# Characterization of Ceramide synthase 2 dysfunctions caused by targeted mutations in transgenic mice

- Dissertation -

zur

Erlangung des Doktorgrades (Dr. rer. nat.)

der

Mathematisch-Naturwissenschaftlichen Fakultät

der

Rheinischen Friedrich-Wilhelms-Universität Bonn

vorgelegt von

Martina van Uelft

(geb. Klahre)

aus

Elsterwerda

Bonn, 2019

Angefertigt mit Genehmigung der Mathematisch- Naturwissenschaftlichen- Fakultät der Rheinischen- Friedrich- Wilhelms- Universität Bonn.

Erstgutachter: PD Dr. Reinhard Bauer
Zweitgutachter: Prof. Dr. Walter Witke
Tag der Promotion: 10.01.2020
Erscheinungsjahr: 2020

## Eidesstattliche Erklärung

Hiermit versichere ich, dass diese Dissertation von mir selbst und ohne Hilfe angefertigt worden ist. Es wurden keine anderen als die angegebenen Hilfsmittel benutzt. Ferner erkläre ich, dass die vorliegende Arbeit an keiner anderen Universität als Dissertation eingereicht wurde.

Teile dieser Arbeit wurden bereits in folgender Originalpublikation veröffentlicht:

Bickert A, Kern P, van Uelft M, Herresthal S, Ulas T, Gutbrod K, Breiden B, Degen J, Sandhoff K, Schultze JL, Dörmann P, Hartmann D, Bauer R, Willecke K. Inactivation of ceramide synthase 2 catalytic activity in mice affects transcription of genes involved in lipid metabolism and cell division. Biochim Biophys Acta Mol Cell Biol Lipids. 2018 Jul; 1863(7):734-749.

Bonn,

MARTINA VAN UELFT

Content

# 1 Introduction

## 1.1 Membranes

A common property of all eukaryotic cells is the presence of a plasma membrane which separates the cell content from the environment (Figure 1.1) (Alberts, 2008; Singer & Nicolson, 1972; Gulbins, 2006). This plasma membrane not only represents a physiological barrier of the cell which allows the maintenance of an internal homeostasis; it is also highly selective and has direct influence on the entry and release of substances. The uptake of metabolically relevant molecules and their release as well as the signal transduction into the cell and vice versa is tightly regulated by the composition of the plasma membrane. Membranes were not only restricted to the cell surface, they can also be found inside the cell, where they contribute to the development of organelles. Most (plasma) membranes consist of the same weight proportions of lipids and proteins (Philips et al., 2009). They build up a lipid bilayer in which different proteins are integrated or associated with (Figure 1.1). Furthermore, membranes can be distinguished by the presence of three main lipid classes, glycerolphospholipids, sterols (cholesterol) and sphingolipids. The composition of each membrane differs from each other due to their diverse functions in different cell types they have to fulfil (e.g. hepatocytes, T cells and neurons). The plasma membrane additionally shows an asymmetric arrangement of their lipids between the inner and outer leaflet. Mechanisms like flip-flop events, lateral diffusion and the vesicular/ specific transport of lipids contribute to this feature (Holthuis et al., 2005; Gulbins et al., 2006, Dupy & Engelmann, 2008). Apart from that, some lipid species are also involved in signalling pathways (Fernandis & Wenk, 2007).

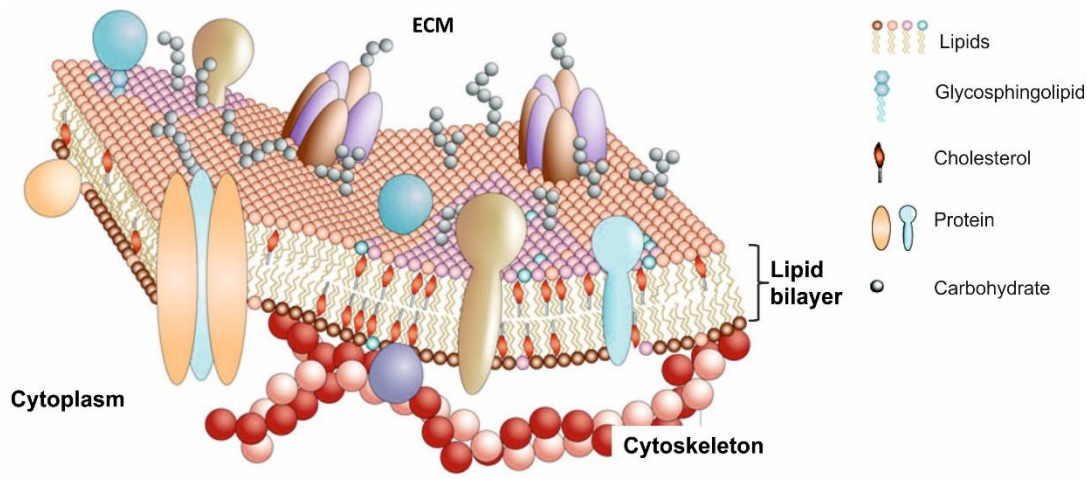


**Figure 1.1: Plasma membrane model**. Depicted is a 3D fluid-mosaic model of the plasma membrane, which is a lipid bilayer in that many different proteins are integrated or associated with. Different lipid classes, e.g. phospholipids, cholesterol and sphingolipids (GSL) build up the membrane, facilitate sorting of proteins into domains upon their physical properties. Segregation leads to generation of the mosaic structure and more detailed membrane organisation. ECM- extracellular matrix; GSL- Glycosphingolipids. (Adopted and modified from Pietzsch, J. 2004; Nicolson et al., 2015)

## 1.2 Lipids

Lipids are one of the main classes of biological molecules besides carbohydrates, nucleic acids and proteins. They are essential components of cell membranes, important for cellular integrity, serve as energy storage, or as signalling molecules involved in signalling pathways. Furthermore, they can be characterized by their amphiphilic character resulting from the carbanion-based condensation of thioesters, or on the other hand by carbocation-based condensation of isoprene units (Fahy et al., 2009). In this respective, lipids can be further divided into the following sub-classes i.e. fatty acids, glycerolipids, glycerophospholipids, prenol lipids, polyketides, saccharolipids, sphingolipids and sterol lipids (Fahy et al., 2005; 2009).

## 1.3 Sphingolipids

Sphingolipids (SL) are one family of eukaryotic membrane lipids, characterized by a high structural variety. They are amphipathic molecules and constituted as a tripartite. In short, SLs consist of a head-group and a sphingoid base (most often C18, Holthuis et al., 2001) which is linked by N-acylation to a fatty acid of varying chain length (C12-36) which can be additionally saturated or non-saturated (Figure 1.2) (Sandhoff, 2010; Mencarelli and Martinez-Martinez, 2012).

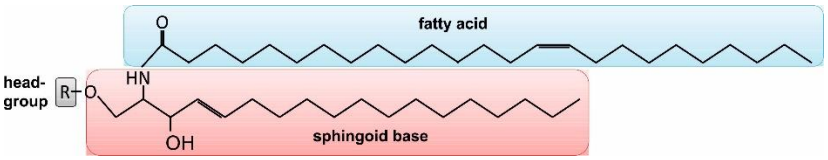


**Figure 1.2: Common structure of sphingolipids**. Shown is a C24:1 Ceramide (d18:1-24:1); a C24:1 fatty acid (blue) is amide-linked to the C2-atom of a C18:1 sphingoid base (red) and a (H)-head-group (grey R). The fatty acid chain length varies between C12 and C36, whereas the sphingoid base commonly consists of 18 C-atoms.

Depending on the (polar) head group bound to the C1-atom of the sphingoid base one can subdivide them into three main classes: ceramides, phosphosphingolipids and glycosphingolipids (Figure 1.3) (Lahiri et al., 2007). Ceramide, the simplest sphingolipid carries a hydrogen atom attached to the sphingoid base. Ceramides are the precursors of all complex sphingolipids, its derivatives and the two known signalling molecules ceramide-1-phosphate (C1P) and sphingosine-1-phosphate (S1P) (Hannun et al., 2002). Next, sphingomyelin (SM) and ceramide phosphoethanolamine (CPE) are the main representatives of the phosphosphingolipids and display eponyms due to the bound head-groups phosphocholine (PC) and phosphoethanolamine (PE) (Figure 1.3). Glycosphingolipids (GSL) represents the last group of SLs, which can be further divided into cerebrosides, globosides and gangliosides depending on the carbohydrate connected by a β-linkage to the sphingoid base (Figure 1.3; Merill, 2011). Briefly, cerebrosides also called monoglycosylceramides contain only one sugar residue. Globosides contain at least two sugar side chains, which can be a combination of the following: D-glucose, D-galactose and N-acetylgalactosamine. Moreover, gangliosides are the third sub-type of GSLs. They carry more than one sugar molecule on their side chain in combination with one or more sialic acids (Kolter et al., 2002; Merill, 2011). While cerebrosides and globosides were referred to as neutral sphingolipids, gangliosides belong to the group of acidic glycosphingolipids due to the presence of at least one sialic acid.

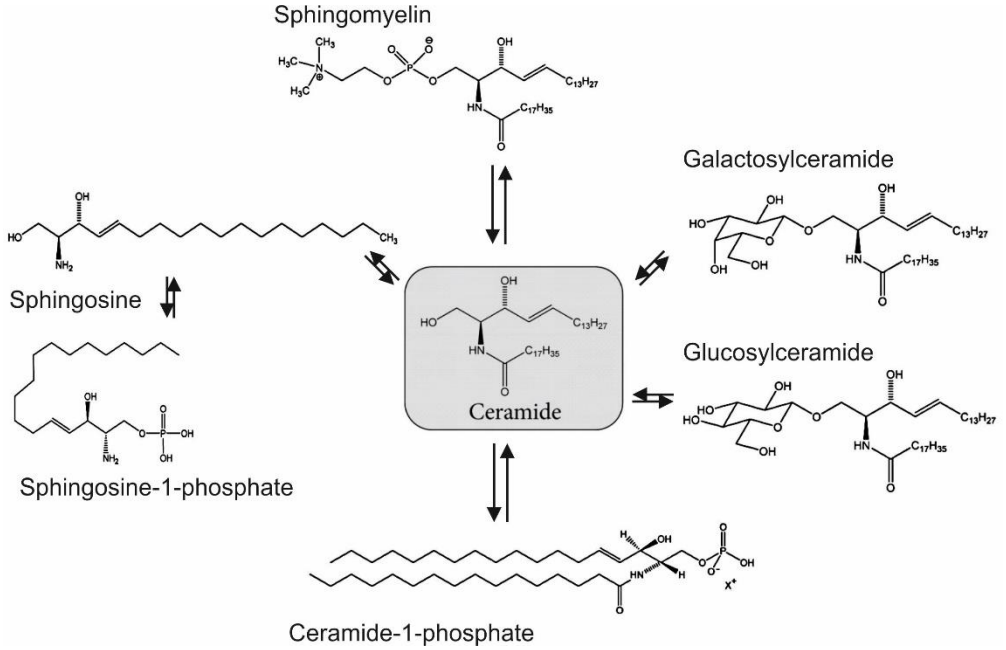


**Figure 1.3: The sphingolipid Ceramide and possible derivatives.** Ceramide displays the key intermediate and central backbone of complex sphingolipids and its derivatives. The most basic structures of glycosphingolipids which in turn themselves are precursor for complex gangliosides were shown on the right side. Sphingomyelin, main component of membranous myelin sheaths is depicted in the upper part. In the lower part and on the left side, the two main signalling molecules sphingosine-1- phosphate and ceramide-1-phosphate were represented (Adopted and modified from Yamashita et al., 2011).

## 1.3.1 Ceramide

Ceramide is the simplest sphingolipid and key intermediate in the sphingolipid metabolism. It is composed of a sphingoid base, a fatty acid of varying chain length (C12 to C36) and a hydrogen atom as the head-group (Figure 1.2 and 1.3) (Grösch et al., 2012; Hannun et al., 2011). On the basis of the incorporated type of sphingoid base, ceramides can be further classified as: dihydroceramides (sphinganine), phytoceramides (phytosphingosine) and ceramide (sphingosine) (Figure A1; Pruett et al., 2008; Alfatah et al., 2019). Finally, the generation of ceramides can either be accomplished by activation of *de novo* synthesis or by constitutive degradation of complex sphingolipids (*salvage* pathway) (Chapter 1.3.1.1 and 1.3.1.2, Figure 1.4).

### 1.3.1.1 *De novo* synthesis

The *de novo* biosynthesis of ceramide occurs exclusively on the cytoplasmic leaflet of the endoplasmic reticulum (ER) and is driven by the stepwise action of many enzymes (Figure1. 4) (Mandon et al., 1992; Tidhar & Futerman, 2013). The first step displays the condensation of L-serine and palmitoyl-CoA to form the sphingoid base 3-ketodihydrosphingosine (3-keto-sphinganine) (Figure 1.4, upper box). The reaction represents the rate-limiting step of the *de novo* synthesis and is catalysed by the serine palmitoyl transferase (SPT) (Hanada et al., 2003) which in turn is regulated by ORMDL proteins (Orm like) (Mandon et al., 1992; Breslow et al., 2010). Consistent with the preference of the SPT for saturated fatty acids, the abundance of palmitoyl-CoA and L-serine, sphingoid bases predominantly with C18 carbons were formed. Subsequently, 3-ketodihydrosphingosine is reduced by the 3-ketophinganine reductase, in a NADPH-dependent reaction to form sphinganine (Figure 1.4, upper box; Stoffel et al., 1968). In the third step, the N-acylation of dihydrophingosine with fatty acids of varying chain length is catalysed by the presence of (dihydro)- ceramide synthases (CerS), more precisely a family of

sphinganine N-acyl-transferases (Figure 1.4 upper part, yellow box, Morell et al., 1970; Guillas et al., 2001; Kolter, 2011) and results in the formation of dihydroceramide. Next, the dihydroceramide desaturase (DES) converts dihydroceramide to ceramide by insertion of a *trans* 4,5 double bond (Rother et al., 1992; Fabrias et al., 2012). Finally, ceramide can be used for the generation of more complex sphingolipids (Figure 1.4, middle box). Therefore, ceramide is transported through vesicular transport or non-vesicular transport by the ceramide transport protein (CERT, van Meer & Holthuis, 200; Hanada et al., 2003 (2)) to the Golgi apparatus, the site of complex SL biosynthesis.

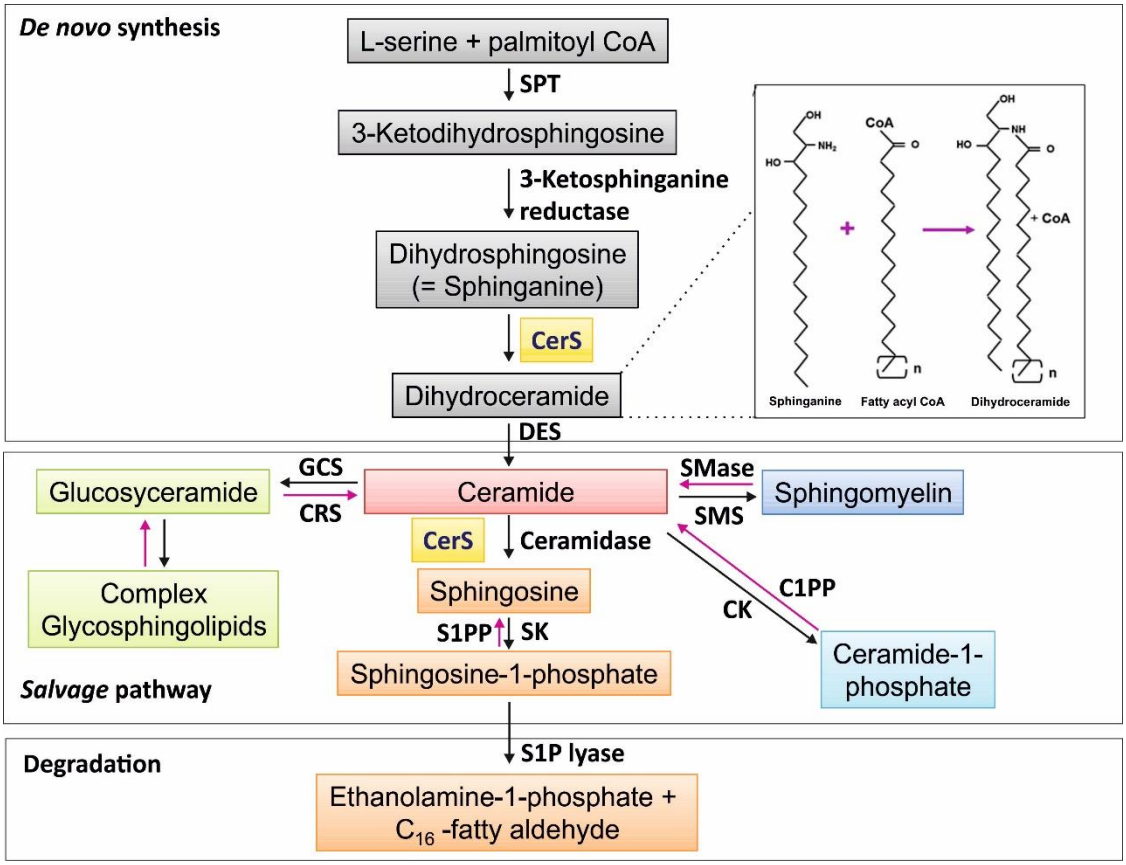


**Figure 1.4: Sphingolipid metabolism.** Depicted is the schematic representation of the sphingolipid metabolism with main steps of biosynthesis and degradation. It starts with the *de novo* synthesis of ceramides in the ER and proceeds with the generation of either complex glycosphingolipids in the Golgi apparatus or the generation of the bioactive molecules S1P and/or C1P. The *salvage* pathway of sphingolipids occurs in endolysosomes and results in the breakdown of higher order SLs (Adopted and taken from Ogretmen & Hannun, 2004).

### 1.3.1.2 *Salvage* pathway

An alternative pathway besides the *de novo* synthesis exists that accelerate the formation of ceramides, by degradation of higher order sphingolipids, the *salvage* pathway (Figure 1.4, middle and lower box, pink arrows; Kitatani et al., 2008; Kolter, 2011; Bikman et al., 2011). This second source is also essential to prevent the cell for accumulation of toxic sphingolipid species. The *salvage* pathway is restricted to late endosomes and/or lysomes and utilises the stepwise action of glycosidases, starting from the non-reducing end thereby giving rise to the formation of ceramide (Sandhoff & Kolter 2003). Furthermore, the degradation is highly dependent on the presence of sphingolipid activator proteins (SAPs, Schultze & Sandhoff, 2014). Mutations within the SAPs or other degrading enzymes could cause severe lysosomal lipid storage diseases also

known as sphingolipidoses. An exception illustrates the degradation of SM, which is hydrolysed by a family of sphingomyelinases (Marchesini et al., 2004). Moreover, those enzymes are distinguished by their preference for acidic, alkaline or neutral pH where they show the highest catalytic activity (Tayama et al., 1993; Hannun & Obeid., 2008). The resulting head-groups and PC can either be re-used or further processed (Sandhoff & Kolter, 2003). The remaining ceramide in turn is further degraded by acid ceramidases which results in the formation of sphingosine and fatty acids (Figure 1.4, lower box) (Linke et al., 2001; Hannun & Obeid, 2008). Thereafter, sphingosine can be further degraded into its building blocks, or 'salvaged' by phosphorylation thereby generating S1P (Spiegel & Milstien, 2003; Ogretman & Hannun, 2004) or reused as the sphingoid base leading to the formation of ceramide by N-acylation processed by ceramide synthases (see Chapter 1.4). Finally, 50- 90 % of the SLs re-generated in the *salvage* pathway are used for the synthesis of new SLs (Kitatani et al., 2008).

### 1.3.2 Sphingosine-1-phosphate and Ceramide-1-phosphate

Sphingosine-1-phosphate displays an important intermediate within the sphingolipid metabolism; and is generated from sphingosine by phosphorylation of the primary hydroxyl group at the C1 atom (Figure 1.3 and 1. 4) (Spiegel & Milstien, 2003). Incidentally, sphingosine is exclusively generated in the *salvage* pathway, by degradation of higher order SLs and not by the *de novo* synthesis of ceramide. This implicates that a tightly controlled turnover of complex SL has developed to cover the actual needs of S1P of the cell (Kitatani et al., 2008; Mao & Obeid, 2008).

Mammalian cells harbour two specific kinases, sphingosine kinase 1 and 2 (SPHK1 or-2) which catalyse the reaction. Both enzymes show a ubiquitous expression pattern, they differ in their intracellular localization (plasma membrane, nucleus) and substrate specificity (Wattenberg et al., 2010; Hatoum et al., 2017). Newly generated S1P can function as an intracellular signalling molecule, which was shown to be involved in the regulation of histone acetylation (Spiegel & Milstien, 2011; Hait et al., 2009; Hatoum et al., 2017). Apart from that, the majority of generated S1P is released into the extracellular space by specialized transporter, where it contributes to the maintenance of a S1P gradient, crucial for lymphocyte trafficking (Proia & Hla, 2010). Moreover, it is capable of interacting with five G-protein coupled receptors (GPCRs) (Regard et al., 2008), termed S1PR1-5, in a form as a second messenger, thereby transducing intracellular signals which regulate cellular proliferation and survival, for example (Proira & Hla, 2010; Hatoum et al., 2017). Next, degradation, i.e. dephosphorylation of S1P is achieved by the action of several lipid phosphate phosphatases and two S1P-specific phosphatases which catalyse the regeneration of sphingosine (Zamora-Pineda et al., 2016). Additionally, breakdown of S1P into its building blocks phosphoethanolamine and hexadecanal is catalysed by S1P lyase (Zhou et al., 1998).

Another bioactive molecule which can be generated upon phosphorylation is C1P- ceramide-1-phosphate. (Figure 1.3 and 1.4, middle box). The formation of C1P is catalysed by the enzyme ceramide kinase (CERK) in the Golgi apparatus (Lamour et al., 2007). C1P is then subsequently delivered to the plasma membrane by C1P transfer protein (Simanshu et al., 2013). Moreover, C1P can either act as an intracellular second messenger, e.g. it was shown to directly interact and activate $cPLA_2$ (cytosolic phospholipases A2), which in turn enhances arachidonic acid formation that triggers inflammatory response (Pettus et al., 2004; Lamour et al., 2007). Apart from that it could also act extracellular, e.g. necessary for the regulation of cell growth and

survival (Ordonez et al., 2018) or as an important key player in the regulation of macrophage chemotaxis (Arana et al., 2010).

## 1.4 Ceramide synthases

Ceramide represents the common backbone of all higher order sphingolipids (GSLs) and is therefore suggested to be the main important sphingolipid species in SL metabolism (Ogretman & Hannun, 2004). In the early 1970s Morell & Randin (1970) characterized the first biochemical dihydroceramide synthase activity. Nevertheless, the genes encoding the ceramide synthases, the central enzymes in the SL metabolism were identified more than 20 years later in yeast strains (D' Mello et al., 1994). There the *lag1* and *lac1* gene were proven to be essential for ceramide synthesis and the name, Lass – longevity assurance gene, arises from the resulting phenotype (Guillas et al., 2001; Teufel et al., 2009); but was re-named into CerS according to their biochemical function (Pewzner-Jung et al., 2006). After their discovery and detailed examination in yeast, further protein database-based searches lead not only to the identification of homologs in mammals (*Mus musculus*), furthermore it turned out that CerSs are encoded throughout the animal kingdom, e.g. *Drosophila melanogaster*, *Danio rerio* (Voelzmann & Bauer, 2010).
To date, the mammalian family of ceramide synthases consist of six members (CerS1-6). All are multi-pass transmembrane proteins, with predicted 5-8 transmembrane domains, depending on the underlying algorithm used for prediction (Levy et al., 2010; Tidhar et al., 2012). Furthermore, their expression is mainly restricted to the ER (Barz & Walter, 1999; Kremser et al., 2013) with the N-terminus facing the ER lumen (Tidhar et al., 2018). Additionally, there is some literature available that point into the direction that some CerS are also present in the Golgi apparatus and mitochondria/ mitochondria associated membranes (Hirschberg et al., 1993; Voelzmann & Bauer, 2010; Gault et al., 2010; Levy et al., 2010). Basically, all of them share the same common feature, the synthesis of ceramides (Mullen et al., 2012).

### 1.4.1 Protein domains and motifs

CerS family members share the presence of several common functional domains and motifs (Figure 1.5). As they are lag1p homologues, all of the mammalian CerS contain a TLC domain (TRAM-Lag-CLN8, Figure 1.5, green region) and all, except CerS1, contain a HOX (homeobox) domain (Figure 1.5, red circles; Levy et al., 2010).

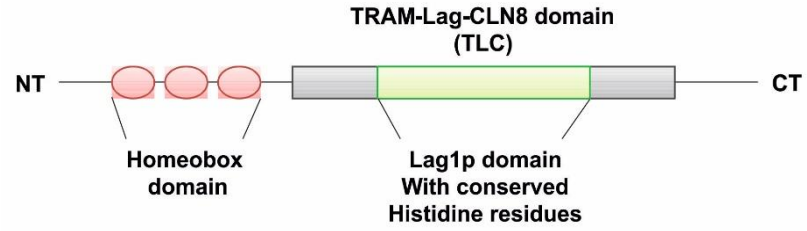


**Figure 1.5: Schematic representation of domain organisation of CerS.** Illustrated is the putative domain structure of mammalian CerS2, N (NT) - as well C-terminus (CT) are indicated. Homeobox domain (red circles) present in all CerS, except CerS1, is N-terminally located. TLC domain harbours the lag1 domain with the two highly conserved histidine residues essential for catalytic activity.

### TLC domain and the lag1 motif

The translocation-associated membrane (TRAM) - motif is present in proteins which facilitate the translocation of proteins. More precisely, they are components of the translocon, a gated channel at the ER membrane (Ng et al., 2010; Fukushima et al., 2018). Even though the lag1 domain shows high sequence similarity to TRAM, Barz & Walter (1999) found no evidence in cell-culture based experiments that support the assumption that CerS are also involved in the structural organisation of the co-translational complex.

The lag1 domain- contains a 52 aa residue stretch, which shows high sequence homology to the yeast lag1 motif (Jiang et al., 1998). In addition it was also shown that only 15 % of the TLC domains are highly conserved and that some distinct mutations within this region, more precisely within the lag1 domain results in the loss of enzymatic activity (Figure 1.6, essential amino acid residues are marked by an arrow; Spassieva et al., 2006; Tidhar et al., 2012).


**Figure 1.6: Lag1 domain of CerS.** Depicted is the highly conserved, 52 amino acids residues in size, lag1 domain, of mammalian CerS. Highly conserved residues were shown in bold faces, conserved residues were not highlighted and 'x' displays non-conserved residues. Arrows indicate that upon its mutation the catalytic activity is lost (Adopted and modified from Spassieva et al., 2006).

On the other hand, not much is known about the functions of the CLN8 motif. It shows high sequence similarity to the ceroid-lipofuscinosis neuronal 8 protein, which is part of a family with further seven members (Winter & Ponting, 2002). Their genetic mutations lead to the development of a lysosomal storage disease where auto fluorescent material accumulates within the lysosomes, which give rise to degeneration of the central nervous system (CNS) (Getty & Pearce, 2010). Furthermore it is suggested that the CLN8 protein might act as a lipid sensor in lipid homeostasis (Winter & Ponting, 2002).

#### 1.4.1.1 The homeodomain (HOX)

Another highly conserved motif, evolutionary present since cnidarias (Voelzmann & Bauer, 2010) and present in many CerS is the homeodomain. On the mammalian system, all CerS, except CerS1, contain this N-terminally located domain. Its function is controversially discussed (Voelzmann & Bauer, 2010). Usually, homeotic genes - master regulators (transcription factors) involved in the specification of the body plan, the determination of the cell fate and further developmental processes (McGinnis et al., 1984; Gehring et al., 1994) - are characterized by the presence of a homeodomain. In contrast to the homeodomain of CerS where the first 15 amino acids (aa) residues are missing (Mesika et al., 2007), they usually contain 60 aa necessary for DNA binding (Gehring 1993). Moreover, nuclear magnetic resonance (NMR) analyses of CerS5 and 6 reveal that both homeodomains have the probability to adopt a 3-helical structure like those of other homeotic genes (Voelzmann et al., 2016; Sociale et al., 2018). Additionally it was shown that *schlank* in *Drosophila* contains two nuclear localization signals (NLS) within the homeodomain, a monopartite-like NLS (NLS1, RPKK, aa78–81) and a bipartite-like NLS (NLS2, RLDKKK-$X_{19}$-RLRR, aa97–125) (Voelzmann, et al., 2016).

### 1.4.2 Expression pattern and substrate specificity

Northern Blot analyses and quantitative real-time PCR experiments of various mouse tissues reveal that each CerS is characterized by a unique expression pattern, with partial overlaps (Mizutani et al., 2005; Levy et al., 2010). Moreover, all CerS catalyse the acylation of sphinganine by fatty acyl-CoAs, which results in the formation of ceramide. Each CerS utilizes a specific subset of fatty acid chain length of C14-C36 (Sandhoff, 2010; Mencarelli and Martinez-Martinez, 2012) for N-acylation. Finally, this results in a broad spectrum of ceramide species available for GSL synthesis in the different tissues (Lahiri & Futerman, 2007; Levy et al., 2010).

### 1.4.3 CerS1 and CerS1-deficient mice

CerS1 is mainly expressed in skeletal muscle and the predominant CerS in brain besides CerS2 (Zhao et al., 2011; Ginkel et al., 2012). Additionally, it shows high substrate specificity towards C18 acyl-CoAs (Levy et al., 2010). Upon its mutation, which leads to CerS1 deficiency in mice, they suffer under Purkinje cell degeneration, accumulation of lipofuscin and cerebellar ataxia, which is in line with decreased levels of myelin-associated glycoprotein (MAG) in the brain and shrinkage of cerebellum (Ginkel et al., 2012).

### 1.4.4 CerS2 and CerS2- deficient mice

*Ceramide synthase 2* is encoded on chromosome 3 at segment 3F2 on the antisense strand between the genes *annexin A9* and *SETdomain* (bifurcated1) in the mouse genome. From the transcribed mRNA of 1981 bp a protein of 380 aa residues is translated with a putative mass of 37 kDa (NCBI, UniprotKB). The genomic organization shares common features with those of a housekeeping gene (Mizutani et al., 2005; Laviad et al., 2008). The first exon and the first part of the second exon are the 5' untranslated region (UTR). The last part of exon 11 harbours the 3' UTR with the polyA signal. A homologous gene of the mouse *cers2* is also encoded in the human genome by the *hcers2* gene, which is localized on chromosome 1. Expression pattern analysis of mouse tissue by Western Blot, qRT-PCR and Northern Blot (Kremser, 2016; Mullen et al., 2012; Schiffmann et al., 2013) indicate that it is not only almost present in every tissue, but also the most abundant with predominant expression in liver, lung and brain (Mizutani et al., 2005; Becker et al., 2008; Kremser, 2016.). Moreover, CerS2-deficient mice ($CerS2^{gt/gt}$) have been intensively studied and the results reveal that the lack of ceramide-species play important roles in many physiological processes (Imgrund et al., 2009/2011; Pewzner-Jung, et al., 2010 i/ii). They maintain brain myelination, cellular homeostasis of the liver and neutrophil migration. Deletion of CerS2 results in the lack of corresponding SL species (C22 and C24/C24:1) and accumulation of C16 and C18 SL, which might be based on a compensatory mechanism or basically due to an increased C16 acyl-CoA level. Furthermore, those mice show a de-regulated S1P-level/gradient which mainly affects the emigration of mature lymphocytes from the thymus into the circulation (blood, lymph node) (Rieck et al., 2017).

### 1.4.5 CerS3 and CerS3- deficient mice

Ceramide synthase 3 is mainly expressed in skin (keratinocytes) and its deficiency leads to defects in the maintenance of the transepidermal water barrier and by this to a transepidermal water loss which causes early lethality of new born mice (Jennemann et al., 2012; Eckl et al., 2013). The severe phenotype can be explained by the unique substrate specificity of CerS3 that mainly uses ultra-long-chain acyl-CoAs (≥ C26) for SL biosynthesis (Park & Park, 2015; Kihara, 2016).

### 1.4.6 CerS4 and CerS4- deficient mice

CerS4 is characterized by a broad expression pattern, but strongest in skin (Ebel et al., 2014 i/ii) and substrate specificity towards C18-C20 acyl-CoA. Two independent, but simultaneously generated CerS4-deficient mouse lines were published and both draw the conclusion that ceramide synthase 4 deficiency results in an age-related hair loss which is based on an altered sebum composition (reduced C18 and C20 SL) in the skin (Ebel et al., 2014; Perters et al., 2015).

### 1.4.7 CerS5 and CerS5- deficient mice

Ceramide synthase 5- deficiency does not result in an obvious phenotype (Gosejacob et al., 2016). The mice are viable and fertile. Under normal conditions, CerS5 is mainly expressed in white adipose tissue (WAT), testes and thymus (Gosejacob et al., 2016) and utilises C16 fatty acids for N-acylation (Levy, 2010; Mizutani et al., 2005). After challenging CerS5-deficient mice in a high fat diet, mice show reduced weight gain and simultaneously a reduction in WAT inflammation pointing into the direction that CerS5 might contribute to ameliorate obesity and its side effects (Gosejacob et al., 2016). Additionally, *in vitro* analyses reveal that the deletion of nearly the entire homeodomain does not affect the catalytic function of the protein (Mesika et al., 2007).

### 1.4.8 CerS6 and CerS6- deficient mice

Similar to CerS5, CerS6 has the same substrate specificity against C16 fatty acids, but also against C14 and shows the highest expression pattern in kidney and intestine (Laviad et al., 2008; Ebel et al., 2014). Furthermore, CerS6-deficiency results in the reduction of C16 ceramide species and the mice show behavioural defects, like clasping of the hind limbs (Ebel et al., 2014). Moreover, it was shown that loss of CerS6 increases the development of experimental autoimmune encephalomyelitis (EAE) (Eberle et al., 2014; Helke et al., 2018).

## 1.5 *Drosophila melanogaster* ceramide synthase - schlank

In contrast to the mammalian system where six CerS are expressed, the fruit fly *Drosophila melanogaster* expresses only one ortholog, the *schlank* gene (Voelzmann & Bauer, 2010; Voelzman et al., 2016; Sociale et al., 2018). Furthermore, it shares protein domain similarities regarding the presents of the homeodomain and similarities regarding the presence of the TLC domain with the lag1 motif essential to maintain its catalytic activity. Moreover, mutations in the catalytic domain results in the characteristic of different phenotypes, including reduced triacylglycerol (TAG) level, developmental delay or early lethality (Bauer et al., 2009; Wulf, 2015). In a recent publication, Sociale et al. (2018) could show that the homeodomain of the schlank protein is membrane-bound, shuttled to the inner nuclear membrane.
Moreover they could show in detailed analysis that the HOX domain interacts with the promoter region of different genes i.e. *lipase3* (*lip3*) and *magro*. Upon mutation of the bipartite NLS2 signal (RLDKKK-$X_{19}$-RLRR, RLDKKK-$X_{19}$-ALAR) within the homeodomain, it loses its function to interact with these regions. Additionally, it was shown that schlank shuttling depends on the energy status of the fly, i.e. under feeding conditions. The homeodomain of the schlank enzyme then suppresses *lip3* expression, however under starvation schlank is released from the promoter region of *lip3*, which results in increased lip3 protein expression and consequently TAG lipolysis (Sociale et al., 2018).

## 1.6 Ceramides and energy metabolism

Mice represent one of the most widely used model organisms to study human diseases and their underlying genetics and molecular mechanisms (Speakmann, 2013). One main field investigated in those studies is the characterization of the energy homeostasis/ metabolism, i.e. the energy expenditure and the main factors involved in regulation and dysfunctions leading to obesity and its comorbidities (Speakmann, 2013). Basically, energy metabolism summarizes all processes and reactions (catabolism and anabolism) involved in food intake and breakdown into its building blocks to obtain energy for cell growth, survival and reproduction (Galgani & Ravussin, 2008). Furthermore, energy metabolism of each organism is influenced by several factors; basal expenditure in combination with physical activity, thermoregulation and the genetic background. During evolution, e.g. periods of fasting and feeding, a tightly controlled multi-factoral network has developed, which is responsible for the regulation of energy intake and expenditure (Galgani & Ravussin, 2008). This network is composed on the one hand of the central nervous system, i.e. the hypothalamus, which regulates appetite and food intake (Yeo & Heisler, 2012) by the release of hormones. Further members of this circuit are the peripheral organs, such as the gastrointestinal tract, including liver and pancreas as well as the adipose tissue (WAT and brown adipose tissue (BAT)) and muscle, which provide and receive information and signals regarding the energy status (Seoena-Collazo et al., 2015). Basically, even more than 90 % of the body energy is stored in form of TAG in adipose tissue despite the restricted capacity to store proteins and carbohydrates for energy production; where the latter one can be further converted and stored as glycogen in liver and muscle (Véret, 2011). Upon saturation of glycogen storages, glucose can also be converted to TAG and subsequently stored in liver and adipose tissue (Véret, 2011). Regardless the genetic background, increased energy consumption (physical activity, fasting state) is accompanied by the depletion of energy storages to maintain cellular processes. On the other hand excessive energy intake (high-fat/caloric-diet), more than required for energy expenditure, is stored in form of fat (TAG) molecules in adipose tissue. If the over nutrition becomes chronically, the organism gained more fat, which in turn results in the onset of obesity (Galgani & Ravussin, 2008). The development of an obese state in turn is a major risk factor for the development and onset of various diseases such as cardiovascular disease and type 2 diabetes as well as atherosclerosis.

### 1.6.1 Ceramide and sphingolipids in the development of metabolic disorders

Ceramide as the key intermediate in sphingolipid metabolism represents not only a membrane component, which facilitates structural integrity, recent publications indicate that ceramides are also involved in the regulation of various cellular processes such as cell growth, proliferation and apoptosis (Bartke & Hannun, 2009), e.g. as a second messenger (Bikman & Summers, 2011). Furthermore, it turned out that there is a correlation between the appearance of certain sphingolipid species and obesity-associated disorders, e.g. atherosclerosis, cardiovascular disease and type 2 diabetes. These findings further highlight the need to elucidate their implication (Holland & Summers, 2008; Bellini et al., 2015).

#### 1.6.1.1 Ceramide and type 2 diabetes

Increasing investigations reveal a strong relationship between the development of type 2 diabetes (T2D) and excessive levels of circulating/accumulating lipids, e.g. free fatty acids (FFA), diacylglycerol (DAG) and phosphatidic acid, concomitant with an altered lipid metabolism, highlighting ceramides as a further important mediator of lipotoxicity and β-cell dysfunction (Bellini et al., 2015). Under normal conditions, the adipose tissue is the main storage for free

fatty acids resulting from dietary-intake (Hajer et al., 2008). Diet-induced obesity results in an overload of adipocytes. Increasing free fatty acid levels accumulate in other peripheral tissue such as liver, pancreas, muscle and serum. There free fatty acids provide an additional source of acyl CoA used for sphingolipid synthesis, which results in increased sphingolipid levels. A direct cause of all these alterations results in insulin resistance and thereby the onset of T2D. Usually, insulin facilitates glucose uptake by regulating the translocation of glucose transporter from intracellular storages to the plasma membrane in adipose tissue and muscle. In liver, insulin signalling prevents the release of glucose, inhibits gluconeogenesis, which results in the storage of glucose as glycogen (Holland & Summers, 2008). Further investigations reveal that elevated ceramide levels antagonize insulin function thereby inducing insulin resistance (Chavez & Summers, 2012). Activation of insulin receptor upon extracellular binding of insulin results in a conformational change and autophosphorylation of the insulin receptor. This in turn leads to the recruitment and phosphorylation of further downstream molecules, e.g. IRS (insulin receptor substrates). Activated IRSs facilitate further activation of phosphatidylinositol 3-kinase (PI3K), which contributes to the activation of Akt/PKB (protein kinase B) and their downstream signalling cascades and targets (Bellini et al., 2015; Ng et al., 2017). Investigations elucidate that Akt/PKB is a direct target of ceramide thereby inducing insulin resistance (Bandet et al., 2019). Ceramide can either interact with protein phosphatase - PP2A, leading to its activation, which prevents further activation of Akt/PKB by mediating its dephosphorylation (Hage et al., 2014, Cazzolli et al., 2001). On the other hand, ceramide was shown to alter insulin signalling, by ceramide-dependent activation of an atypical PKCζ (Protein kinase C). Activated PKC prevents translocation of Akt/PKB to the plasma membrane (Powell et al., 2003; Turban&Hajduch, 2011).

#### 1.6.1.2 Diet-induces obesity and the role of ceramide synthase deficient mice

With the generation and analysis of ceramide synthase knockout mice the question raises whether the overall altered ceramide content causes insulin resistance or the increase in a specific ceramide species. Experiments regarding the expression of CerS2 in liver, white adipose tissue and skeletal muscle of obese human and mouse model indicate a positive correlation between *cers6* mRNA expression and the grade of obesity (Turpin et al., 2014). Additionally, they showed that CerS6-deficient mice, fed a high-fat-diet (HFD) were protected from diet-induced obesity and glucose intolerance (Turpin et al., 2014). These findings were also supported by results obtained from Raichur et al (2019). Here, obese mouse mutants (ob/ob) and obese HFD-mouse models were treated with CerS6 antisense oligonucleotides (ASO) to knockdown CerS6. ASO treatment results in down-regulation of CerS6 expression and subsequent reduction in subcutaneous and visceral fat reduced C16:0 ceramide plasma levels as well as improved glucose tolerance and insulin sensitivity (Raichur et al., 2019). Further data existing from analysis of β-cell function showing that elevated ceramide levels, resulting from high palmitate and glucose content and increased CerS4 expression, induces activation of PP2A (Veret et al., 2014) and inhibits nuclear translocation of the transcription factors PDX-1 and Mafa, thereby causing the loss of pancreatic β-cell function (Poitout et al., 2008; Veret et al., 2014). Haplo-insufficient expression of CerS2 results in increased ratio of fat to lean mass and mild insulin resistance, which was shown by Raichur and colleagues (2014). Moreover they could verify that elevated CerS6 expression and C16:0 ceramide levels than the loss of very-long chain ceramides causes these alterations. CerS2$^{gt/gt}$ mice showed an even more pronounced phenotype regarding insulin resistance and C16:0 ceramide levels (Park et al., 2014).

## 1.7 Immune system

The immune system shows the ability of a multi-cellular organism to protect themselves from a broad spectrum of pathogens, e.g. bacteria, viruses and parasites, which can cause severe infections (Kenneth et al., 2012; Iwasaki & Ruslan, 2015; Lodish et al., 2016). This host-defence complex system has formed during the course of evolution and comprises a coordinated interaction of various structures (e.g. skin barrier, effector cells) and processes (e.g. chemokine production, phagocytosis) (Dranoff, 2004; Kenneth et al., 2012; Lodish et al., 2016). The mammalian immunity can be further subdivided into the innate and adaptive immune system (Kenneth et al., 2012).

The majority of all immune responses depict a coordinated and highly connected response of both pathways. The innate immune response against bacteria for example, is mainly mediated by phagocytic cells (dendritic cells (DCs), macrophages), which stimulate/ activate the adaptive immune response and thus activate the clonal expansion of highly specific T lymphocytes and the production of antibodies by B cells (Janeway et al., 2001; Kenneth et al., 2012).

B cells, also known as B lymphocytes, belong to the group of effector cells of the adaptive immune system and they are characterized by the generation and secretion of specific antibodies upon their activation (Cano & Lopera, 2013; Nutt et al., 2015).

During maturation, T lymphocytes either differentiate into the lineage of CD4+ or CD8+ T cells. Primarily, CD8+ T cells further differentiate into cytotoxic T cells when they develop their effector functions (Cox et al., 2013). On the other hand, CD4+ T cells differentiate into T helper (Th) cells of various sub-lineages, more precisely into Th1, Th2, Th17, Th9, Tfh and Treg (Cano & Lopera, 2013; Carbo et al., 2014). The differentiation into one of these lineages depends on the type of antigen presenting cell (APC) in combination with its activation state, but depends also on the type of antigen and cytokines present in the microenvironment (Cox et al., 2013).

### 1.7.1 Thymus

The thymus is a flat- two-lobed organ. Each lobe is surrounded by a capsule, and can be further subdivided into lobules, where each lobule is separated by trabeculae, a strand of connective tissue (Garland, 2001). Additionally, each lobule consists of two main regions, the cortex and the medulla (Figure 1.7).

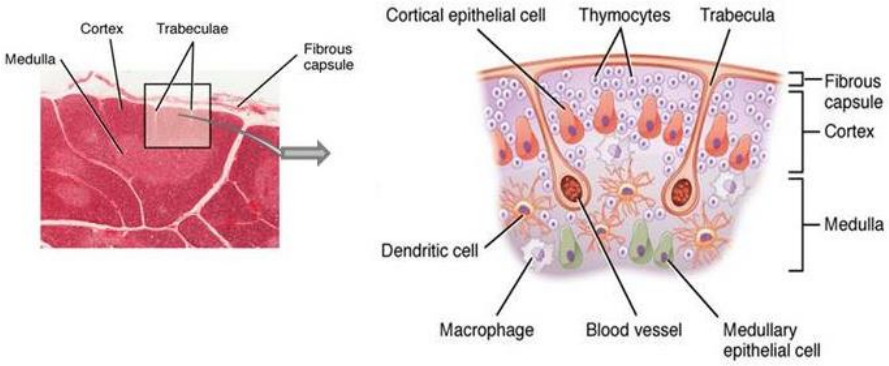


**Figure 1.7: Thymus.** Histological section of H&E staining from thymus (left) and graphical overview (right) of detailed thymic organization (Figure adopted and modified from "Location, Structure, and Histology of the Thymus" von Philschatz. Lizenz: CC BY 4.0).

### 1.7.2 T cell development - Thymopoiesis

The T cell development can be divided into several stages each requiring a distinct microenvironment provided by the thymus, more precisely by thymic stromal cells, thymic epithelial cells, endothelial cells, fibroblasts and their expression of chemokines (Figure 1.8; Takahama, 2006; Nitta & Suzuki, 2016).

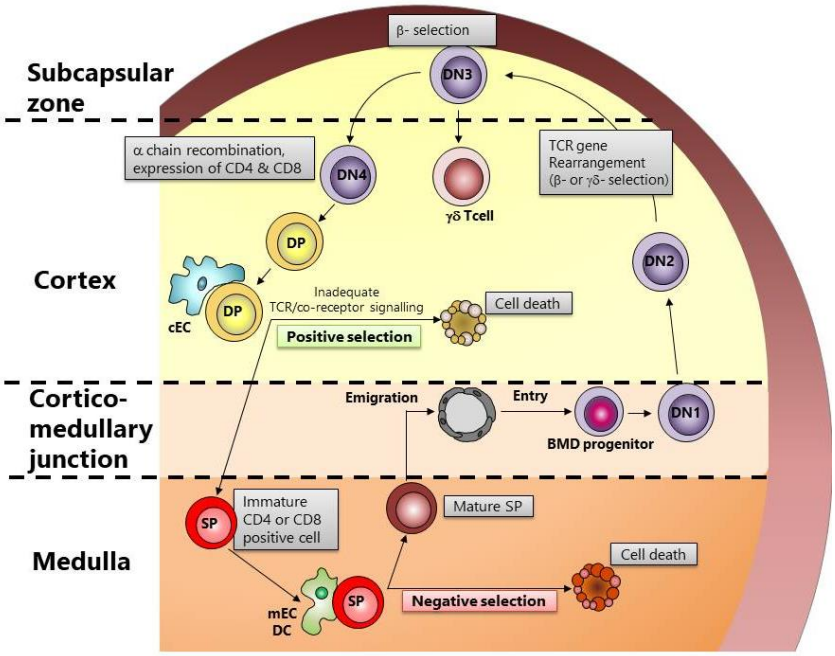


**Figure 1.8: T cell development.** Bone marrow derived (BMD) progenitor cells enter the thymus at the cortico-medullary junction and give rise to the group of CD4/CD8 double-negative (DN) cells. Upon differentiation they migrate into the subcapsular zone (SCZ) and back to the cortex and transform into DN1($CD44^+CD25^-$), DN2($CD44^+CD25^+$), DN3($CD44^-CD25^+$) and DN4($CD44^-CD25^-$). Afterwards they differentiate into CD4/CD8 double positive (DP) thymocytes and undergo positive selection, via TCR$\alpha\beta$:self-peptide-MHC signalling. Positive selection is mediated by cortical epithelial cells (cEC) which induce, upon appropriate signalling, the development into either CD4 or CD8 lineage. Immature single positive (SP) thymocytes enter the medulla and interact with medullary epithelial cells (mEC) or dendritic cells (DC) in a second control point, the negative selection (development of self-tolerance). Mature SP cells migrate to the cortico-medullary junction an leave the thymus to become naïve T cells circulating in the periphery. (Adopted and modified according to Takahama, 2006; Cano & Lopera, 2013; Nitta & Suzuki, 2016).

Initially, bone marrow derived (BMD) progenitors enter the thymus at the well-defined cortico-medullary junction and migrate to the cortex. Each differentiation step can be monitored by the cell surface expression of different markers e.g. CD25, CD44 and CD4 as well as CD8 (Godfrey et al., 1993; Ceredig & Rolink, 2002). BMD progenitors belong to the group of CD4/CD8 double negative thymocytes that undergo various differentiation steps from double negative (DN) stage to the double positive (DP) stage and finally give rise to the stage of mature single positive (SP) thymocytes, which leave the thymus and enter secondary lymphoid organs (e.g. spleen and lymph nodes). Moreover, cells of each differentiation step colonize a distinct area of the thymus (Figure 1.8; Zuniga-Pflücker, 2004). First, the DN stage can be further divided into DN1 ($CD44^+$/ $CD25^-$), DN2 ($CD44^+$/ $CD25^+$), DN3 ($CD44^-$/$CD25^+$) and DN4 ($CD44^-$/ $CD25^-$). Stage DN2 and DN3 are characterized by the V(D)J rearrangement at the TCR$\gamma$, $\delta$, and $\beta$ loci. Successful rearrangement of the TCR $\beta$-chain results in differentiation of the cells into the DN4 stage, which

undergo further differentiation and proliferation to become double positive thymocytes (Figure 8, left side) (DP= αβTCR$^+$, CD4$^+$/CD8$^+$/CD44$^-$/CD25$^-$) (Singer & Bosselut, 2004). Upon positive selection, a control point for DP thymocytes, only those receive further survival signals that express a functional TCR which has low/intermediate avidity/affinity in binding of a self-peptide presented on an MHC I or II molecules by cortical epithelial cells. According to the interaction with either MHC class I or class II molecules, DP cells in turn down-regulate either CD8 or CD4 and thereby differentiating into immature CD8$^+$ or CD4$^+$ single positive cells (Figure 8, Medulla, SP cells are CD4$^+$ or CD8$^+$- CD62L$^{low}$/CD69$^{high}$) (Takahama 2006, Takaba & Takayanagi, 2017). Interestingly, 95 % to 99 % of all DP cells were eliminated during the step of positive selection (Cano & Lopera, 2013). Single positive (SP) thymocytes enter the medulla and interact with auto-antigen presenting cells (mTecs, DCs) to become mature single positive thymocytes (CD4$^+$ or CD8$^+$- CD62L$^{high}$/CD69$^{intermediate}$) (Klein et al., 2014).

The positive selection by cortical epithelial cells in combination with the negative selection by DCs and macrophages give rise to the generation of a T cell repertoire capable to distinguish between self and non-self (foreign, Figure 1.8). Any dysregulation in the development and generation of T cells or the thymus can cause immunodeficiency (lack of T cells) or autoimmunity (auto reactive T cells) (Klein et al., 2014; Takaba & Takayanagi, 2017). Finally, naïve T cells leave the thymus and enter secondary lymphoid tissues e.g. spleen and lymph nodes.

### 1.7.3 S1P signalling and thymic egress

Thymocytes that have successfully undergone positive and negative selection developed into mature single positive T cell (CD4$^+$ or CD8$^+$- CD62L$^{high}$/CD69$^{intermediate}$) which enter the circulation and become part of the adaptive immune system (Saba, 2017).

The process of thymic emigration largely depends on the maintenance of an S1P gradient between the thymic interstitium and the blood (Proia & Hla, 2017). First, high S1P level at the cortical junction the exit site for thymocytes, is generated by neural crest-derived pericytes and to a minor extend also by vascular endothelial cells (Resop et al., 2016; Saba, 2017). On the other hand, activity of intracellular S1P lyase in DCs (and thymocytes) and to minor extend in thymic epithelial cells results in low interstitial S1P concentration (Schwab, 2005; Resop et al., 2016). This chemical gradient is highly essential for chemotaxis of mature thymocytes, i.e. to exit the thymus and enter the periphery (Schwab et al., 2005; Yanagida & Hla, 2017). This condition can also be monitored by appearance of certain cell surface marker. Immaturity is depicted by expression of: S1PR1$^{low}$/CD69$^{high}$/CD61L$^{intermediate}$. After maturation where thymocytes become sensitive to S1P, they start expression of the S1P receptor (S1PR1) (Carlson et al., 2006; Resop et al., 2016). Furthermore, CD69 expression is mutually antagonized by S1PR1 expression, and expression of CD62L also increases, which represents another important factor for homing mature thymocytes to peripheral lymphatic tissues (Resop et al., 2016). To this end, mature thymocytes are recruited along the S1P gradient to the perivascular space from which they had entered the thymus (Yanagida & Hla, 2017). Based on even higher S1P levels in the blood (generated by erythrocytes) (Saba, 2017), thymocytes transmigrate across the vessel wall, enter the blood circulation and become naïve T cells (Saba, 2017). Even though Resop (et al., 2016), Zamora-Pineda (et al., 2016) and colleagues could show, that S1P lyase in DCs is essential to maintain S1P gradient, whereas the exact intrathymic distribution and the contribution of other present cell types need to be elucidated (Zamora-Pineda, et al., 2016; Yanagida & Hla, 2017).

All these findings were further supported by experiments performed with mice deficient in S1PR1 (S1PR1$^{-/-}$) (Resopt et al., 2016; Matloubian et al., 2004) in hematopoietic stem cells. Briefly, those

mice have almost no naïve T cells in the blood and periphery (Resop et al., 2016). Furthermore, they verified that $CD69^{low}$ but not $CD69^{high}$ thymocyte migrate towards the S1P gradient in combination with high expression of $CD62L^{high}$ (L-selectin), necessary for homing cells to peripheral lymphoid tissues (Feng et al., 2002; Shiow et al., 2006; Resop et al., 2016).

Despite these findings it was shown that maintenance of ceramide, i.e. sphingolipid metabolism by ceramide synthases is additionally necessary to regulate the S1P homeostasis/ gradient (Newton et al., 2015). In detail, it was shown that CerS2 is a potent regulator in these homeostasis and that upon its deficiency, the S1P gradient is disrupted (Pewzner-Jung et al., 2010 i ; Rieck et al., 2017). Moreover, $CerS2^{gt/gt}$ mice show elevated S1P levels within the thymic interstitium and significantly increased levels in the plasma (Rieck et al., 2017). Furthermore, this marginal distortion is sufficient that mature single positive CD4 or CD8 thymocytes respond and internalize S1P-bound-S1PR1, which in turn results in the accumulation of thymocytes at the exit site, next to a T cell lymphopenia in the periphery (Rieck et al., 2017).

## 1.8 Manipulation of gene function

### 1.8.1 Conventional gene targeting via homologous recombination

One way to analyse gene function is the manipulation of the gene of interest, caused by ubiquitous deletion or alteration, i.e. upon the insertion and expression of a non-conditional construct.

However, depending on the essentiality of the given gene during embryonic development or adulthood, the non-conditional approach could cause early lethality or lead to the development of pleiotropic effects, which in turn interfere with the analyses of the desired gene and preclude the generation of a new mouse line (Rajewsky & Kühn, 1996). Another possibility to bypass this problem is the application of a conditional approach which allows the analysis of the desired gene in a tissue and/or developmental (time) specific manner (Schultze et al., 1996; Rickert et al., 1995). To facilitate the functionality, the approach requires two different recombinase-driven systems, the Cre/loxp and Flp/frt (Kuhn et al., 1995; Feil et al., 2009; Bouabe & Okkenhaug, 2013). First, the Cre-recombinase (causes recombination) is derived from the bacteriophage P1 (Sternberg & Hamilton, 1981; Hoess et al., 1982) and the Flp (Flippase) from the yeast *Saccharomyces cerevisiae* (McLeod et al., 1986). Both recombinase proteins form dimers in the activated stage, capable to recognize a specific 34 bp long sequence. This in turn consists of an asymmetric 8 bp long core, depicting the orientation that is flanked by 13 bp long inverted repeats (Lewandowski, 2001). Furthermore, the core sequence is termed loxP-site (locus of X over P1) or frt-sites (Flp-recognition target) respectively. Each recombinase specifically recognizes its sites of action (loxP/frt) and mediate different kinds of recombination (Bouabe & Okkenhaug, 2013). If the desired DNA sequence is flanked by two sites pointing in identical direction, Cre causes a deletion. However, it should be considered, that after recombination one of the recognitions sites remain in the genomic locus (Kano et al., 1998; Lam & Rajewsky, 1998; Lewandowski, 2001), but the inserted loxP/frt sites do not interfere with the expression of the gene. On the other hand, sites with opposite directions cause inversion of flanked region. Furthermore, the recombination mechanism of the Flp/frt system is analogous to Cre/loxP and describes an alternative tool, which can be combined with the latter one to enhance the conditional approach. To achieve manipulation of gene function in mice, a gene-targeting-vector construct with desired mutation and loxP/frt-sites has to be generated and inserted via homologous recombination into embryonic stem cells (ESCs), following blastocyst injection. After generation of mice, which harbour the mutated allele flanked by loxP/frt sites, animals can

be crossed with mice expressing the Cre/Flp-recombinase under the control of a specific promoter. This in turn allows not only a tissue/cell type specific expression, but also a temporally manipulation upon application of Cre-ER(T) approach, where the Cre-recombinase is coupled to a modified estrogen-receptor (ER) and thus Cre-mediated recombination only occurs after administration of Tamoxifen (artificial modified estrogen) (Feil, 1996). The Cre/loxP and Flp/frt systems have become a powerful tool to analyse and investigate the cellular and molecular functions of a given gene (Bouabe & Okkenhaug, 2013).

# 2 Aim of the study

The ceramide synthase (CerS1-6) gene family encodes a key enzyme in lipid metabolism of eukaryotes. They are highly conserved and catalyse the formation of ceramides, which can act as bioactive lipids and secondly are precursors for all complex sphingolipids. All ceramide synthases harbour a highly conserved lag1 domain necessary for the catalytic function and all CerS, except CerS1, additionally contain a homeodomain (HOX) whose role is controversially discussed, but under intensive investigations to unravel its functions. Ceramide synthases differ in their expression pattern and substrate specificity towards the fatty acyl-CoAs used for N-acylation.

Most of the studies done so far have been performed with CerS2$^{gt/gt}$ mice that carry a gene trap insertion within the genomic locus of *cers2*. This in turn results in the complete loss of the mCerS2 protein (i.e. lag1 domain and homeodomain) accompanied by complete loss of function (Imgrund et al., 2009; Pewzner-Jung et al., 2010 i/ii), which causes the development of severe phenotypes in the mice, e.g. hepatocellular carcinoma, demyelination/ myelin sheath defects and T cell lymphopenia.

For this reason, two new conditional transgenic mouse lines had to be generated by homologous recombination in order to study the functions of each protein domain independently from each other: the CerS2$^{H212A/H213/A}$ and the CerS2$^{Del79-120}$ mouse line. This involved the construction of the two conditional gene targeting constructs, their transfection into embryonic stem (ES) cells, as well as the screening of positive ES cells clones, i.e. verification of correct homologous recombination. Finally, generation of the conditional CerS2$^{H212A/H213/A}$ and the CerS2$^{Del79-120}$ transgenic mice results after blastocyst injections and subsequent breeding with Cre-recombinase-expressing mice.

The conditional CerS2$^{H212A/H213/A}$ mouse line should offer the possibility to analyse the phenotypes arising from the loss of catalytic activity independently from those caused by the homeobox domain; and the CerS2$^{Del79-120}$ mouse line should shed light on the function of the homeodomain. In order to pursue and further investigate the endogenous expression of the mutated proteins, an IRES-eGFP reporter cassette was additionally integrated after the stop-codon of each manipulated *cers2*-coding sequence. Detailed analysis of hepatic alterations, lipid and energy metabolism as well as the immune status of the mice was to be carried out in this PhD thesis. This included biochemical, histological and immunological approaches as well as the analyses of the transcriptome and feeding behaviour of the mice.

# 3 Material

Materials used for this thesis, except explicitly mentioned, were already described before (Degen 2003; van Uelft 2012; Ginkel 2013).

## 3.1 Buffer, stock solutions and cell culture media

***Chemicals, enzymes and radioactivity***

All standard chemicals for the preparation of commonly used buffers and solutions were of analytical grade and purchased from the following companies: Difco, Fluka, GibcoBRL, Invitrogen, Merck, PAA, Roche, Roth, Serva and Sigma. Enzymes and nucleotides were ordered from Roche, New England Biolabs, MWG-Biotech or Promega. Furthermore, all buffer and stock solutions were prepared with double distilled water ($ddH_2O$) and stored at room temperature (RT) if not mentioned otherwise. The pH was adjusted either with 1N HCl or 1N NaOH. Radioactivity ($P^{32}$) for Southern blot analysis was purchased from Hartman Analytic GmbH under consideration of the calibration date and the half-life of the isotope.

### 3.1.1 Nucleic acid sample preparation buffer and stock solutions

#### 3.1.1.1 Genomic DNA preparation buffer and stock solutions

| | | |
|---|---|---|
| ES-lysis buffer (pH 8.0) | 50 mM | NaCl |
| | 20 mM | Tris-HCl |
| | 100 mM | EDTA |
| | 0.5 % (w/v) | SDS |
| | 2 mM | $CaCl_2$ |
| | | Steril filtrate, aliquots |
| Add the following prior usage: | | |
| | 50 $^{\mu l}/_{ml}$ | Proteinase K |
| | 100 $^{\mu l}/_{ml}$ | RNase200 |
| Laird Buffer | 100 mM | Tris-HCl |
| | 200 mM | NaCl |
| | 5 mM | EDTA |
| | 0.2 % (w/v) | SDS |
| | 200 $^{\mu g}/_{\mu l}$ | Proteinase K |
| TE Buffer (pH 8.0) | 10 mM | Tris-HCl |
| | 1 mM | EDTA |
| | | Autoclave 20 min at 121°C |
| Proteinase K – Stock Solution | 20 $^{mg}/_{ml}$ | Proteinase K |
| | | Store at -20°C |
| RNase 2000 | 0.2 % | RNase A (Roche) |
| | 2000 $^{U}/_{ml}$ | RNase T1 (Roche) |
| | | ad 10 ml $ddH_2O$, aliquots, store at -20°C |
| Sodium acetate (pH 4.8) | 3 M | Sodium acetate |
| | | Autoclave 20 min at 121°C |

#### 3.1.1.2 Plasmid preparation

| | | |
|---|---|---|
| Alkaline Lysis buffer I | 50 mM | Glucose |
| (pH 8.0) | 25 mM | Tris-HCl |
| | 10 mM | EDTA |
| | | Autoclave 20 min at 121°C, store at 4°C |
| Add the following prior usage: | | |
| | 3 $^{\mu l}/_{ml}$ | RNase 2000 |
| Alkaline Lysis buffer II | 0.2 M | NaOH |
| | 1 % (w/v) | SDS |
| Alkaline Lysis buffer II | 5 M | Potassium acetate |
| (pH 5.5) | 3 M | Glacial acetic acid |

#### 3.1.1.3 Agarose gel electrophoresis buffer

| | | |
|---|---|---|
| DNA Sample Buffer (6x) | 0.25 % (w/v) | Bromophenol blue |
| | 0.25 % (w/v) | Orange G |
| | 30 % (v/v) | Glycerol |
| TAE Buffer (pH 8.0) | 2 M | Tris |
| (50x) | 100 mM | EDTA |
| | 35.5 ml | Glacial acetic acid |
| | | Adjust pH with acetic acid |
| TBE Buffer (pH 8.3) | 1 M | Tris |
| (10x) | 0.83 M | Boric acid |
| | 10 mM | EDTA |

#### 3.1.1.4 Southern Blot buffer

| | | |
|---|---|---|
| Depurination Buffer | 0.25 M | HCl |
| Denaturation Buffer | 0.5 M | NaOH |
| | 1.5 M | NaCl |
| SSC (20×) | 3 M | NaCl (pH 7.5) |
| | 0.3 M | Trisodium citrate |

### 3.1.2 Protein preparation buffer; and stock solutions

#### 3.1.2.1 Immunoblot analysis buffer

| | | |
|---|---|---|
| APS (10%) | 10 % | APS (Ammoniumpersulfat) |
| | | Store at 4 °C |
| Blocking Buffer | 5 % (w/v) | Milk powder in TBS-T |
| Complete™- (25x) | 1 tablet | Complete™ (Roche) |
| | 2 ml | distilled water |
| | | Store at -20°C |

| | | |
|---|---|---|
| Urea Sample Buffer (2x) | 40 mM<br>1 mM<br>9 M<br>5 % (v/v)<br>0.01 % (w/v)<br>5 % (v/v) | Tris-HCl (pH 6-8)<br>EDTA<br>Urea<br>SDS<br>Bromphenol blue<br>2-Mercaptoethanol |
| Stacking Gel Buffer (pH 6.8) | 0.5 M<br>0.4 % (v/v) | Tris-HCl<br>SDS<br>Store at 4°C |
| Separation Gel Buffer (pH 8.8) | 1.5 M<br>0.4 % (v/v) | Tris-HCl<br>SDS<br>Store at 4°C |
| SDS Running Buffer (10x) (pH 8.8) | 0.25 M<br>1.92 M<br>1 % (v/v) | Tris-Base<br>Glycine<br>SDS<br>Autoclave 20 min at 121°C |
| Transfer Buffer (pH 8.3) | 20 mM<br>150 mM<br>20 % (v/v) | Tris Base<br>Glycine<br>Methanol |
| PonceauS staining solution | 0.2 % (w/v)<br>1 % (v/v) | Ponceau S<br>Acetic acid |
| TBS (pH 7.5) (10x) | 100 mM<br>1.5 M | Tris- HCl<br>NaCl |
| TBS-T (1x) | Dilution of 1:10<br>0.1 % | in $ddH_2O$<br>Tween20 |

#### 3.1.2.2 Immunofluorescence microscopy solutions (IF)

| | | |
|---|---|---|
| Blocking Solution | 5 % NGS | PBS or Oldenburg buffer |
| Dako | | Fluorescence mounting medium, Dako |
| Oldenburg buffer (pH 7.6) | 50 mM<br>256 mM<br>3 % (w/v) | Tris-base<br>NaCl<br>Triton X-100 |

### 3.1.3 Bacterial cell culture; buffer and stock solutions

#### 3.1.3.1 Antibiotics for used for cultivation

| | | |
|---|---|---|
| Ampicillin Stock | 50 $^{mg}/_{ml}$ | Ampicillin in $ddH_2O$<br>Sterile filtrate and store at -20°C<br>Final concentration 100 $^{\mu g}/_{ml}$ |
| Chloramphenicol Stock | 20 $^{mg}/_{ml}$ | Chloramphenicol in ethanol abs<br>Sterile filtrate and store at -20°C<br>Final concentration 20 $^{\mu g}/_{ml}$ |

| | | |
|---|---|---|
| Kanamycin A Stock | 25 $^{mg}/_{ml}$ | Kanamycin A in $ddH_2O$<br>Sterile filtrate and store at -20°C<br>Final concentration 25 $^{\mu g}/_{ml}$ |
| Tetracycline Stock | 10 $^{mg}/_{ml}$ | Tetracycline in $ddH_2O$<br>Sterile filtrate and store at -20°C<br>Final concentration 10 $^{\mu g}/_{ml}$ |

#### 3.1.3.2 Solution for generation of chemically or electro- competent cells

| | | |
|---|---|---|
| $LB_0$ Agar (1 l) | 10 g<br>5 g<br>10 g<br>15 g | Bacto-Trypton<br>Yeast- Extract<br>NaCl<br>Agar<br>Autoclave 20 min at 121°C |
| $LB_0$ Medium (1 l) | 10 g<br>5 g<br>10 g | Bacto-Trypton<br>Yeats-Extract<br>NaCl<br>Autoclave 20 min at 121°C |
| $CaCl_2$ Stock | 100 mM | $CaCl_2$ |

### 3.1.4 Embryonic stem cell culture; medium, buffer and stock solutions

| | | |
|---|---|---|
| ES- EDTA (pH7-8) | 5 mM | EDTA in ES-$PBS^-$ (Invitrogen)<br>Substitution of 200 µl 10 N NaOH<br>Autoclave 20 min at 121°C |
| ES- Gelatine Stock | 1 % | Pork Skin, Type A Gelatine<br>Autoclave 20 min at 121°C and store at 4°C |
| 2i ES medium | 500 ml<br>5 %<br>1mM<br>1 x<br>1 x<br>1 x<br>0.007 % (v/v)<br>0.1 %<br>1 µM<br>3 µM | GlasgowMEM<br>FCS<br>Sodium pyruvate (100 mM, Gibco)<br>non-essential amino acids (100 x, Invitrogen)<br>Penicillin/Streptomycin (100 x, Gibco)<br>L-Glutamine<br>2- Mercaptoethanol<br>LIF (1000 $^{U}/_{ml}$)<br>MEK1-2 inhibitor (Millipore)<br>GSK3 inhibitor (Miltenyi Biotec) |
| ES freezing medium (2x) | 17.5 ml<br>2.5 ml<br>5 ml | 2i ES medium<br>FCS<br>DMSO |
| 2i ES selection medium | 350 $^{\mu g}/_{ml}$ | G418 Stock solution in 2i ES medium |
| G418 Stock | 50 $^{mg}/_{ml}$<br>100 mM | G418 Sulphate<br>PIPES<br>Sterile filtrate and store at -20°C |

| | | |
|---|---|---|
| 2-Mercaptoethanol Stock | 0.7 % | 2-Mercaptoethanol in ES- $H_2O$<br>Store at -20°C |
| ES- Trypsin | 400 ml<br>1 mM<br>1 %<br>0.025 % | $PBS^-$<br>ES-EDTA- solution (1.85 $^g/_l$ , pH8.0)<br>Chicken serum<br>Trypsin |
| HBS Buffer | in<br>0.02 M<br>2.5 M | $PBS^-$<br>Hepes<br>Glucose<br>Store at -20°C |
| KCl Solution | 0.56 % | KCl |

### 3.1.5 Cell culture; medium, buffer and stock solutions

| | | |
|---|---|---|
| MEF medium | 500 ml<br>1 %<br>1 %<br>1 %<br>10 %<br>1 %<br>1 % | GlasgowMEM<br>L-glutamine (1 %)<br>Non- essential amino acids<br>Sodium pyruvate<br>FBS<br>2-Mercaptoethanol<br>Penicillin/Streptomycin, store at 4 °C |
| HEK medium | 500 ml<br>10 %<br>1 %<br>1 % | DMEM<br>FBS<br>Non- essential amino acids<br>Penicillin/Streptomycin, store at 4 °C |
| 2 x MEF freezing medium | | MEF medium supplemented with 20 % DMSO and 10 % FCS. |
| 2 x HEK freezing medium | | HEK medium supplemented with 20 % DMSO and 30 % FCS. |
| Poly L-lysine stock | 1 $^{mg}/_{ml}$ | Poly L-lysine in $ddH_2O$ |
| Poly L-lysine working solution | 50 $^{mg}/_{ml}$ | Poly L-lysine |

### 3.1.6 FACS experiments; buffer and stock solutions

| | |
|---|---|
| Lymphoprep™ | Density gradient medium (Stem cell technologies) |

| | | |
|---|---|---|
| Red blood cell (RBC) lysis buffer<br>(pH 7.6) | 142 mM<br>100 µM<br>1 mM | $NH_4Cl$<br>EDTA<br>$NaHCO_3$ |

## 3.1.7 Lipid Biochemistry

### 3.1.7.1 Ceramide synthase activity assay

| | | |
|---|---|---|
| BSA (fatty acid free) | | Sigma-Aldrich |
| Dihydrosphingosine, D-erythro, [4,5-$^3$H] | | Biotrend Chemicals GmbH |
| Sphinganine | | Sigma-Aldrich |
| NBD-sphinganine | | Avanti Polar Lipids |
| (omega(7-nitro-2-1,3-benzoxadiazole- 4-yl)(2S,3R)-2 aminooctadecane-1,3-diol) | | |
| AcylCoAs | | Avanti Polar Lipids |
| HEPES- KOH (pH 7.4) | 0.5 M | HEPES<br>Adjusted the pH 7.4 with KOH (2 M) |
| Homogenization Buffer | 20 mM | HEPES/KOH$_7$ |
| | 25 mM | KCl |
| | 0.25 M | Sucrose |
| | 2 mM | $MgCl_2$ |
| | | Store at -20°C |
| | Add fresh | |
| | 1 mM | PMSF |
| | 1 $^{µl}/_{ml}$ | Aprotinin (200 $^{U}/_{ml}$) |
| | 1 $^{µl}/_{ml}$ | Leupeptin (1 $^{mg}/_{100µl}$) |
| Reaction Buffer | 20 mM | HEPES/KOH |
| | 25 mM | KCl |
| | 0.25 M | Sucrose |
| | 2 mM | $MgCl_2$ |
| | 0.34 $^{mg}/_{ml}$ | BSA (fatty acid free), store at -20 °C |

## 3.1.8 Histological staining solutions

### 3.1.8.1 Hematoxylin and eosin staining (H&E)

| | | |
|---|---|---|
| Eosin staining solution | 0.1 % (w/v) | EosinY<br>Filtered solution can be used several times |
| Hematoxylin | 0.1 % | Mayer's Hemalum solution |

### 3.1.8.2 Oil Red O

| | | |
|---|---|---|
| OilRedO® stock solution A | 0.5 g | OilRedO® |
| | 100 ml | 99 % isopropanol |
| OilRedO® stock solution B | 60 ml | OilRedO® stock solution A |
| | 40 ml | dd$H_2O$ |
| | | Incubate for 24 h and filtrate, storage at RT |

## 3.2 Antibodies

### 3.2.1 Primary antibodies

| Antigen | Host | Dilution | Company |
|---|---|---|---|
| **CerS2** | Rabbit | 1:750 (IB) | Kremser et al., 2013 |
| **CerS4** | Rabbit | 1:300 (IB) | Ebel et al., 2014 |
| **CerS5** | Sheep | 1:2000 (IB) | Gosejacob et al., 2016 |
| **CerS6** | Mouse | 1:500 (IB) | Santa Cruz Biotechnology |
| **GAPDH** | Mouse | 1:10.000 (IB) | Millipore |
| **GAPDH** | Rabbit | 1:10.000 (IB) | Millipore |
| **GFP** | Chicken | 1:500 | Abcam |
| **V5** | Mouse | 1:1000 (IB) | Invitrogen |

### 3.2.2 Secondary antibodies

| | Antigen | Host | Dilution | Company |
|---|---|---|---|---|
| **Alexa Fluor 488** | Rabbit | Goat | 1:1000 (IF) | Invitrogen |
| **Alexa Fluor 562** | Mouse | Goat | 1:1000 (IF) | Invitrogen |
| **HRP conjugate** | Mouse | Goat | 1:10.000 (IB) | Dianova |
| **HRP conjugate** | Rabbit | Goat | 1:10.000 (IB) | Dianova |
| **HRP conjugate** | Sheep | Goat | 1:10.000 (IB) | Dianova |

### 3.2.3 FACS antibodies

| Target | Clone | Conjugate | Host | Use | Company |
|---|---|---|---|---|---|
| **CD3** | | Fluorochrome | | FC | Biolegend |
| **CD4** | GK1.5 / RM4 | Fluorochrome | Rat | FC | Biolegend |
| **CD8a** | 53-6.7 | Fluorochrome | Rat | FC | Biolegend |
| **CD19** | | Fluorochrome | | FC | Biolegend |
| **CD25** | 7D4 / PC61 | Fluorochrome | Rat | FC | Biolegend |
| **CD45** | 30- F11 | Fluorochrome | Rat | FC | Biolegend |
| **CD45.1** | A20 | Fluorochrome | Mouse | FC | Biolegend |
| **CD62L** | MEL14 | Fluorochrome | Rat | FC | Biolegend |
| **CD69** | H1.2F3 | Fluorochrome | Armenien hamster | FC | Biolegend |

## 3.3 Primer molecules

All oligonucleotides were ordered from MWG Eurofins, HDSL and diluted to 100 pmol/µl.

| Primer | Sequence (5‘ → 3‘) | Application |
|---|---|---|
| **5’SB BAC for** | ATGTGCCTAACGGGAAACAG | Amplification of 5‘SB probe (477 bp) |
| **5’SB BAC rev** | ATGTGGCCAGAAACAAGACC | |
| **3’SB BAC for** | GTTTAACTACGCGGGATGGA | Amplification of 3’SB probe (415 bp) |
| **3’SB BAC rev** | GAGTTGCAGCATGACAAGGA | |
| **Ctrl 2 for (3’HR for)** | GTACAAGTAAAGCGGCCTCG | Genotyping of 3’ HR region (bp) in ES cells/ mice |
| **Ctrl 3 rev (3’HR rev)** | CATCATAGAACTGGCGTGTG | |
| **HA_loxP_2_for** | TAGGGCTTCGTGTTGGTCTT | Genotyping of CerS2-ES cells and mice |
| **HA_loxP_1_rev** | CCGCTGGTCTGGTAGAAATG | |
| **5’ctrl for (5’HR for)** | GGGATCTGTGCAGGGTTTTC | Genotyping of 5’ HR region (bp) in ES cells/ mice |
| **5’ctrl rev (5’HR rev)** | CGATGGAGAAATTGGCAAGC | |
| **USP_Flp** | TAAGGTCCTGGTTCGTCAGTTTGTGG | Verification of presence of Flp recombinase in mice |
| **DSP_Flp** | GTGATATTATCCCATTCCATGCGGGG | |
| **Pgk1_for** | GCTGTTCTCCTCTTCCTCATCTCC | Verification of presence of PGK-Cre recombinase in mice |
| **Int-Cre_rev** | TCCATGAGTGAACGAACCTGGTCG | |
| **del79-120_for** | GAGGCTGAGGACTCAGCATC | Verifcation of deletion in CerS2Del mice |
| **del79-120_rev** | CCCACTTCCCAGTACTCACA | |
| **PvuII_alt_for** | GCTCTTCAGCATTGCCTCTG | Verification of point mutation in CerS2H/A mice |
| **PvuII_alt_rev** | CTGTGAGGAAGCCTAACCTC | |
| **HA_Cre_rev** | CGCGTGAATTTCGACGGTAT | |
| **Nnt- WT for** | GGGCATAGGAAGCAAATACCAAGTTG | Verification of NNT mutation in mice |
| **Nnt- Mut for** | GTGGAATTCCGCTGAGAGAACTCTT | |
| **Nnt-com rev** | GTAGGGCCAACTGTTTCTGCATGA | |
| **frt_SalI/AsiSi_for** | ACGCGTCGACGCGATCGCCAACCGCGCCACTCAGAG | Amplification of 5’HR-SOE fragment (379bp) |
| **frt_AatII_rev** | TGCTGACACCGACGTCACCCGCGCACAGACTTACT | |
| **frt_AatII_for** | GTGCGCGGGTGACGTCGGTGTCAGCATCACCTAAGG | Amplification of 3’HR-SOE fragment (570bp) |
| **frt_SalI_rev** | GCGTGTCGACCAATGGTGCGCTGGGGGA | |
| **E3-11wt MfeI for** | TTACAATTGTCTTCCTGAGGCTGAGGACT | Amplification of genomic region of exon3 to exon11 |
| **E3-11wt MfeI rev** | AATCAATTGAACCACAAGGGAGGCCTAAG | |
| **E3-11 PspOMI_ for** | TTAGGGCCCTCTTCCTGAGGCTGAGGACT | Amplification of genomic region of exon3 including tga |
| **E3-11 BstEII/PspOMI rev** | TAAGGGCCCGGTAACCCTAGGACAATGGTTCAGTCATTC | |
| **E3-11 H/A for** | GAACAGATCATCGCAGCTGTGGCCACTATC | Introduction of H/A mutagenesis |
| **E3-11 H/A rev** | GATAGTGGCCACAGCTGCGATGATCTGTTG | |
| **3’ HR_XhoI_for** | CCGCTCGAGCTGCCTCCCACATCAATGCA | Amplification of 3’HR region, insertion of XhoI/ApaI resctrion site |
| **3’HR_ApaI_rev** | TTGGGCCCATGCCAAACTTGAAGGCAA | |
| **IRES_SapI/AsiSI for** | CAAGCGGAAGAGCGCCCAAGCGATCGCCAACCGCGCC ACTCAGAG | Amplification of 3’frt-SOE fragment (571bp |
| **IRES_NdeI rev** | AGCCTGCGACCATATGACCCGCGCACAGACTTACT | |

| Primer | Sequence (5‘ → 3‘) | Application |
|---|---|---|
| **IRES_NdeI for** | TGTGCGCGGGTcatatgGTCGCAGGCTTTCACCCAT | Amplification of 5'frt-SOE fragment (388bp) |
| **IRES_BstEII/ClaI rev** | taatcgataggtaaccCTAGGACAATGGTTCAGTCATTC | |

## 3.4 Plasmids

| Plasmid | Description | Company |
|---|---|---|
| **loxP frt dualneo frt loxP** | Contains neomycin cDNA controlled by a dual (pro- and eukaryotic) promoter, flanked by frt and loxP sites | H. Wende (MDC Berlin) |
| **pBSK_IRES_eGFP** | eGFP expression vector with internal ribosomal entry site | Tress, 2006 |
| **pDTA** | pDTA containing mammalian expression vector | H. Wende (MDC Berlin) |
| **pCDNA3.1 TOPO Blunt** | Cloning and expression vector, suitable for mammalian cell culture systems | Invitrogen |
| **pCDNA3.1 V5-His-TOPO** | Cloning and expression vector; suitable for the mammalian cell culture systems. Expression lead to generation of C-terminally V5/6xHis tagged proteins. | Invitrogen |

## 3.5 Hybridization probes

| Probe | Description | Application |
|---|---|---|
| **Internal CerS2 probe** | 400 bp fragment that binds within the coding region of CerS2 (exon 8-10) | CerS2 Southern Blot |
| **eGFP probe** | Digestion fragment of GFP from the IRES-eGFP vector | CerS2 Southern Blot |

## 3.6 Bacterial artificial chromosomes

| BAC | Description | Source |
|---|---|---|
| **BMQ 325-K4** | Comprise the genomic sequence of CerS2 | Sanger Institut |

## 3.7 Eukaryotic cell lines

| Cell line | Description | Reference |
|---|---|---|
| **HM1** | Murine embryonic stem cells isolated from agouti-coloured-male blastocysts (SV129P2/OlaHsd line) | Magin et al., 1992 |
| **HEK-293T** | human embryonic kidney cells | Own stock |
| **Macrophages** | Murine macrophages derived by differentiation of primary bone marrow cells | Primary cell culture |
| **CerS2 H212/213A** | HM1 founder line for blastocyst injection, heterozygous for mutated CerS2 allele, based on homologous recombination with CerS2H/A-exchange vector | Bickert et al., 2018, Present study |
| **CerS2 del 79-120** | HM1 founder line for blastocyst injection, heterozygous for mutated CerS2 allele, based on homologous recombination with CerS2 del-exchange vector | Bickert et al., 2018, Present study |

## 3.8 Bacterial strains

| Strain | Description | Reference |
|---|---|---|
| **E. coli XL1-blue** | *rec*A1, *end*A1, *gyr*A96, *thi-1*, *Δ(mcr)*A183, *Δ (mcr*CB-*hsd* SMR-*mrr)*173, *sup*E44, *rel*A1, *lac*[F'*pro*AB *lacIq*Z *Δ* M15 Tn10, *(Tetr 12.5 µg/ml)]* | Bullock et al., 1987 |
| **DH10B** | F'*mcrA (mrr-hsd*RMS-*mcr*BC*) 80lac*Z M15 *lac*X74 *rec*A1 *deo*R *ara*D139 *(ara-leu)*7697 *gal*U *gal*K *rps*L (StrR) *end*A1 *nup*G | Invitrogen<br>Liu et al., 2003 |
| **Top10** | F- *mcrA* Δ( *mrr-hsd*RMS-*mcr*BC) Φ80*lac*ZΔM15 Δ *lac*X74 *rec*A1 *ara*D139 Δ(*araleu*)7697 *gal*U *gal*K *rps*L (StrR) *end*A1 *nup*G | Invitrogen |
| **DH5α** | F-*φ80lac*ZΔM15 *Δ(lac*ZYA-*arg*F)U169 *rec*A1 *end* A1 *hsd*R17*(rk-, mk+) pho*A *sup*E44 *thi-1 gyr*A96 *rel*A1 *ton*A (confers resistance to phage T1) | Invitrogen |
| **DY380$^{\alpha}$** | *mcrA Δ( mrr-hsd*RMS-*mcr*BC) Φ80*lac*ZΔM15 Δ *lac*X74 *deoR recA1 endA1 araD139 Δ(ara, leu)7697 galU gal490 pglΔ8 rpsLnupG λ(cI857ind1) Δ{(cro-bioA)<>tetRA}(Tet$^{R}$)* like DH10B, λ Red$^{+}$ | Liu et al., 2003 |

## 3.9 Transgenic mouse lines

| Mouse line | Description | Reference |
|---|---|---|
| **CerS2floxH212/213A** | The CerS2 coding region is flanked by loxP sites, after Cre-mediated recombination the CerS2H212/213A mutation is expressed under control of endogenous promoter. | Bickert et al., 2018, Present study |
| **CerS2 H/A** | Derived from an ES cell clone in which the genomic locus of CERS 2 was mutated by the insertion of the CerS2 H212/213A vector. Expresses the CerS2 H212/213A mutation and eGFP reporter; leads to the exchange of two histidine residues to alanine residues at position 212 and 213 of the CerS2 peptide sequence. | Bickert et al., 2018, Present study |
| **CerS2floxDel79-120** | The CerS2 coding region is flanked by loxP sites. After Cre-mediated recombination the mutated CerS2 del79-120 protein is expressed, which lacks 42 amino acid residues (aa79-120) within the peptide sequence. | Bickert et al., 2018, Present study |
| **CerS2 Del** | Derived from an ES cell clone in which the genomic locus of CERS 2 was mutated by the insertion of the CerS2 del79-120 vector. Expressed a homeodomain-truncated CerS2 protein (Δaa79-120) and eGFP repoter; controlled by endogenous *cers2* promoter. | Bickert et al., 2018, Present study |
| **Deleter-FLPe** | Ubiquitous expression of Flp-recombinase; controlled by human β-actin promoter. | Rodriguez et al.,2000 |
| **PGK-Cre** | Ubiquitous expression of Cre-recombinase; controlled by the PGK-promoter. | Lallemand et al.,1998 |

## 3.10 DNA ladder and Protein marker

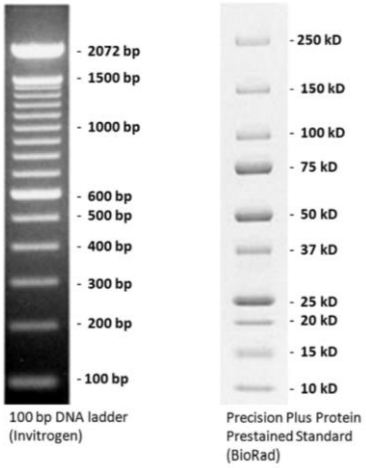


## 3.11 Lipid Standards for TLC Analyses

Lipid standards were ordered from Avanti polar lipids.

| Lipid standard | Application |
|---|---|
| **NBD-Sphinganine (D18:1)** | TLC |
| **Cholesterol (Chol)** | TLC |
| **Cholesterol ester (CE)** | TLC |
| **Diacylglycerol (DAG)** | TLC |
| **Triacylglycerl (TAG)** | TLC |
| **Free fatty acid (FFA) (C16:O)** | TLC |

# 4 Methods

Unless explicitly mentioned otherwise, all standard laboratory methods used in this thesis were carried out and prepared as previously described (van Uelft, 2012; Ginkel, 2013; Bickert, 2016).

## 4.1 Nucleic acid biochemistry

### 4.1.1 Analytical plasmid preparation (Mini prep, quick & dirty)

The analytical plasmid preparation method provides a fast and rapid technique for the purification and analysis of plasmid DNA from bacteria.

2 ml LB-selection medium was inoculated with a single colony of transformed bacteria and cultured overnight (ON) (180 rpm, 37°C). 1.5 ml of the bacteria culture was harvested in a centrifugation step (1 min, 13,000 rpm). The supernatant was discarded and the bacteria pellet re-suspended in 100 µl alkaline lysis buffer I. Then, 200 µl of alkaline lysis buffer II was added, the mixture was inverted several times (lysis of membrane) and incubated for 2 min at RT. Next, 150 µl of alkaline lysis buffer III was added, to precipitate proteins, cell debris and other cellular components. The mixture was inverted for several times, followed by a centrifugation step (10 min, 13.000 rpm, RT). The supernatant was subsequently transferred into a fresh tube containing 0.5 ml isopropyl alcohol (or 70 % ethanol). Samples were vigorously mixed and the plasmid-DNA precipitated in a centrifugation step (10 min, 13.000 rpm). The supernatant was removed, the pellet air-dried and resuspended in 100 µl dd$H_2O$.

### 4.1.2 Preparative plasmid isolation (Midi prep)

The preparation of plasmid-DNA in pure and high amounts was performed according to the standard protocol of either the Jetstar Plasmid Purification Midi Kit (Genomed) or the PureLink™ HiPure Plasmid Midiprep Kit (Invitrogen). 50 ml of LB-selection medium was inoculated and cultured overnight (180 rpm, 37°C). The plasmid was resuspended in 100 µl to 150 µl TE buffer and stored at -20°C.

### 4.1.3 Endotoxin-free preparation (Maxi prep)

Isolation of high, pure and endotoxin-free DNA amounts, suitable for the transfection of embryonic stem (ES) cells, was performed using the EndoFree MaxiKit (Qiagen). The purified plasmid DNA was resuspended in 200 µl sterile endotoxin-free TE buffer and stored at -20°C.

### 4.1.4 Isolation of genomic DNA

#### 4.1.4.1 Isolation of genomic DNA from embryonic stem cells

The verification of homologous recombination in embryonic stem (ES) cells after electroporation was done by PCR reaction (see chapter 4.5). To isolate genomic DNA, the half amount of a 48-well plate, confluent covered with HM1 cells, was transferred into a fresh PCR tube after trypsinization. Cells were centrifuged (5 min, 13.000 rpm) and the supernatant was discarded. Next, the cell pellet was resuspended in 40 µl PCR-lysis buffer (1x) supplemented with 0.4 µl Proteinase K and incubated at 55°C for 2 h. The cell lysate was gently mixed before setting up the PCR reaction. For Southern blot analysis, the genomic DNA extracted from a confluent T25 cell culture flask was used. The medium was removed and the cells washed twice with $PBS^-$. Immediately, 1.5 ml ES-lysis buffer was added and the cells were incubated for 1 h on a seesaw (RT). The solid, jelly-like suspension was then transferred to a fresh 15 ml Falcon tube and incubated at 55°C ON. The genomic DNA isolation was performed by

phenol/chloroform extraction. After adding 2 ml Roti® -Phenol/Chloroform the suspension was thoroughly mixed and centrifuged (15 min, 6.000 rpm, RT) resulting in two phases. The lower organic phase was left intact and the upper aqueous phase was transferred to a fresh tube containing 3 ml ice-cold isopropyl alcohol. The suspension was inverted several times until the DNA precipitates. The visible genomic DNA clot was picked with a sterile tip, transferred to a fresh tube containing 500 µl 70 % ethanol and precipitated by centrifuged (5 min, 6.000 rpm). Next, the DNA pellet was washed again with 70 % ethanol and then air-dried. Finally, the genomic DNA was resuspended in 200 µl TE buffer and incubated at 55°C for at least ON.

#### 4.1.4.2 Isolation of genomic DNA from tail tips and ear clip biopsies

The genotype of transgenic mice used in the experiments was determined by PCR on genomic DNA level (chapter 3.2). To isolate genomic DNA, 400 µl Laird buffer supplemented with 4 µl Proteinase K was added to the tail tips or ear clip biopsies. The tissue lysis was performed at 55°C ON. After a centrifugation step (13.000 rpm, 10 min, RT), the supernatant was transferred to a fresh reaction tube containing 0.5 ml isopropyl alcohol. The suspension was vigorously mixed and the DNA precipitated by centrifugation (13.000 rpm, 10 min, 4°C). Furthermore, the supernatant was removed and the DNA pellet washed with 0.5 ml of 70 % ethanol (13.000 rpm, 5 min). Next, the supernatant was discarded, the DNA pellet air-dried and resuspended in 100 µl dd$H_2O$. Finally, 1 to 2 µl of this DNA solution were used for further PCR analyses.

### 4.1.5 Photometric estimation of DNA/RNA concentration

Quantification of nucleic acid (DNA or RNA) concentration was performed with the NanoDrop2000 from Peqlab. Based on the absorption maximum of DNA or RNA at 260 nm the device not only displays the amount of nucleic acid in comparison to a blank control, it also determines the purity of the sample by the ratio of 260 nm/ 280 nm.

### 4.1.6 Sequence validation

Validation of correct base pair composition of plasmids, vector fragments and PCR products was performed in a sequencing reaction (GATC Biotech).

## 4.2 Molecular cloning

### 4.2.1 Restriction digestion, dephosphorylation and ligation

***Restriction digestion*** **-** The digestion of template DNA (vector, PCR product) was performed with type II restriction endonucleases. The cleavage occurs at or near specific recognition sites, which results in the generation of blunt or sticky ends (cohesive ends) at the cutting sites. A standard protocol has a reaction volume of 20 µl containing 1-2 µg DNA, 2 U of the restriction endonuclease and was incubated at the corresponding temperature (most often 37°C) for 1 to 2 h. Depending on the enzymes that were used, single or double digestions reactions were also performed.

***Dephosphorylation*** **-** Next, dephosphorylation of the vector backbone with alkaline phosphatase (Roche) was performed to prevent self-ligation events. Usually, 1 µg vector backbone was incubated with 1 µl alkaline phosphatase and 1 µl RAPiD buffer (10 x) in a final volume of 10 µl, for 10 min at 37°C. For inactivation of the enzyme, the reaction mixture was incubated at 72°C for 2 min.

***Ligation -*** Ligation of DNA fragments (vector and insert) for the generation of new recombinant DNA sequences was performed with the T4-DNA-ligase (NEB). Usually, the ratio between vector and insert was 1:7 that was incubated with 1 µl T4-DNA-ligase, 2 µl T4-DNA-ligase buffer in a final volume of 20 µl. The ligation was incubated at 18°C ON.

### 4.2.2 Generation of competent cells, transformation and "Recombineering"

The transformation describes a method that allows the uptake of extra-chromosomal DNA by prokaryotes. The membranes of those cells have been chemically modified to achieve the artificial competence. Usually there are two main methods for the generation of competent cells. First, it can be achieved through the application of calcium chloride and second through electroporation.

***Recombineering -*** Recombineering displays a method that allows the partial exchange/ homologous recombination of/between bacterial DNA (plasmid, BAC) and an introduced linear dsDNA containing two short homology arms (Liu et al. 2003, Zhang et al., 1998). Based on this technique, the RecET system (plasmid) from the Rac pro-phage (GeneBridges) is needed which promotes the homologous recombination in electro competent cells.

#### 4.2.2.1 Generation of $CaCl_2$ competent cells

The generation of chemically competent cells starts with the inoculation of 3 ml $LB_0$ medium with a single colony of the desired *E.coli* strain at 37°C, ON (225 rpm). Next, 0.5 ml of the pre-culture was used to inoculate another 50 ml $LB_0$ medium. The culture was incubated again at 37°C in a shaker-incubator at 225 rpm and the $OD_{600}$ determined every 30 to 60 minutes. When the culture reaches a value of 0.4 to 0.6 the culture flask was cooled on ice and the bacteria were harvested (10 min, 3.000 rpm, 4°C). The supernatant was carefully discarded, the cell pellet resuspended in 20 ml cold 0.1 M $CaCl_2$ and left on ice for at least 20 min. After another centrifugation step (10 min, 3.000 rpm, 4°C), the supernatant was discarded and the cell pellet carefully resuspended in 3 ml 0.1 M $CaCl_2$ The bacteria suspension was incubated on ice for at least one hour and then supplemented with glycerol (20 % end concentration). Finally, aliquots of 50 µl volume were prepared and snap frozen in liquid nitrogen for long-term storage (-80°C).

***Transformation -*** The transformation represents the uptake of newly generated plasmids into bacteria. Chemically-competent *E.coli* (50 µl) were thawed on ice and gently mixed with the ligation reaction. The mixture was incubated on ice for another 20 min before the heat shock was applied (1 min, 42°C). Afterwards, 250 µl $LB_0$ medium was added and the cells incubated in a shacking heat block at 37°C for 1 h. Finally, bacteria were grown on LB agar plates supplemented with appropriate antibiotic at 37°C ON. The selection of positive clones was performed with an analytical plasmid preparation (see chapter 3.1.1) followed by enzymatic digestion of 3 µl vector DNA and analysis of resulting fragments in an agarose gel.

#### 4.2.2.2 Generation of electro-competent cells (BAC)

The generation of electro-competent cells starts with the inoculation of 3 ml $LB_{Chl}$ medium with a single colony of the desired *E.coli* strain at 37°C, ON (225 rpm). Next, 2 ml of the pre-culture were used to inoculate another 100 ml $LB_{Chl}$ medium. The culture was further incubated at 37°C in a shaker-incubator at 225 rpm. Finally, with an $OD_{600}$ value of 0.7 the culture was cooled on ice and the cells were harvested (2 x 50 ml, 10 min, 2.900 xg, 4°C). The supernatant was carefully discarded and the cell pellet resuspended in 40 ml glycerol solution (10 %). The cells were again centrifuged (10 min, 4.000 xg, 4°C), the supernatant removed and the cells

resuspended in 40 ml glycerol solution (10 %). This step was repeated and the cell suspension centrifuged at 5.800 xg, 10 min at 4°C. Cells were resuspended in 40 ml glycerol solution (10 %). Next, the cells were harvested for 10 min at 7.300 xg, 4°C. The supernatants were very carefully removed and the two cell pellets recombined and resuspended in 40 ml glycerol (10 %). After a final centrifugation step (10 min, 9.000 xg, 4°C) the supernatant was fully removed and the cells resuspended in 400 µl glycerol (50 %). Aliquots containing 26 µl of BACs were prepared and snap frozen in liquid-nitrogen for long term storage (-80°C).

#### 4.2.2.3 Electroporation

The generation of CerS2-BAC- containing *E.coli* with the pRedET plasmid was carried out according to the manufacturer's instructions (Gene Bridges). Briefly, one aliquot of cells (BAC) were thawed on ice and 1 µl pRedET plasmid added. Next, the suspension was transferred to a pre-cooled electroporation cuvette and the electroporation was performed (1350 V, 10 µF, 5 ms). Finally, the cells were resuspended in 1 ml $LB_0$ medium and incubated for 1 h at 30°C. Cells were grown on LB agar plates supplemented with Tetracycline (30 µg/ml) /Chloramphenicol (15 µg/ml) at 30°C overnight.

#### 4.2.2.4 Recombineering procedure

The recombineering procedure was also performed according to the manufacturer's instructions (Gene Bridges). An ON culture of *E.coli* containing the CerS2-BAC and pRedET plasmid was prepared in LB medium supplemented with Tet/Chl (30°C). The next day, a fresh 1.4 ml culture was inoculated with 30 µl ON culture and incubated for 2 h at 30°C. Next, 50 µl 10 % L-arabinose were added and the culture incubated for 45 min at 37°C, which leads to the expression of the inducible pRedET plasmid. Furthermore, cells were prepared for electroporation procedure (3 x 30 s, 11.000 rpm, 4°C). After each centrifugation step, the supernatant was removed and the cell pellet resuspended in 1 ml $ddH_2O$, except for the last step. Here the supernatant was removed; the cells resuspended in the remaining water and transferred to a pre-cooled electroporation cuvette. Additionally, 100 µg or 200 µg of the linearized vector was added and the electroporation performed (1350 V, 5 ms). Afterwards, 1 ml $LB_0$ medium was added and the cells incubated for 50 min at 37°C. Cells were plated on LB agar plates containing Tetracycline (10 µg/ml) and Kanamycin (25 µg/ml) and grown at 30°C ON.

#### 4.2.2.5 Preparation of glycerol stocks

Glycerol stocks were prepared for long-term storage of the desired plasmid DNA. Therefore, 850 µl of an ON culture were mixed with 150 µl of sterile 100 % (v/v) glycerol solution in a safe-lock cap. The glycerol stock was stored at -80°C until usage. Prevent the cap from freezing and thaw cycles. For recovery, the cap was opened under sterile conditions and a sterile pipette tip was used to scrape some of the frozen material from the top of the glycerol stock. The tip in turn was directly used to inoculate 2 ml of LB medium supplemented with antibiotic. The culture was grown ON at 37°C.

## 4.3 Eukaryotic cell culture

### 4.3.1 Cell counting and calculations (Neubauer chamber)

The determination of correct cell number in suspension was performed using a hemocytometer (Neubauer chamber). The device is a microscopic slide with a grid and an appertaining cover slip, which in combination form a space of defined volume. The resulting space can be filled with the cell suspension of interest. Furthermore, the grid (3x3 mm) consists of four large squares (each 1x1 mm) and each large one consists of 16 smaller squares. Usually, four large squares were counted to determine the cell concentration per ml (see formula).

$$\frac{cells}{ml} = \left(\sum_{i=1}^{4} xi\right) \div 4 \times 10^4 \times dilution\ factor$$

**Equation 1:** The cell concentration per ml is the average number of counted cells of four squares multiplied by $10^4$ multiplied by the dilution factor. ($10^4$ describes the total volume of one square, 1 mm x 1 mm x 0.1 mm; 0.1 $mm^3$ = 1 ml).

For cell culture and immunological experiments, the total cell numbers in the analysed compartments were obtained by counting. The numbers of lymphocyte populations in thymus, spleen and blood were obtained by flow cytometric analyses (see Chapter 4.11) and calculated based on their relative frequencies.

### 4.3.2 HEK cell culture

HEK293T cells were maintained in a humidified incubator at 37°C with 5 % $CO_2$. The cells were cultured in DMEM supplemented with 10 % fetal bovine serum (FBS). To maintain the viability of the cell line, medium was replaced daily or every second day and the cells sub-cultured once confluent (90 %). Therefore, the medium was removed, the cells washed with 1 x $PBS^-$ and 1/10 of the culture volume of trypsin/EDTA solution was added. The cell culture dish was gently rotated and incubated for 2-3 min at 37°C. Additionally, it was necessary to tap the plate at the bottom to detach remaining cells. Subsequently, preheated medium was added and the cell suspension drawn in a pipette and rinsed two to four times to dissociate cell aggregates. Finally, the appropriate volume of cell suspension was transferred to a fresh cell culture dish and filled up to final volume with preheated medium.

### 4.3.3 MEF cell culture

Immortalized mouse embryonic fibroblasts (MEFs) derived from $CerS2^{gt/gt}$ mice were already generated (M van Uelft, Master thesis). Cells were maintained in a humidified incubator at 37°C with 5 % $CO_2$. The cells were cultured in Glasgow-MEM supplemented with 10 % FBS and 1 % P/S on untreated cell culture dishes. To maintain their viability, cells were split at a confluence of 80 to 90 % and the medium replaced daily or every second day.

### 4.3.4 Transient transfection with Metafectene (S10 cell culture dish)

The transient transfection of almost confluent S10 cell culture dishes was prepared with the Metafectene Kit according to the manufacturer's instructions (Biontex). Metafectene, a cationic lipid transfection agent covers the DNA and facilitates its internalization. The transfection mixture consists of two different solutions. Solution A contains 15.7 µg DNA diluted in 700 µl 1 x $PBS^-$. Component B contains 63.16 µl Metafectene reagent in 700 µl 1 x $PBS^-$. After an incubation step of 5 min at RT, solution A was gently added to the transfection reagent and incubated for 15 min at RT. During the incubation step, cells were prepared. In detail, the

medium was removed and the cells washed with 1 x $PBS^-$. Next, 11.7 ml DMEM (w/o FBS, w/o Pen/Strep) was put on top of the cells and the transfection solution added drop-wise. The transfection was carried out for 5 h at 37°C. Finally, the medium was replaced by complete DMEM and cells were incubated for 24 h in a humidified incubator at 37°C, 5 % $CO_2$.

### 4.3.5 HM1 embryonic stem cell culture (mouse)

HM1 embryonic stem cells had been isolated from agouti-coloured, male mice blastocysts from the mouse strain Sv129P2/OlaHsd (Magin et al., 1992). They grow on gelatine-coated culture dishes in the presence of soluble LIF, MEK 1 and GSK3 (2i WT medium). To maintain viability of ES cells, 2i-WT medium was replaced daily or every second day.

#### 4.3.5.1 Gelatine coating of cell culture ware

Cell culture ware (plates, flasks) were coated with 0.1% gelatine to allow a better adhesion of HM1 ES cells. The appropriate volume of 0.1% gelatine working solution was used to prepare the cell culture ware. Gelatine solution was incubated for at least 15 min at 37 °C. Afterwards, the gelatine solution was removed and the cell culture ware ready for the cultivation of HM1 ES cells.

#### 4.3.5.2 Passaging of HM1 ES cells

After complete removal of the medium, the cells were washed with an appropriate amount of 1 x $PBS^-$. Next, pre-warmed trypsin/EDTA solution was added (1/7 vol.), the culture flask gently rocked to ensure entire coverage of the cells and incubated for 5 min at 37°C. The culture flask or dish was then tapped at the bottom to detach remaining cells. The reaction was stopped after addition of 2 volumes of 2i-ES medium. The cells were transferred to a fresh falcon tube and centrifuged for 5 min, 800 rpm, RT. Finally, the medium was removed; the cells resuspended in 2i-ES medium by pipetting up and down to obtain single cell suspension. According to the dilution factor, the appropriate volume of cells was transferred to a new gelatine- coated- culture dish containing pre-warmed 2i-ES medium.

#### 4.3.5.3 Cryo conservation

For future experiments (blastocyst injection, karyotyping etc.) and as a general back up, it was necessary to store some aliquots of the cell lines in use. The cryopreserved cells were kept in a combination of the cryoprotective agent DMSO and complete medium.
Initially, the medium was removed, cells were washed in 1 x $PBS^-$ and then trypsinized. The cell suspension was transferred to a fresh falcon tube and centrifuged for 5 min, at 800 rpm, RT. Next, the supernatant was removed and the cells resuspended in the appropriate amount of freezing medium. Finally, 1 ml aliquots of the cell suspension were generated in cryogenic storage vials and placed in a freezing container, which allows a gradual freezing of the cells (1°C/min). Aliquots were incubated for two days at -80°C and then transferred to a liquid nitrogen freezer for long-term storage.

#### 4.3.5.4 Electroporation

The stable transfection of HM1 ES cells was performed by electroporation. The gene targeting vector (200-350 µg) was cleaned up with the Qiagen-Endo free Maxi-prep kit, linearized by restriction digestion and resuspended in endotoxin-free TE buffer (80 µl). Next, the cells of a confluent culture dish (T75) were harvested; following centrifugation resuspended in HBS-buffer and the cell concentration was determined. Finally, 0.8 ml HBS-buffer containing 3 x $10^7$cells and the linearized targeting vector were transferred into a fresh pre-cooled

electroporation cuvette and the electric pulse applied (0.8 kV, 3 µF; time const. 0.1, Biorad GenePulser). Afterwards, the cells were incubated for 10 min at RT and resuspended in 20 ml complete 2i-ES growth medium and seeded in different dilutions.

#### 4.3.5.5 Selection of stable integration and homologous recombination

The antibiotic selection of HM1 cells having the neomycin resistance gene stable integrated was performed 24 h after electroporation by the application of 2i-ES medium supplemented with G-418 (350 µg/ml). The medium was changed every second day and the selection period finished ten days after application of G-418 for the first time. Ideal cell clones were picked under the microscope with a 200 µl pipette and each dissociated in 96-well flat bottom dish, which was coated with gelatine before. Once the dish was confluent (80 %), the culture was split in half. Half of the culture was used for genotyping analysis (3'HR PCR) and the other half was transferred into a fresh dish (48-well flat bottom dish). Positive clones were further expanded to 24-well (5'HR PCR analysis) → 12-well → 6-well flat bottom dish. Each positive clone from a 6-well plate was again split in half. Each half was sub cultured on a T25 cell culture flask. The cells of one confluent T25 flask were cryopreserved (3 x 1ml) and the other half further expanded on three T25 culture flasks for karyotyping analysis, genomic DNA preparation and cryopreserved for blastocyst injections.

#### 4.3.5.6 Karyotyping

Karyotype analysis for each positive ES cell clone was prepared to check for chromosomal anomalies, such as aneuploidy. The application of colcemid results in the arrest of cells in the metaphase of the cell division cycle, where the chromosomes are most condensed.
Therefore, the cells were fed 2 h before with fresh medium which was replaced by 2 ml 2i-ES medium containing 20 µl colcemid (Demecolcine (10 µg/ml), Sigma) and incubated for 1 h at 37°C. Thereafter, the cells were washed twice with pre-warmed 1 x $PBS^-$ and trypsinized and the reaction stopped by medium addition. The cell suspension was centrifuged (5 min, 800 rpm) and the supernatant removed. Initially, 1 ml 0.56 % KCl solution was added dropwise and the pellet resuspended by flicking the tube. Afterwards, 3 ml KCl were additionally added and the suspension incubated for 10 min at RT. Cells were centrifuged (5 min, 800 rpm), the supernatant removed, then incubated with 2 ml methanol : acetic acid solution (3:1) for 5 min at RT. The procedure was repeated after centrifugation (5 min, 800 rpm). Finally, a minimum of three slides per clone were prepared and the cells dropped from at least 10 cm above the surface of the slide. Afterwards, the slides were stained with Giemsa solution and fixed in Entellan Neu (Merck). Counting of chromosomes of about 20 cells under a microscope ensures selection of clones with mostly 40 chromosomes, needed for blastocyst injection.

## 4.4 Generation, handling and analysis of transgenic mice

### 4.4.1 Generation of the CerS2$^{Flox}$, CerS2$^{H212A/H213A}$ & CerS2$^{Del79-120}$ vector

The generation of both exchange vectors was performed with standard cloning techniques using enzymatic modifications. Plasmid DNA was cut with restriction endonucleases (NEB) and the backboned dephosphorylated with alkali phosphatase (RAP, Roche), followed by T4 DNA ligase mediated ligation. Thereafter, transformation into chemically competent bacteria, growth and clone selection was performed as described (see Chapter 4.2).

#### 4.4.1.1 Generation of the conditional CerS2$^{H212A/H213A}$ vector

1st step: (pCR2.1 TOPO:5'SOE)
The first step depicts the generation of the the 5' homology region (HR) entry side. Initially, two DNA fragments (379bp/570bp) flanking the 5'HR were generated in a PCR reaction on the basis of the BAC vector (frt_SalI/AsiSi_for and frt_AatII_rev; frt_AatII_for and frt_Sal_rev). In a following overlap extension PCR reaction, with both PCR fragments as templates and the application of the external forward and reverse primer, generation of the full-length 5'SOE fragment (924bp) was achieved, which was directly cloned into the pCR2.1 TOPO vector (Invitrogen). The external forward and reverse primer introduce an additional SalI restriction side which was needed for further cloning steps. Additionally, the introduction of an AatII restriction side within the DNA fragment was necessary for the insertion of the 5' HR region in a recombineering step. Third, we additionally inserted an AsiSI restriction at the 5' end, downstream of SalI as a backup.

2ndstep: (dual loxP/frt-Neo:5'SOE)
Next, after linearization of the dual loxP/frt-Neo vector with SalI, the 5'SOE fragment was inserted upstream of the neomycin resistance cassette.

3rd step: Truncation of Ampicillin resistance gene
Afterwards, the ampicillin resistance gene was truncated via ScaI/PsiI double digestion. Both enzymes create blunt ends, which were ligated in a T4-DNA-ligase mediated step that results in the circularization of the vector.

4th step: (5'SOE-frt-Neo_ΔAmp:E3-11 genomic sequence)
In the next step, the genomic sequence of exon three to eleven (E3-11 wt) was amplified by PCR (E3-11 wt MfeI for/ E3-11 wt MfeI rev) on the BAC-DNA and directly inserted into the TOPO Blunt vector (Invitrogen). The primer inserted on the 5' and 3' end of the fragment an MfeI restriction site. E3-11wt was subcloned by compatible end ligation (MfeI, EcoRI) between the loxP (locus of X over P1) and frt (flippase recognition target) site upstream of the neomycin cassette.

5th step: (E3-11wt-frt-Neo_ΔAmp:E3-11 H/A)
Next, a second fragment containing the genomic region of exon 3 until the stop codon was amplified via PCR (E3-11 PsPOMI_for/ E3-11 BstEII/PspOMI_rev) and subcloned into the TOPO Blunt vector. The generation of the point mutations, H212A and H213A, create an additional PvuII restriction site and were introduced by mutagenesis PCR (E3-11 H/A for and E3-11 H/A rev, Figure A2). The resulting fragment was inserted between the loxP and frt site downstream of the Neo cassette by PspOMI/NotI compatible end cloning.

6th step: Recombineering of the 5' homology region (5'HR-Neo:CerS2)
After linearization of the frt_Neo_D Amp:CerS2-vector with AatII, it served as a retrieval vector in a recombineering- mediated gap repair step using electrocompetent, CerS2-BAC/ pRedET containing, *E. coli*. The recombination procedure extended the 5' HR to its full length.

7th step: (pDTA:3'HR)
Briefly, the 3' homologous region (3'HR) needed for homologous recombination in ES cells was amplified via PCR (3'HR_XhoI_for/ 3'HR_ApaI_rev) from the BAC. The resulting fragment was subcloned into pDTA (diphtheria toxin A) containing vector upon double restriction digestion with XhoI/ApaI.

8th step: (pBSK-IRES-eGFP:3'HR-pDTA)
Next, the 3'HR-pDTA fragment was subcloned by XhoI/PsiI restriction into the pBSK vector, downstream of the IRES-eGFP cassette (IRES- internal ribosomal entry side, eGFP- enhanced green fluorescent protein).

9th step: (IRES-eGFP/3'HR-pDTA:frt-SOE)
In this step, we generated the entry site for the 5'HR-Neo:CerS2 vector which was generated during the first six steps of the cloning procedure. Initially, two DNA fragments homologous to the 5' and 3' region of the 5'HR-Neo:CerS2 vector were amplified by PCR (IRES_SapI/AsiSI for;IRES_NdeI rev and IRES_NdeI for;IRES_BstEII/ClaI rev). In the next step, both DNA fragments serve as templates for an overlap extension PCR to generate the full-length frt-SOE fragment needed for the final ligation step. The external forward/ reverse primer (IRES_SapI/AsiSI for and IRES_BstEII/ClaI rev) used in the second PCR reaction additionally inserted a SapI/AsiSI restriction site upstream and a BstEII/ClaI restriction site downstream of the fragment. Finally, the frt-SOE fragment was inserted upstream of the IRES-eGFP-3'HR-pDTA cassette by SapI/ClaI restriction. Additionally, the insertion leads to the desired deletion of a NotI restriction site.

10th step: (CerS2$^{H212/213A}$ vector)
The final step was initially designed as a recombineering step which should combine both generated plasmids. Briefly, after generation of electro-competent E3-11wt-frt-Neo_ΔAmp: E3-11 H/A/pRedET containing cells, the recombineering step with NdeI linearized IRES-eGFP/3'HR-pDTA:frt-SOE did not results in the generation of any positive clone. Therefore we changed our strategy and performed a normal T4-DNA-ligase mediated ligation. After restriction of both plasmids with AsiSI/BstEII, we subcloned the 5'HR-Neo:CerS2 fragment upstream of the IRES cassette which results in the generation of the final CerS2H212A/2H13A gene targeting vector.

### 4.4.2 Generation of the conditional CerS2Del 79-120 vector

The generation of the conditional gene-targeting vector was completed on the basis of the CerS2H212A/H213A targeting vector and *cers2* DNA fragments amplified from the BAC clone. Finally, the final vector carries a deletion of amino acid 79 to amino acid 120 within the homeodomain of the CerS2 protein. With this approach we attempted to generate a truncated CerS2 protein, which should be not affected in its catalytic activity.

1st step: (TOPO blunt: E3-11, Δaa79-120)
The first step includes the amplification of exon 3 to 11 in a PCR reaction in the basis of the BAC vector and directly inserted into the TOPO Blunt vector. Afterwards, the coding sequence for amino acid residues 79 to 120 was deleted in a two-step mutagenesis PCR.

2nd step: (dual loxP/frt-Neo: E3-11, Δaa79-120)
In this step, the truncated coding region from E3-11, Δaa79-120 was cloned into the dual loxP/frt- Neo vector by compatible end cloning with NotI/PspOMI.

3rd step: (Cers2Del79-120 vector)
Next, the mutated sequence was subcloned by BsiWI/BstEII restriction into the conditional CerS2$^{H212A/H213A}$ gene targeting vector. The insertion of the mutated E3-11,Δaa79-120 fragment leads to the replacement of the E3-11 H/A coding region. The CerS2Del79-120 gene-targeting vector represents the final vector.

### 4.4.3 Generation and breeding of mice

A detailed description for the generation of transgenic mice based on ES cells and blastocyst injection was published some years ago by Nagy et al., 2003. The injection of correct recombined ES cell clones into C57BL/6N blastocysts, as well as the implantation of these manipulated cells in pseudo-pregnant mice was done by W. Krzyzak, LIMES GRC. The identification of genetically modified mice after injection through homologous recombination is based on the fur colour marker (agouti). Sv129/OlaHsd ES cells are characterized by the inhibition of melanine production in the hair follicle, which in turn results in the dominant expression of agouti-colored fur. Therefore, only high-extent fur coloured chimeras (male) were bred with C57BL/6N female mice to obtain heterozygous transgenic mice. Those mice in turn where either crossed with ubiquitious Flp-recombinase expressing mice (Rodriguez et al., 2000) resulting in the deletion of the neomycin cDNA or in case of the conditional deletion, heterozygous males ($CerS2^{+/floxH212/213A}$ and $CerS2^{+/flox\text{-}del79\text{-}120}$) were mated to female PGK-Cre (Lallemand et al., 1998) recombinase expressing mice for ubiquitious deletion of the wild type DNA sequence via the Cre/loxP system. Afterwards, heterozygous CerS2+/H212/213A:PGK-Cre and CerS2+/del79-120:PGK-Cre mice were bred with C57BL/6N mice to outcross PGK-Cre from the genome. Thereafter, interbreeding of heterozygous mice from each mouse line resulted in homozygous transgenic $CerS2^{H212A/H213A}$ or $CerS2^{Del79\text{-}120}$ mice. CerS2+/flox-delNeo (HA or del79-120):Flp mice were backcrossed with C57BL/6N mice to increase the C57BL/6 background and to delete the Flp-recombinase. Genotyping of mice for correct homologous recombination was verified by PCR analyses (see chapter 4.5).

### 4.4.4 Mouse handling

All mice were kept under standard housing conditions with a 12 h/12 h dark-light cycle in a specific pathogen free environment (SPF) and with water and food *ad libitum*. The cages were renewed once a week. If not mentioned otherwise, experimental animals were killed by cervical dislocation. Tissues were dissected and directly used for further analyses or snap-frozen and stored at -80°C for future experiments. Additionally, if not mentioned otherwise 6 to 10-week old males with a genetic background of 75 % C57BL/6N were used in all experiments.

#### 4.4.4.1 Measurement of food intake

The following experiments were performed with littermates from heterozygous breedings (WT and +/H/A). For analysis, male as well as female mice were used and the experiment started at the age of eight weeks. All animals were kept in IVCs (individually ventilated cages), with stainless steel grid, wood shavings and nesting material. The mice were fed a normal chow (LASQCdiet® Rod16, LASvendi) containing 16.9 % protein, 4.3 % fat and 4.3 % fibres. Sterile water from one drinking tube was also available *ad libitum*.
First, animals were separated at an age of eight weeks and acclimated to individual cages for 5 days. Afterwards, food and water intake was measured every day for a period of 14 days (to the nearest of 0.1 g). Food spillage was under detection level <1g/d and not taken into account. The food was renewed every second day. The body weight was measured once a week and started three weeks prior the beginning of the test.

## 4.5 Polymerase chain reaction (PCR)

Analyses of homologous recombination in embryonic stem (ES) cell clones and genotyping of transgenic mice was performed by polymerase chain reaction (PCR). It describes an in vitro method for the amplification of a defined and short nucleotide sequence; in which double-stranded DNA, harbouring the region of interest, serves as the template for the reaction (Mullis and Faloona, 1987). The programs and reaction mixture used for each PCR are listed below as well as the expected fragment sizes for the respective alleles. The following concentrations of ingredients were applied (unless indicated otherwise): dNTPs (10 mM each), $MgCl_2$ (25 mM), primer molecules (100 pmol/µl), Taq-Polymerase (5 U/µl).

### 4.5.1.1 PCR analysis for verification of 3' homologous recombination in ES cell clones

| Component | Volume |
|---|---|
| **Go-Taq buffer (5x)** | 5 µl |
| **$MgCl_2$** | 3 µl |
| **dNTPs** | 0.5 µl |
| **2 ctrl for (3'HR for)** | 0.1 µl |
| **3 ctrl rev (3'HR rev)** | 0.1 µl |
| **$H_20$** | 15.1 µl |
| **Go-Taq polymerase** | 0.2 µl |
| **DNA** | 1 µl |

| Temperature | Time | Cycles |
|---|---|---|
| 95°C | 2 min | 1 |
| 95°C | 30 s | |
| 65°C | 60 s | 34 |
| 72°C | 2:10 min | |
| 72°C | 10 min | 1 |

Fragment size: CerS2 wild type allele: --- bp, CerS2H/A or CerS2 Del allele: 1.9 kb.

### 4.5.1.2 PCR analysis for verification of 5'loxP homologous recombination in ES cell clones

| Component | Volume |
|---|---|
| **Go-Taq buffer (5x)** | 5 µl |
| **$MgCl_2$** | 2 µl |
| **dNTPs** | 1 µl |
| **HA loxP for_2 (LoxP for)** | 0.2 µl |
| **HA loxP rev_1 (LoxP rev)** | 0.2 µl |
| **$H_20$** | 15.25 |
| **Go-Taq polymerase** | 0.25 µl |
| **DNA** | 1 µl |

| Temperature | Time | Cycles |
|---|---|---|
| 95°C | 5 min | 1 |
| 95°C | 60 s | |
| 58°C | 30 s | 34 |
| 72°C | 90 s | |
| 72°C | 10 min | 1 |

Fragment size: CerS2 wild type allele: 402 bp; Flox allele: 484 bp; H/A or Del allele: 519 kb.

### 4.5.1.3 5' Long Amp PCR – Analysis of 5' external homologous recombination

| Component | Volume |
|---|---|
| **Long Amp buffer (5x)** | 5 µl |
| **dNTPs** | 0.75 µl |
| **5' ctrl for** | 0.1 µl |
| **5' ctrl rev** | 0.1 µl |
| **DMSO** | 0.75 µl |
| **$H_20$** | 15.6 |
| **LongAmp polymerase** | 0.2 µl |
| **DNA** | 1 µl |

| Temperature | Time | Cycles |
|---|---|---|
| 94°C | 1 min | 1 |
| 94°C | 30 s | |
| 61°C | 30 s | 30 |
| 68°C | 3min 20 s | |
| 68°C | 10 min | 1 |

Fragment size: CerS2 HA/ or Del allele: 5.6 kb.

#### 4.5.1.4 Verification of the CerS2 H212/213A point mutation (Nested PCR)

| A) Component | Volume |
|---|---|
| **Go-Taq buffer (5x)** | 5 µl |
| **$MgCl_2$** | 2 µl |
| **dNTPs** | 1 µl |
| **PvuII_alt_for** | 0.2 µl |
| **HA_Cre_rev** | 0.2 µl |
| **$H_20$** | 15.35 |
| **Go-Taq polymerase** | 0.25 µl |
| **DNA** | 1 µl |

| Temperature | Time | Cycles |
|---|---|---|
| 95°C | 2 min | 1 |
| 95°C | 30 s | |
| 59°C | 30 s | 34 |
| 72°C | 90 s | |
| 72°C | 5 min | 1 |

Fragment size: CerS2 wild type allele: --- bp, CerS2H/A allele: 1200 bp.

| B) Component | Volume |
|---|---|
| **Go-Taq buffer (5x)** | 5 µl |
| **$MgCl_2$** | 2 µl |
| **dNTPs** | 1 µl |
| **PvuII_alt_for** | 0.2 µl |
| **PvuII_alt_rev** | 0.2 µl |
| **$H_20$** | 15.35 |
| **Go-Taq polymerase** | 0.25 µl |
| **DNA** | 1 µl |

| Temperature | Time | Cycles |
|---|---|---|
| 95°C | 2 min | 1 |
| 95°C | 30 s | |
| 58°C | 30 s | 34 |
| 72°C | 30 s | |
| 72°C | 5 min | 1 |

Fragment size: CerS2 wild type allele: 343 bp, CerS2H/A allele: 343 bp (after *Pvu*I digestion 222 bp and 121 bp).

#### 4.5.1.5 Verification of the CerS2 D79-120 allele

| Component | Volume |
|---|---|
| **Go-Taq buffer (5x)** | 5 µl |
| **$MgCl_2$** | 1 µl |
| **dNTPs** | 0.5 µl |
| **del79-120_for** | 0.5 µl |
| **del79-120_rev** | 0.5 µl |
| **$H_20$** | 15.3 |
| **Go-Taq polymerase** | 0.2 µl |
| **DNA** | 2 µl |

| Temperature | Time | Cycles |
|---|---|---|
| 95°C | 2 min | 1 |
| 95°C | 30 s | |
| 60°C | 30 s | 30 |
| 72°C | 1 min | |
| 72°C | 5 min | 1 |

Fragment size: WT allele: 887 bp; Del allele: 762 bp.

#### 4.5.1.6 Flp genotyping PCR

| Component | Volume |
|---|---|
| **Go-Taq buffer (5x)** | 5 µl |
| **$MgCl_2$** | 2 µl |
| **dNTPs** | 1 µl |
| **USP_Flp** | 0.2 µl |
| **DSP_Flp** | 0.2 µl |
| **$H_20$** | 15.25 |
| **Go-Taq polymerase** | 0.25 µl |
| **DNA** | 1 µl |

| Temperature | Time | Cycles |
|---|---|---|
| 95°C | 5 min | 1 |
| 95°C | 60 s | |
| 58°C | 60 s | 34 |
| 72°C | 90 s | |
| 72°C | 10 min | 1 |

Flp recombinase allele: 1200 bp fragment.

#### 4.5.1.7 PGK-Cre PCR

| Component | Volume |
|---|---|
| **Go-Taq buffer (5x)** | 5 µl |
| **$MgCl_2$** | 2 µl |
| **dNTPs** | 0.2 µl |
| **Pgk1_for** | 0.2 µl |
| **Int-Cre_rev** | 0.2 µl |
| **$H_20$** | 16.3 µl |
| **.Go-Taq polymerase** | 0.1 µl |
| **DNA** | 1 µl |

| Temperature | Time | Cycles |
|---|---|---|
| 94°C | 5 min | 1 |
| 94°C | 30 s | |
| 60°C | 50 s | 35 |
| 72°C | 90 s | |
| 72°C | 10 min | 1 |

PGK-Cre recombinase allele: 500 bp fragment.

#### 4.5.1.8 NNT genotyping PCR

When breeding mice with C57BL/6J background we were aware to check for the mutation of the NNT (nicotinamide nucleotide transhydrogenase) gene to avoid mitochondrial redox abnormalities that could interfere with our analyses of the lipid metabolism.

| Component | Volume |
|---|---|
| **Go-Taq buffer (5x)** | 5 µl |
| **$MgCl_2$** | 3 µl |
| **dNTPs** | 0.5 µl |
| **WT for** | 0.1 µl |
| **Mut for** | 0.1 µl |
| **Com rev** | 0.1 µl |
| **$H_20$** | 14 µl |
| **Go-Taq polymerase** | 0.2 µl |
| **DNA** | 1 µl |

| Temperature | Time | Cycles |
|---|---|---|
| 95°C | 5 min | 1 |
| 95°C | 60 s | |
| 58°C | 60 s | 30 |
| 72°C | 60 s | |
| 72°C | 5 min | 1 |

Fragment size: wild type allele: 579 bp, NNT allele: 793 bp.

#### 4.5.1.9 Mutagenesis PCR

The generation of the designed deletion or point mutation within the homeodomain/ lag1 domain of the *cers2* gene, was done with the PCR-based *Dpn*I-mediated-mutagenesis method. The insertion of the mutation is performed by the presence of two complementary long-chain oligonucleotides that carry the desired mutation. After amplification of the whole vector in a standard PCR reaction the template is cleaved by *Dpn*I. Next, verification of amplification was done by analysis of 10 µl of the PCR reaction in an agarose gel. The remaining 40 µl were incubated with *Dpn*I to digest remaining plasmid (1 h, 37°C) and then directly transformed into competent *E.coli* cells.

| Component | Volume |
|---|---|
| **GC buffer (5x)** | 10 µl |
| **DMSO** | 1.5 µl |
| **dNTPs** | 1.0 µl |
| **Primer A** | 0.12 µl |
| **Primer B** | 0.12 µl |
| **$H_20$** | ad 50 µl |
| **Phusion polymerase** | 0.5 µl |
| **DNA template plasmid** | 15 ng |

| Temperature | Time | Cycles |
|---|---|---|
| 98°C | 30 s | 1 |
| 98°C | 10 s | |
| 55°C | 30 s | 19 |
| 72°C | 30 s/kb | |
| 72°C | 15 min | 1 |

## 4.6 Radioactive Southern blot hybridisation

For Southern blot analyses, genomic DNA from wild type, CerS2$^{H212A/H213A}$- and CerS2$^{Del79-120}$-ES- cell clones was extracted as described before (see chapter 3.1.4.1). Depending on the genotype, different digestions were performed following standard protocols. Verification of correct and single insertion of the corresponding exchange vector into the genomic locus of *cers2* was carried out with two different internal probes in combination with internal/external restriction digestion. After electrophoretic separation on an agarose gel, the gel was incubated in depurination buffer at RT for 10 min. Next, the agarose gel was rinsed in $ddH_2O$ and incubated in denaturation buffer for 30 min at RT. The transfer of genomic DNA onto Hybond-$N^+$ membrane (Amersham Biosciences, UK) was performed overnight. The sample slots were marked and the membrane washed with 2 x SSC. Application of UV-light to the membrane results in fixation and cross-linking of the DNA. The internal probes (50 ng) were diluted in 30 µl $ddH_2O$. Next, 5 µl of random hexamer primer solution was added and incubated at 100°C for 5 min. Afterwards, 2 µl Klenow polymerase (1 U/ml), 10 µl labelling buffer (containing non-radioactive dATP, dGTP and dTTP) as well as 2 µl $\alpha$-$^{32}$P-dCTP (Hartmann Analytic) were added and incubated at 37°C for 45 min, which results in the generation of radioactively labelled probes. Hybridization of the probes with the membrane was performed in QuickHyb solution (Stratagene) at 68°C for 2 hours. To remove unbound-probes, the membrane was washed several times in decreasing amount of SSC buffer containing 0.1 % SDS at 68°C (2 x SSC down to 0.1 x SSC). Finally, an X-ray film was exposed to the membrane at -70°C overnight and analysed afterwards.

## 4.7 DIG Southern blot

The CerS2-BAC containing bacteria were analysed according to the manufacturer's instruction of the DIG High Prime SB labelling Kit (Roche). Briefly, large scale plasmid purification was prepared following the protocol of the PureLink HiPure Plasmid Maxiprep Kit (Invitrogen). Next, 2 µg of BAC were digested with desired enzyme according to the protocol of NEB overnight at 37°C. The fragments were separated by agarose gel electrophoresis, transferred on PureLink HiPure Plasmid Maxiprep Kit onto Hybond.-N membrane and cross-linked. After hybridization probe, labelling and analysis of the corresponding DNA fragments was prepared following the DIG High Prime Kit.

## 4.8 Protein Biochemistry

### 4.8.1 Protein extraction

#### 4.8.1.1 Generation of cell culture lysates

Cells, HEK cells and MEFs, were grown on S10 cell cultures dished to yield appropriate amounts for immunoblot analysis. Once confluent (80-100 %), the medium was removed and the cells washed with 1 x $PBS^-$. Next, 500 µl 1 x $PBS^-$ was added, the cells scraped from the plate and centrifuged (2 min, 1.000 rpm, 4°C). The supernatant was removed, the cell pellet resuspended in 250 µl pre-cooled homogenisation buffer and passed 10 times through a 27 G needle. Subsequently, the cell lysate was centrifuged (10 min, 960 rpm, 4°C) and the supernatant transferred to a fresh reaction tube and stored at -80°C. Protein concentration was prepared following manufacturer's instructions of the BCA assay kit (Sigma-Aldrich).

#### 4.8.1.2 Generation of tissue lysates

Mouse tissue homogenates were generated using a Precellys homogenizer. Therefore, 1 ml/g wet weight of homogenisation buffer, supplemented with protease inhibitor cocktail (complete, PMSF, aprotinin and leupeptin), was added and the cells homogenized. Next, cell debris was removed in a centrifugation step (10 min, 13.000 g, 4°C) and the supernatant transferred to a fresh reaction tube. Storage of tissue homogenates was performed at -80°C and the protein concentration determined with the BCA assay kit (Sigma-Aldrich).

### 4.8.2 Quantification of protein concentration

The BCA method was used for the determination of the protein concentration of cell and tissue homogenates. All measurements were carried out in duplicates and all following steps prepared according to manufacturer´s instructions (BCA assay kit, Sigma-Aldrich). The $OD_{550}$ was determined and the amount of protein calculated as a function of the OD value (y-axis) and the corresponding concentration (x-axis) drawn in a graph.

### 4.8.3 Immunoblot analysis

#### 4.8.3.1 SDS- PAGE and transfer of proteins

| Component | Stacking gel | Separating gel |
|---|---|---|
| **Acrylamid** | 1 ml | 8 ml |
| **Stacking gel buffer** | 4.5 ml | --- |
| **Separating gel buffer** | --- | 5 ml |
| **Glycine** | --- | 2.5 ml |
| **ddH2O** | 4 ml | 4 ml |
| **APS (10%)** | 120 µl | 45 µl |
| **TEMED** | 12 µl | 1. µl |

Depending on the type of lysate (tissue, cells) 25 µg up to 50 µg of protein lysate were mixed with 2 x Urea buffer, filled up to a final volume of 20 µl with water and heated for 10 min at 75°C. Next, the protein lysate was separated by SDS-PAGE in 1 x SDS running buffer (stacking gel 20 mA/gel; separating gel 25 mA/gel). All applied gels were of the following composition as summarized in the table. Briefly, the stacking gel causes a concentration of the samples in front of the separating gel, whereas the separating gel leads to the separation of the proteins regarding their molecular mass. The transfer of proteins onto nitrocellulose membranes (Hybond-ECL, GE Healthcare) was performed with the wet transfer method in transfer buffer for 2 hours (150 mA, 4°C). Finally, the transfer was verified by Ponceau S staining.

#### 4.8.3.2 Immunoblot analysis via chemiluminescence (ECL)

To avoid unspecific antibody-binding, the membrane was incubated in blocking solution for 1 h at RT. Afterwards; the primary antibody solution was prepared in blocking solution and the membrane incubated overnight at 4°C. The antibody solution was removed and the membrane washed with TBS-T (3 x 10 min). Next, the membrane was incubated with secondary antibody solution prepared in TBS-T and incubated for 1 h at RT. Afterwards, the secondary antibody solution was discarded and the membrane washed with TBS-T for several times. Finally, the membrane was incubated with Amersham ECL Prime Western Blotting Detection reagent (GE Healthcare) and developed using the VersaDoc imaging system (Bio-Rad). Afterwards, the membrane was washed with TBS-T and stored either at 4°C/in TBS-T or was air-dried and placed between two Whatman-papers for further analyses.

#### 4.8.3.3 Regeneration of membranes

For further immunodetection analyses of already analysed membranes, it was necessary to remove the antibody complexes. Initially, the membrane was equilibrated in TBS-T, when air-dried before, and then incubated in Restore PLUS Western Blot stripping buffer solution (ThermoFisher Scientific) for 10 min at RT. Finally, the membrane was incubated with fresh stripping buffer solution (10 min, 37°C), then washed with TBS-T (2 x 10 min) and then ready for further analyses.

### 4.8.4 Immunofluorescence analysis

Dilutions and references of all antibodies used for immunofluorescence analyses are described in Chapter 2.2.

For immunofluorescence analysis of cell culture cells (HEK293T, pMEFs), 13 mm glass cover slips were PLL coated and placed into culture dish. 24 h after transfection or once confluent, the medium was removed and the cells washed with 1 x $PBS^-$. Fixation of cells on cover slips was performed upon incubation in appropriate volume of 4 % PFA/$PBS^-$ solution for 5 min on ice and following incubation for 10 min at RT. Fixation solution was discarded and the cells washed with Oldenburg buffer. Perforation of membranes was achieved upon incubation of fixed cells in 400 µl ethanol for 5 min at -20°C. Cells were washed with Oldenburg buffer (2 x 10 min, RT), covered with 500 µ blocking solution and incubated for 1 hour at RT. Next, blocking solution was discarded and primary antibody solution ($1^{st}$ antibody, 5 % NGS, Oldenburg buffer) added and incubated either overnight at 4°C or at least for 1 h, RT. Afterwards, cells were washed with Oldenburg buffer (3 x 10 min, RT) and secondary antibody incubation performed for 1 h (RT) in blocking solution. Finally, staining solution was removed and nuclei stained by incubation in washing solution supplemented with 0.5 mg/ml bisbenzimide (1:1000, HOECHST 33258 stain, Sigma) for 10 min (RT).The staining solution was discarded, the cells washed three times with Oldenburg buffer and mounted with Glycerol mounting medium (Dako). Slides were imaged with a Laser Scanning Microscope (Zeiss).

## 4.9 Lipid analysis

### 4.9.1 Ceramide synthase activity assay

The *de novo* generation of ceramides was determined in an *in vitro* ceramide synthase activity assay either with radioactive- or NBD- labelled substrate. All samples were performed as duplicates.

#### 4.9.1.1 Radioactive-labelled CerS assay

First, cell homogenates of transfected/un-transfected HEK293T cells or primary MEFs were prepared as described (van Uelft, 2012). Initially, 12.5 µg of protein in a final volume of 50 µl homogenisation buffer was prepared. Next, the [$^3$H] sphinganine/BSA/sphinganine solution was prepared and incubated for 20 min on ice. Each sample reaction consists of 0.25 µl [$^3$H] sphinganine, 0.1 µl sphinganine and 44.65 µl reaction buffer. Furthermore, acylCoA/HEPES solution (5 M) was prepared and stored at RT. The radioactive-labelled substrate solution was mixed with the protein homogenate and incubated for another 2 min at 37°C. After pre-incubation, the reaction was started by addition of 5 µl acylCoA/HEPES. Both solutions were mixed very well to achieve homogenous distribution of the components. After an incubation step of 20 min at 37°C, the reaction was terminated by the addition of 375 µl

chloroform/methanol (1:2, v/v). The solution was vigorously mixed (vortex) and lipid extraction performed according to the protocol of Bligh and Dyer (1959).

#### 4.9.1.2 NBD-labelled CerS assay

First, cell homogenates of transfected/un-transfected HEK293T cells or primary MEFs were prepared in homogenisation buffer supplemented with protease inhibitors as described (see chapter 4.8.1.1). Next, 25 µg of homogenate were diluted in a final volume 50 µl homogenisation buffer and the 10 µM NBD- sphinganine (omega (7-nitro-2-1,3-benzoxadiazol-4-yl)(2S,3R)-2-aminooctadecane-1,3-diol, Avanti Polar Lipids) solution prepared for each reaction (45 µl) as a master mix. After incubation of 2 min at 37°C, the NDB-sphinganine was added to the protein homogenate and incubated for another 2 min at 37°C. The reaction was started upon addition of 50 µM acylCoA (Avanti Polar Lipids). After incubation of 20 min at 37°C the de novo synthesis was stopped and the lipids were extracted following addition of 375 µl chloroform/methanol (1:2, v/v). Finally, the solution was well mixed (vortex) and the lipid extraction performed according to the protocol of Bligh and Dyer.

#### 4.9.1.3 Lipid extraction (Bligh and Dyer)

Lipid extraction started with the addition of 375 µl chloroform/methanol (1:2, v/v) solution. The solution was vigorously mixed and briefly centrifuged (1 min, 2.500 rpm). Next, 125 µl chloroform were added to each sample, vigorously vortexed and centrifuged (1 min, 2,500 rpm). Furthermore, 125 µl dd$H_2O$ were added, again vigorously vortexed and centrifuged (1 min, 3.000 rpm). After phase-separation, the lower organic phase was transferred to a fresh reaction tube and air-dried in a speed vac apparatus or under $N_2$-flow in a heating module at 37°C. Finally, the lipids were resuspended in 15 µl chloroform/methanol (1:1) and stored at -20°C until HPTLC analyses were performed.

### 4.9.2 High-performance thin layer chromatography (HPTLC)

HPTLC analysis was used to separate and analyse different lipid classes from a diverse lipid mixture. The separation of the analytes is based on their solubility in the liquid mobile phase (solvent) and their affinity to the stationary phase. For TLC (thin layer chromatography) analysis, lipid extracts were dissolved in appropriate volume of chloroform/methanol (1:1, v/v).

**[$^3$H]-labelled lipids**

Radioactive-labelled lipids loaded on HPTLC silica gel 60 plates (Merck) were developed in chloroform/methanol/glacial acetic acid (190:9:1). Afterwards, the plate was air-dried and [$^3$H] sphinganine/BSA/sphinganine mixture of known concentration (2 x 1 µl, 2 x 5 µl) was added to the plate for further quantification analyses. Finally, a [$^3$H]-sensitive screen was put on top of the TLC plate and exposed for 20 to 24 h. Visualization was performed with the BAS reader (Fuji) and the AIDA software tool used for quantification purposes.

**NBD-labelled lipids**

Initially, TLC silica gel 60 plates (Merck) with applied NBD-labelled lipids were developed in chloroform/methanol/water (8:1:0.1, v/v) and air-dried. Afterwards, different volumes of NBD-sphinganine standards were spotted onto the plate for quantification analyses. Finally, the fluorescence was detected using a Rolera MGI plus EMCCD camera (494/20 and 572/28 emission filter) in combination with the GelPro analyser software (Media Cybernetics). Quantification of fluorescence intensity was performed with ImageJ.

### 4.9.3 Lipid extraction from mouse tissue (liver, muscle and WAT)

Mouse tissues used for lipid extraction were collected and stored at -80°C. Prior to homogenisation in a Precellys® homogenizer (Peqlab Biotechnology), the wet weight was determined and the appropriate amount of tissue (50 mg wet weight/ml) transferred to a fresh precellys tube containing a small amount of $ddH_2O$ (3 x 10 sec, 5.000 rpm, RT). Afterwards, homogenates were transferred to fresh Pyrex screw cap tubes and filled up with $ddH_2O$ to a final volume of 800 µl. Next, samples were mixed with 3 ml chloroform/methanol (1:2, v/v). Afterwards, 1 ml chloroform were added and the solution mixed well by vortexing. Then, 1 ml $ddH_2O$ was added to each sample, followed by vigorous vortexing. After phase separation (2.500 rpm, 5 min, RT), the lower organic phase (1.8 ml) was transferred to a fresh glass screw cap tube. The solvent was evaporated under $N_2$-flow at 37°C and the lipids extracts resuspended in small volume of 180 µl chloroform/methanol (1:1, v/v).

For TLC analysis, 5 µl of lipid extracts (corresponding to 1 mg tissue) as well as 5 µl of lipid standard (cholesterol, cholesterol ester, DAG and TAG) were spotted onto the plate (HPTLC Silica gel 60, Merck) and developed in *n*-hexane/diethylether/acetic acid (70:30:1, v/v/v). Afterwards, the plates were air-dried and incubated in 10 % $CuSO_4$/ 8 % $H_2PO_4$ solution until the plate was completely covered with the solution. Next, the plate was heated to 180°C for several minutes to visualize the separated lipids (Yao & Rastetter, 1985). Quantification was done with ImageJ.

### 4.9.4 Lipid extraction from mouse feces

Mouse feces were collected at different time points and stored at -80°C until further analysis. For lipid extraction, 100 mg feces were transferred to fresh tube and dried for 1 hour at 37°C. Afterwards, feces were ground using pestle, resuspended in 400 µl $ddH_2O$ and transferred to fresh Pyrex screw cap tube. Next, 1.5 ml chloroform/methanol (1:2, v/v) were added and the storage lipids extracted. 0.5 ml chloroform was added to each sample followed by the addition of 0.5 ml $ddH_2O$. After each step, the lipid mixture was vigorously mixed by vortexing. For phase separation, the samples were centrifuged (10 min, 2.500 rpm, RT) and the lower phase transferred to a fresh glass screw cap tube. The solvent was evaporated and the remaining lipid extract resuspended in 100 µl chloroform/methanol (1:1, v/v). For TLC analysis of lipid composition see chapter 4.9.1.3.

## 4.10 Histological analysis

Mouse tissue samples were fixed in 4 % paraformaldehyde (PFA), methanol-free PBS for 24 h at 4°C. Afterwards, the tissues were embedded in paraffin. Microtome sectioning and the stainings were performed by Melanie Thielisch.

Paraffin sections used for H&E, PAS, Elastica and IHC staining's were deparaffinised and rehydrated as followed. First, the sections were incubated for 20 min at 60°C in the incubator. Next, the slides were incubated in Xylol (2 x, 10 min) and run through a descending alcohol series (2x 100 %, 96 %, 90 %, 80 %, 70 % and $ddH_2O$).

### 4.10.1 H&E (hematoxylin and eosin) staining

The H&E staining is a combination of two single stainings and is one of the most widely used overview staining. First, hematoxylin stains all basophilic structures like the nuclei of cells blue and the counter staining with eosin, all acidophilic (eosinophilic) structures in red/pink and orange (cytoplasm, mitochondria, collagen and keratin).

Briefly, the sections were deparaffinised as described above and then incubated for 3 min in Mayer's hemalum solution (VWR) and again washed three times in tap water. Next, the sections were incubated in Eosin-staining solution (VWR) for 3 min at RT and washed with tap water (3 x). Finally, the slides were shortly incubated in an ascending alcohol series. Entellan was dropped onto the slides and covered (air bubble-free) with a cover slip.

### 4.10.2 PAS staining

The periodic acid- Schiff (PAS) staining allows detection of polysaccharides such as glycogen or glycoproteins (mucos). For interpretation, glycogen, mucus substances, basement membranes and fungal organisms were magenta colored. The nuclei are stained in blue, by hematoxylin counter staining.

First, the sections were deparaffinised as described and rinsed in distilled water. Then, the slides were incubated in periodic acid for 5 min (RT, Roth) and washed under running tap water for at least 3 min. Slides were again rinsed in distilled water, then incubated in Schiff's reagent (15 min, RT, Roth) and washed with tap water. Next, the slides were rinsed in distilled water and incubated for 2 min in Mayer´s hemalum solution (VWR). Afterwards, the slides were washed in tap water, run through ascending alcohol series and mounted with Entellan.

### 4.10.3 Elastica van Gieson Staining (Merck)

This staining is a combination of the Weigert and Van Gieson Trichrome staining and highlights the connective tissue and elastic fibers.

Deparaffinised slides were incubated for 10 min in Elastin solution according to Weigert's protocol and rinsed under tap water. Next, slides were incubated for 5 min in a mixture of Weigert's solution A and B (1:1) and rinsed with tap water. Finally, the sections were incubated for 2 min in Picrofuchsin solution, incubated for 1 min in 70 % ethanol and run through ascending alcohol series before they were mounted with Entellan.

#### 4.10.3.1 Immune histochemistry

It describes a common application, where applied (conjugated) antibodies selectively bind their antigen and can be used in turn for detection.

Sections that have been deparaffinised were incubated in 1.2 % $H_2O_2$/PBS solution for 10 min. After another incubation step in 10 mM sodium acid buffer (pH 6) for 40 min at 95°C, the sections were blocked in 1 % BSA/PBS-T additionally supplemented with 10 % donkey serum (30 min). The primary antibody was diluted in 1 % BSA/PBS-T solution and incubated overnight at 4°C. The staining solution was removed, slides washed with $PSB^-$ (3x 3 min) and then incubated with the secondary antibody solution (in PBS) for 1 hour at RT. The sections were again washed with $PBS^-$ (3x 3 min) and stained with NovaRED (Vectorlaboratories). Finally, a hematoxylin- counterstaining for nuclei was prepared and sections were mounted.

### 4.10.4 Oil Red O staining

The Oil Red O staining utilizes a lysochrom diazo dye for the staining of neutral, storage lipids (TAG, cholesterol ester) and also some lipoproteins. Preparation of frozen sections and the staining procedure were done by Melanie Thielisch.
Briefly, fresh tissue was taken from a mouse which was killed by cervical dislocation. Next, the tissue was directly embedded in Tissue-Tek® O.C.T.TM compound (Sekura), frozen on dry ice and stored at -80°C. Cryo sections of 8- 10 µm thickness were prepared and mounted on glass

slide. Sections were incubated for 5 min (RT) in formalin and washed with tap water. Next, the slides were shortly equilibrated in 60 % isopropanol followed by an incubation step of 10 min in Oil Red O solution B for 10 min (RT). The staining reaction was terminated by incubation in 60 % isopropanol. Finally, the slide was rinsed with distilled water and a counterstaining with Mayer´s hemalum solution (2 min) was performed. Afterwards, the slide was rinsed with distilled water and a drop of Kaiser's glycerol gelatine added and covered with cover slip.

## 4.11 Flow cytometry

The flow cytometry is a laser-based technology which allows the counting, sorting and profiling of cells in a heterogeneous fluid mixture (e.g. tissue homogenate, blood sample). The analysis is based on the expression of a combination of specific antigens on the cell surface which were detected by antigen-specific-fluorochrome-conjugated antibodies. Thereby it is possible to specify not only the cell type, but also its biological function and developmental stage. Additionally, next to an extracellular, an intracellular staining of proteins is also possible.

### 4.11.1 Dissection of thymus and spleen

Mice killed by cervical dislocation were placed in dorsal recumbency and the prepping area cleaned with 80 % ethanol. Initially, the abdomen was opened with sterile dissection instruments and the spleen removed. Next, the thoracic cavity was opened and the thymus removed. Each organ was subsequently transferred to a fresh reaction tube containing 0.5 ml 1 x PBS and stored on ice until FACS analysis were performed (see Chapter 4.11.4).

#### 4.11.1.1 Isolation of lymphocytes from thymi and spleen

For the preparation of lymphocyte single cell suspension, thymi and spleens were prepared as described (3.10.2). Next, each organ was placed in a 40 µm cell strainer placed in a S10 cell culture dish which was filled with 8 ml ice-cooled PBS (1 x) and chilled on ice. To achieve single cell suspension, each organ was passed with gentle pressure through the cell strainer with a sterile plunger of a 10 ml syringe. The suspension was transferred to a fresh falcon tube, the cell strainer rinsed with 1 x PBS and also collected in the corresponding falcon. After centrifugation for 10 min at 1.200 rpm at 4°C, the supernatant was removed, the lymphocytes from thymi samples resuspended in 10 ml 1 x PBS and stored on ice. Lymphocytes from spleen samples were resuspended in 5 ml red blood cell (RBC) lysis buffer and incubated for 5 min at RT. The hypotonic buffer conditions results in the burst of erythrocytes whereas lymphocytes remain intact. The reaction was terminated after the addition of 30 ml PBS followed by a centrifugation step (1.200 rpm, 8 min, 4°C). Next, the supernatant was removed, lymphocytes resuspended in 10 ml PBS (1 x) and stored on ice. Finally, an aliquot from each sample was taken, mixed with Trypan blue and the cells counted (see Chapter 4.3.1).

### 4.11.2 Blood collection by intracardiac puncture

The blood collection as a terminal procedure by intracardiac puncture was performed with mice that had been anaesthetized (overdose) with isoflurane. The mouse was placed in dorsal recumbency and the prepping area cleaned with 80 % ethanol. Next, the heart was directly punctured, by inserting the needle (27G needle on a 1 ml syringe) at the base of the sternum under the left side to the xiphoid process. Finally, the blood was carefully withdrawn and the mice killed by cervical dislocation. Subsequently, the blood was transferred to a fresh reaction tube (1.5 ml) and gently mixed with 0.5 M EDTA (up to 50 µl/ 500 µl blood) to avoid

coagulation. In the next step, the blood was diluted with 1 x PBS supplemented with 2 % FCS and 2 mM EDTA to a final volume of 1.2 ml and was stored at RT until PBMCs isolation and FACS analysis were performed.

### 4.11.3 Isolation of PBMCs from whole blood samples

The isolation of PBMCs from whole blood samples was done by density gradient centrifugation. Diluted whole blood samples were carefully layered onto a 3 ml Lymphoprep™ (density gradient medium, Stem cell technologies) that had been prepared in a fresh 15 ml falcon tube. In order to prevent the gradient from destruction during centrifugation step, the brakes from the centrifuge were switched off. After centrifugation (20 min, 800 x g, RT), the PBMC-containing interphase was carefully harvested and transferred to a fresh falcon tube containing 10 ml 1 x PBS. An additional centrifugation step was performed (10min, 300 x g, 4°C) and the supernatant carefully removed. The pellet was resuspended in 10 ml 1 x PBS and once more centrifuged (10 min, 120 x g, 4°C) to pelletize the PBMCs whereas the platelets-containing supernatant can be carefully removed afterwards. Finally, the PBMCs were resuspended in 1 to 2 ml 1 x PBS and a small aliquot prepared to count the cells (Trypan blue added to exclude dead cells). The PBMC suspension was stored on ice until further experiments were performed.

### 4.11.4 Flow cytometry

As mentioned before, the flow cytometry represents a laser-based technology, which allows the simultaneously analysis of various parameters of a single cell suspension. First, cells were arranged by hydrodynamic focusing; and depending on their size and granularity, the laser light is differentially scattered and absorbed when passing two detector systems. First, the forward scatter detector (FSC) is placed in line with the laser beams and detects the light which passes the cells. Meaning, the bigger the cells are, the less light passes them and the less can be detected. This in turn gives information about size of the cells. The second detector, the sideward scatter detector (SSC) is arranged in a defined angle to the laser beams which allows the measurement of light that is scattered by the cells. The level of scattering in turn is based on e.g. the intracellular amount of granules or other membrane compartments and gives some information about the internal complexity. Additionally, each laser is able to excite several fluorochromes simultaneously. The emission of those fluorochromes were separated by specific band pass filters and measured by an additional set of detectors.

#### 4.11.4.1 Flow cytometric analysis of cell surface marker

The staining of cell surface antigens for flow cytometric analyses was performed with 1 x $10^6$ cells. The appropriate amounts of single cell solution from each sample that have been prepared as described (Chapter 3.10.3 and 3.10.4) were transferred to flow cytometry tubes, containing 1 ml PBS (1 x). After a centrifugation step (8 min, 1.200 rpm, 4°C), the supernatant was removed and the cells resuspended in 100 µl PBS buffered antibody staining solution. The dilution of antibodies was prepared according to the manufacturer's instructions. Incubation was performed for 20 min at 4°C in the dark. Next, the cells were diluted with 1 ml PBS (1 x) and again centrifuged (8 min, 1.200 rpm, 4°C). Afterwards, the supernatant was decanted, the cells resuspended in 200 µl PBS and stored on ice. The analysis of the cells was performed at the Canto II flow cytometer. In one experiment, propidium iodide (200 ng/ sample), was added to the samples directly before the measurement was started. Propidium iodide is a fluorescent-

DNA intercalating dye and was used to stain dead cells as it can pass through porous membranes.

## 4.12 Statistical analysis

For statistical analysis of obtained data a two-tailed Student's t-test for independent groups was performed. *p*-values lower than 0.05 were regarded as statistically significant. Values are presented as mean ± SEM.

# 5 Results

The present thesis is divided into three parts. The first part focuses on *in vitro* experiments. The second part summarizes the cloning strategy and generation of two conditional mouse lines: CerS2$^{H212A/H213A}$ or CerS2$^{Del79-120}$, later abbreviated as CerS2H/A or CerS2Del. The last section summarizes the characterization and analysis of the dysfunctions caused by the targeted mutations *in vivo*. Some of the experiments were done in cooperation with Dr. A. Bickert and Dr. P. Kern and already published (Bickert et al., 2018) prior to this thesis was finished.

## 5.1 Bioinformatics analysis of ceramide synthase 2

### 5.1.1 CerS2 transmembrane topology prediction studies and analyses suggest an ER-luminal orientation of the N-terminus and cytoplasmic localisation of the homeodomain

Despite the intensive investigations done to elucidate the detailed functions of each ceramide synthase, e.g. consequences from a loss of function; not much is known about the 3D-structure and transmembrane topology of the whole protein. This may be explained by the lack of X-ray crystallographic analyses. However, there are several software tools and databases available, which allow the prediction of domains and motifs, based on the comparison (blast/alignment) of similarities to already well-characterized proteins.
All applied database searches, alignments, and experiments were performed to gain more insights into the protein structure and to avoid impairment of important sites necessary for the catalytic function of the CerS2 protein (Figure 5.1 A and B). This issue becomes even more crucial when mutation constructs of the CerS2 protein were generated, which probably affect the functionality of the homeodomain by leaving the protein structure and catalytic activity intact.

So far it is already known, that the CerS2 protein consists of two domains, the homeodomain and the TLC domain (Figure 1.5, Figure 5.1, Chapter 1.4). Posttranslational modification analyses were performed with the NetNGlyc1.0/ NetOGlyc3.1 server and the NetPhos3.1 prediction tool in order to validate, at which sites the protein is possibly glycosylated or phosphorylated. This is of great importance due to modifications, which should be introduced into the protein sequence. Here, the generated mutations should not interfere with those sites leading to their impairment. The NetNGlyc1.0 prediction revealed two possible glycosylation sites within the peptide sequence at position N19 and N81 (Figure 5.1, A/B, black asterisks, Figure A3). The possible function of the glycosylated N18 and its contribution to the catalytic activity were later on further investigated (Chapter 5.1.3). The NetOGlyc3.1 prediction does not indicate any O-glycosylated amino acids in the CerS2 protein (data not shown).

Results from the NetPhos3.1 prediction revealed that several amino acid residues within the peptide sequence of CerS2 can be phosphorylated (Figure A4). Some of the predicted phosphorylation sites within the C-terminus of the CerS2 protein could be confirmed by experiments of Sassa et al (2016). It should also be noted that the phosphorylation itself influences the catalytic activity of the protein (Sassa et al., 2016).

Next, the CerS2 protein was analysed regarding the presence of a nuclear localisation signal. The NLStradamus software tool recognizes a putative NLS region within the peptide sequence of the homeodomain, but its value does not reach the threshold-line (Figure 5.1 D, lower section). Another result from the NucPred server suggests that this "RRRR-motif" within the

homeodomain of the CerS2 peptide sequence could function as an NLS signal (Figure 5.1 D, middle section). Since it was known from schlank, the well-characterized ceramide synthase from *Drosophila melanogaster*, that it harbours two NLS motifs (Chapter 1.5), were the second one, the NLS2 (RLRR-motif), was proven to be essential for nuclear localization (Voelzmann, 2013; Sociale et al., 2018.). Following that, we performed another protein sequence alignment of CerS2 with schlank to determine whether the NLS1 and/or NLS2 motif is also present in CerS2 peptide sequence (Figure 5.1 D). The obtained results indicate that the NLS2 ("RLRR") motif from the fruit fly is highly conserved (from insects to mammals) and present in the CerS2 peptide sequence (here "RRRR"). Additionally it turned out that those amino acids are the same as that predicted by the NucPred server (Figure 5.1 D).

Next, membrane topology predictions indicated that CerS2 has either six or seven transmembrane domains (data not shown). The N-terminus is thereby facing the ER lumen, based on the predicted glycosylation site and the fact that the enzymes, necessary for its glycosylation, are located in the ER lumen (Tidhar et al., 2018). Another representative prediction result performed with the Phyre$^2$ server suggests, that the CerS2 protein consists of seven TMDMs and that the homeodomain is located between the first and second transmembrane domain (Figure 5.1 B). Furthermore it predicted that the C-terminus is facing the cytoplasm, which is in line with prediction analyses performed by Tidhar et al. 2018. Additionally, it was also shown by nuclear magnetic resonance (NMR) analyses, that the homeodomain of CerS5 and 6 can adopt a typical 3D-structure, composed of three $\alpha$-helices (Figure 5.1 C; UniProtKB (Q9D6K972cqx.1.A. and Q8C172); Voelzmann, 2013; Sociale et al., 2018). Based on these findings protein-blast and alignment analyses were performed with the Swiss-Model-/ and Phyre$^2$ server to predict the possible structure, which can be adopted by the CerS2 protein (Figure 5.2 B and C). The findings from the Swiss-Model server clearly indicate that the homeodomain of CerS2 has low sequence similarity of 37.97 % to CerS5 (Figure 5.1 C); however it suggests that it can adopt the same secondary structure of three alpha helices, which is located between the first and second large transmembrane spanning domain. The Phyre$^2$ prediction supports this assumption (Figure 5.1 B) and it additionally gives an overview, upon homology modelling, that the tertiary structure of the CerS2 protein is mainly composed of alpha helices (Figure 5.1 B). With all these findings we gained further information about the possible protein structure, which is needed for the following steps.

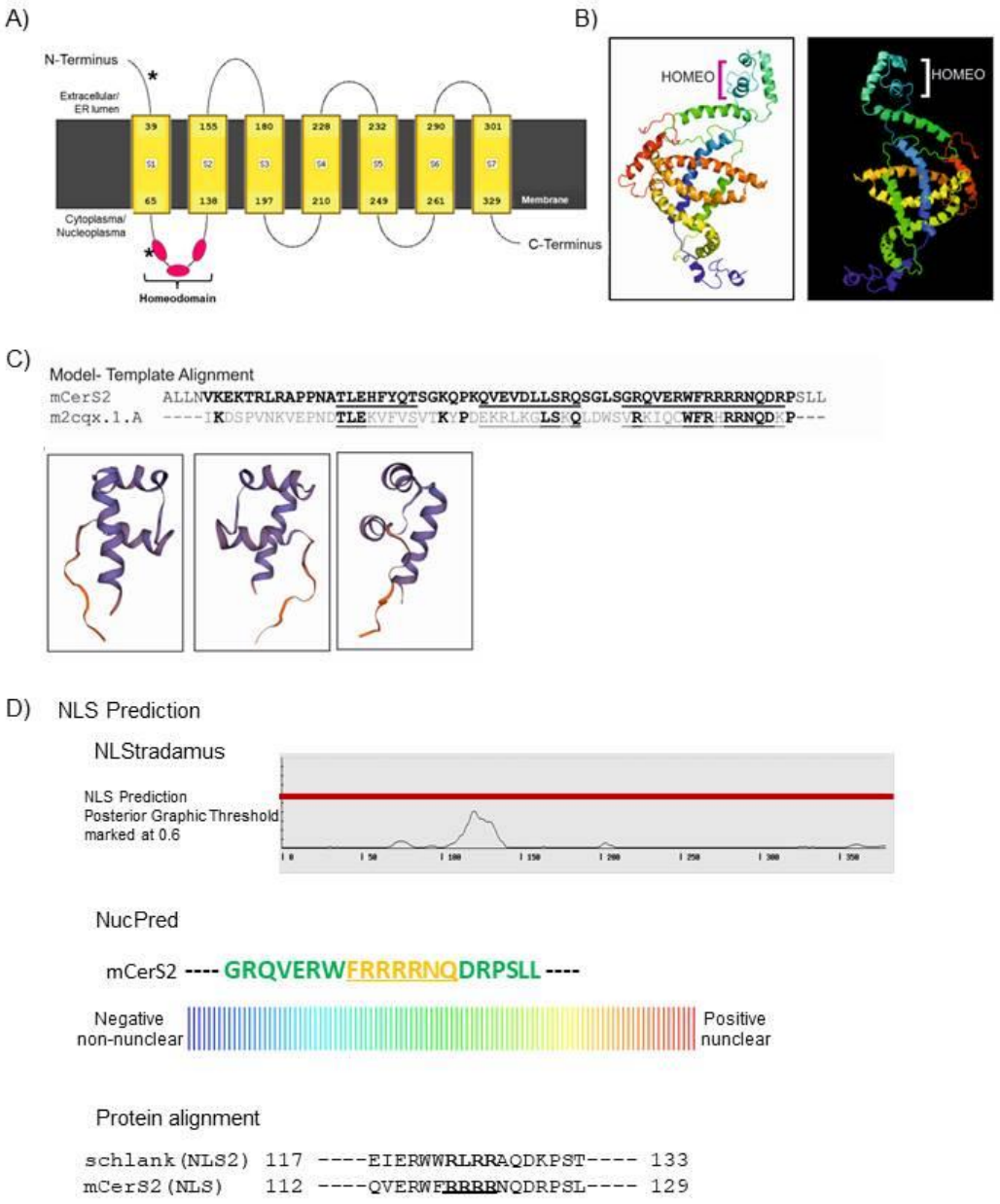


**Figure 5.1: Bioinformatics analysis of mouse ceramide synthase 2. (A)** Graphical representation of the CerS2 protein (homeodomain aa 67-128; TLC domain aa 131-332). Predicted 2D model suggests the presence of seven transmembrane domains arising from the peptide sequence. N- terminus faces the ER lumen (extracellular space). C-terminus is directed against the cytoplasm. Asterisks highlight possible glycosylation sites at position N19 and N81. Purple circles depict positions of alpha helices of the homeodomain. **(B)** Phyre[2] 3-D homology modelling results. Homeodomain is shown in light green/blue at the top of the protein. **(C)** Swiss-Model homology modelling result. Homeodomain of CerS2 shares 37.93% sequence identity with the CerS5-template (m2cqx.1.A). Model-Template-Alignment highlighted position of alpha helices. Conserved amino acids are in black. 3D-structures predict the possible formation the homeodomain of CerS2 can adopt. **(D) Upper section** show NLStradamus prediction results performed to identify NLS signals within the CerS2 protein. Identified signal between aa 100 and 150 does not reach threshold line. **Middle section** summarize the NucPred- NLS prediction results for the identification of an NLS signal (bold faces, yellow). Color-code indicates probability. **Lower section** show results of NLS-prediction based on the sequence alignment of Cers2 and schlank (Results were obtained and modified from indicated server, Phyre[2] and Swiss Model, NucPred, NLStradamus).

### 5.1.2 Mutations in the lag1 and not of the homeodomain affects the catalytic activity *in vitro*

As it was described at the beginning of Chapter 1.4, all ceramide synthases, except CerS1, are composed of two sequence motifs; the N-terminally located homeodomain and the C-terminally located TLC domain (Figure 1.5).

In order to investigate the function of the homeodomain and TLC domain independently from each other in mice, different constructs were generated and tested *in vitro*. Each CerS2-construct suitable for the expression in a mammalian cell culture system carries a defined mutation within one of the protein domains (Figure A5). The cDNA of *cers2* was amplified via PCR and directly cloned into the pcDNA3.1/V5-His TOPO® TA vector (Invitrogen). The defined mutations were introduced by mutagenesis PCR. Next, the mutant constructs were either overexpressed in HEK293T cells or immortalized MEFs derived from CerS2$^{gt/gt}$ mice. 24 hours after transfection, cells were harvested, protein lysates generated and transfection efficiency tested via immunoblot analyses. 25 µg of protein lysates were subsequently subjected to the *de novo* synthesis assay and incubated for 20 min with 10 µM NBD-sphinganine [(omega (7-nitro- 2-1,3-benzoxadiazole-4-yl) (2S,3R)- 2amino- octadecane-1,3-diol)] and 50 µM acyl-CoA at 37°C. Reactions were determined by addition of chloroform/methanol; lipids were extracted according to the protocol of Bligh & Dyer and separated on methanol HPTLC plates. Quantitative analyses of fluorescence intensities were performed in comparison to applied standards with ImageJ, Excel, and GraphPad. All values derived from the different assays were put as relative ceramide synthase activity. The CerS2H212A/H213A-V5-His expression vector construct was already cloned (van Uelft, 2012) and is characterized by the replacement of two highly conserved consecutive histidine residues by two alanine residues (aa 212 and 213, Figure 5.2 A and B). The defined deletion of amino acid residues 79-120 within the homeodomain was generated under consideration of a ClustalO sequence alignment with CerS5 and 6; and in accordance to similar experiments done with CerS1 and 5 (Figure 5.2 E) (Spassieva et al., 2006). Here, the CerS5-stop and CerS5del87-128-stop vector (Gosejacob, 2017) was used as a positive control for our truncated CerS2 protein construct. Additionally, it is necessary to mention that untransfected HEK 293T cells endogenously express CerS2 and CerS5, which leads to a background signal of *de novo* generated ceramides. Immortalized MEFs derived from CerS2$^{gt/gt}$ mice showed no endogenous CerS2 activity, due to the lack of the CerS2 protein. Results of immunoblot analyses illustrate that transfected HEK 293 cells or MEFs express the CerS2 constructs in the same ratio (Figure 5.2 C and F). Furthermore, overexpression of WT CerS2 (Figure 5.2 D and G) and CerS5 (Figure A5) results in increased levels of *de novo* generated ceramide in comparison to controls. Increased activity was undetectable in lysates from CerS2H212A/H213A transfected MEFs (Figure 5.2 D). These findings suggest that the two histidine residues seem to be necessary to maintain the catalytic activity of CerS2. Therefore, the histidine to alanine replacement mutation is suitable to study the effect of a catalytically inactive protein where the homeodomain is still present.

Next, the deletion of amino acids 87-128 within the homeodomain of CerS5 does not result in reduced *de novo* synthase activity (Figure A6) and was therefore used as an internal positive control for our experiments. Crude lysates of CerS2Del79-120 transfected HEK293 cells show minor reduction in *de novo* synthase activity against its preferred substrates C24:1 and C22:0-acylCoA in comparison to WT CerS2 control (Figure 5.2 G). Based on these results we conclude that the deletion (aa 79-120) within the homeodomain of the CerS2 peptide sequence and its minor effects on the catalytic activity allow the investigation of the possible function of the homeodomain *in vivo*.

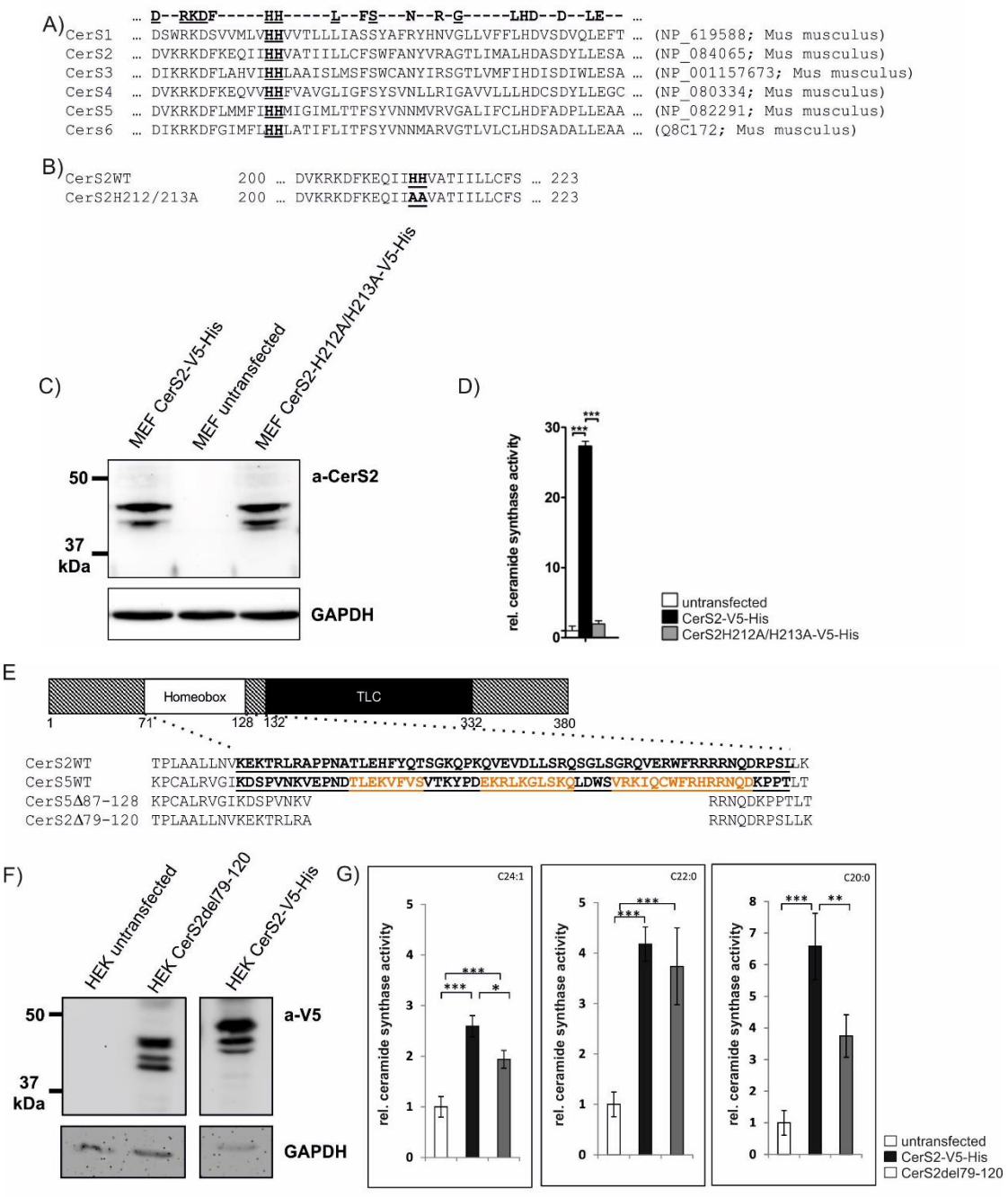


**Figure 5.2: Analysis of ceramide synthase activity *in vitro*. (A)** ClustalO alignment results. Alignment of all mouse CerS indicate high conservation of histidine residues within the putative active centre. **(B)** Amino acid modifications introduced into the Lag1 domain of the mouse CerS2 protein. Two consecutive histidine residues were replaced by two alanine residues at position 212 and 213. Mutations were introduced by mutagenesis PCR. **(C)** Immunoblot analysis of crude cell lysates with an anti-CerS2 antibody. MEF$^{gt/gt}$, were either not or transiently transfected with CerS2 WT (49.9 kDa) or CerS2H212A/H213A mutant constructs, both C-terminally V5 and His tagged (49.7 kDa). GAPDH served as a loading control. **(D)** NBD-dihydroceramide synthase activity assay using NBD-sphinganine and C24:1-acyl-CoA as substrates. Densitometric analysis was performed after lipid extraction and separation by thin layer chromatography. **(E)** Schematic representation of predicted domains in mCerS2 (according to swissprot). ClustalO alignment result of the amino acids sequence of the HOX motif present in CerS5 and CerS2. Underlined amino acids highlight homeodomain; bold-colored faces depict putative alpha helices (according to UniProt blast analysis and protein sequence alignments). **(F)** Immunoblot analysis of control and transiently transfected HEK cells. Proteins were detected with anti-V5 antibody, GAPDH served as the loading control. **(G)** Quantitative analysis of NBD-ceramide synthase activity performed with different acyl-CoAs as substrates. **(D/G)** Data are means ± SEM; n=2-3 (D), n=3-6 (G); unpaired t-test, *P<.05; **P<.01; ***P<.001. (Data of panel C/D and F/G(C24:1) were already published in Bickert et al., 2018.)

### 5.1.3 Identification of glycosylation sites

Based on the previously performed bioinformatic analyses a CerS2-N19Q- protein construct was additionally generated aimed to verify if the glycosylation itself influences catalytic activity. First, transient transfection of the CerS2-WT (control), CerS2H212/213A and CerS2Del79-120 construct was performed in primary MEFs. Protein lysates of transfected cells were generated 24 h after transfection and subsequently analysed via immunoblot analyses with or without treatment of PNGAseF (Figure 5.3 B). Here we could show that both modified CerS2 proteins (H/A and Del) were glycosylated, which results in a band shift after incubation with the amidase (Figure 5.3 B). Transfection of HEK cells with the CerS2N19Q construct results in the generation of a CerS2 protein with lower kDa mass (appr. 44 kDa) in comparison to the CerS2-WT control (appr. 49.9 kDa; Figure 5.3 C). Additionally, activity assays performed with protein lysates of CerS2-N/Q or WT transfected cells indicate that the presence or absence of the glycosylation does not negatively influence catalytic activity (Figure 5.3 C and D).

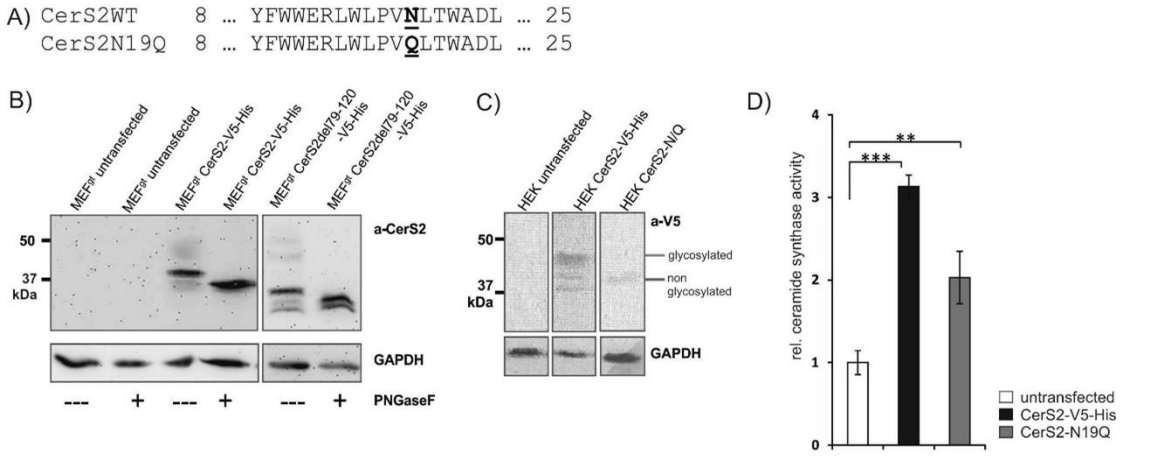


**Figure 5.3: Glycosylation studies of ceramide synthase 2**. **(A)** Shown is the N-terminal sequence section from amino acid 8 to 25 of CerS2 wild type and N-glycosylation site modified CerS2. **(B)** Verification of glycosylation. Crude lysates of MEF$^{gt/gt}$ transfected cells were incubated ± PNGaseF and analysed via immunoblot analyses performed with anti-CerS2. GAPDH served as a loading control. **(C)** Immunoblot analysis of transfected HEK cells with CerS2N/Q construct. Transfection efficiency was verified anti-V5 staining. GAPDH served as a loading control. **(D)** Quantitative analysis of [$^3$H]-sphinganine/ ceramide synthase assay performed with 25µg protein extract from transfected HEK cells. Data are means ±SEM; n=3 (CerS2-V5-His control), *n=2* (CerS2N/Q-V5-His).**, p<0.01; ***, p<0.001.

## 5.2 Generation of two conditional CerS2 gene targeting constructs (H212A/H213A and Del79-120) requires a number of cloning steps

The second part of the thesis focuses on the generation of two conditional mouse lines. Two *cers2*-gene-targeting-vector constructs were designed and generated for homologous recombination in ES cells. Blastocyst injection results in the generation of chimeric mice, which serve as the basis for the generation of new transgenic mouse lines.

### 5.2.1 Bacterial artificial chromosome (BACs)

The generation of the *cers2* gene targeting constructs requires the presence of long homology arms flanking both sides of the mutated sequence for correct homologous recombination in ES cells. The commercially available BMQ 325-K4, BAC (Source BioScience) should contain the genomic locus of *cers2,* needed for recombination, which was verified via Southern Blot analysis.

#### 5.2.1.1 Southern Blot analysis of the *cers2*-BAC and probe generation

Southern blot probes were amplified by PCR with specific primers based on template DNA (WT) extracted from mouse liver (C57BL/6N). The generated 5' probe (5' SB BAC for/ 5' SB BAC rev) has a size of 477 bp and binds within the first intron. The generated 3' probe (3'SB BAC for/ 3'SB BAC rev) has a size of 415 bp and covers exon10 as well as a part of the downstream and upstream intron sequence (Figure 5.4 A). Next, the *cers2*-containing BAC was extracted from an overnight culture and 2 µg BAC DNA was either digested with HindIII, EcoRV or BglII respectively. Digested DNA was separated on an agarose gel, blotted onto Hybond-N membrane and cross-linked. Next, labelling of probes, hybridisation, and detection of labelled DNA fragments was prepared. Finally, the verification of the expected band sizes after restriction and separation on an agarose gel showed that the BAC (BMQ 325-K4) contains the coding region of the *cers2* gene (Figure 5.4 B). Meaning, the 5' probe detects the expected fragments at 3.4 kb upon HindIII digestion and the bigger 7.4 kb fragment, which covers the 5' region of the *cers2* gene (Figure 5.4 B). On the other hand, analyses performed with the 3' probe after BglII restriction results in the detection of a 6.3 kb fragment as expected (E2-E11/3'UTR; Figure 5.4 B). The 3' probe allows also the detection of a 5 kb fragments, which covers the middle part of the genomic sequence of *cers2* and show partial overlap with the bigger fragment detected with the 5' probe. Based on these findings we conclude that the BAC could be used for further cloning steps and the recombination step to integrate the large 5'UTR region into the gene targeting vector.

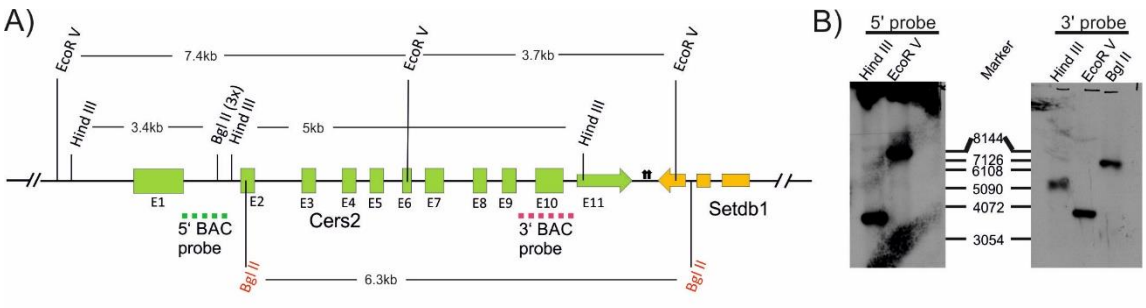


**Figure 5.4: DIG Southern Blot analysis of CerS2-BAC. (A)** Schematic representation of the genomic *cers2* locus. Restriction and binding sites of BAC-probes and the expected fragment sizes are highlighted. **(B)** Autoradiograms of DIG Southern Blot analysis.

### 5.2.2 Generation of the conditional CerS2H212A/H213A vector

The generation of the conditional gene-targeting vector was done with the aid of different expression vectors and *cers2* DNA fragments amplified from the BAC clone. Initially, two plasmids were generated in nine steps (1-6, 7-9) and combined in a final ligation step (10) (Figure 5.5). Finally, the generated vector should introduce two mutations within the coding region of CerS2, which leads to the replacement of two histidine residues (aa 212 and 213) by two alanine residues in the protein sequence. Furthermore, the use of the endogenous promoter in combination with an IRES cassette results in the additional expression of a downstream eGFP- reporter protein.

1st step: (pCR2.1 TOPO:5'SOE):
The first step depicts the generation of the entry side for the 5' homology region needed for the recombineering step.

2ndstep: (dual loxP/frt-Neo:5'SOE):
The 5'HR-SOE fragment was then inserted into the dual loxP/frt-Neo vector, upstream of the neomycin resistance cassette.

3rd step: Truncation of Ampicillin resistance gene:
Next, the ampicillin resistance gene was truncated, which was necessary for further selection steps of positive clones.

4th step: (5'SOE-frt-Neo_ΔAmp:E3-11 genomic sequence):
In the next step, the genomic sequence of exon three to eleven (E3-11 wt) was subcloned by compatible end ligation (MfeI, EcoRI) between the loxP and frt site upstream of the neomycin cassette.

5th step: (E3-11wt-frt-Neo_ΔAmp:E3-11 H/A):
Next, the H212/213A fragment was generated and inserted between the loxP and frt site downstream of the Neo cassette by PspOMI/NotI compatible end cloning.

6th step: Recombineering of the 5' homology region (5'HR-Neo:CerS2):
After linearization of the frt_Neo_D Amp:CerS2-vector with AatII, the recombination procedure extended the 5' HR to its full length.

7th step: (pDTA:3'HR):
The 3' homologous region (3'HR) was amplified and subcloned into pDTA (diphtheria toxin A) containing vector.

8th step: (pBSK-IRES-eGFP:3'HR-pDTA):
The 3'HR-pDTA fragment was subcloned downstream of the IRES-eGFP cassette (IRES- internal ribosomal entry side, eGFP- enhanced green fluorescent protein).

9th step: (IRES-eGFP/3'HR-pDTA:frt-SOE):
The entry site for the 5'HR-Neo:CerS2 vector (Step 1-6) was generated and inserted upstream of the IRES-eGFP-3'HR-pDTA cassette. Additionally, the insertion leads to the desired deletion of a NotI restriction site.

10th step: (CerS2H212/213A vector):
The final step was initially designed as a recombineering step but did not result in the generation of any positive clone. Therefore we changed our strategy and performed a normal T4-DNA-ligase-mediated ligation, which results in the generation of the final CerS2H212A/H213A gene targeting vector (Figure 5.5).

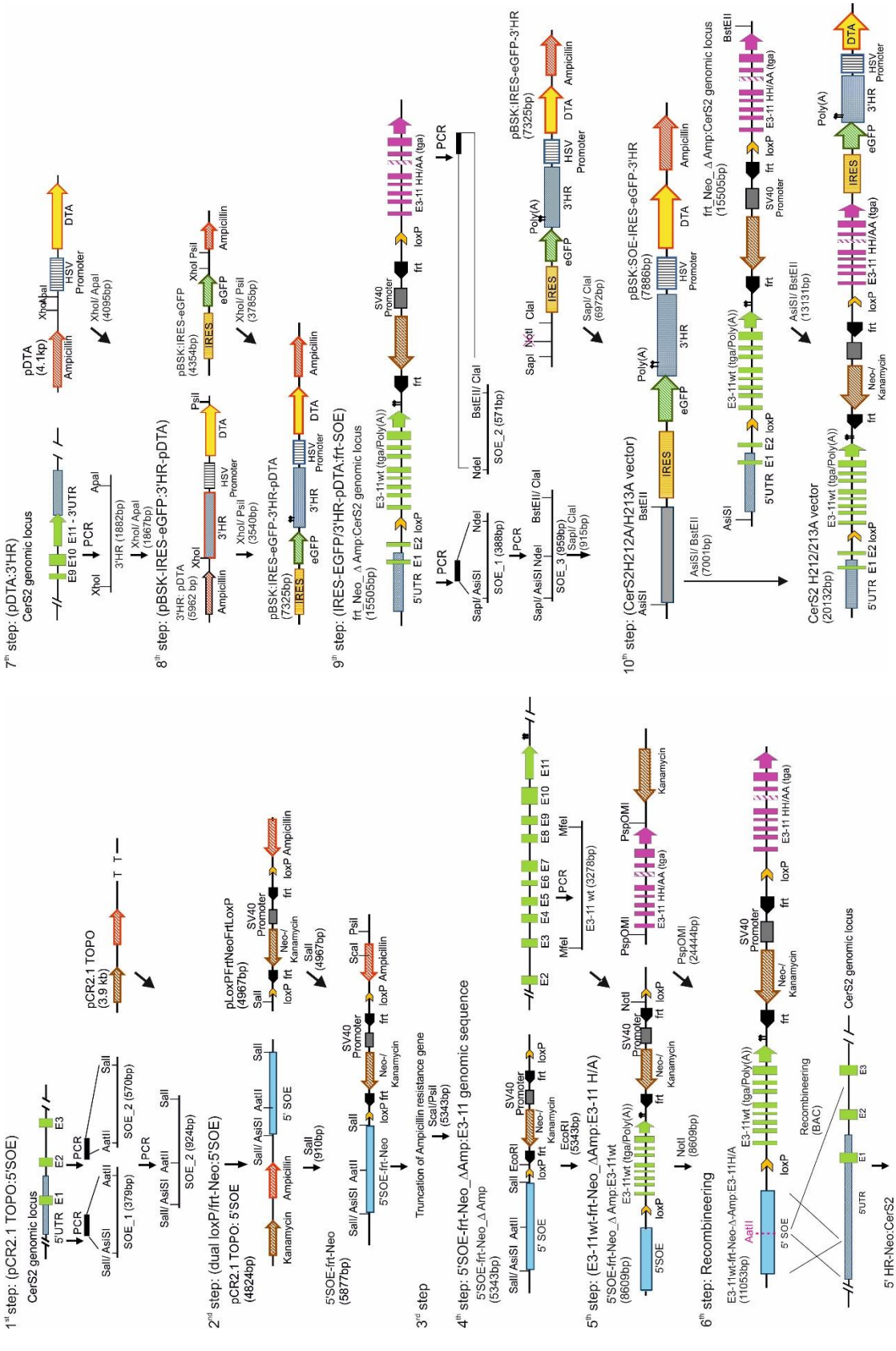


**Figure 5.5: Generation of the CerS2H212A/H213A gene targeting vector.** Graphical overview of the different cloning steps required for the generation of the CerS2 H/A gene targeting vector, which introduced a replacement of two consecutive histidine residues by two alanine residues at position 212 and 213 after homologous recombination.

### 5.2.3 Generation of the conditional CerS2Del79-120 vector

The generation of the conditional gene-targeting vector was completed on the basis of the CerS2H212/213A targeting vector and *cers2* DNA fragments amplified from the BAC clone (Figure 5.6). Finally, the final vector carries a deletion of amino acid 79 to amino acid 120 within the homeodomain of the CerS2 protein. With this approach, we attempted to generate a truncated CerS2 protein, which should be not affected in its catalytic activity (Figure 5.6).

1st step: (TOPO blunt: E3-11, Δaa79-120)
First exons 3 to 11 were amplified and amino acid residues 79 to 120 deleted in a two-step mutagenesis PCR.

2nd step: (dual loxP/frt-Neo: E3-11, Δaa79-120)
The truncated coding from step one was cloned into the dual loxP/frt- Neo vector by compatible end cloning (NotI/PspOMI).

3rd step: (CerS2Del79-120 vector)
The mutated sequence was inserted into the conditional CerS2H212A/H213A gene targeting vector. The insertion of the mutated E3-11,Δaa79-120 fragment leads to the replacement of the E3-11 H/A coding region. The CerS2Del79-120 gene-targeting vector represents the final vector.

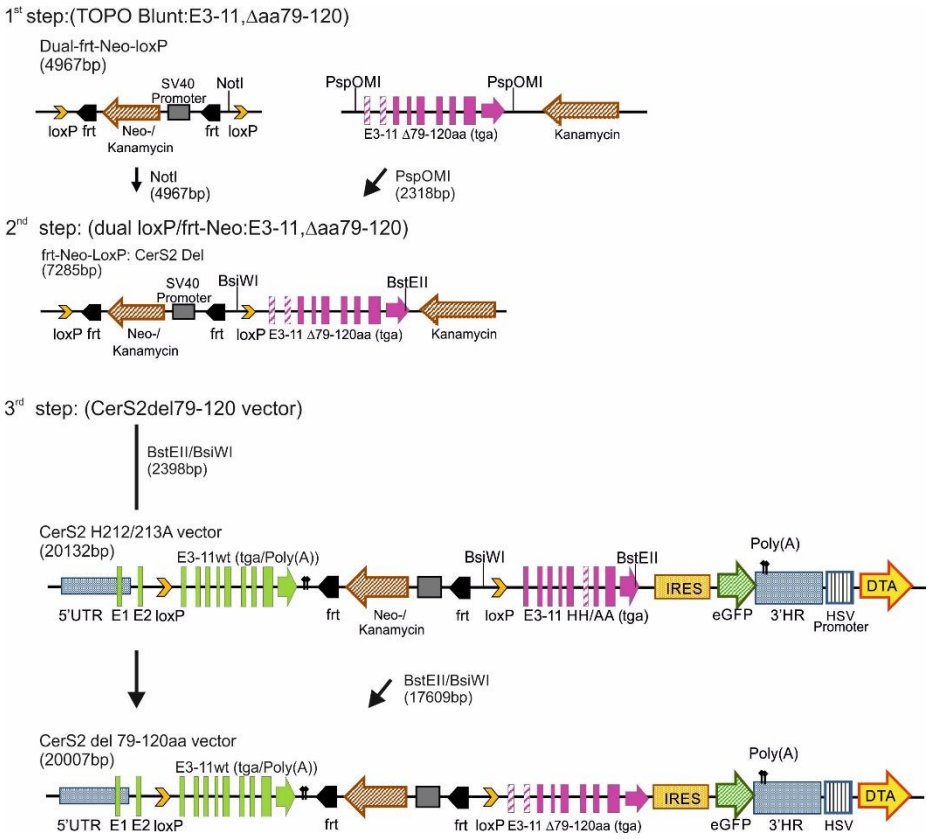


**Figure 5.6: Generation of the CerS2Del79-120 gene targeting vector.** The main cloning steps leading to the generation of the CerS2Del79-120 targeting vector are illustrated. The deletion of amino acids 79 to 120 results in the truncation of the homeodomain of the CerS2 protein sequence.

### 5.2.4 Analysis of the conditional gene targeting vector constructs

The integrity of each plasmid generated during the different cloning steps as well as the final conditional gene targeting constructs was verified by restriction digestion analysis followed by partial sequencing (GATC Biotech). The expected fragment sizes of both targeting constructs were confirmed after restriction analysis (Figure 5.7 A and B). Furthermore, verification by sequencing revealed the absence of undesirable mutations, which could lead to modifications of loxP and frt sites or to further modifications within the peptide sequence. Only one silent mutation within exon 4 (mutation: GGG→ GGA; Gly) was detected. Three further mutations had been detected within the sequence of different introns. Two were located in the 5$^{th}$ intron between exon 5 and 6 of the WT fragment and the last one in the 9$^{th}$ intron, between exon 9 and-E10 located in the H/A or Del fragment.

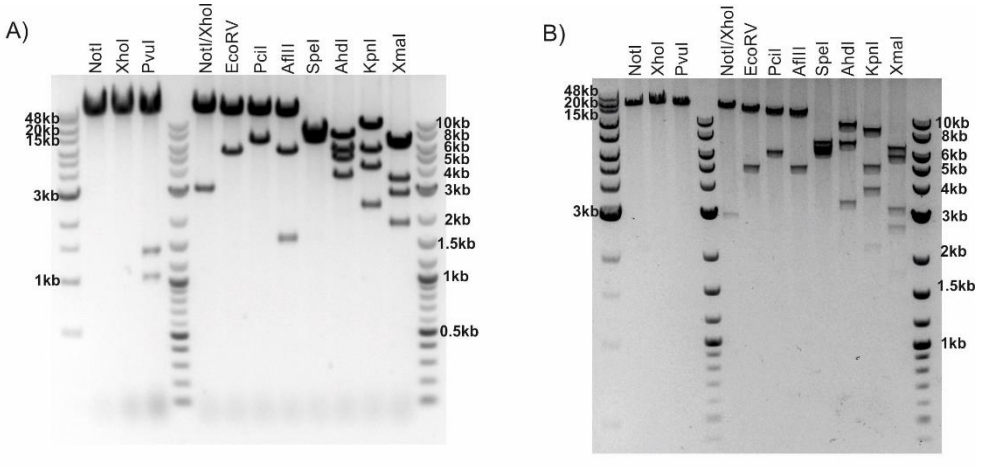


C)

| Enzyme | CerS2H212/213A vector | CerS2del79-120 vector |
|---|---|---|
| **NotI** | linearized (20.1kb) | linearized (20kb) |
| **XhoI** | linearized (20.1kb) | linearized (20kb) |
| **PvuI** | linearized (20.1kb) | linearized (20kb) |
| **NotI/XhoI** | 17.2/ 2.9 | 17.1/ 2.9 |
| **EcoRV** | 14.8/ 5.3 | 14.8/ 5.2 |
| **PciI** | 13.8/ 6.3 | 13.7/ 6.3 |
| **AflII** | 13.3/ 5.3/ 1.5 | 13.4/ 5.1/ 1.5 |
| **SpeI** | 7.2/ 6.6/ 6.3 | 7.2/ 6.5/ 6.3 |
| **AhdI** | 7.0/ 5.3/ 4.4/ 3.4 | 9.6/ 7.0/ 3.4 |
| **KpnI** | 8.7/ 5.3/ 3.9/ 2.2 | 8.7/ 5.2/ 3.9/ 2.2 |
| **XmaI** | 6.6/ 5.9/ 3.2/ 2.6/ 1.8 | 6.6/ 5.9/ 3.1/ 2.6/ 1.8 |

**Figure 5.7: Agarose gel electrophoresis of the targeting vectors digested by restriction enzymes. (A)** Analysis of the CerS2H212A/H213A vector. **(B)** Analysis of the CerS2Del79-120 vector. All fragments show the expected size. **(C)** Overview of fragments resulting from the application of different restriction enzymes.

Finally, the obtained results verify the accurate generation of the CerS2 H212A/H213A vector, containing a homologous region at the 5' end (5'HR) followed by a loxP site and the genomic sequence of exon 3 to 11. Furthermore, an frt-flanked neomycin resistance gene followed by the 3'located second loxP site, the H212A/H213A mutation fragment, a downstream IRES-driven eGFP reporter and the 3'HR-DTA selection cassette. On the other hand, the restriction and sequencing results also indicate the correct generation of the CerS2Del79-120 vector which enclosed also the 5'HR, the 5'loxP the genomic region of E3 to 11, the Neo-cassette, the 3'loxP followed by the E3 to 11, Δaa79-120 fragment, followed by an IRES-eGFP cassette, the 3'HR, and DTA selection cassette.

## 5.3 Generation and analysis of targeted mutations after homologous recombination in ES cell clones

### 5.3.1 Set up of sensitive PCR for verification of homologous recombination

The generation of different PCR-test constructs beforehand was necessary to ensure fast and reliable PCR-based analyses of correct homologous recombination of stable transfected ES cell clones (Figure 5.8).

First, a 3'HR test vector, which contains additionally 520 bp upstream of the 3'homologous region in comparison to both conditional constructs, was generated. A highly sensitive PCR was established and showed the expected results, even if only 100 fg genomic DNA was present in the reaction mixture (3'ctrl for and 3'ctrl rev). Here, correct 3' homologous recombination leads to the generation of a fragment of 1.9 kb (Figure 5.8 A). Next, the final CerS2H212A/H213A-vector was used for the generation of a second PCR to further verify correct 5' homologous recombination of the construct (HA_loxP_2_for and HA_loxP_1_rev; Figure 5.8 B). The test PCR showed the expected fragment sizes, which should be detected after homologous recombination in a heterozygous *cers2*$^{H212A/H213A}$ or *cers2*$^{Del79-120}$ background (WT, 466bp; H/A or Del 548bp).

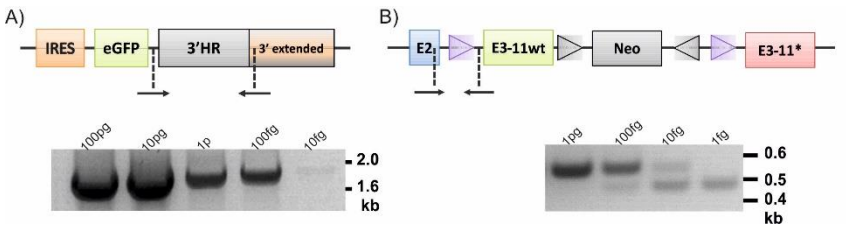


**Figure 5.8: ES cell clone test PCR. (A)** Schematic representation of the 3'HR-control vector used for the development of the 3'HR test PCR. Primer binding sites were depicted as arrows. Prolonged 3' region shown in orange. The grey fragment depicts the 3' homology region used as the template. **(lower section)** PCR results for the amplification of the desired fragment of 1.9 kb. A highly sensitive primer pair detects and amplifies fragments down to 100fg DNA in the reaction mixture. **(B)** Schematic representation of the internal 5' region from the gene targeting constructs used for modification in ES cells. Primer binding sites were depicted as arrows (loxP PCR). **(lower section)** PCR results based on the amplification of the loxP site containing fragments of the mutated allele. PCR primer show high sensitivity even with low amounts of DNA in the reaction mixture (WT: 466bp; H/A or Del: 584bp).

### 5.3.2 Generation and analysis of targeted HMI ES cells reveal the presence of several positive ES cell clones

The generation of genetically modified HMI ES cell clones began with an electroporation step. Therefore, both gene targeting vector constructs were linearized by NotI restriction and 350 µg of linearized DNA was electroporated into the HMI ES cell line. Next, the homologous recombination of the negative diphtheria toxin A (DTA) selection cassette outside of the 3' homology region results in cell death, which minimizes the amount of false positive ES cell clones. Furthermore, the application of G-418 supplemented ES cell medium during the first ten days of cultivation further reduces the number of false positive clones. Afterwards, growing ES cell clones were picked as described (see Chapter 4.3.5.5) and analysed by 3'HR-ctrl PCR (3'ctrl for and 3'ctrl rev). Correct 3' homologous recombination was accompanied by the amplification of a 1.9 kb fragment and relevant ES cell clones were further expanded (Figure 5.9 A). In the next step, ES cell clones were analysed by PCR, regarding the correct homologous recombination of the 5' region of the construct (loxP PCR and 5'HR PCR, Figure 5.9 A). Finally, 50 out of 364 analysed ES cell clones were positively tested for stable 5' and 3' integration of

the CerS2H212A/H213A construct on one allele of the *cers2* gene. For the second cell line, 550 ES cell clones were picked, which may have integrated the CerS2Del79-120 mutation into their genome. Here, 33 ES cell clones could be identified by 3' and 5' HR PCR analyses to be positive for correct recombination of the construct (Figure 5.9 B). Next, all positively tested ES cell clones were further expanded and subjected to Southern Blot hybridization analyses following karyotyping and blastocyst injection (Chapter 5.3.3 - 5.3.5).

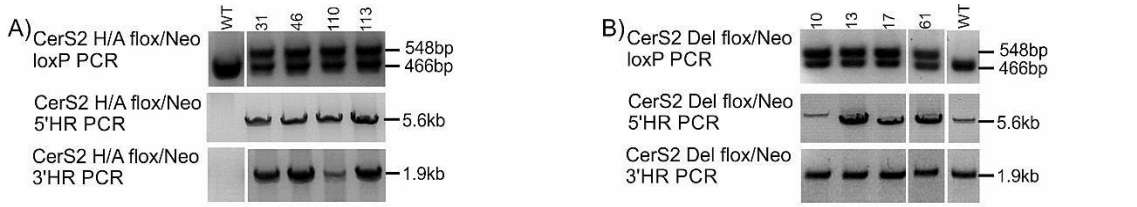


**Figure 5.9: PCR analysis of homologous recombination in ES cells. (A)** Verification of correct homologous recombination in ES cell clones of the CerS2H212A/H213A gene targeting vector. Shown are the PCR results for correct insertion of the 5' (loxP) and 3' end of the construct and the PCR results of the long amplification PCR of the external 5' region. **(B)** PCR analysis of homologous recombination of the CerS2Del79-120 construct in ES cells. 5'-loxP, 3' and 5' external long amplification PCR results are shown (Figure adopted and modified according to Bickert et al., 2018).

### 5.3.3 Southern Blot analysis lead to verification of positive ES cell clones

Briefly, positive selected ES cell clones were expanded and the genomic DNA extracted and digested with EcoRV (Figure 5.10 A). Resulting fragments were separated corresponding to their size by agarose gel electrophoresis, transferred and immobilized on a membrane. Hybridization with radioactively labelled *cers2* internal 3' probes was done as described (see Chapter 4.6). For the CerS2 H212A/H213A ES cell clones, a fragment of approximately 3.7 kb was detected as expected and represents the wild type allele (Figure 5.10 B). Next, correct homologous recombination results in the generation of a heterozygous background, which lead to the presence of two bands with almost the same size (EcoRV: 5.1/ 5.2 kb; Figure 5.10 B). These bands were detectable in all analysed ES cell clones and not present in the WT control as expected. Furthermore, heterozygous ES cell clones carrying one mutated *cers2*$^{Del79\text{-}120}$ allele were characterized by the presence of the *cers2* WT band at 3.7 kb and two bands at approximately 5.1 kb (Figure 5.10 A). The autoradiogram reveal that almost all analysed ES cell clones show the presence of the expected fragment sizes (Figure 5.10 C). Clone 129 showed only one weak signals for the wild type fragment and no signal for the mutated allele and was therefore not further analysed. The same situation was observed for clone 170 and 204. Here, only a weak signal for the mutated allele was detectable whereas the wild type signal was under the detection limit. Additionally, for clone 123 and 129 a bigger band at approximately 7 kb was detected, which indicate failures in homologous recombination and those were discarded.

Multiple insertions or integration at the wrong locus were further verified by the application of a second internal probe (Figure 5.11 A-C). Genomic DNA was either digested with EcoRV (CerS2H/A) or PsiI (CerS2Del). Correct homologous recombination results in the detection of either a 5.1 kb fragment (CerS2H/A, Figure 5.11 B) or a 20.8 kb fragment (CerS2Del, Figure 5.11 C). The GFP probe does not bind within the WT allele. The autoradiogram of *cers2H/A*-mutated ES cell clones showed no indication of the appearance of additional bands, pointing out to successful homologous recombination. The same was verified for *cers2Del*-mutated ES cell clones. No additional bands were detected in every examined sample, except the expected at

20.7 kb (Figure 5.11 C). However, Southern Blot hybridisation with the internal GFP probe rather implicates the absence of a detection signal for clone 53, 92, 123 and 204. Those were not further analysed by karyotyping analysis nor used for blastocyst injection.

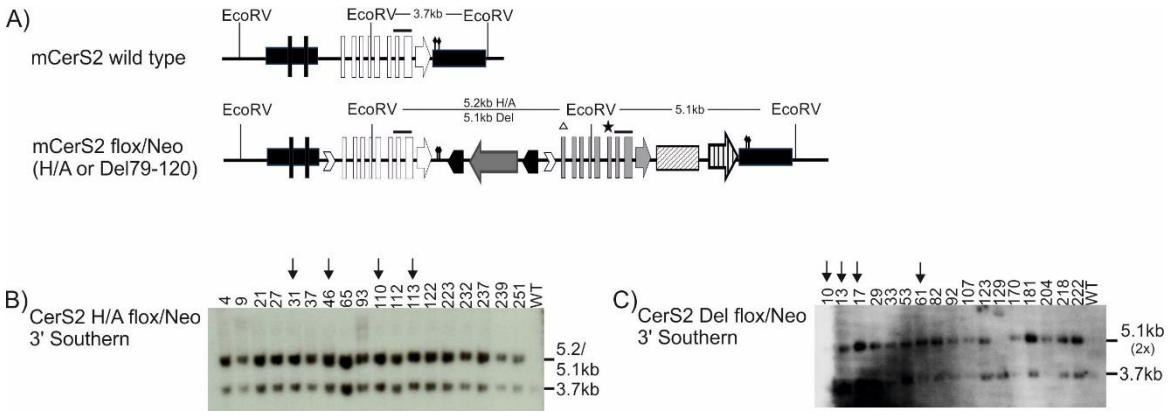


**Figure 5.10: Southern Blot analysis of homologous recombination in ES cell clones (I). (A)** Graphical overview of the Southern Blot strategy used for the verification of correct homologous recombination in ES cell clones. Internal 3'probes (black bar) as well as the resulting fragment sizes after EcoRV restriction are indicated. **(B/C)** Autoradiogram results from SB analysis of indicated ES cell clones. Genomic DNA was digested with EcoRV. The WT allele showed an expected band at 3.7 kb. After recombination, we verified two bands for each targeting construct either at 5.1/5.2 kb (CerS2H212A/H213A) or 2x 5.1 kb for the CerS2Del79-120 mutation. Results were partially published in Bickert et al., 2018.

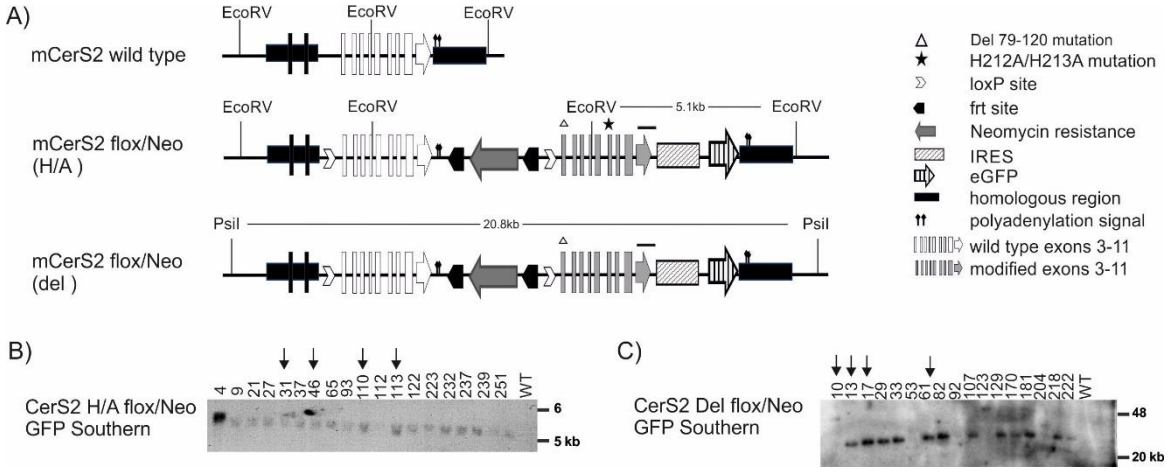


**Figure 5.11: Southern Blot analysis of homologous recombination in ES cell clones (II). (A)** Graphical overview of the strategy used for the verification of correct homologous recombination in ES cell clones. Internal 3' GFP-probe (black bar), as well as the resulting fragment sizes after EcoRV or PSiI restriction, are indicated. **(B/C)** Autoradiogram results from SB analysis of indicated ES cell clones. Genomic DNA was digested with EcoRV. The WT allele showed no band as expected. After recombination we verified one band for each targeting construct either at 5.1 kb (CerS2H212/213A) or 20.8 kb for the CerS2Del79-120 mutation respectively. Results were partially published in Bickert et al., 2018.

### 5.3.4 Southern Blot analysis with external probes causes unexpected problems

Initially, genomic DNA was digested with PsiI/BssSI and subjected to Southern Blot hybridisation. Due to unexpected problems with the 5' external probes (high GC-content), which showed no results either generated by PCR or by restriction digestion, we changed our strategy. Verification of correct 5' insertion of the construct was done by a long PCR

amplification approach (Figure 5.9). Briefly, the upstream primer (5'ctrl for) binding site is outside of the construct whereas the downstream primer (5'ctrl rev) binds within the gene targeting locus. As expected, all examined ES cell clones either from the CerS2H212A/H213A or the CerS2Del79-120 line showed one specific band at 5.6 kb (5'HR PCR) confirming the correct insertion of the 5' region at the desired genomic locus (Figure 5.9).

In summary, 12 of 364 analysed ES cell clones (3.29 %) were positively tested for the correct homologous recombination of the CerS2H212A/H213A construct. Additionally, 13 out of 550 ES cell clones (2.36 %) analysed by Southern Blot hybridisation exhibit also the correct integration of CerS2Del79-120 construct.

### 5.3.5 Karyotyping of CerS2H212A/H213A or CerS2Del79-120 ES cells

ES cell clones positive for one of the mutated alleles were subjected to karyotype analysis in order to detect chromosomal abnormalities. Here we focussed on numerical changes and analysed whether the correct number of chromosomes is present after recombination events.

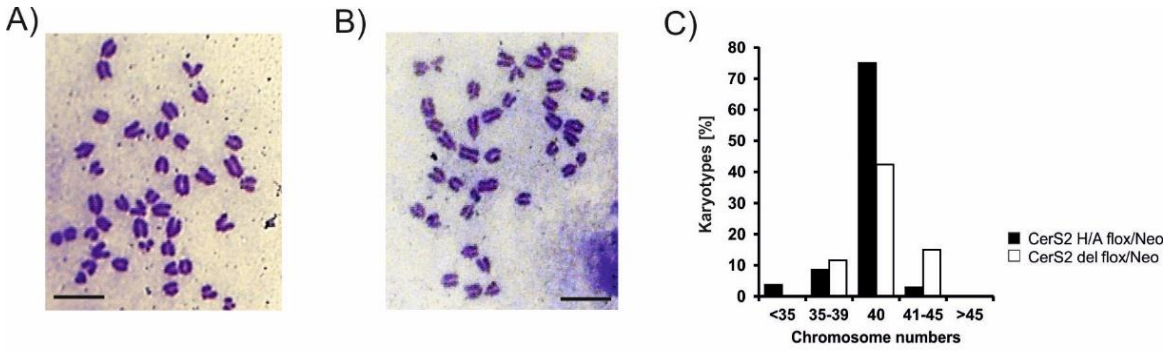


**Figure 5.12: Verification of karyotypes. (A)** Chromosome spread from ES cell clone #110 (CerS2H/A flox/Neo). **(B)** Chromosome spread of clone #13 from CerS2Del ES cell line. **(C)** Shown are the mean values of spreads counted for each ES cell clone. 25 spreads per CerS2H/A ES cell clone (n=3) were counted. 28 spreads per CerS2Del ES cell clone (n=3) were counted. Condensed chromatin stained with Giemsa solution. Bar, 10 µm.

Cells were arrested in the metaphase of mitosis after application of colcemid. Highly condensed chromosomes were stained with Giemsa solution and slides analysed by light microscopy (Figure 5.12 A and B). At least 20 spreads per sample (ES cell clone) were counted and the mean calculated. Figure 5.12 (A-B) demonstrate two representative pictures of metaphase spreads, one from each clone subjected to blastocyst injection. The graph depicts the summary of counted spreads from all analysed ES cell clones. Each column indicates the percentages of counted chromosomes (Figure 5.12 C).
Finally, ES cell clone number 31, 46, 110 and 113 positive for the CerS2H212/213A allele displayed the expected number of 40 chromosomes. For the Del79-120 mutation, clone numbers 10, 13, 17 and 61 showed the correct number of 40 chromosomes.

## 5.4 Analysis and characterization of the conditional mouse lines

### 5.4.1 Generation and breeding of mice with mutated *cers2* alleles

ES cell clones (Sv129P2/OlaHsd), positively tested for the homologous integration of the CerS2H212A/H231A allele or the CerS2Del79-120 allele, were subjected to blastocyst injection (C57BL/6NCrl, done by W. Krzyzak; LIMES-GRC). Resulting chimeric male mice were bred with C57BL6/NCrl mice at the age of seven weeks (Figure 5.13). Germline transmission was successful when agouti colored offspring was born (Figure 5.13 B).

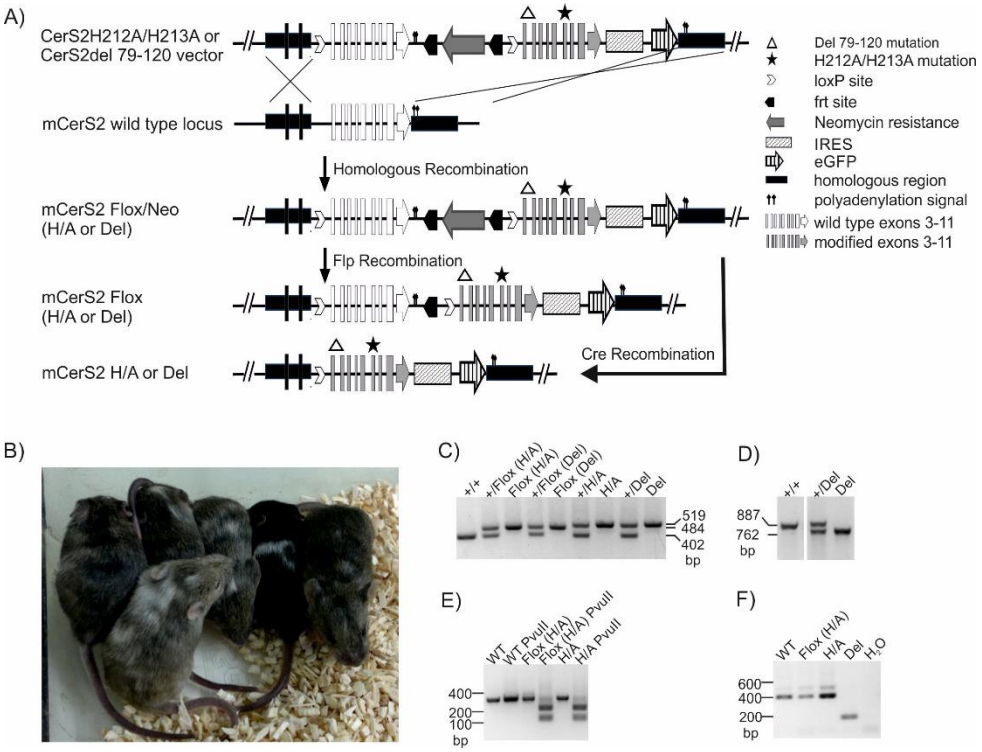


**Figure 5.13: Generation and analysis of CerS2 conditional mice. (A)** Schematic representation of the homologous recombination strategy in ES cells for the conditional CerS2H212A/H213A and CerS2Del79-120 construct. Flp and Cre-recombination results in the deletion of frt-sites or loxP-site flanked regions after breeding with the desired mouse line. Flp-recombination leads to deletion of internal neo selection cassette. Cre-mediated recombination leads to deletion of the wt fragment of the *cers*2 gene with neo cassette and thereby to the expression of mutated CerS2 allele in the desired tissue. **(B)** Chimeric mice resulting from blastocyst injection. **(C)** Genotyping analysis. Tail tip gDNA from WT, heterozygous and homozygous mice was analysed in a two primer-based PCR to verify the presence of the 5'loxp site. Expected fragment sizes: WT- 402 bp; Flox- 484 bp; H/A- and Del- 519 bp. **(D)** Validation of the 79-120 deletion on the genomic level. Expected fragment sizes: WT- 887 bp; deletion- 762 bp. **(E)** Validation of H/A Mutation. PCR analysis on genomic DNA extracted from mouse liver, following PvuII restriction of amplified fragments. Expected fragments: PCR amplicon 343 bp; after PvuII digestion 222 bp and 121 bp. **(F)** PCR verification of deletion on cDNA level. Expected fragments sizes: WT, Flox (H/A), 424 bp; Del, 298 bp. Resulting fragment size for Del mutation was about 188 bp (Figure adopted and modified from Bickert et al., 2018).

The graphical overview of the homologous recombination of the wild type locus by the *cers2* gene targeting constructs in ES cells is shown in Figure 5.13 A. Initially, breedings of chimeric mice with deleter-Flp mice, lead to the deletion of the neomycin resistance cassette, which might influence the transcription of neighbouring loci (Olson et al., 1996). The resulting Flox-

mice (Flox) represents, on the one hand, the basis of further conditional mice, where the H/A and Del mutation can be expressed in a tissue-specific manner upon breeding with the appropriate Cre-mouse lines. It should be noted that the Flox mice express the endogenous *cers2* gene and serve as an additional control in in the following experiments. This was done in advance in case if the introduction of the targeting construct influences the expression level. In parallel, we set up breedings of heterozygous-chimeric mice with pgk-Cre-expressing mice. The Cre recombinase is under control of the ubiquitously expressed phosphoglycerate kinase 1 promoter (pgk), which results in the deletion of the loxP-flanked CerS2wt-neomycin cassette in every tissue. Finally, the CerS2H/A or CerS2Del mutation is expressed under the control of the endogenous CerS2 promoter. Furthermore, an eGFP reporter protein separated by an IRES cassette (internal ribosomal entry site) will be expressed simultaneously and also under the control of the endogenous *cers2* promoter.

For our experiments, we used homozygous animals generated from heterozygous breedings of three different mouse lines (Flox/+; H/A/+ and Del/+). With this approach, we obtained animals needed for our investigations, as well as littermate controls. First, homozygous wild type (WT) animals and Flox (CerS2:CerS2H/A) mice were used as controls. Second, homozygous CerS2H/A or Del mice were used to analyse the consequences of the targeted mutations.

Genotyping of all mice was done by PCR regarding the presence or absence of the 5' loxP site (Figure 5.13 C). Additionally, the desired mutations were easily verified by PCR analyses. First, the histidine to alanine point mutation at position 212 and 213 within the peptide sequence was designed in a way that an additional PvuII restriction site was created (Figure 5.13 E). After Nested-PCR amplification, the generated fragment (343 bp) for each sample was extracted from agarose gel and restricted with PvuII (done by A. Bickert). As indicated, the mutation leads to the generation of an additional PvuII restriction site and thereby to the generation of two smaller fragments after digestion (222 bp / 121 bp; Figure 5.13 E). Amplified WT-DNA was unsusceptible to digestion. Next, the verification of the deletion within the homeodomain of the *cers2* gene was based on the amplification of the corresponding cDNA (Figure 5.13 D and F). As the results indicate, the obtained fragment of approximately 188 bp was smaller than expected (298 bp). Additional sequencing analyses pointed out, that the genomic locus was modified as designed, where exon 3 and 4 are still present and that a complete loss of exon3 and exon4 occurs during transcription (sequence analysis of cDNA). Furthermore, the lack of the exon 3 and 4 in the transcribed mRNA results in the deletion of amino acids residues 59 to 137 within the peptide sequence. This, in turn, affects a much larger region of the homeodomain/ protein as it was designed (del 79-120, Figure A7). All these findings are also in contrast to those obtained in *in vitro* experiments (Chapter 5.1.2).

### 5.4.2 CerS2H212A/H213A and CerS2Del79-120 mice show an increased mortality rate

Usually, the offspring of heterozygous breedings segregates into the ratio of 1:2:1 (25%: 50%: 25%). Preliminary analyses regarding the Mendelian ratio gained from $CerS2^{(+/gt)}$ breedings indicated that the lack of CerS2 protein somehow alters the ratio of the expected phenotypes. This, in turn, lead to further analysis of littermates obtained from Flox, H/A and Del mice. The findings from more than 40 breedings of heterozygous Flox mice (+/Flox x +/Flox) show, that those were born according to the Mendelian ratio (Figure 5.14 A), although they show a reduction in *cers2*-mRNA level and protein expression (Figure 5.14 A/B). In contrast, results obtained from heterozygous H/A (+/HA x +/HA) breedings showed a strong reduction of the

expected homozygous CerS2H/A mice (Figure 5.14 A). Results obtained from CerS2Del mice were already published and not further investigated (Figure A8, Bicket et al., 2018). Moreover, re-evaluation of litter-parameter revealed that CerS2H/A and CerS2Del mice show an increased mortality and that the mice die immediately after birth or within the first 14 days after birth (Figure 5.14 B); indicating that the mutation (H/A) influences the life expectancy.

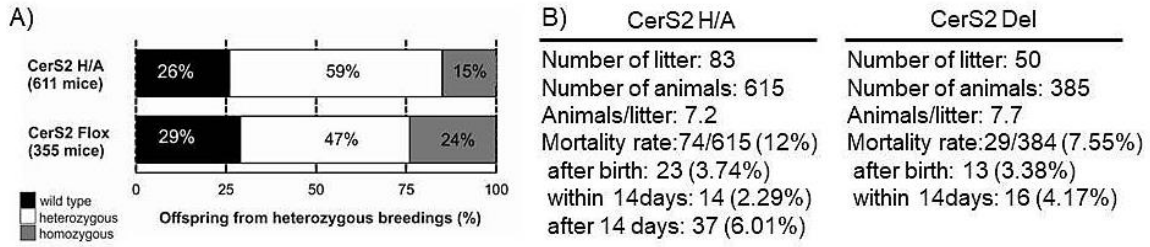


**Figure 5.14: Mendelian Ratio and mortality rate is altered in CerS2 mutated mice. (A)** Resulting percentage of offspring gained from heterozygous breedings of CerS2H/A and Flox mice. Total numbers of mice are shown in brackets. **(B)** Analysis of litter rate and corresponding mortality rate of CerS2H/A and -Del mice. Numbers were obtained from Mausoleum (software).

### 5.4.3 CerS2H212A/H213A and CerS2Del79-120 proteins were expressed to different extent in comparison to endogenous CerS2

The following experiments (section 5.5.3 – 5.5.4) summarize the first steps in the detailed analyses of the newly generated CerS2$^{H212A/H213A}$ and CerS2$^{Del79-120}$ mice. Parts of this experimental section were done in cooperation with Dr. A. Bickert and Dr. P. Kern, and were already published (Bickert et al., 2018). Here, only main findings are mentioned in the sake of completeness.

The CerS2 H212A/H213A and CerS2Del79-120 mutation constructs were designed in a way that the expression of each mutated CerS2 protein is characterized by the simultaneous expression of an enhanced GFP reporter protein under the control of the endogenous CerS2 promoter, which is facilitated by an IRES cassette.
Total protein extracts of liver, kidney, brain and five other tissues from CerS2-WT, -Flox, -H/A and CerS2Del mice were generated. The presence of the mutated CerS2 or GFP protein was determined by immunoblot analyses using the anti-CerS2 (Kremser et al. 2013) or the anti-GFP antibodies (Figure 5.15). For protein extracts from WT and Flox controls, a protein migrating at approximately 45 kDa was detected in all analysed tissues, displaying the expression of endogenous CerS2. Furthermore, strongest expression was detectable in liver, lung, and spleen (Figure 5.15 A; Figure A9). On the other hand, expression of mutated CerS2H/A protein (44.9 kDa) was also examined (Figure 5.15 A, Figure A9). However, protein expression levels of CerS2 from Flox and H/A mice were significantly reduced in liver, kidney and brain in comparison to WT control (Hsp90) (Figure 5.15 A). Furthermore, no Del79-120 protein was detectable under normal exposure conditions (Figure 5.15 A). More accurate analysis of quantitative mRNA expression revealed that the mutated CerS2-WT, -H/A and -Del transcripts were reduced to 50 % in Flox, H/A and Del mice (Figure 5.15 B). These findings are in line with the reduced protein levels found in Flox and H/A mice. Sequencing of *cers2*-Del cDNA

transcripts showed complete loss of exon 3 and 4 (data not shown), which would code for a protein lacking aa 59-137 (Figure A7).
Verification of eGFP expression showed the presence of the GFP-reporter protein in all analysed tissues from CerS2H/A and CerS2Del mice. This, in turn, implicates specificity of the anti-GFP antibody as no protein was detected in the WT and Flox control. Furthermore it supports also the assumption that the bicistronic transcripts were expressed to similar extent. Additionally, expression levels of CerS4, 5 and 6 were also verified, since it is suggested that they can compensate the lack of one CerS by up-regulation of another CerS (Figure 23, C). The analyses confirm increased expression levels of CerS5 and CerS6 in CerS2H/A and -Del mice in comparison to WT and Flox control. Moreover, in comparison to these findings, the expression level of CerS4 remains unaltered in the liver.

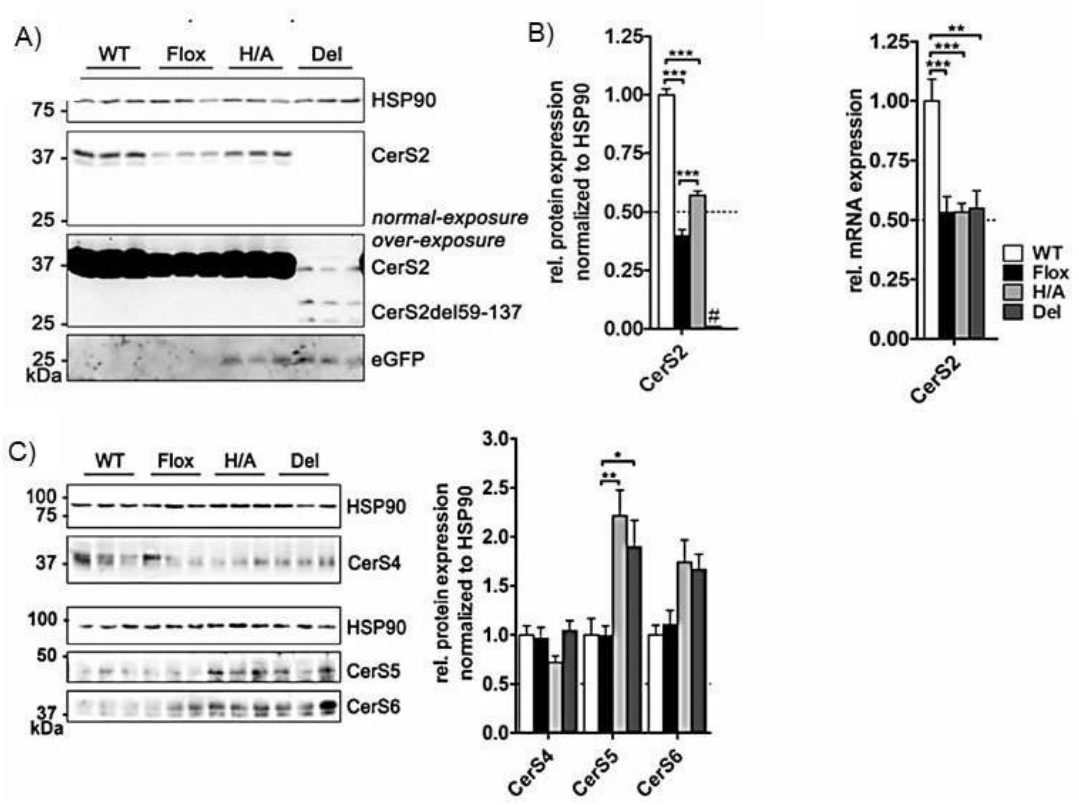


**Figure 5.15: Protein expression and mRNA level in mouse liver. (A)** Protein expression analyses of mutated CerS2 (H/A and Del 79-120) and GFP in Flox, H/A and Del mice. WT mice served as the control. Expression of wild type and modified CerS2 protein is lower in Flox and H/A mice in comparison to WT control. Very low CerS2 protein level were detectable in Del mice and appeared only after strong overexposure. HSP90 serve as loading control. The graph shows the densitometric analysis of CerS2 expression relative to WT control. **(B)** Quantitative RT-PCR analysis of CerS2 mRNA expression level. Data are mean values ± SEM (n= 5-6). **(C)** Immunoblot analysis of CerS4, 5 and 6 expression. HSP90 served as the loading control. Shown are relative expression levels in comparison to WT control. Data are means ± SEM; Quantification of A/C) was based on two individual experiments (n=6). Unpaired t-test, *P<.05; **P<.01; ***P<.001. (Data adopted and modified from Bickert et al., 2018).

### 5.4.4 Targeted mutations lead to loss of catalytic activity and an altered sphingolipid content in CerS2H212A/H213A (and Del79-120) mice

To prove that the catalytic activity is indeed lost in CerS2H/A mice and unaffected in CerS2Del mice, it was necessary to perform ceramide synthase activity assays *in vitro*. In line with the loss of protein in CerS2Del mice is the strong reduction of synthase activity, detected in liver extracts (Figure 5.16 A). Additionally, the H/A mutation leads to the desired loss of the catalytic activity, when liver protein extracts of mouse mutants were analysed. Reduction of CerS2 WT protein level in Flox mice results also in reduced ceramide synthase activity. Furthermore, activity assays performed with extracts from CerS2H/A and CerS2Del mice showed increased activity against C16 and C18 acyl-CoAs, due to elevated protein levels of CerS5 and CerS6 (Figure 5.16 B). Activity against C14 acyl-CoA remains unaltered (Figure 5.16 B).

Additional Mass Spectrometry analyses of liver lipids from CerS2-WT, -Flox, -H/A and -Del mice indicate that the reduction of CerS2 protein in the genetic background of Flox mice has no impact on the sphingolipid levels (Figure A10). On the other hand, the loss of catalytic activity and/or protein in CerS2H/A and CerS2Del mice results in the depletion of very long chain ceramides, hexosylceramides and sphingomyelin (C22-24) as expected (Figure A10). Additionally, the depletion of C22-24 sphingolipids was accompanied by a significant increase in C16 (C18)- sphingolipid species and an increase in sphinganine (d18:0) levels (Figure A10). Moreover, these obtained results from CerS2H/A and CerS2Del mice are in line with previous findings from CerS2$^{gt/gt}$ mice (Imgrund et al., 2009).

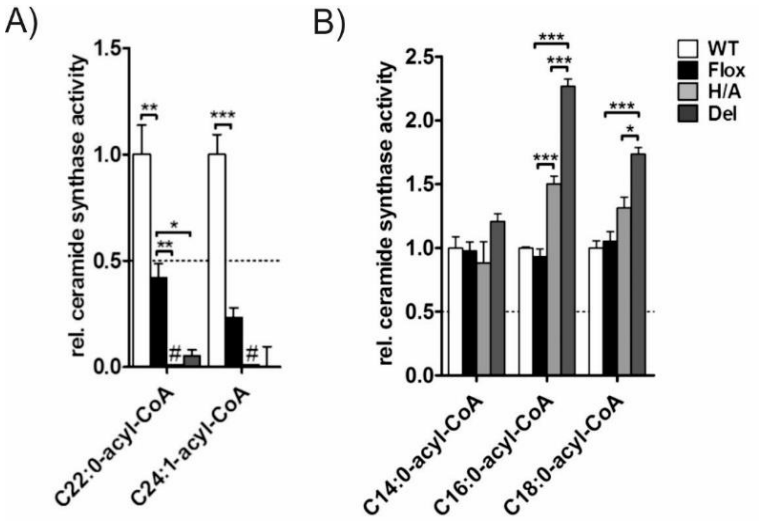


**Figure 5.16: Analysis of Ceramide synthase activity in liver. (A)** Quantitative analysis from NBD-sphinganine based ceramide synthase activity assay performed with C22:0 or C24:1 acyl-CoA. Lipids were separated and detected on TLC plate, after termination of the reaction. **(B)** Quantitative TLC results based on protein extracts incubated with [4,5- 3H] sphinganine in combination with either C14:0-, C16:0 or C18:0 acyl-CoA. Data are mean values (n=4, 3). Unpaired t-test, *P<.05; **<.01; ***P<.001 (Figure was taken from Bickert et al.,2018).

### 5.4.5 CerS2H212A/H213A and CerS2Del79-120 mice show altered transcriptome expression and reduced expression of genes involved in lipid metabolism

In order to gain more insights into the pathophysiological alterations of liver in CerS2H/A and CerS2Del mice, transcriptome analyses were performed by Oaklabs on 80x60K Mouse Array XS chips (Agilent technologies). Total RNA extracts from liver of CerS2WT, Flox, H/A and Del mice (n=4 animals per genotype) were prepared by A. Bickert. Further processing of raw data was done in cooperation with Prof. Dr. Joachim L. Schultze (Bickert et al., 2018). The primary focus on the bioinformatic results is based on differential expressed genes between CerS2Flox (control) and CerS2H/A mice. Here, 1464 genes were up- and 265 down-regulated (Figure 5.17 A and B). Additionally, differentially expressed genes were further analysed by Gene ontology (GO)-enrichment analysis, which allows clustering of genes in respect to cellular processes and molecular function they are involved in (Figure 5.17 C). The most prominent down-regulated genes belong to lipid metabolic processes, e.g. responsible for fatty acid synthesis (Figure 5.17 C). Furthermore, these results are in line with previously generated qRT-PCR analyses, which showed decreased expression of genes involved in fatty acid- synthesis, - elongation and –transport as well as TAG synthesis (Figure A11). Additional analyses of up-regulated genes showed over-representation of those related to cell division and DNA conformational changes (Figure 5.17 B and C).

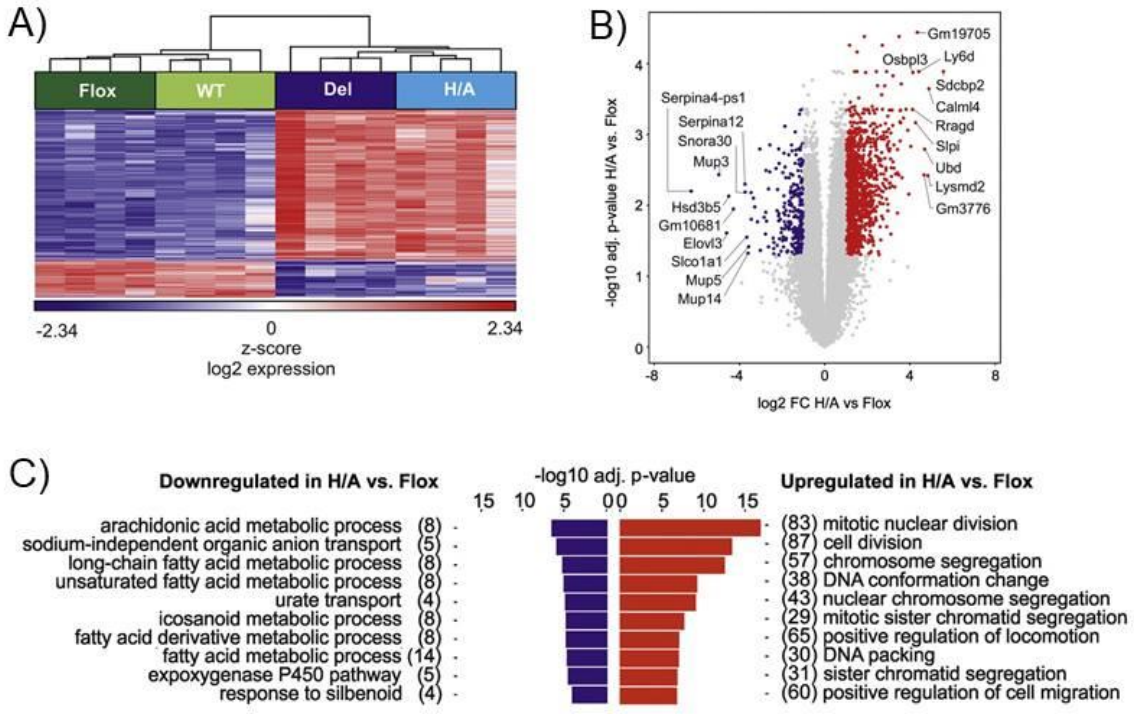


**Figure 5.17: Liver transcriptome analysis. (A)** Hierarchical clustering of the 1000 genes, showing highest differential expression within the data set. **(B)** Vulcano Plot depicts comparison of 10 most differential down (blue) or up-regulated (red) genes between CerS2H/A and Flox mice. **(C)** GO-enrichment analysis of differentially expressed genes derived from the comparison of CerS2H/A and Flox mice. Numbers in brackets refer to the amount of genes enriched per GO-term. Blue depicts down- and red bars up-regulated genes. (n=4 animals per genotype).(Figure adopted and modified from Bickert et al., 2018).

## 5.4.6 Energy metabolism

### 5.4.6.1 Body weight and food intake is altered in CerS2H212A/H213A mice

As it was discussed in the introduction (Chapter 1.6.1), CerS have been shown to be involved in the regulation of diet-induced obesity and their comorbidities. Moreover, recent findings suggest that the C16/C24 ceramide ratio could possibly serve as a new biomarker for the onset and progression of altered energy metabolism resulting in cardiovascular pathologies (Tippetts et al., 2018).

To investigate a possible role of CerS2 and its catalytically inactivation under normal feeding conditions, CerS2H/A mice were investigated regarding body weight increase and food intake (Figure . CerS2WT and CerS2H/A mice were fed a normal chow (16.9% protein, 4.3% fat and 4.3% fibres). Male mice, as well as female mice, were investigated separately to rule out sex-dependent alterations. Measurement of body weight started with eight weeks of age; was determined once a week and carried out for eight weeks. Determination of food and water intake was performed daily for a period of 14 days. To avoid biased results concerning the experimental conditions (e.g. social separation), animals were acclimated to individual cages for five days prior to the beginning of the experiment.

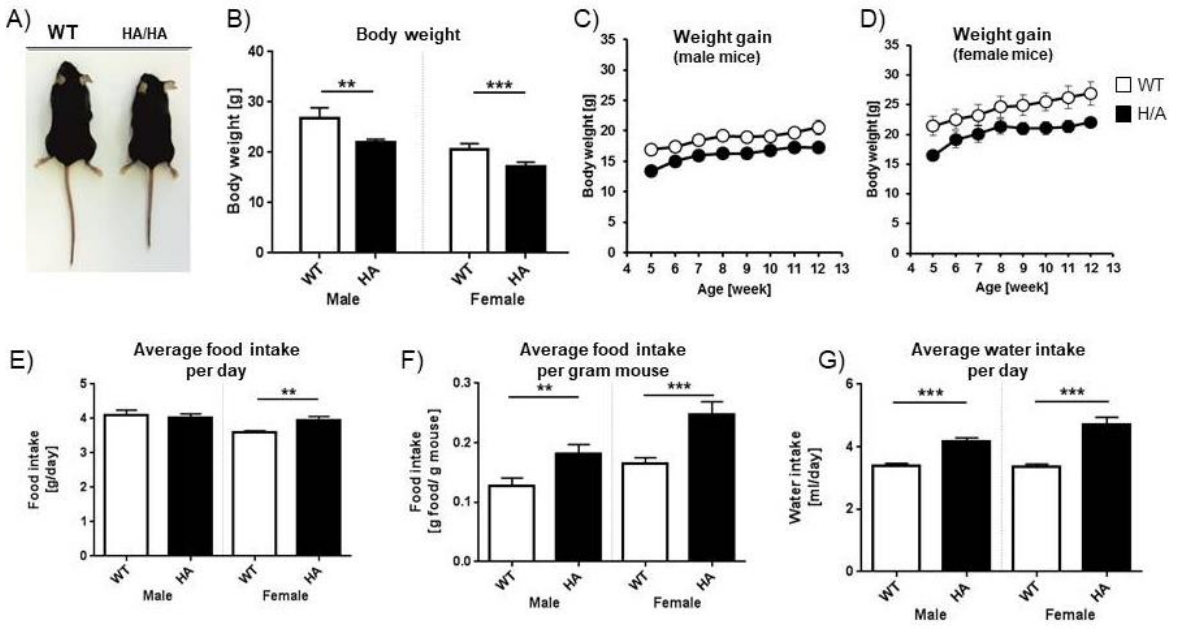


**Figure 5.18: Analyses of weight gain and food intake. (A)** Comparison of 12-week old WT and CerS2 H/A male mice. **(B)** Comparison of body weights from male and female mice. **(C/D)** Growth curve illustrating genotype-dependent differences in weight gain. Data were depicted as means (±SEM) of eight consecutive weeks, with three animals (n=3) per genotype and sex. **(E)** Average of food intake per day. **(F)** Average of food intake per gram mouse weight. **(G)** Average of water intake per day. **E/F/G**; Data were shown as means from individual experiments, means ±SEM; unpaired t-test; **P<.01; ***P<.001; WT, n= 3; H/A, n=3.

The obtained results reveal that CerS2 H/A male, as well as female mice, show significantly reduced body size and body weight (Figure 5.18 A and B). Moreover, both genders show reduced body weight gain in comparison to their WT littermates (Figure 5.18). These findings are in line with reduced body sizes of analysed CerS2H/A and CerS2Del mice, and correlate in some points also with decreased tissue weights (Figure A8 B and C). Determination of food intake (g/day) revealed no differences between CerS2H/A male mice and WT control group (Figure 5.18 E). This is in contrast to the observed results from female mice. Here, CerS2H/A

female mice eat significantly more than the WT animals (Figure 5.18 E). Based on significantly reduced body weights obtained from CerS2H/A mice, we also determined the amount of food intake per gram mouse (g food/ g mouse). The results indicate that male mice take up 36 % more food per gram body weight than the WT animals (Figure 25, F). The same results were obtained for female mice (H/A), which eat about 15 % more than the control group (Figure 5.18 F). Additional determination of water intake (ml/day) reveals also an increased consumption for CerS2H/A mice in comparison to WT mice (Figure 5.18 G).

### 5.4.6.2 Storage lipid content and composition is altered in mutated mice

Based on previous findings, e.g. altered food intake/water consumption of CerS2H/A mice, further investigations regarding the intestinal lipid absorption were performed. Additional analyses of the storage lipid content of liver, adipose tissue (WAT) and muscle were also done.

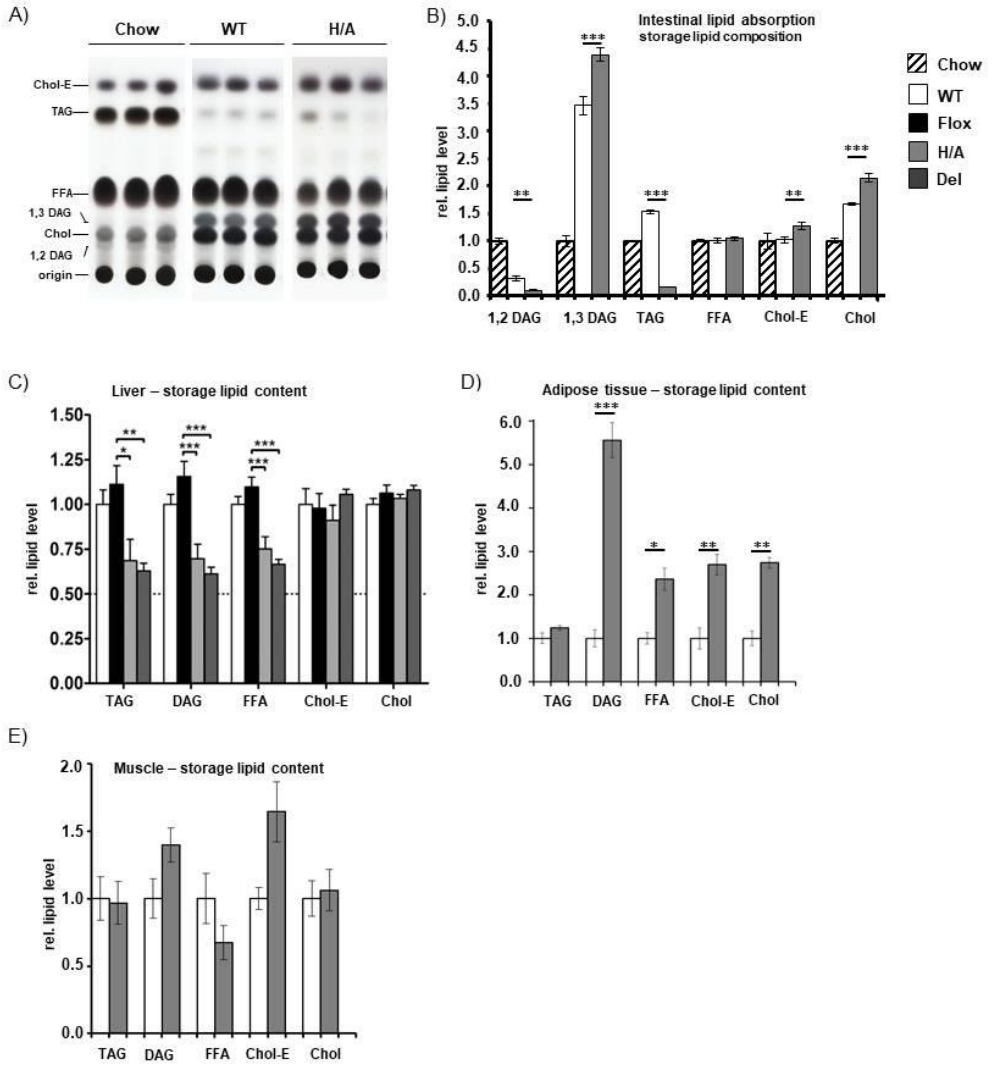


**Figure 5.19: Analyses of storage lipid contents. (A)** Representative thin layer chromatography analysis of lipid extracts generated from feces and normal chow diet. **(B)** Quantitative analysis of intestinal lipid absorption (WT, n=3; H/A, n=3). **(C)** Quantification of liver storage lipids (n=6 quantified from two individual TLC plates, Bickert et al., 2018). **(D)** Quantification results obtained from adipose tissue (WAT). **(E)** Relative storage lipid content in muscle extracts. B/D/E, Data are means ±SEM, unpaired t-test; *P.5; **P<.01; ***P<.001. ( C) taken from Bickert et al., 2018)

Feces of male mice were collected once a week during the period of food (water) intake measurements (n=3). Lipid extracts were generated as described and separated on TLC plates. Values were depicted as relative amounts in comparison to diet lipid content and indicate several differences between CerS2WT and H/A mice (Figure 5.19). Here, 1,3 DAG and TAG level of feces extracted from CerS2H/A mice were significantly reduced in comparison to their WT littermates (Figure 5.19 A and B). In contrast, 1,2 DAG level was elevated in CerS2H/A when compared to WT control. FFA levels remain unaltered between WT and H/A mice. Relative amounts of cholesterol-ester and cholesterol were increased in feces of CerS2H/A mice (Figure 5.19 A and B).
Next, in comparison and consistent with the decreased weight gain of CerS2H/A mice they also showed alterations in adipose tissue and liver storage lipid content (Figure 5.19 C and D). CerS2H/A mice exposed a strong decrease in TAG, DAG and FFA levels in liver. Cholesterol-ester and cholesterol level remain unaltered in liver of CerS2H/A mice (Figure 5.19 C). Investigation of adipose tissue showed, on the one hand, a strong reduction in tissue mass (Figure 5.19 A; Figure A8), followed by an altered lipid composition. Unexpectedly, TAG level was not altered in CerS2H/A mice, whereas DAG, FFA as well as cholesterol-ester and cholesterol levels were elevated in comparison to WT animals.
Finally the storage lipid composition in muscle showed high variance, which does not reach significance in any of the quantified lipid species in CerS2H/A mice, i.e. lipid levels were not altered (Figure 5.19 E).

#### 5.4.6.3 Liver and adipose tissue of CerS2H212A/H213A mice exhibit altered cell size, decreased lipid droplet formation and loss of glycogen content

In addition to investigations regarding the storage lipid content and coherent development of body size and weight, we performed histological analyses of WAT and liver.

First of all, it was evident that CerS2H/A mice show a significant loss of adipose tissue mass (Figure 5.20 A; Figure A8). Further hematoxylin and eosin (H&E)-staining on cryo-sections of epididymal WAT indicate further differences between CerS2WT and H/A mice. Adipose tissue sections derived from CerS2H/A mice showed normal sized adipocytes interspersed with areas of multiple, smaller adipocytes, which were absent in WT control samples (Figure 5.20 C-E). Additionally, adipocytes of CerS2H/A genetic background showed significantly reduced cell diameter (WT: 75.5µm ± 2.29; H/A: 48.6µm ± 4.2, Figure 5.20 B), concomitant with higher density packaging (H/A: >100cells/ROI; WT: ∅36cells/ROI; Figure 5.20 B).

Next, analysis of Oil-RedO-staining on liver cryo-sections of CerS2H/A mice were performed (Figure 5.21 A-D). Signals derived from the staining patterns highlighted reduced/ lack of lipid droplet formation in liver of CerS2H/A mice in comparison to their WT littermates. These findings are in line with the reduction in TAG content, quantified by TLC analyses (Figure 5.19 C). Further verification of glycogen content of liver-paraffin-sections stained with periodic acid Schiff-(PAS)- reagent showed also strong reduction in PAS signal in CerS2H/A mice (Figure 5.21, E-H). Here only few, but strong PAS-positive cells were scattered over the liver nodule. All other cells showed a rather pale, weak staining pattern. In contrast are the obtained staining signals of CerS2WT liver sections. Here, PAS-staining pattern showed the expected uniform distribution of glycogen content over the liver lobules (Figure 5.21 E / G).

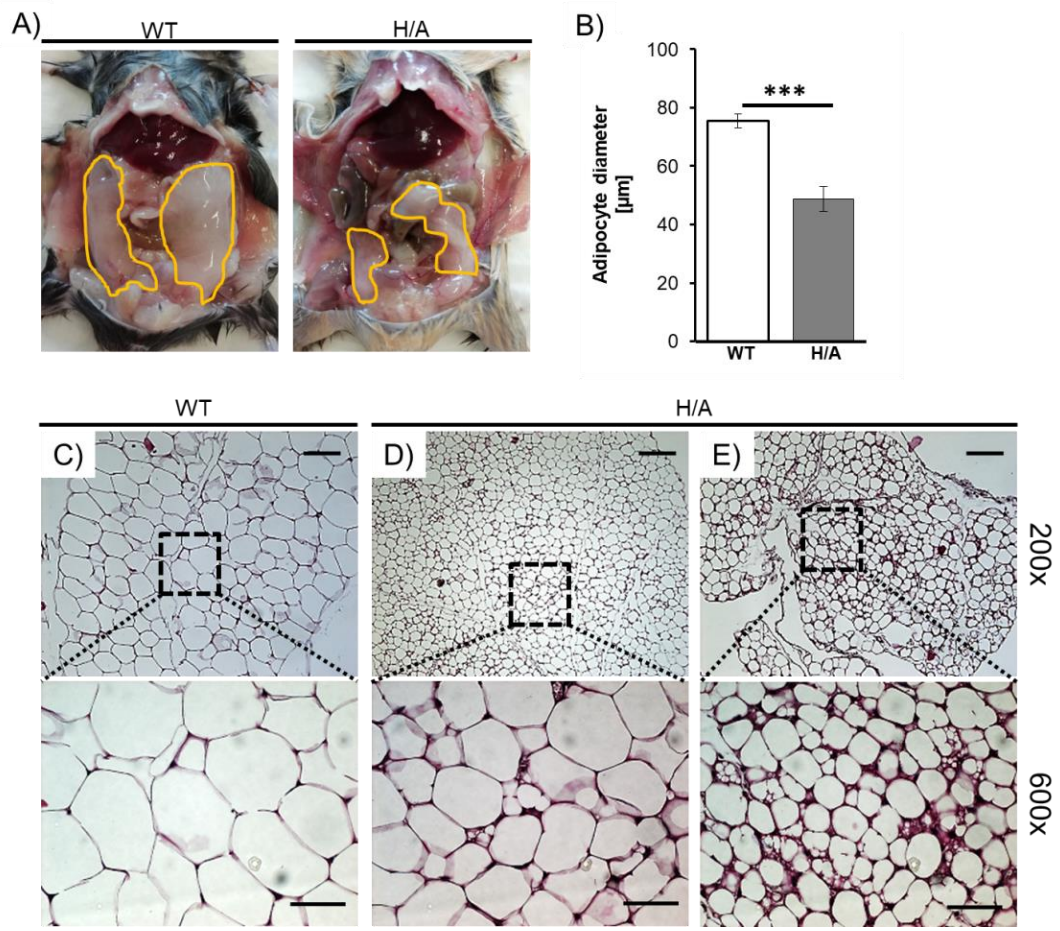


**Figure 5.20: Histological analysis of epididymal adipose tissue. (A)** Photographs of representative eWAT morphology from CerS2WT and H/A mice. **(B)** Quantification of adipocyte diameter. Data shown as means ±SEM (n=4, six cells measured per sample). Unpaired t-test, ***P<.001. **(C-E)** H&E-staining of eWAT derived from 12-week-old male mice. Genotypes and magnifications are indicated. Dotted scares in upper row depict the regions of magnification shown in lower row. Scale bars, 200x: 100µm; 600x: 50µm. Abbreviation: eWAT-epididymal white adipose tissue.

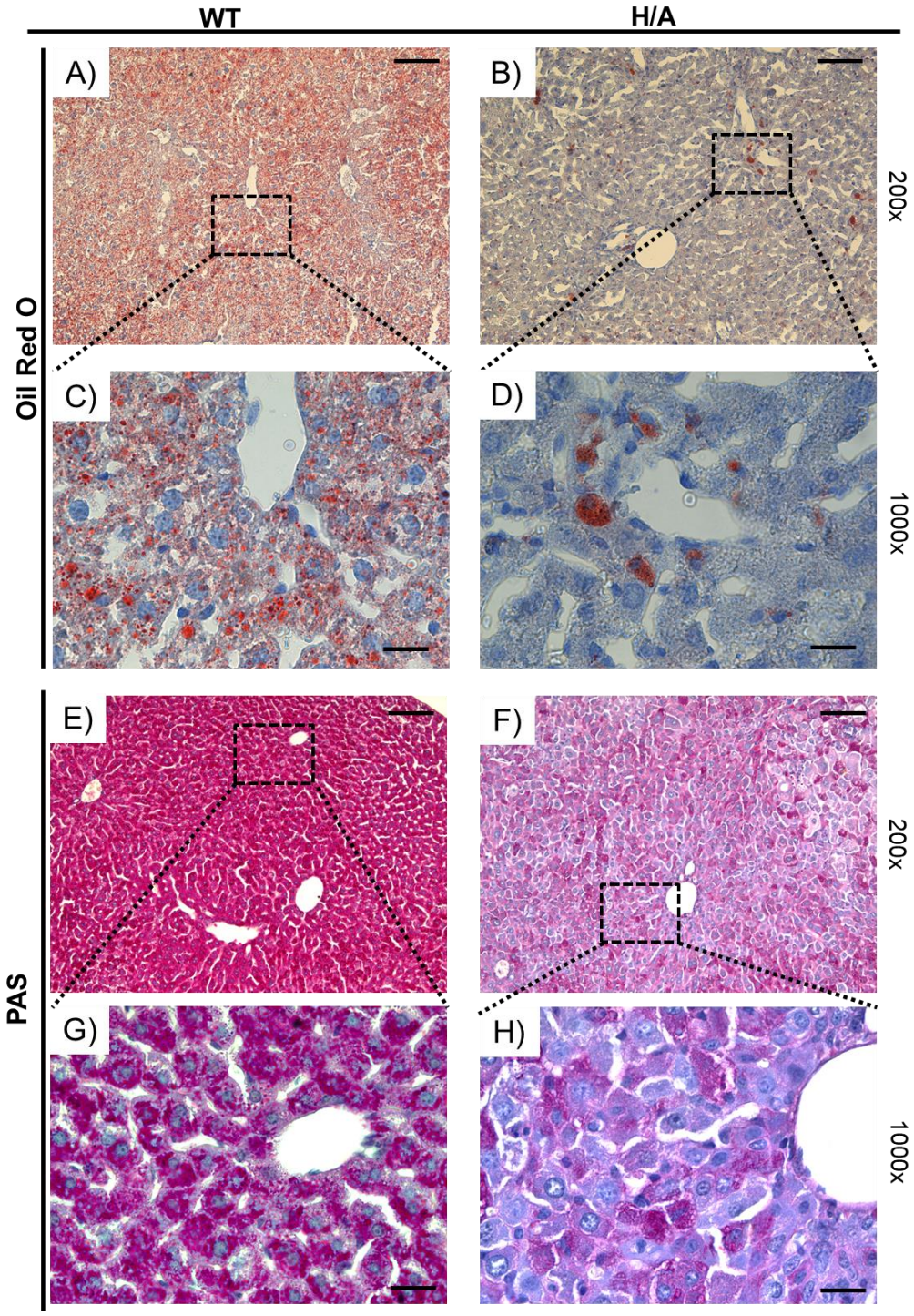


**Figure 5.21: Histological analysis of liver sections. (A-D)** Oil Red O staining performed in liver sections from CerS2WT and H/A mice. **(C/D)** Magnification of dotted square highlighted in A) and B). WT hepatocytes show intracellular lipid droplet accumulation, which is lost or rather strong decreased in hepatocytes of CerS2H/A mice. **(E-H)** Shown are glycogen (PAS) stainings of liver sections from CerS2WT and H/A mice. **(E/F)** Dotted squares represent areas of higher magnification shown in G) and H). (**E/G)** Hepatocytes show strong PAS-positive staining, which depicts high glycogen content. **(F/H)** Hepatocytes show pale. Weak PAS-positive signals indicating low glycogen content. Scale bars correspond to: A/B, E/F: 50µm, C/D, G/H: 20µm.

### 5.4.7 Histological analysis of CerS2H212A/HA213 (and CerS2Del79-120) mice indicate alterations in the tissue architecture of some organs

Detailed investigations concerning the cell-type specific expression pattern of the CerS2 protein were already performed for most of the tissues on the basis of CerS2$^{gt/gt}$ mice, in combination with the application of a highly-specific custom-made anti-CerS2 antibodies (Imgrund et al., 2009; Kremser et al.,2013). It was shown that CerS2 is expressed in hepatocytes (liver), oligodendrocytes and glial cells (brain), in the respiratory epithelium and pulmonary alveoli of the lung as well as in the renal corpuscle and proximal tubular cells of the kidney. The following histological investigations, in addition to those of chapter 5.4.6, were performed with the aim to verify, whether previous findings could be transferred to the newly generated CerS2H/A and Del mice. Tumor formation analyses of 8-week-old mice were done in cooperation with Prof. D. Hartmann (Bickert et al., 2018).

#### 5.4.7.1 Liver of CerS2H212A/H213A and CerS2Del79-120 mice showed loss of liver architecture and early onset of tumor formation

Gross anatomy of liver tissue extracted from 20-week-old CerS2H/A or WT mice does not indicate any morphological differences (Figure 5.22 A). Organs show the same structural architecture composed of four lobes. Detailed H&E stainings performed on PFA-sections of 20-week-old mice indicate that livers of CerS2H/A (Del, data not shown) mice were characterised by several alterations in contrast to their WT littermates, where no histopathological changes of liver architecture were observed (Figure 5.22 B-I). Hepatocytes of WT control livers showed the typical arrangement in one-cell-layer thick plates, which were separated by sinusoids (Figure 5.22 D and F). Furthermore, the overall architecture of liver lobes showed classical shape with a central vein and portal fields (portal vein, hepatic artery and bile duct) at the periphery (Figure 5.22 D and F). Moreover, WT hepatocytes are roughly polyhedral shaped, containing one or two nuclei. The cytoplasm of all hepatocytes showed equal appearance with typical glycogen and lipid-rich content (Figure 5.22 B and C). These findings are in contrast to that found in CerS2H/A (and Del) mice. Here, one cell-layer thick plates of hepatocytes were irregularly interspersed by cells or cluster of cells, which lack sinusoids (Figure 5.22 F/G/I). Additionally, sections indicate a glycogen and lipid-free cell-content and pale-stained cytoplasm (Figure 5.22 G and H). Moreover, hepatocytes found in CerS2H/A mice showed a significant reduction in diameter compared to WT control and on the other hand enlarged and irregular stained nuclei (Figure 5.22 B and C).
In the following step, the presence of tumor cells was also confirmed by proliferating-cell-nuclear-antigen (PCNA) staining. Sections showed enriched PCNA-positive nuclei in CerS2H/A mice (Figure 5.23 A-C). Results were also confirmed by a high expression level of beta-catenin, a prominent marker of hepatic tumorigenesis (Figure 5.23 D). All these findings indirectly indicate by high expression of either PCNA or beta-catenin a loss of normal liver architecture and point out to an onset and development of hepatocellular carcinoma in CerS2H/A mice.

Analyses of CerS2Del mice showed comparable differences in liver architecture as those found in CerS2H/A mice (Bickert et al., 2018). First, Oil-Red O and PAS- staining performed on live - sections revealed the same loss of lipid droplets and lack of glycogen content as found in CerS2H/A mice (data not shown). Findings regarding altered cell morphology and nuclei diameter of CerS2Del hepatocytes are in line with those found CerS2H/A mice (data not shown). Verification of the tumor marker ,PCNA and beta-catenin, revealed also increased expression, which lead to the assumption that CerS2Del mice are as well characterized by an early onset of liver-tumor formation (Figure 31, A-D).

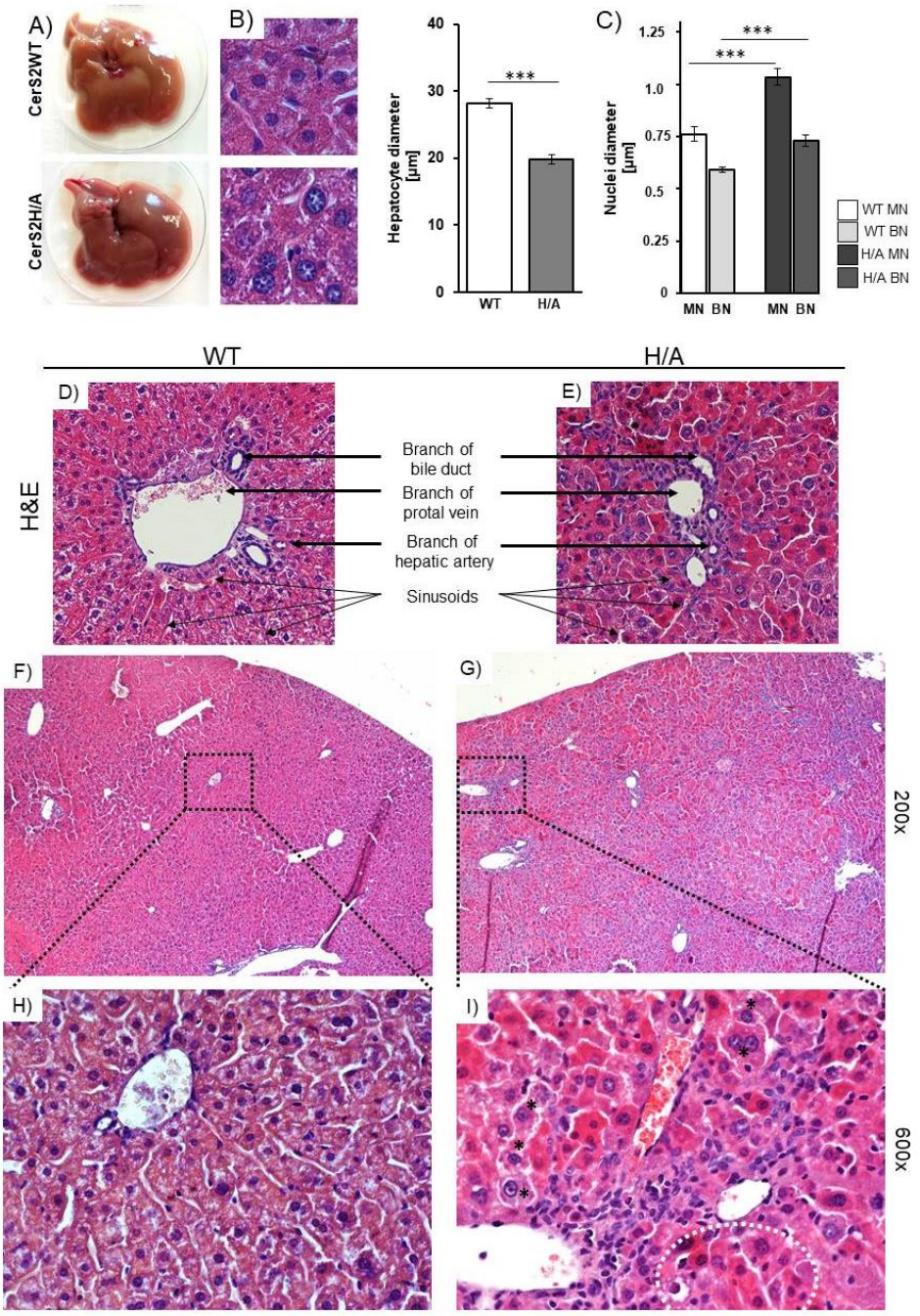


**Figure 5.22: Hepatic histopathology in 20-week-old CerS2H/A mice (H&E stainings). (A)** Gross anatomy of liver from CerS2WT and H/A mice. **(B)** Representative pictures of liver sections used to determine the diameter of hepatocytes and their nuclei. Graphs depict quantification of hepatocyte diameter found in WT and H/A mice or determination of nuclei diameter, which differentiates between mononuclear (MN) and bi-nuclear (BN) hepatocytes. Data shown as means ±SEM (hepatocytes: n=3, ten cells measured per sample; Nuclei: n=3, ten nuclei per group (MN/BN), per sample were measured). Unpaired t-test, ***P<.001. **(C/D)** Overview of portal fields from WT and H/A mice. Portal field composed of central vein, artery (A) and bile duct (BD). **(E)** WT liver section, showed normal architecture and distribution of hepatocytes in one-cell layer thick plates. **(F)** Overview of liver section from CerS2H/A mice. Normal hepatocytes (white asterisk) were interspersed with hepatocellular carcinoma cells (white dotted line), which results in loss of liver architecture. **(G/H)** Magnification of dotted areas in D) and E). **(G)** Glycogen- and lipid-rich hepatocytes show roughly polyhedral shape with marginal positioned cytoplasm. **(H)** Altered H/A-liver architecture is depicted by loss of typical morphology of hepatocytes, lack of lipid and glycogen-droplets as well as enlarged nuclei diameter.

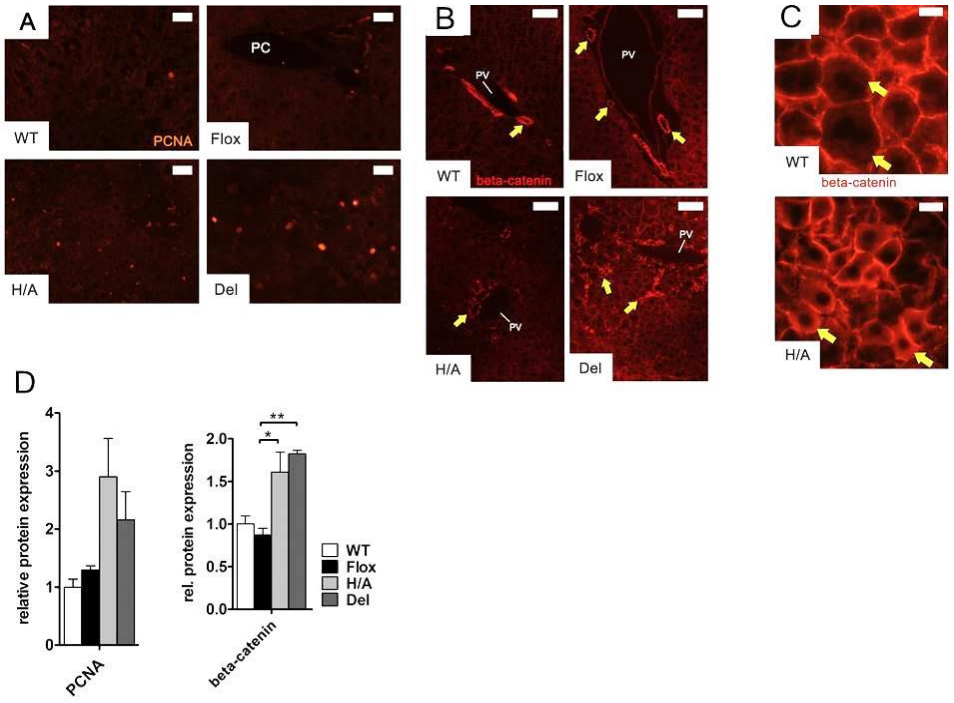


**Figure 5.23: Analysis of tumor markers in CerS2WT, Flox, H/A and Del mice. (A)** Liver sections were stained for the presence of proliferator cell nuclear antigen (PCNA). In WT and Flox showed rare PCNA-positive nuclei in contrast to H/A and Del mice. (**B)** Beta-Catenin staining of liver sections. Arrows indicate regions of high expression. **(C)** CerS2WT liver sections stained with anti-beta-catenin antibodies. Resulting signal are restricted to the membranes of hepatocytes (arrows). CerS2H/A mice showed additional cells showing beta-catenin signals in the cytoplasm (arrow). **(D)** Immunoblot analysis of PCNA and beta-catenin protein expression in liver. Data are means ± SEM, normalized to GAPDH (PCNA) or PDH (beta-catenin); n = 3; Unpaired t-test, *P<.05; **P<.01. Scale bars correspond to: A) 25µm, B) 500µm, C) 25µm. (Figure adopted and modified from Bickert et al., 2018).

### 5.4.7.2 CerS2H212A/H213A mutation does not influence splenic architecture but alters glycogen content and macrophage presence

In the next step, we analysed overall architecture as well as glycogen and macrophage content of spleen from CerS2H/A mice. In general, the spleen is not only responsible for clearing blood from circulating particles and aged erythrocytes, it also plays an important role as a peripheral lymphoid tissue (Grossi & Lydyard, 1998). Initially, histological analysis of H&E staining performed on PFA-sections of spleen from CerS2H/A and WT mice showed no differences in the overall architecture (Figure 5.24). Both showed the typical separation into red and white pulp with interspersed trabeculae (Figure 5.24 A and B). Additional PAS-staining indicated decreased PAS-signal in the sub-capsular zone and red pulp of CerS2H/A mice (Figure 32, C/D). Immunohistochemical staining performed with an anti-F4/80 antibody indicate also reduced F4/80 positive signal (macrophages) in the red pulp of CerS2H/A mice in comparison to sections from WT animals (Figure 5.24 E-H).

Subsequently, the thymus was also examined, which is another important immunological organ, since it is the place of thymocyte maturation. Semi-thin sections either stained with H&E or F4/80 do not indicate any alterations (data not shown). Thymi of both genotypes show a typical architecture/distribution of cells, with larger pale-red stained cells in the medulla and dark-blue positive cells in the cortex. H&E staining does not allow differentiation between B-cell and T-cell content in the cortex. Additionally, no differences were detected in the distribution and content of macrophages (F4/80 staining) in any of the analysed CerS2WT or H/A thymi sections.

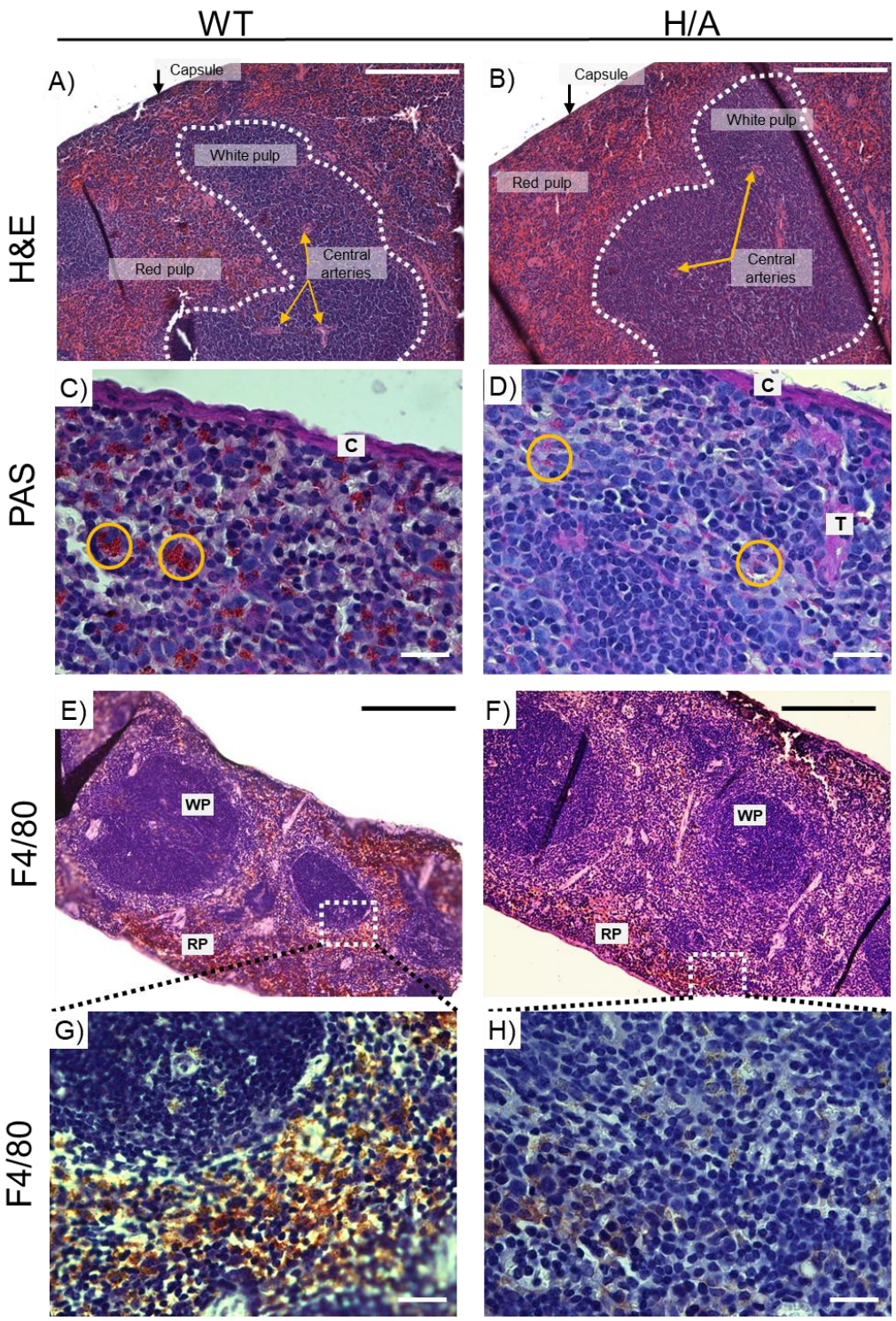


**Figure 5.24: Histological analyses of spleen. (A/B)** H&E staining of PFA-fixed spleen sections derived from CerS2H/A and WT mice. Main structural components were highlighted. **(C)** PAS staining shows strong positive signals (yellow circle) in the sub-capsule region and red pulp of WT sections. **(D)** PAS staining of spleen from CerS2H/A mice shows a reduction in PAS-positive signals in the sub-capsular region and the red pulp. **(E/F)** Immunhistochemical staining of F4/80 positive cells. **(G/H)** Magnification of white dotted square from G and H. **(G)** Strong F4/80 positive signals detected in red pulp. **(H)** Pale, weak staining of F4/80 positive cells in red pulp. Abbreviations: C-capsule; T- trabeculae; RP-red pulp; WP- white pulp. Scale bars correspond to: A/B and E/F bar) 100µm, C/D and G/H white bar) 50µm.

### 5.4.7.3 Kidney of CerS2H212A/H213A mice showed reduced glycogen storage

The kidney is a bilateral organ and involved in the regulation of blood pressure (fluid level), waste excretion and reabsorption of nutrients, e.g. of glucose, amino acids, and water.

The next step was to identify, whether the ablation of catalytic activity of the CerS2 protein and the corresponding lack of specific ceramide/sphingolipid species cause alterations of the kidney architecture thereby affecting glycogen content. Initially the overall architecture, investigated by H&E staining, showed no alterations between CerS2H/A and WT mice (Figure 5.25 A and B). Differences become only obvious in PAS stainings performed on PFA-sections, as expected. Here, the proximal convoluted cells from CerS2WT mice show the typical strong PAS-positive signal of the brush border (microvilli), as well as PAS-positive signals of basement membranes of the glomeruli. This is in contrast to the obtained pale and weak signals in sections of CerS2H/A kidneys (Figure 5.25 C-F); indicating reduced glycogen content or possibly altered morphology of those cells. Again, these results are consistent with recent findings found in liver and spleen.

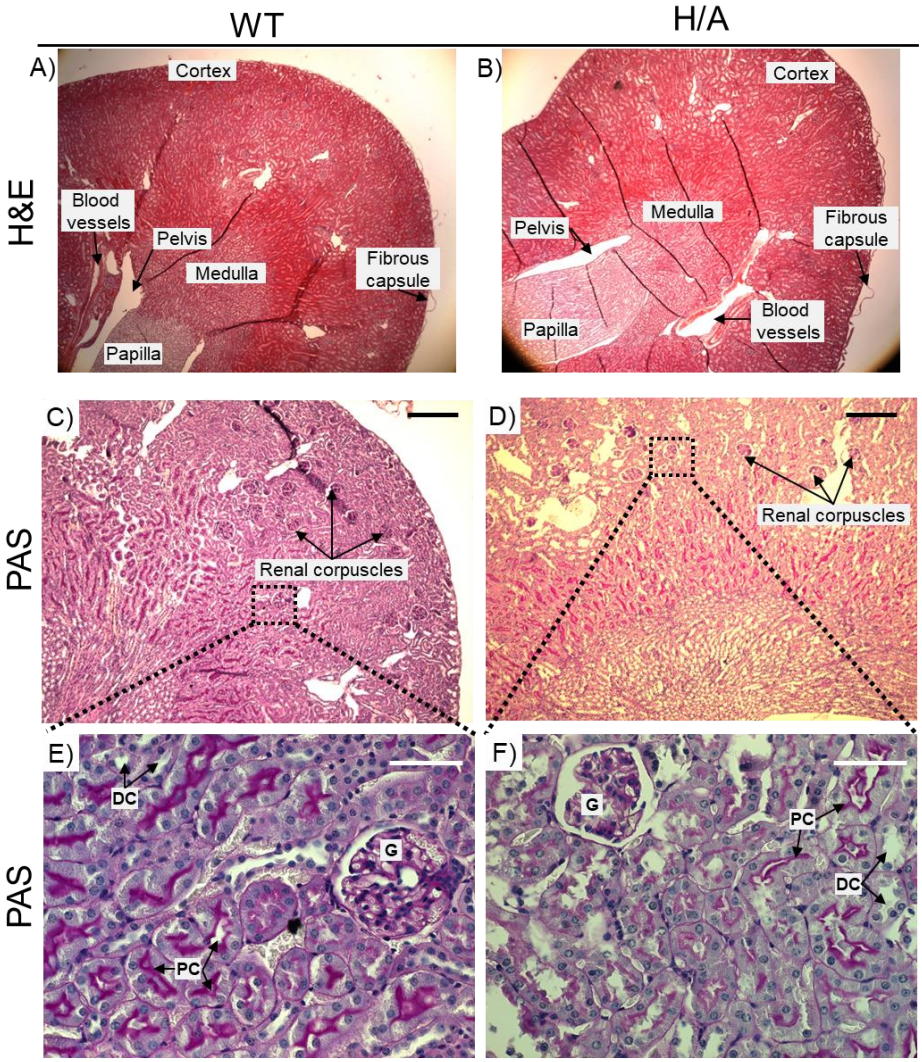


**Figure 5.25: Histological analyses of kidney. (A/B)** H&E-staining of kidney sections depict typical architecture. Structural components were highlighted. **(C/D)** PAS-staining of PFA-sections obtained from WT and CerS2H/A mice. **(E)** Magnification of C. **(F)** Higher magnification indicates pale, weak staining of kidney cells (PC) and glomeruli in CerS2H/A mice. G- Glomerulus, DC- distal convoluted cells, PC- proximal convoluted cells. Scale bars correspond to: C/D) 200µm, E/F) 100 µm.

#### 5.4.7.4 Histological analysis of large intestine (colon) indicate no differences between CerS2H212A/H213A and WT mice

Previous analysis regarding the storage-lipid content of feces derived from CerS2H/A mice indicated alteration in the composition (Chapter 5.4.6.2). To verify if these alterations are based on an altered histology of the intestine, we investigated colon sections of several CerS2H/A and WT mice. After PFA-fixation, sections were either stained with H&E or PAS (Figure 5.26). Analyses of those showed no alterations in overall architecture nor mucine content (heavily glycosylated protein) (Figure 5.26 A-D). Here, CerS2H/A and WT animals show typical structural organisation of the colon and strong mucine content in goblet cells as expected (Figure 5.26, E-H). Whether the sub-cellular structure (e.g. protein composition of the plamamembrane) is disturbed to some extend cannot be clarified with the preformed stainings. For this reason, it would be appropriate here to conduct in-depth analysis by means of electron microscopy. Based on these findings, we initially assume that the uptake of nutrients is not altered.

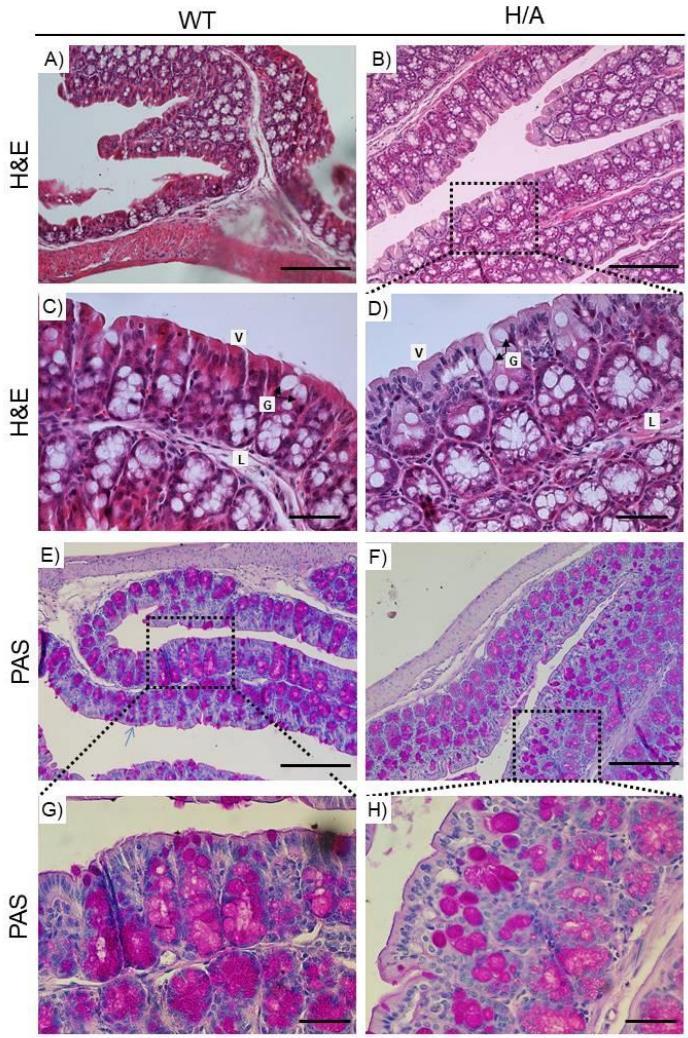


**Figure 5.26: Histological analyses of colon sections. (A/B)** H&E staining of PFA-fixed colon-sections derived from CerS2H/A and WT mice. **(C)** Magnification of A). **(D)** Magnification of B), no alterations were observed between the two genotypes. Structural components are indicated; V-microvilli, G-goblet cells, L-lamina propria. **(E/F)** PAS-staining of WT and CerS2H/A colon sections. **(G)** Higher magnification of E). **(H)** Magnification of F). Rich glycogen-content of goblet cells is stained in purple. No differences were obtained between WT and CerS2H/A sections. Scale bars correspond to: A/B and E/F bar) 100µm, C/D and G/H white bar) 50µm.

## 5.4.8 Immune status of CerS2H212A/H213A mice

### 5.4.8.1 Background and introductory remarks

The adaptive immunity (differentiation between self and non-self) depends on the presence of lymphocytes, e.g. on an ever-changing TCR (T cell receptor) repertoire, that is produced by the maturation of new T cells in the thymus as it was described in the introduction (Chapter 1.7.2). Recent studies revealed that emigration of terminally differentiated thymocytes from the thymus into the circulation (periphery) occurs along an S1P (sphingosine-1-phosphate) gradient and is suggested as a two-stage process. Briefly, thymocytes undergo a differentiation and maturation process which leads to the up-regulation of CD62L (L-selectin, cell adhesion molecule) and S1PR1 (sphingosine 1 phosphate receptor 1), among other surface markers. Finally, single positive thymocytes migrate into the perivascular space, by passing the basement membrane of the surrounding blood vessel from where they enter the bloodstream (Figure 8).

As it was hypothesized and proven for CerS2$^{gt/gt}$ mice, the maintenance of the S1P gradient between the thymus, blood and peripheral tissues, e.g. spleen, lymph nodes, is essentially necessary and the main key player in the facilitation of thymic egress of single positive thymocytes (Rieck et al., 2017).

In the following section of the present study, analyses were performed to verify, whether these findings could be transferred to the newly generated CerS2H/A mice. Detailed investigations of the efficiency of thymic egress as well as quantitative measurements of single positive T cells in blood and spleen were done. It is also worthy of note, that the reduced body size of CerS2H/A mice (Figure 5.27, Figure A8) could have an influence on the absolute cell numbers, which are integral parts of the calculations and results. To overcome this bias, cell counts of wild type control mice and of respective H/A mutated animals were represented in different outputs (Figure 5.29). First, as frequencies or unmodified numbers (cell count/raw data). Second, as weight-corrected numbers, which were normalized to the average of mouse weights of wild type and H/A mice (cell count per g mouse, weight-corrected data). Furthermore, it should be remarked that the results are based on analysis exclusively performed with male mice to rule out gender/hormone-specific phenotypes. Additionally, we also analysed Flox mice to exclude that the reduced CerS2 protein expression influences the thymic egress. The results reveal that Flox mice behave like wild type mice. From this point of view, we conclude that the remaining CerS2-WT-protein level is sufficient to maintain the S1P gradient in those mice.

### 5.4.8.2 CerS2H212A/H213A mutation affects thymic egress of single positive thymocytes

First, to verify if the CerS2H/A mice show the same deficiency in emigration like the CerS2$^{gt/gt}$ mice, flow cytometry analyses were performed. Therefore, cells of thymi from wild type, Flox and H/A mice were isolated and frequencies as well as total numbers of immature and mature single positive thymocytes determined (Figure 5.27, 5.29). Immature cells still need to undergo the process of negative selection and are not allowed leaving the thymus in comparison to the terminally differentiated, mature single positive T cells. Furthermore, mature single positive T cells express the S1PR1 receptor which enables them to migrate along the S1P-gradient. The different expression of the surface markers CD62L and CD69 were used to discriminate between immature (CD62L$^{low}$/CD69$^{high}$) and mature (CD62L$^{high}$/CD69$^{intermediate}$) T cells (Figure 5.28).

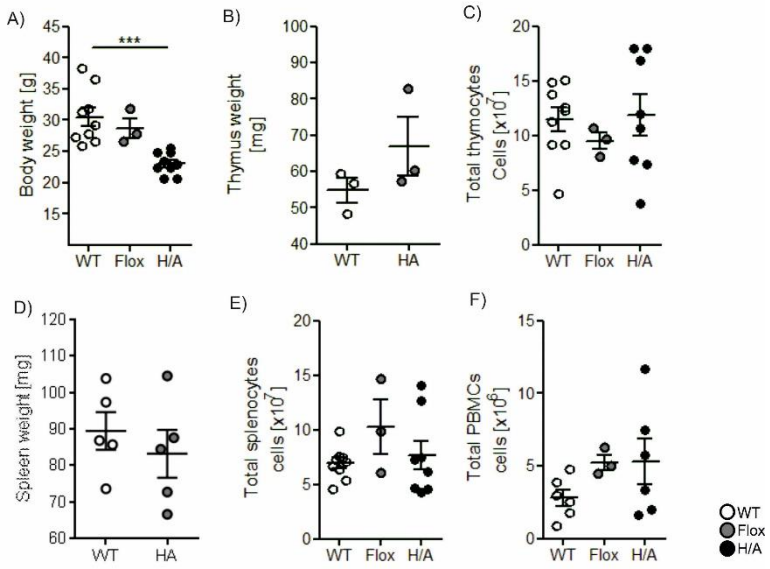


**Figure 5.27: Characteristics of CerS2H/A mice. (A)** Body weights of male wild type (WT, n=9), Flox (Flox, n=3) and CerS2 H/A (H/A, n=9) mice at middle age (10-17 weeks). Weight is significantly reduced in CerS2H/A male mice. **(B/C)** CerS2 H/A mutation does not result in reduced thymi weight (n=3, ±SEM), nor reduced total thymocyte counts (WT, n=9; Flox, n=3; H/A, n=9; ±SEM). **(D/E)** Catalytically inactive CerS2 (H/A) protein does not influence the spleen weight as well as the total cell counts. (D: WT, n=5; H/A, n=5; ±SEM. E: WT, n=9; Flox, n=3; H/A, n=8; ±SEM.). **(F)** Total PBMCs/ml blood is not altered in CerS2H/A mice (WT, n=6; Flox, n=3; H/A, n=6; ±SEM). Dots represent individual mice; wild type, white dots; Flox, grey dots; H/A, black dots. Data were pooled from individual experiments. Unpaired t-test, ***P<.001.

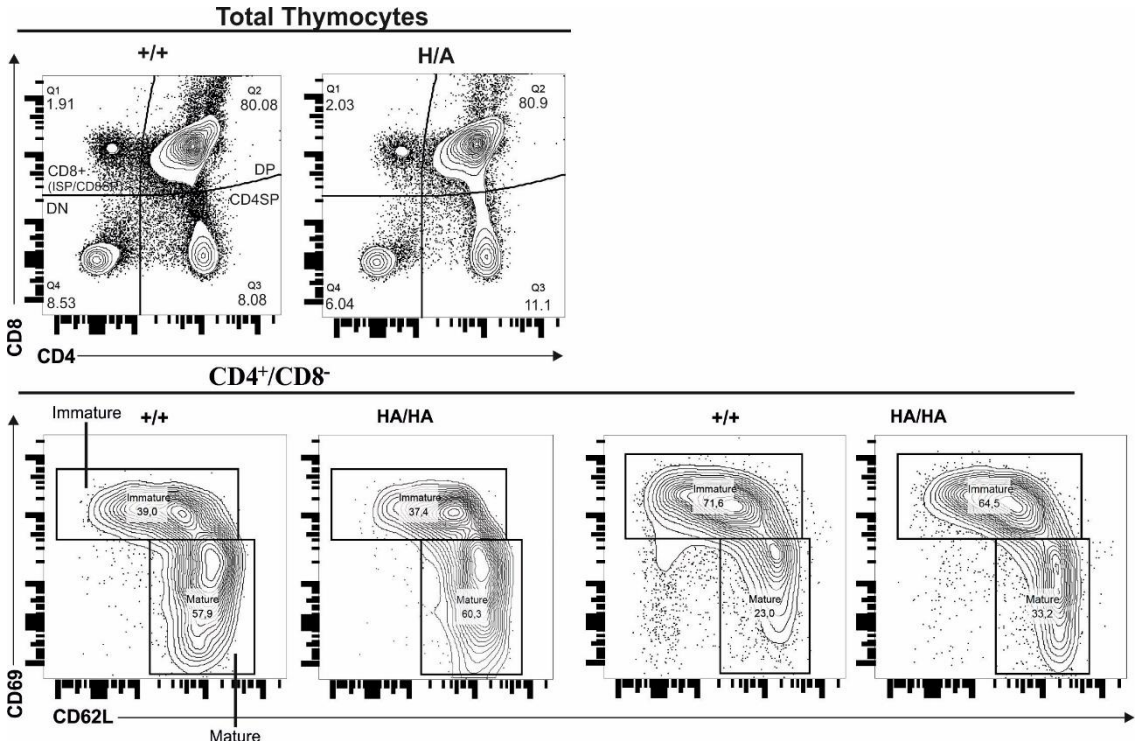


**Figure 5.28: Thymi flow cytometry plot**. Representative overview of flow cytometric identification of immature ($CD62L^{Low}/CD69^{high}$) and mature ($CD62L^{high}/CD69^{intermediate}$) $CD4^+/CD8^-$ and $CD4^-/CD8^+$ thymocytes of male WT and H/A mice. Numbers indicate percentages of subpopulations within the parental gate. DN, double negative; CD8+ (ISP-immature single positive /CD8 SP), CD8 positive cell population composed of CD8+ single positive cells and CD8 positive, CD3low cells; CD4SP, CD4 single positive cells, DP double positive.

Initially, the determination of thymi weight revealed no significant differences (Figure 5.27 B) despite the altered body weight (Figure 5.27 A). Furthermore, the number of total thymocytes was also not altered (Figure 5.27 C). Flow cytometric analyses showed that the presence of a catalytically inactive CerS2H/A protein in male mice lead to a significant increase in the frequency, counts and numbers of mature $CD4^+/CD8^-$ thymocytes (Figure 5.29 A). In case of $CD4^-/CD8^+$ thymocytes significant differences were detectable in frequencies; whereas counts (raw data) and absolute numbers (weight corrected data) show a tendency of accumulation which does not reach significance, upon high variability (Figure 5.29 B). Numbers and weight corrected cell counts of immature thymocytes were not affected. Next, quantitative analysis regarding the frequency of immature thymocytes of the $CD4^+$subpopulation was significantly decreased, whereas immature $CD8^+$ cells were not affected (Figure 5.29 A and B).

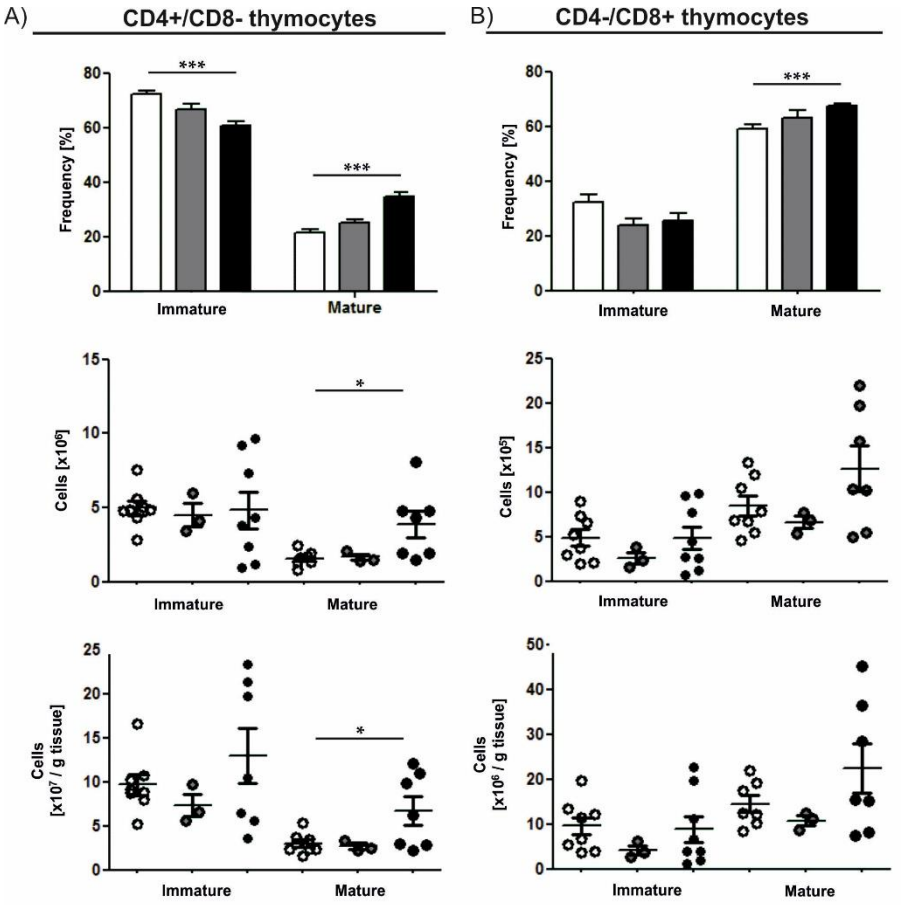


**Figure 5.29: CerS2H/A-modified mice showed selective accumulation of mature thymocytes**. **(A)** Frequencies, counts (raw data) and weight corrected data revealed significant increase in mature single positive CD4+/CD8- cells. **(B)** Frequencies of mature CD8+/CD4- thymocytes show a significant increase. Significance is lost after weight correction. **(A/B)** Frequencies and counts (raw data) of respective single positive cells were determined by flow cytometry. For calculation of weight corrected data, total counts of the subpopulation of interest was normalized to the corresponding thymi weight/ average of thymi weight (WT). Bar graphs represent means ±SEM, dots in scatter plots represent individual mice (unpaired t-test; *P<.05, ***P<.001; WT, white bars, dots, n=8; Flox, grey bars and dots, n=3; H/A, black bars and dots, n=7)). (Remark: CD8+ mature, counts P=0.1356; CD8+ mature, weight corr. P=0.2059.)

### 5.4.8.3 CD69 surface expression is altered in CerS2H212A/H213A mice

CD69 and S1PR1 mutually antagonize each other upon transcriptional regulation (Zamora-Pineda et al., 2016; Saba et al., 2017), i.e. the up-regulation of one cell surface protein leads to the down-regulation of the other one. Under normal conditions, CD69 expression is low on mature thymocytes, whereas the S1PR1 expression is high, which in turn enables the cells to migrate along the S1P gradient and leave the thymus. Based on these considerations and on the lack of an adequate antibody for the determination of S1PR1 on the cell surface for flow cytometric analysis, we measured the expression level of CD69 as an indicator for S1P/ S1PR1 (Figure 5.30).

The results clearly demonstrate that the expression level of CD69 on the cell surface, of both $CD4^+$ and $CD8^+$ mature thymocytes, is significantly down-regulated (Figure 5.30 A and B). Based on these findings and on the lack of quantitative SP1 measurements, we can only assume that the surrounding microenvironment contains either (I) higher amounts of S1P in the H/A mutant mice than in the wild type littermates or (II) the T cell development is somehow affected which causes the unequal expression of CD69. To exclude an impaired T cell development, we preceded with further flow cytometric analyses based on the surface marker CD25 and CD44.

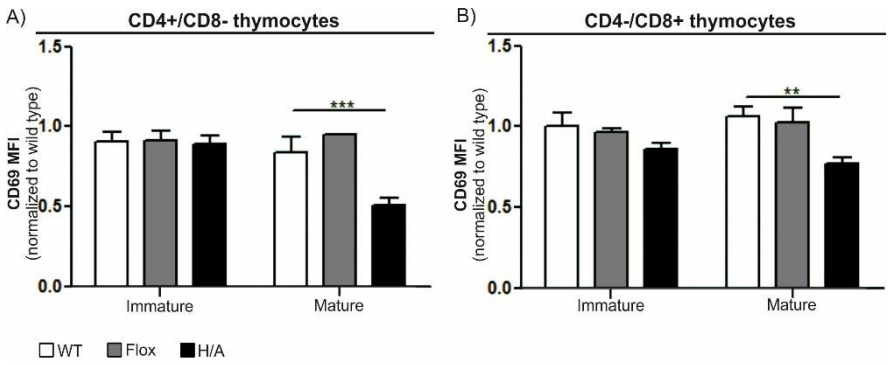


**Figure 5.30: CD69 surface expression on thymocytes.** CerS2H/A mutation lead to reduced CD69 surface expression on mature thymocytes. Thymocytes from indicated genotypes were analysed by flow cytometry and CD69 expression depicted as mean fluorescence intensity. CD69 MFIs of immature and mature $CD4^+/CD8^-$ **(A)** and $CD4^-/CD8^+$ **(B)** respectively were normalized to expression on wild type controls. Data were pooled from individual experiments, means ±SEM; unpaired t-test; **P<.01; ***P<.001; WT, n= 8; Flox, n=3; H/A, n=8.

### 5.4.8.4 Early T cell development is not affected in CerS2H212A/H213A male mice

The T-cell development describes a tightly controlled process and any malfunction during the different stages can cause server diseases like autoimmunity, immunodeficiency and cancer as it was extensively discussed in the introduction (see Chapter 1.7). First, bone-marrow-derived progenitors migrate into the thymus, where they build up the thymocyte cell population and differentiate to mature single positive naïve T-cells. The development (TCR gene configuration) starts with the double negative (DN) stage which can be further subdivided into DN1 → DN2 → DN3 → DN4 (Figure 5.31 A). Many surface markers were expressed during each stage and can be monitored. Here we used the CD25 in combination with the CD44 marker to identify cells of each developmental stage (Figure 5.31 A and B) (Hager-Theodorides et al., 2007).

Flow cytometry analyses revealed that the mutation of CerS2's catalytic activity has a negligible impact on the T cell development in male mice. The overall frequency, counts and weight corrected numbers of DN cells showed no significant changes between wild type and CerS2H/A male mice (Figure 5.31 C, left chart). Interestingly and despite the normal DN values, analysis of subpopulations DN1 to DN4 showed striking differences. The counts and weight corrected counts for DN1 revealed a significant loss of DN1-cells in H/A mice. Furthermore, DN2 cells showed a strong decrease in cell counts (P=0.1401) and weight corrected cell counts (P=0.0563) but does not reach significance (Figure 5.31 C, middle). Reduction in cell counts of DN3 subset reached only significance after weight correction (Figure 5.31 C, right chart). Cells counts and weight corrected cell counts of DN4 subset were also decreased but do not reach significance (Figure 5.3).

Additional quantification of double positive (CD4+/CD8+) cell amounts was performed to determine whether this mild loss of cells will continue or gain strength with further differentiation (Figure 5.31 D). Basically, no difference in frequency, counts and weight corrected numbers of double positive (DP) cells were detectable between wild type mice and their H/A littermates; pointing out that T cell development and differentiation is unaffected in H/A male mice and does not contribute to the accumulation of single positive thymocytes.

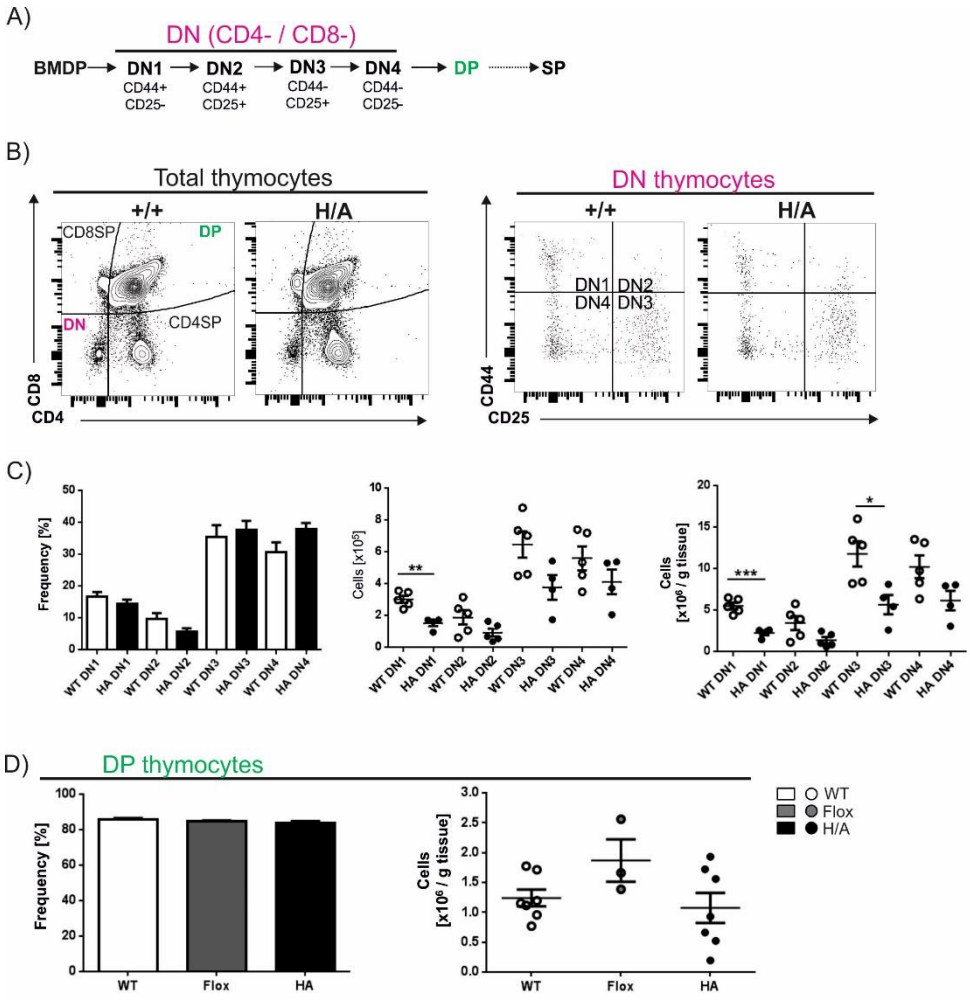


**Figure 5.31: T-cell development in CerS2 H/A male mice is not affected by its catalytically inactivation. (A)** Overview of the differentiation stages of bone-marrow-derived-T-lineage progenitors to mature, naïve T-cells. Differentiation starts with DN1 stage ($CD44^+/CD25^-$). Further differentiation reveal up-regulation of CD25,

DN2 stage ($CD44^+/CD25^+$). DN3 is characterized by TCRβ rearrangement and down-regulation of CD44. DN4 ($CD44^-/CD25^-$) end up in DP (double positive, $CD4^+/CD8^+$) which undergo further TCRα rearrangement and develop to terminally differentiated SP (single positive), naïve T-cells (CD4 (MHCII) or CD8 (MHCI)). **(B)** Representative overview of flow cytometric identification of lymphocytes from thymi (left section, $CD4^+$ vs $CD8^+$) and expression of CD44 and CD25 of double negative subpopulation (left). **(C)** Quantification of frequencies, counts and cell numbers of different thymi-DN subsets. DN1 show significantly reduced counts and numbers of cells. (Data were pooled from individual experiments, means ±SEM. Dots in scatter plot depict individual mice; unpaired t-test;*P<.05; **P<.01; ***P<.001; WT, n= 5; H/A, n=3.) **(D)** Quantification of frequencies and cell numbers from DP cells. Analysed subpopulation reveals no difference. Data were pooled from individual experiments, means ±SEM; WT, n= 7; Flox, n=3; H/A, n=7.

### 5.4.8.5 CerS2H212A/H213A mice develop a mild T cell lymphopenia

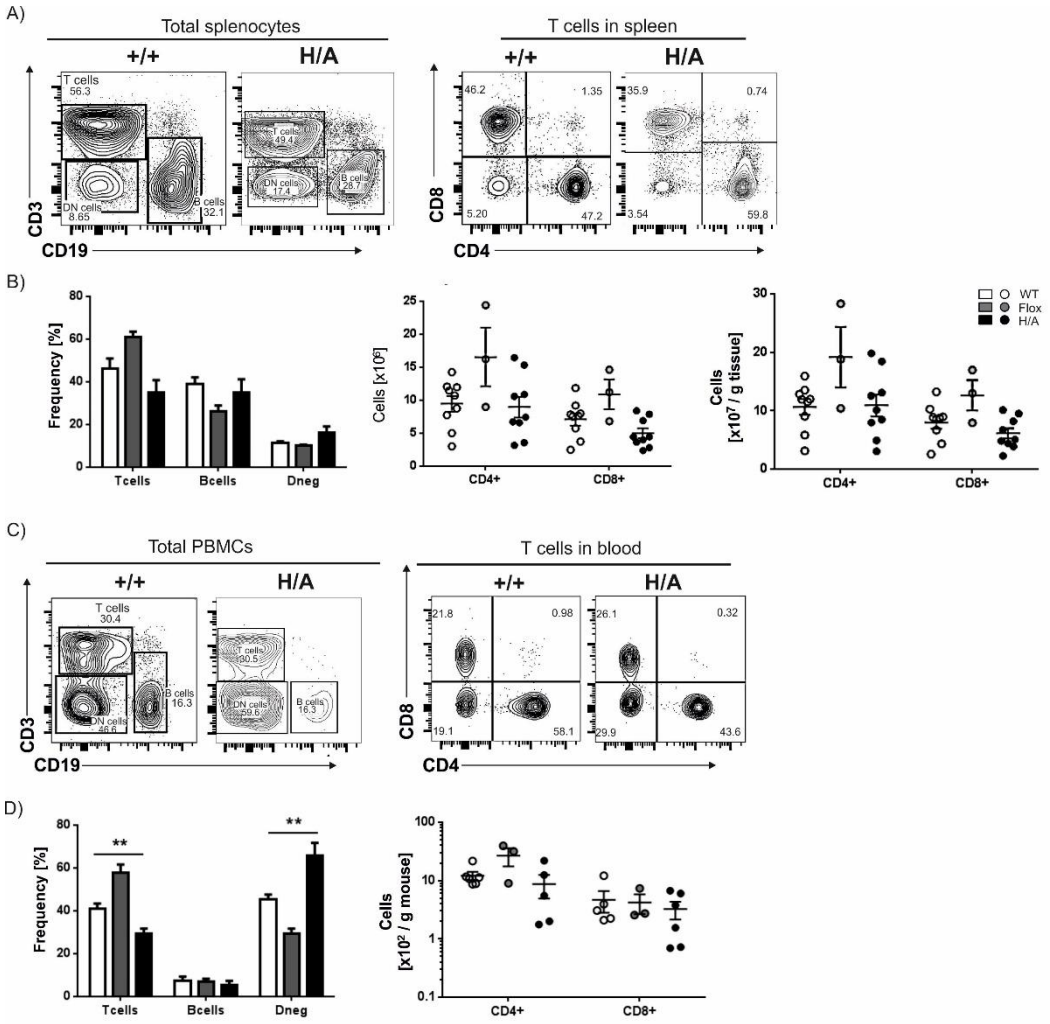


**Figure 5.32: Quantification of T cell content in spleen and blood. (A)** Representative flow cytometry analyses of T cells in spleen. **(B)** Quantification of counts (left chart, raw data) and total numbers (right chart, weight corrected data) of $CD4^+$ and $CD8^+$ T cells in the spleen. (WT, n=9; Flox, n=3; H/A, n=9). **(C)** Representative picture of flow cytometry results obtained from T cell analysis of blood. **(D)** Quantification of frequencies and counts of single positive T cells in blood. Frequency of H/A mice reveal reduction in single positive T cells (left chart). Weight correction of total number showed reduced T cell content which does not reach significance (right chart). Data were pooled from individual experiments, means ±SEM. Each dot in scatter plot depicts individual mice; WT, n= 5; Flox, n=3; H/A, n=5.

The next step was to identify if the accumulation of egress-competent T cells in the thymus leads to a decreased amount of circulating naïve T cells in the periphery (blood/PBMCs) and lymphoid tissue (spleen). Here, a reduced number of T cells (T cell lymphopenia) could cause severe infections of CerS2H/A mice due to limited immune response mediated by the adaptive immune system. Based on these considerations, cells were first subdivided upon the expression intensity of CD3 and B220 on the cell surface (Figure 5.32 A). $CD3^{high}$-expressing cells were further analysed regarding the expression of CD4 and CD8 (Figure 5.32 A).

The organ weight, as well as, the total cell number of splenocytes, is not affected by the expression of the mutated CerS2H/A protein (Figure 5.32 D/E). These results are consistent with findings from total cell numbers of PBMCs (blood, Figure 5.32 F.), i.e. no alterations were observed. Further flow cytometry analyses of splenocytes reveal a mild reduction in the frequency of $CD3^{high}$ positive cells, which does not reach significance (Figure 5.32 B). Further sub-gating of $CD3^{+}$ cells, regarding the expression of CD4 and CD8, indicate that counts and weight corrected cell counts show a reduction of $CD8^{+}$ T cells, whereas $CD4^{+}$ T cells were not affected (Figure 5.32 B).

In contrast, the overall immune cell composition of isolated PBMCs is affected by alterations in thymic egress of single positive T cells (Figure 40, C/D). Here, frequencies of T cells were significantly reduced, in contrast frequencies of double negative cells ($CD3^{low}$/$CD19^{low}$) increased, whereas frequencies of B cells remain unaffected (Figure 40, D left graph).

In summary, the present results indicate that the reduced body weight of CerS2H/A mice neither has an influence on the organ weight of the thymus or spleen, nor on the number of total cell counts. Furthermore, CerS2H/A mice show a significant increase of mature CD4+ and CD8+ thymocytes. The accumulation is not based on altered differentiation or developmental delay, since counts and weight corrected numbers of double negative/positive cells were not affected. Furthermore, the accumulation of T cells in thymus causes a mild reduction in T cell content in the periphery (spleen, blood). Moreover, CerS2H/A-mature-single-positive thymocytes are characterized by reduced CD69 surface expression levels. These findings strongly suggest an altered S1P gradient between the thymus interstitium and blood, since up-regulated S1PR1 expression mutually antagonizes CD69 surface level. All findings indicate the presence of a mild peripheral T cell lymphopenia and are in line with previous findings from $CerS2^{gt/gt}$ mice.

# 6 Discussion

CerS2, a member of the mammalian CerS family (CerS1-6), describes a key enzyme in sphingolipid metabolism, which catalyses the production of C22-24 ceramides. Additionally to the TLC (TRAM-Lag-CLN8) domain, harbouring the lag1 domain, which essential for catalytic activity (Spassieva et al., 2006; Tidhar et al., 2012), CerS2 is characterized by the presence of a further domain, the homeodomain. So far, not much is known about the structure and orientation as well as the detailed function and molecular mechanisms facilitated by the homeodomain in mammals (Mesika et al., 2007; Voelzmann, 2013). Additionally, it is already known from recent publications and experiments performed by the Willecke lab (Imgrund et al., 2009; Kremser et al. 2013) and Futerman-group (Pewzner-Jung et al., 2010 i/ii) that CerS2 is ubiquitously expressed. More precisely, results verified expression of CerS2 in hepatocytes (liver), oligodendrocytes and glial cells of the brain, in the respiratory epithelium and pulmonary alveoli of the lung, as well as in the renal corpuscle and proximal tubular cells in kidney, but also to a lower extent in thymus and spleen (Kremser et al., 2013; Kremser, 2016). Upon deletion of CerS2, i.e. the loss of catalytic activity, mice lack C22/24/24:1 ceramides and sphingolipid species and possibly drives the (compensatory) increase in C16/C18 ceramide species. Moreover, CerS2-deficiency results in the development of severe phenotypes, e.g. demyelination of neurons in the CNS its comorbidities and development of hepatocellular carcinoma (Imgrund et al., 2009; Pewzner-Jung et al., 2010 i/ii). Again, all these findings were obtained in mice, which completely lack CerS2-protein expression. Based on that it is nearly impossible to distinguish, which of the upcoming phenotypes and alterations are based in the loss of catalytic activity (C24-ceramides) and which are a consequence by loss of proper homeodomain function. To further investigate the in vivo function of the lag1 motif and the homeodomain independently from each other, we aimed to deplete catalytic activity and on the other hand, we tried to abolish homeodomain interaction. Therefore, the conditional transgenic mouse lines CerS2$^{H212A/H213A}$ and CerS2$^{Del79\text{-}120}$ were established.

## 6.1 Bioinformatics analysis and basic experimental setup (CerS2)

### 6.1.1 CerS2 – Orientation, Transmembrane topology, and Domain structure

The successful generation of two conditional mouse lines emphasises the need to understand the protein structure and topology, besides the knowledge of how CerS2 might be post-translational regulated. However, not much is known about the possible orientation of the CerS2 protein, its putative 2D-/ 3D-structure and the correct number of transmembrane domains and the common knowledge is based on sequence alignments and homology prediction analyses. All those findings as well as findings from publication of *in vitro* experiments, performed with all ceramide synthases, resulted in the generation and investigation of different CerS2-overexpression constructs to unravel, which targeted mutation might be most suitable for following *in vivo* analysis.

***Posttranslational modifications and localisation of the termini***

First, N-glycosylation prediction tools identified amino acid residue 19(N) and residue 81(N) to be possibly glycosylated. Overexpression of CerS2-WT-V5/His and CerS2Del79-120 with subsequent PNGaseF treatment of the generated protein lysates resulted in a band shift, i.e. reduced mass, for the WT and Del constructs. Based on these results we concluded that both proteins were glycosylated. Additionally, a previously tested CerS2Del74-96 construct showed

also the ability to be glycosylated (data not shown; van Uelft, 2012). All these constructs have a common feature, the lack of amino acid residue 81 and retention of aa19 (N). For that reason, it was supposed that only aa19(N) gets glycosylated and not aa81(N). This assumption is further strengthened by the loss of nearly the same mass (~3 kDa) in immunoblot analyses in all PNGaseF treated protein lysates in comparison to the CerS2WT construct, i.e. counting for only one glycosylation site within the protein. Additional generation of an N19Q-CerS2-V5/His construct could also further clarify that position 19(N) is glycosylated, since protein extracts from overexpressing cells showed a reduced mass in comparison to WT control and treatment with PNGaseF does not result in further band shift (data not shown). Ceramide synthase activity assay performed with protein lysates from N19Q-CerS2-/ CerS2-WT-V5/His expressing cells, showed equal synthase activity, strengthen the assumption that glycosylation is not necessary to maintain catalytic activity. These findings were also supported by Mitzutani (2005) where he could show that CerS2-(N19Q) is characterized by a, lack of glycosylation, but nothing was mentioned about the influence on catalytic activity. Additionally, they could also show that CerS5 and 6 were glycosylated in the N-terminus and that loss of glycosylation in CerS6 does not negatively influence catalytic activity, which is in line with our findings (Mitzutani et al., 2005). Taken together these findings also indirectly indicate the localization of the N-terminus of CerS2. More precisely, until now no cytoplasmic glycosylation complex has been identified, implying that N-terminus has to face the ER-lumen, where to this days the N-glycosylation enzymes are located (Stanley et al., 2017).

Moreover, it was shown by Sassa and collaborators that the mouse as well as human CerS2, protein can be C-terminally phosphorylated (S341, T346, S348, S349) and that phosphorylation is facilitated by the action of protein kinase CK2 (casein kinase 2; Sassa et al., 2016). Furthermore, they could show that lack/degree of phosphorylation influences catalytic activity. This interesting fact implicates a further indirect hint concerning the C-terminal localisation. Filhol (2003) and Bibby & Lichtfield (2005) identified that the two different subunits ($\alpha/\beta$) of CK2 show either cytoplasmic or nucleocytoplasmic localisation (Filhol et al., 2003; Bibby & Lichtfield, 2005). These findings lead to the conclusion that aa341-349 at the C-terminus face the cytoplasm, where they are easily accessible for CK2. This, in turn, also implicates that CerS2 must have an uneven number of transmembrane domains (5 or 7). Unfortunately, this assumption could not be further confirmed by transmembrane domain (TMD) prediction analyses, due to inconsistent results predicting, five, six or seven TMDs.

### *Localisation and function of the homeodomain of CerS2*

Regardless of previous findings, all collected data were re-evaluated regarding the localization of the homeodomain within the protein. As a result of these investigations, we can hypothesize that the homeodomain is localized between the first and second transmembrane domain. Additional findings obtained by homology prediction analyses reveal also that the homeodomain of CerS2 has the same probability to adopt a 3D-structure composed of three alpha helices, like CerS5 and 6. As this helix-turn-helix motif, where each alpha helix is connected by a loop to the following, is a common feature of transcriptional regulators, we further assume that CerS2 might regulate the expression of certain genes. However, the homeodomain of CerS2,5 and 6 might slightly differ from those of homeotic genes, since some alignment analyses predict that the first 15 amino acid residues of the consensus sequence may be missing (Levy et al., 2010; Voelzmann, 2013). On the other hand, our considerations are in line with recent findings from our group (Sociale et al., 2018). Sociale et al. could show that the homeodomain of schlank, the ceramide synthase in the fruit fly, adopt a 3x $\alpha$-helix-

conformation. Furthermore she also showed that the NLS2 motif within the third alpha helix is able to interact with the promoter region of lipase 3. Even more detailed investigations further confirmed that the homeodomain of CerS2 is also able to interact with the promoter region of lipase 3, when overexpressed in S2 cells. Furthermore, re-expression of CerS2-WT in the fat body of KINLS2-mutant flies repressed lipase3 expression and restores the endogenous situation to some extent (Sociale et al., 2018). Unfortunately, this current data could not have been taken into considerations of generating homeodomain-deletion constructs, since they have been made several years ago.

### 6.1.2 CerS2 expression vectors for *in vitro* experiments

In order to study the functions of the lag1 domain and those of the homeodomain independently from each other, bioinformatics analyses (e.g. sequence alignments) supported the information, necessary for the generation and testing of different mutation. The different constructs (Figure A5) were transiently transfected into HEK 293T cells or immortalized *cers2*-deficient MEFs. Overexpression was verified via immunofluorescence analyes of fixed cells, immunoblot analyses of protein lysates and in vitro assays. First, the replacement of the two highly conserved histidine residues by two alanine residues was done in respect to experiments performed with CerS1 (Spassieva et al., 2006). Our findings obtained for the CerS2H212A/H213A construct are in line with that of CerS1, where we could show that replacement-mutation results in loss of catalytic activity and that they are essentially necessary to maintain catalytic activity needed for N-acylation of the long chain base. Additionally, immunofluorescence and immunoblot experiments show strong expression of modified CerS2H/A protein, which lead to the conclusion that the introduced modification does not influence protein glycosylation, expression, and conformation. This, in turn, strengthened the assumption that the H/A mutation is suitable to study consequences arising from loss of catalytic activity and lack of C22/24-ceramide species independent from homeodomain function.

In contrast, no suitable CerS2-construct could have been initially generated in which the catalytic activity was not altered after modification of the homeodomain. With the help of published data of CerS5, we finally generated a deletion construct based on protein sequence alignments. Briefly, Mesika et al., (2007) showed that aa 87-128 can be deleted within the peptide sequence of CerS5, which does not alter its catalytic activity. As indicated in the beginning, sequence alignments of CerS2 and CerS5 resulted in the identification of the appropriate amino acids within the homeodomain of CerS2 and lead to the generation of the CerS2Del79-120 construct. The obtained results regarding the catalytic activity (after transient transfection and protein lysate preparation) in in vitro experiments are in line with that published for CerS5-(Δ87-128). Here, overexpressed CerS2Del79-120 and CerS2WT constructs show similar expression levels as well as similar levels of catalytic activity. Based on that we could show that the deletion of certain nucleotides (bp-bp) within the cDNA of cers2 lead (I) to the generation of the mutated-CerS2Del97-120 protein and (II) that the mutation does not alter catalytic activity, but affect the function of the homeodomain.

### 6.1.3 Future perspective – Unravelling homeodomain function *in vitro*

The generation of different CerS2-deletion constructs indicated that the catalytic activity is not dependent on the presence of the homeodomain; but that certain deletions negatively influence its conformation, thereby affecting protein expression and its function. Within this question, it would be helpful to deconstruct the 3D-conformation of the protein and how it is exactly integrated in the membrane and which parts are freely accessible.

Another recent finding verified that eleven residues at the C-terminus (aa291-301) of CerS2 might be responsible for the acyl chain specificity of each CerS protein (Tidhar et al., 2018). This newly identified "acyl-CoA-binding-motif" represents a further domain by which the catalytic activity could be regulated, e.g. positive/negative feedback loop dependent on substrate availability. Another possibility could be that it depicts an indirect measuring unit, which determines the body's energy status (feeding vs fasting state). This indirect measurement of nutrient supply and energy status could additionally affect the intracellular localisation of CerS2 and the other CerS proteins, i.e. facilitating shuttling from the ER to the nucleus, where the homeodomain might fulfill its function as a transcriptional regulator.

This assumption and additional function of CerS2 is further supported by recent findings obtained from schlank, the Ceramide synthase family member of the fruit fly (Sociale et al., 2018). Here Sociale et al. could show that schlank is energy-dependent shuttled from the ER to the nucleus or vice versa, to force/repress gene expression (Sociale et al., 2018). Therefore, the same approach could be used to further investigate and unravel the molecular mechanisms resulting in gene expression and are based on homeodomain function of CerS2:

(I) Different CerS2-tagged-overexpression constructs need to be generated and overexpressed in a suitable cell system. After verification of the expression level (immunoblot), catalytic activity (*in vitro* assay) and subcellular localisation (immunofluorescence) of the modified CerS2 proteins, the transfected cells can be challenged by application of different concentrations of acyl-CoAs (C16/18/C24:1, 2/5/10µM), sphinganine (2/5µM) and BSA (control); and the subcellular localization monitored upon fixation of the cells and immunofluorescence analysis with appropriate antibodies.

(II) The following constructs could be used: CerS2-NLS2 (RRRR→ ARAR), which carries a mutation within the homeodomain, the CerS2H212D construct, which has a mutation of within the Lag1 motif, and the CerS2Δ291-301 (ΔYPLELYPAFFG)-construct, which shows a deletion of the putative fatty acid binding region.

Based on previous findings, we speculate that the CerS2-constructs, modified within the acyl-CoA binding site, do not correspond to acyl-CoA application and remain in the ER-membrane. Additionally, it is suggested that the CerS2-WT, CerS2-NLS2, as well as CerS2H212D proteins show an altered subcellular localization (ER → nuclear membrane). Additionally, the CerS2-NLSII-mutated construct should show an altered localisation but an abrogated DNA-binding capability. Meaning, a different sub-cellular localization, would again strengthen the assumption that the homeodomain might function as a transcriptional regulator upon nutrient stimulation. In the next step, it might be indispensable to elucidate by chromatin immunoprecipitation (ChIP) assays whether the different constructs have the potential of DNA-binding and which genes are affected. It would also be of great interest to see, whether the homeodomains of other CerS might also function as a transcriptional regulator.

## 6.2 Generation and features of the gene targeting constructs & homologous recombination in ES cells

The conditional CerS2$^{H213A/H212A}$ and CerS2$^{Del79-120}$ exchange vectors used for homologous recombination of the *cers2* locus in ES cells were shown in Figure 5.5 and 5.6. Both contain at their 5' end the same homology region, which consist of a part of exon1 until exon2 as well as a minor part of the intron downstream of exon2 from the *cers2* gene. This is followed by the remaining genomic region of *cers2*, which is flanked by two loxP sites and an frt-flanked Neomycin-resistance cassette. Downstream of the loxP-flanked region is either the part of the construct containing the CerS2H212A/H213A mutation or the CerS2Del79-120 mutation. This is followed by an IRES-eGFP cassette and the 3'homology region, required for homologous recombination. eGFP was the reporter protein of choice since it smaller in size (720 bp) than the ß-galactosidase, *lacZ*, reporter gene (3kb). Another advantage is shown by the fact that eGFP shows a strong fluorescence signal when stimulated by UV-light compared to other members of the GFP-family (YFP, CFP; Patterson et al., 2001). This combined with the application of specific antibodies against GFP, allows the use of different approaches (e.g. IF and IHC) to additionally monitor cers2 expression.

PCR and Southern blot analyses of ES cell clones were done to verify correct insertion of the exchange vectors. In case for the CerS2$^{H212A/H213A}$ line, 12 out of 364 analysed ES-cell clones were positively tested. This represents a final recombination rate of 3.29 %. On the other hand, 13 out of 550 ES cell clones were positively tested for correct recombination (recombination rate: 2.36 %). The low recombination efficiency might be due to a relatively inaccessible (heterochromatic) region of the mouse genome. Moreover, karyotype analyses were performed for a minimum of four positive ES cell clones (Chapter 5.3.5). Finally, blastocyst injection of clone #110 (CerS2$^{H212A/H213A}$) and clone #61 (CerS2$^{Del79-120}$) resulted in the birth of several high-extend-agouti-fur-colored chimeric mice, which were either used for the generation of the new CerS2$^{H212A/H213A}$ (CerS2H/A) or the CerS2$^{Del79-120}$ (CerS2Del)mouse line.

Backcrossing of CerS2H/A mice with C57BL/6 (N) and Flp-recombinase (B6/J) expressing mice lead to the generation of the Flox-control mouse line (Rodriguez et al., 2000), which express the CerS2WT gene and lack the neomycin resistance gene. Mice show a C57BL/6 content of at least 87.5 %. Additionally, backcrossing of CerS2H/A chimeric mice with C57BL/6 (B6/N) and pgk-Cre (B6/J) expressing mice results in the loss of the loxP-flanked, "CerS2WT-frt-neomycin fragment" and the expression of the H212A/H213A-mutated *cers2* gene. Mice show a C57BL/6 content of 75 %. Backcrossing of CerS2Del mice with C57BL/6 (B6/N) and pgk-Cre (B6/J) mice lead to the replacement of the loxP-flanked "CerS2WT-frt-neomoycin-fragment" by the CerS2Del79-120 fragment, with a corresponding C57BL/6 content of 75 %.

Additionally, all mice were further investigated by PCR-analysis regarding the expression of the mutated nicotinamide (NAD) nucleotide transhydrogenase (NNT) gene. Here it was shown by Toye and others (Toye et al. 2005; Freeman et al. 2006) that the C57BL/6 J strain is positive for this mutation, which affects insulin secretion and glucose tolerance (Raichur et al., 2014; Park et al., 2014). To avoid any interaction of this mutation within the background, mice were backcrossed to a NNT-mutation-free (i.e. NNT-WT) background.

## 6.3 Biochemical characterization of targeted mutations in transgenic mice

### 6.3.1 CerS2 expression in CerS2H212A/H213A mice

Immunoblot analyses of several mouse tissue lysates verify the expression of the mutated CerS2 protein in CerS2H/A mice (Figure 5.15). Results of liver lysates indicate that the protein is glycosylated and that the mutation of the genomic locus does not result in abrogated transcription, which would have resulted in the loss of protein or altered protein mass. For both, CerS2H/A and Flox mice, we detected a protein running at equal height as that of WT lysates. This further implicates that genomic manipulation leads to gene expression and protein generation. However, the degree of protein expression in CerS2H/A and Flox mice of liver and several other tissues was not always comparable to that found in WT mice. In line with these findings are also the reduced mRNA levels of CerS2 found in both, CerS2H/A and Flox mice (Figure 5.15). Based on these findings we speculate that maybe the remaining loxP (H/A) or frt-loxP-flanked-CerS2H/A-locus in Flox mice or the position of the first loxP site within the intron between exon2 and 3, somehow interfere with the transcription. In addition; it should be noted that the analyses of the genomic locus of CerS2H/A mice as well as the cDNA transcripts of *cers2*$^{H212H/H213A}$ show the presence of the H/A mutation. Moreover, the replacement-mutation resulted in the generation of an additional PvuII restriction site, which was easily used to determine double histidine to double alanine mutation (Figure5.13).

Verification of downstream eGFP-reporter protein expression (facilitated by the interaction of the endogenous *cers2*-promoter and the presence of an upstream-IRES-cassette) showed the presence of the GFP protein in immunoblot analyses (5.15). GFP-expression levels in CerS2H/A mice were comparable to that found in CerS2Del mice. No GFP-expression was detected in Flox mice as expected. Based on this, we cannot conclude that eGFP expression reflects the endogenous level of CerS2 expression; we can only say that the eGFP reporter protein is expressed and is an appropriate way to monitor the overall expression of CerS2 in various tissues.

### 6.3.2 Protein degradation in CerS2Del79-120 mice

Surprisingly, verification of CerS2Del protein expression by immunoblot analyses of liver lysates and of several other tissues indicated a lack of protein expression. Even after strong overexposure, we could hardly detect a CerS2Del protein. This leads to the assumption, that the CerS2Del protein is either not translated, or directly degraded after translation. These results are in contrast to the findings obtained in *in vitro* experiments. There we could show that deletion of nucleotides 235 to 360 (126bp) within the cDNA sequence of *cers2*, corresponding to aa79-120 of the peptide sequence, results after transiently transfection in protein expression where the catalytic activity is not affected.

Besides that, verification of GFP-reporter protein expression results in the detection of the expected band upon normal exposure conditions. Furthermore, expression levels are comparable to the signals found in CerS2H/A mice. This in turn leads to the conclusion, that the endogenous promoter in combination with the IRES-cassette is working, which enables eGFP expression. And, that on the other hand, some unexpected alterations occurred that cannot be explained so far, which either adversely affect translation of the *cers2* mRNA or cause the early degradation of the CerS2Del protein.

### 6.3.3 Catalytic activity and mass spectrometric analyses

The CerS2H212A/H213A mutation was designed in order to replace two histidine residues (imidazole side chains) which function as a coordinating ligand in the catalytic centre, by two alanine residues. The alanine residues itself do not have the probability to switch between a protonated and un-protonated state, thereby inhibiting ceramide synthesis. Liver extracts were generated and results from radioactively-labelled ([4,5-$^{3}$H]-D-*erythro* sphinganine) *in vitro* assays indicate that desired HH/AA mutation lead to loss of catalytic activity; and are in line with previously performed cell culture experiments (Figure 5.2 and 5.3).

Coincident with the loss of CerS2Del protein is the lack of catalytic activity determined in liver lysates generated from CerS2Del mice.

Moreover, reduced ceramide synthase activity detected in liver lysates of CerS2Flox mice are in line with reduced *cers2* mRNA and protein levels, but does not proceed into altered sphingolipid content. Here, mass spectrometric analyses indicated same ceramide and sphingolipid levels like determined for WT control. This indirectly implicates that roughly 50 % of the *cers2* mRNA and protein are suitable to maintain sphingolipid content.

On the other hand, catalytic inactivation (H/A) or the lack of CerS2Del protein resulted in a strong decrease of C22:0, C24:0 and C24:1 ceramide species in liver extracts. Interestingly, observed reductions were accompanied by significant increases in short-chain ceramide levels (C16/18). However, increased levels were not able to restore total sphingolipid content. Since it is conceivable that the ceramide synthases mutually regulate each other, we subsequently examined the mRNA and protein expression levels of CerS4, 5 and 6. Protein expression level of CerS4 was not altered (Figure 5.15). On the other hand, immuno blot analyses of liver protein extracts showed increased expression levels of CerS5 and 6 (Figure.5.15). Additionally, these observations fit into the assumption that CerS5 and 6 are responsible for the increase in C16/18 sphingolipid levels, suggesting a compensatory mechanism, possibly aimed to reduce accumulating amounts of LCB and acyl-CoAs.

### 6.3.4 Future perspective – CRISPR/Cas9 vs traditional ES cell culture

The previously obtained results regarding the newly generated CerS2Del line strengthen the assumption that those mice were not suitable to investigate the putative functions of the homeodomain. Those mice show with the loss of the remaining nucleotides from exon3 and 4 in the mRNA, an even bigger deletion within the homeodomain of the protein than intended (Δ79-120 vs Δ59-137). Furthermore, the deletion results in an early stop of translation or rapid degradation of the protein, which unfortunately results in mice deficient for CerS2.

One solution represents the generation of a new mouse line, where the desired mutation should be re-defined and possibly be based on recent findings obtained by the analysis *schlank*, the ceramide synthase in the fruit fly (Sociale et al., 2018). At the present time two suitable methods are available, homologous recombination of a gene targeting construct or the homology-direct-repair with a designed oligonucleotide and gRNA, facilitated by Cas9 (CRISPR/Cas9).

The first method, homologous recombination of a conditional vector, allows the investigation of the targeted-mutation in a cell-type-specific manner, without affecting the whole organism (Figure 6.1). Furthermore, it facilitates monitoring the expression by the integration of an additional reporter gene (Bouabe & Okkenhaug, 2013). However, the disadvantages are not negligible. First, the approach is expensive and very time consuming (1 year), which requires the (I) design and generation of a conditional gene targeting vector, (II) the homologous

recombination, as well as the selection and verification of many ES cell clones (>200). Since ES cells could show low frequency of recombination events (Deng et al., 1992; Hasty et al., 1991). Furthermore, the success depends also on the availability to perform (III) microinjection of positive-selected ES cells into blastocysts and the subsequent transfer of those into the uterus of pseudopregnant foster mice. Next, breeding (IV) of chimeric mice, that showed coat-color chimerism with WT mice to pass the genetic modification onto the offspring and (V) breeding with appropriate Cre/ Flp mouse lines to establish the desired tissue-specific mutation, describes in additioan very time-consuming aspect.

Here, the conventional technique could be used for the generation of a CerS2NLSII line based on the already existing conditional gene targeting constructs and is illustrated in Figure 6.1. Briefly, the generation of the amino acid exchanges (RRRR→ARAR) can be achieved by the application of *DpnI*-mediated mutagenesis PCR. Here long-oligonucleotides (primer) introduce the modifications and simultaneously initiate amplification. The mutated DNA-fragment can then be transferred by normal cloning steps into the CerS2H/A-vector to generate the final CerS2NLSII-vector suitable for homologous recombination in ES cells.

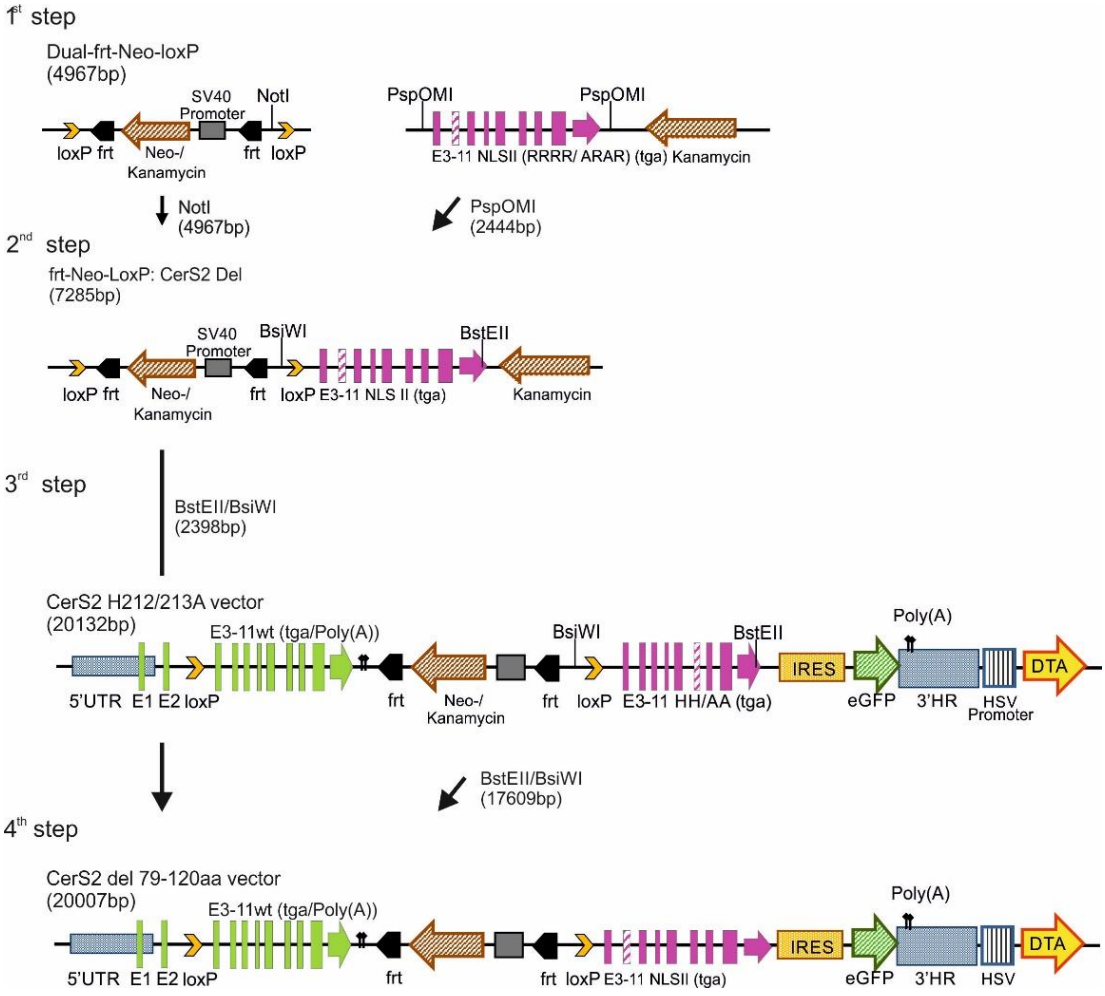


**Figure 6.1: Generation procedure of the CerS2NLS II gene targeting vector.** Graphical overview of the different cloning steps required for the generation of the CerS2NLSII-gene-targeting vector, which introduced a replacement of the RRRR (NLSII) residues by ARAR residues within the homeobox domain.

On the other hand, with the application of the CRISPR/Cas9 system (clustered regulatory interspaced short palindromic repeats/ CRISPR associated (Cas) protein number 9) one could circumvent much of these aspects. The new mice could carry a mutation within the putative NLS2-motif ('RRRR'- 'ARAR') of the *cers2* gene (Figure 6.2). The application of the CRISPR/Cas9 technology is suggested to be very efficient and faster than the conventional-gene-targeting approach (Hsu et al., 2014; Wang et al., 2013).

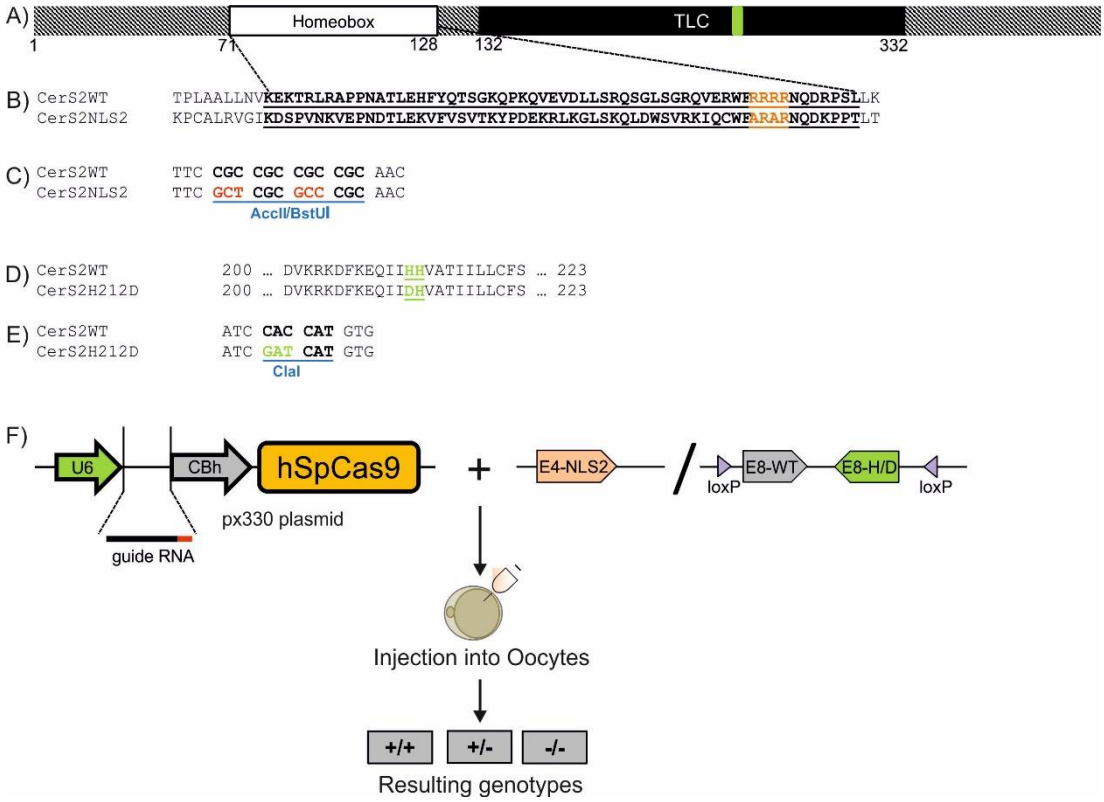


**Figure 6.2: CerS2 gene manipulation by CRISPR/CAS9. (A)** Schematic representation of predicted domains in mCerS2 (according to swissprot). **(B)** Alignment result of the amino acid sequence of the homeodomain present in CerS2. Underlined amino acids highlight homeodomain; bold-coloured faces depict putative NLS2 ('RRRR') signal in CerS2 WT protein. Sequence below shows possible NLS2 mutation. **(C)** Genomic DNA sequence of WT and NLS2 mutated CerS2 region. Mutation results in the introduction of an additional AccI/BstUI cleavage site. **(D)** Alignment result of the amino acid sequence containing two highly conserved histidine residues in the lag1 motif. **(E)** Genomic DNA sequence of CerS2 WT and CerS2H212D replacement. Mutation results in deletion of endogenous DraIII restriction site and introduction of a new ClaI site. **(F)** CRISPR/Cas9 approach requires the generation of the px330 plasmid (Addgene), containing the desired guide RNA. U6 promoter is already cloned in frame, as well as the CAS9 endonuclease. The right side depicts the generated oligonucleotides suitable for homology direct repair. Px330 vector in combination with one of the oligonucleotides is injected into fertilized oocytes. The following founder generation possibly contain WT, heterozygous and/or homozygous mice.

Briefly, it requires the presence of a Cas9 endonuclease, a target recognition CRISPR-RNA, which shows sequence homology to the region desired for mutation; and a Cas9-recruiting tracer RNA; both also termed as single guide RNA (sgRNA). The guide with a 'protospacer-adjacent motif (PAM)', depicts a specific sequence pattern of 20 nucleotides (N) followed by an NGG-motif (20N-NGG) (Mali et al., 2013; Young et al., 2015), which has to be mutated in the oligonucleotide delivered for homology direct repair. Microinjection of either a plasmid coding for the guide RNA and the Cas9 (pX330 vector, Addgene, Mashiko et al., 2014) or co-injection

of sgRNA and the mRNA of Cas9 into fertilized oocytes should lead to induction of CRISPR/Cas9 machinery. Cas9 is recruited to the desired genomic DNA sequence in a site-specific manner, mediated by the sgRNA. Next, Cas9 cleaves 3nt upstream of the PAM site, which results in double-strand brake (Jinek et al., 2012; Cong et al., 2013; ;Mali et al., 2013), which in turn can be repaired by two mechanisms; (I) non-homologous-end-joining (NHEJ) or by (II) homology direct repair (HDR) (Young et al., 2015; Chu et al., 2015). The NHEJ utilizes host-own proteins for the recognition and repair of the double-strand break and depicts an error-prone process, i.e. it results in indels (Young et al., 2015), which is not favourable. The second and preferred repair mechanism is the HDR. Here, co-injection of an oligonucleotide, which shares sequence homology to the targeted gene, results in direct repair by homologous recombination. Modification of the oligonucleotides can result in the insertion of directed mutations, which alter gene function; Chu et al., 2015). Furthermore, in combination with the Cre/loxP approach one could also generate a conditional CerS2H212D mouse line, which expresses a catalytically inactive version of the protein upon breeding with Cre-expressing mice (Fig.). Additionally, one has to consider that the efficiency of integration of loxP-site containing oligonucleotides by HDR is rather low (Wang et al., 2013; Bishop et al., 2016).

## 6.4 Analysis of energy metabolism of CerS2H212A/H213A and CerS2Del79-120 mice

One main significant risk of health is the development of obesity and the progression of its comorbidities, caused by constant nutrient-oversupply. The recent literature summarizes many investigations and findings regarding CerS function and sphingolipid content in the development of diet-induced obesity. Among them are studies performed with CerS5 and 6-deficient mice, indicating that loss of C16:0 ceramide species protects mice from weight gain after feeding a high-fat diet (Turpin et al., 2014; Gosejacob et al., 2016). Additionally, CerS5-deficient mice showed improved glucose-homeostasis and reduced adipose tissue inflammation (Gosejacob et al., 2016). On the other hand, heterozygous deletion of CerS2 expression resulted in reduced C24:0/24:1 ceramide levels and increased C16 sphingolipid levels inducing mice to become susceptible to diet-induced obesity and the development of steatohepatitis and insulin resistance (Raichur et al., 2014).

### 6.4.1 Weight gain and lipid content in CerS2H212A/H213A mice

To investigate basal consequences arising from homozygous impairment of CerS2´s catalytic activity in respect to the development of weight gain and growth, CerS2 WT and H/A mice were fed a normal chow. For the first time, we could show that food-intake is altered in male as well as female mice, i.e. mice ingest more food per gram body weight than WT littermates (Figure 5.18). Surprisingly, the mice gain less weight over time. Additional findings obtained from CerS2$^{gt/gt}$ mice are in line with our results (Park et al., 2014). They could verify that CerS2 depletion protects mice from weight gain (obesity) either fed a low-fat or high-fat diet (Park et al., 2014).

Moreover, analysis of CerS2H/A mice indicate, that loss of catalytic activity impairs hepatic storage-lipid levels, which is not based on altered intestinal lipid absorption (Figure 5.19). More precisely, TLC analysis of lipid composition of feces from CerS2H/A mice showed a strong reduction in 1,2 DAG and TAG level in comparison to WT control samples (Figure 5.19). These findings lead to the conclusion that secretion of bile salts as well as pancreatic juice is not altered and leads to intestinal lipid digestion. Furthermore, equal FFA content between CerS2WT and H/A mice suggests normal absorption by enterocytes. Additional H&E staining

on colon sections did not indicate alterations in tissue architecture (Figure 5.26). PAS-staining also indicated equal glycogen-content in colon sections of CerS2H/A and WT mice (Figure 5.26).

Further investigations of liver- , adipose tissue- and muscle lipid composition highlighted several alterations. First, TLC analysis of liver-lipid extracts indicate a strong reduction in TAG, DAG and FFA-levels and are in line with findings obtained in CerS2gt/gt mice (Figure 5.19/ 5.20, Imgrund et al., 2009; Park et al., 2014). Second, OilRedO staining verified also loss of lipid droplet formation/accumulation in liver sections of CerS2H/A mice (Figure 5.21). These results are also in line with previously published findings of schlank-mutant flies, where the loss of catalytic activity leads to reduced TAG level and enhanced lipase3 (TAG lipase) and brummer (ATGL lipase) expression (Bauer et al., 2009). In addition, PAS-staining indicated reduced glycogen-content; and H&E staining indicated loss of normal liver architecture, reduced hepatocyte diameter as well as a reduced number of bi-nucleated hepatocytes besides an abnormal increase of nuclei-diameter (Figure 5.22). Findings of liver architecture alterations were further supported by immunoblot analysis determining enhanced expression levels of tumor marker and indirectly depicted the early onset of liver cancer development and are possibly reasonable for destruction of liver architecture. However, it should be noted that tumor formation could also be an indirect consequence of an additionally altered signalling pathways (Figure 5.23).

Analysis of CerS2H/A-adipose-tissue mass and lipid composition revealed a reduction in weight and surprisingly inhomogeneous distribution of adipocytes with varying cell diameter. Furthermore, lipid content showed significantly increased DAG level, next to slightly elevated FFA, cholesterol and cholesterol-ester level. These findings somehow differ from that obtained in CerS2gt/gt mice, where no alterations were observed (Park et al., 2014). On the other hand, these findings are comparable to that found in mutated-schlank (schlankG0061 and schlankG0349) larvae (Bauer et al., 2009). As the name implies, schlank-deficiency results in slim-shaped larvae and decreased fat accumulation in the fat body in comparison to WT. Based on these findings and recent publications, we assume that homeodomain of CerS2, like that of schlank, possibly function as a transcriptional regulator of genes involved in lipogenesis and lipolysis. More precisely, we assume a decreased repression of lipolysis, resulting in the up-regulation of lipases, concomitant with decreasing storage lipid levels and reduced adipose tissue mass. Simultaneously, depleted glycogen-storages of CerS2H/A mice also fit in this assumption. It might describe a possible consequence of altered FFA uptake, arise from higher energy-demand of tumor cells or might be a consequence of mitochondrial dysfunction (Park et al., 2013). Here, "starvation-condition", e.g. lack of lipid accumulation in CerS2H/A-hepatocytes drives breakdown of glycogen to obtain glucose as remaining energy source. This assumption is further supported by our own results and those obtained from Park (2013). They and we could show that intestinal glucose-absorption/ glycogen-content of enterocytes is not altered and that liver gluconeogenesis was increased to satisfy high-energy demand (Park et al., 2013). Another possible explanation for an altered lipid uptake and "starvation-like" phenotype of hepatocytes could be based on an altered hepatic plasma membrane composition as suggested for CerS2gt/gt mice (Park et al., 2013/ 2014). They indicate that loss of very-long-chain sphingolipid species (C22-24) possibly results in a compensatory increase of short-chain ceramides (C16/18), responsible for altered membrane fluidity. However, preliminary experiments performed with membrane sheets of CerS2-derived hepatocytes did not indicate alterations in lateral diffusion of overexpressed IR (insulin receptor, Figure A12). Based on these findings it is more likely that ablation of specific sphingolipid species was

responsible for transmembrane transporter/receptor dysfunction, i.e. proper function depends on the interaction of sphingolipid with specific acyl chain length N-acylated to the sphingoid long chain base.

At least, no alterations were observed in TLC analysis of muscle lipid content between CerS2H212/213A and WT mice. These findings fit into the assumption that CerS1 and not CerS2 is the pre-dominantly expressed CerS in muscle; and that catalytic inactivation does not negatively influence lipid/energy metabolism in that tissue.

### 6.4.2 Transcriptome analysis of liver enzymes involved in lipid synthesis

Another aim of this study was to link present phenotypic alterations, observed in liver of newly generated CerS2H/A mice to up- and down-regulated genes, thereby elucidating involved signalling pathways.

Initially and based on previous findings obtained from analyses of *schlank* in *D. melanogaster* and CerS2$^{gt/gt}$ mice, we re-capitulate gene expression of those involved in fatty acid uptake, -synthesis and lipolysis by qRT-PCR analyses (Figure A11, Bauer et al., 2009; Pewzner-Jung 2010ii; Sociale et al., 2018). In detail, we could verify that ablation of catalytic activity negatively influences the expression of *de novo* fatty acid synthesis, as well as negatively regulate the expression of enzymes involved intra-hepatic TAG synthesis (Figure A11). Moreover, decreased C24-ceramide levels somehow induce lipolysis, which might be a mechanism to compensate decreased fatty acid uptake. On the other hand, lipolysis depicts the counter-part of *de novo* synthesis and could be influenced by homeodomain function. The detected decreased expression levels of ELOVL3 and 6, possibly result in reduced C16-24:0 saturated fatty acid (SFA) levels (Sassa & Kihara, 2014), which is hypothetically determined by the newly identified "acyl-CoA-binding motif" within the C-terminus of CerS2 (Tidhar et al., 2018). Additionally, we assume that this "indirect" measurement of a "fasting-state" induces lipolysis. Since the homeodomain of CerS2H/A mice is not affected, it is thought to facilitate this regulatory mechanism. We speculate that upon decreased FFA-level, the CerS2H/A protein is shuttled from a nuclear localisation to an ER localisation, resulting in the inhibition of gene-repression, which in turn initiates lipase generation and ended up in TAG degradation (also see Sociale et al., 2018 for comparison).

### 6.4.3 Future perspective – conditional CerS2H212A/H213A expression in liver and brain

#### 6.4.3.1 CerS2H212A/H213A expression in liver & energy metabolism

In this study, the focus of characterising CerS2H/A (Del) mice was initially based on re-capitulation of already described phenotypes obtained from CerS2$^{gt/gt}$ mice, to decipher alterations driven by the loss of catalytic activity.

In that respect, future studies should either focus on (I) the generation of a liver-specific CerS2H/A expressing mouse line or on (II) challenging of already existing mice by high-carbohydrate diet, to investigate if and how glycogen-content is restored in liver. Additionally, it would also be of great interest to investigate the lipid content of enterocytes by OilRedO staining and TLC analysis to further support, that either depletion of specific lipid class than altered membrane fluidity is responsible for function/dysfunction of CD36/FAT transporter and that ablation of catalytic activity possibly does not influence enterocyte lipid composition. Moreover, expression of glucose transporter and enzymes involved in

gluconeogenesis/glycogen- break down in muscle, adipose tissue and liver could be further investigated to gain more insights into glucose homeostasis and to verify if catalytic inactivation cause alterations. Additionally, it might be important to analyse serum levels of e.g. albumin, leptin, glucose and insulin, to unravel if the mice show further alterations, which might explain the increased food intake and reduced weight gain.

#### 6.4.3.2 CerS2H212A/H213A expression in brain & behavioural test

It was already suggested that CerS2-deficiency lead to an altered ratio of expected genotypes after birth and was proven by analysis of littermates derived from heterozygous breedings of CerS2H/A or Del mice. Here, we could show that catalytic inactivation negatively influences the yield of homozygous mice (Figure 5.13). Moreover, analyses strengthen the assumption that the inactivation of CerS2 also influences the survival rate of homozygous mice (H/A and Del) during the first two weeks of lifespan (Figure 5.14). Preliminary findings, based on routine observations during the course of single animal assessment, indicate that CerS2H/A and Del mice did not only suffer under increased mortality rate, they developed also behavioural alterations (Figure 5.14). In detail, 11/62 (17.7%) CerS2H/A mice showed hind limb paraplegia and other 7/62 (11.3%) epileptic behaviour, which exacerbate with rising age. Similar numbers were obtained for CerS2Del mice, where 14/47 (29.8%) show hind limb paraplegia and 3/47 (6.38%) an epileptic phenotype. Until now, only liver phenotypes and alterations were investigated, but the recent findings in combination with the brain-phenotype (demyelination, reduction of myelin-associated protein-MAG) observed in CerS2$^{gt/gt}$ mice strengthen the importance to intensify investigations of brain-development in CerS2H/A (Del) mice. More precisely, one could generate a mouse line, which exclusively expresses CerS2H/A in oligodendrocytes, the cell type in the brain responsible for myelination of never fibres. The main advantage of this tissue-specific mutation, results in decreased side effects arising from loss of catalytic activity/C22-24 sphingolipid classes in other tissues. Further, lipid content analysis by mass spectrometry and activity assay could be used to determine current-lipid state and behavioural analyses test (Open-field behavioural habituation, One-trial object recognition or Anxiety-like behaviour in the elevated plus-maze) could decipher if and how demyelination impairs processing and signalling.

## 6.5 Immune status of CerS2H212A/H213A mutated mice

The precise development, proper differentiation and egress of naïve T cells is of fundamental importance to maintain the functions of the adaptive immune system, which are responsible for the protection of the organism against invading pathogens or harmful agents (Kenneth et al., 2012; Lodish et al., 2016). The main key player in thymic emigration depicts the tightly controlled maintenance of a chemically gradient by the sphingolipid S1P, which is present in low levels in the thymic interstitium and in high levels at the cortico-medullary junction/ blood (Resop et al., 2016; Saba, 2017). Upon positive and negative selection, thymocytes undergo a developmental program from immature to mature state. In line with this is the up-regulation of certain cell surface marker, that enables them to respond and migrate along the S1P gradient and finally to leave the thymus into circulation to become an active part of the adaptive immune system. It is known from several studies, that the S1P gradient is kept by the action of intracellular S1P lyase in dendritic cells (Schwab, 2017; Zamora-Pineda et al., 2016) and to a minor extent also in epithelial thymic cells. On the other hand, the precise regulatory mechanisms that control the exact architecture are yet not fully elucidated and require further investigations (Yanagida & Hla, 2017).

With the present study and the newly generated conditional CerS2H/A mice we wanted to recapitulate recent findings performed with non-conditional CerS2$^{gt/gt}$ mice (Rieck et al., 2017). Based on the insertion of a gene trap construct into the *cers2* gene locus, the mice are depicted by a loss of functional CerS2 protein, which is in line with the lack of CerS2-acyl-CoA specific ceramides and sphingolipids (Imgrund et al., 2009). Furthermore, mice show a compensatory increase in C16 and C18 sphingolipids (Imgrund et al., 2009; Pewzner-Jung et al., 2010 i/ii). Moreover, CerS2-deficiency leads to the distortion of the S1P gradient between thymus and blood. This, in turn, results in the accumulation of mature single positive T cells and a T cell lymphopenia in the periphery (Rieck et al., 2017). They propose a model in which CerS2 expression in endothelial cells maintains the S1P gradient in the thymus and that it additionally limits the level of circulating S1P (Rieck, 2017). Thereby they highlight CerS2 as a novel factor for regulation of S1P homeostasis next to SPHKs and SP1 lyase (Rieck, 2017; Pham et al., 2010).

### 6.5.1 Early T cell development is not affected in CerS2H212A/H213A male mice

The adaptive immunity is highly dependent on the thymus and its function to provide a unique cell and microenvironment needed for proper T cell development and function (Takahama et al., 2006). In this course, bone marrow derived progenitor cells enter the thymus via the cortico-medullary junction and undergo several sequential differentiation and proliferation steps, which are further characterized by a distinct migration, i.e. each subpopulation covers a specific region of the thymus (Ceredig & Rolink, 2006; Zuniga-Pflücker, 2004). Furthermore, maturation is explained by the emergence of a divers TCR repertoire and the differentiation into the CD4 or CD8 positive lineage. Upon positive and negative selection, non-functional or self-reactive T cells were eliminated. Upon that, only about 1-5 % of those cells survive and express a functional and self-tolerant TCR. Moreover, they proceeded further signalling to complete the development and become part of the peripheral T cell repertoire (Cano & Lopera, 2013).

The recent findings show that ablation of CerS2 catalytic activity does not alter T cell development of male mice in general. However, we detected a significant reduction in cells of developmental stage DN1 and DN3, whereas DN2 and DN4 showed only tendency of reduced amounts. Furthermore, the minor amount of DN cells in CerS2H/A mice does not continue or gain strength in the subpopulation of double positive cells. Here, CerS2H/A mutated mice show similar frequencies, counts (raw data) and cell numbers after weight correction in comparison to their wild type littermates.

With regard to analysis performed in female mice (data not shown) we could also verify recent findings performed with CerS2$^{gt/gt}$ mice (Rieck et al., 2017). So far, female mice show an altered T cell development upon mutation of CerS2's catalytic activity and/or on the occurrence of its comorbidities. Additionally, it must be taken into consideration that these findings need further support on the basis of low replications and high variability.

Taken together these findings indicate that CerS2 plays a minor role in the T cell development of male mice in comparison to female mice. However, these findings need further investigations. First of all, the robust reproduction of results for female mice and later on the involvement of CerS2 in the process of hormone-driven thymic and T cell development, by quantification of specific sex-related hormone levels in the blood.

### 6.5.2 CerS2H212/213A mutation affects thymic egress of single positive thymocytes and induces mild T cell lymphopenia

The precise mechanisms, which contribute to the generation of the S1P gradient between the perivascular space / blood and thymus, were not fully understood so far. However, it is well characterized that low S1P levels in the thymic interstitium and high S1P levels in the perivascular space/ blood are crucial to allow proper migration and egress of single positive mature T cells (Resop et al., 2016; Schwab et al., 205; Yanagida & Hla, 2017). Furthermore, the maintenance of this gradient is thought to be the result of a well-controlled, 'S1P-synthesis-export-degradation-cycle' which requires the interaction of different cell types and enzymes (Zamora-Pineda, et al., 2016; Resop et al., 2016; Yanaga & Hla, 2017). Furthermore, it was verified that uptake via S1PR1 and intracellular S1P degradation, by S1P lyase, in dendritic cells is needed to facilitate low interstitial S1P level and to a minor extent the expression of S1P lyase and dephosphorylating enzymes in thymic epithelial cells (Zamora-Pineda et al., 2016; Saba, 2017). On the other hand, high S1P level at the thymic exit site (cortical junction/perivascular space) is facilitated by neural crest-derived pericytes, which generate and secrete S1P (Saba, 2017). Moreover, high level of S1P in blood plasma is maintained by the involvement of many cell types (e.g. hepatocytes, erythrocytes), which synthesise and subsequently release S1P (Gazit et al., 2016). The transport of S1P is carried out either by HDL and LDL-associated apolipoprotein M or by albumin (Gazit et al., 2016).

The observed results for CerS2H/A mice indicate an accumulation of mature CD4 and CD8 positive T cells within the thymus. Additionally, those cells were further characterized by the down-regulation of CD69, which we used as a marker for high S1PR1 expression due to the lack of an appropriate S1PR1 antibody in combination with the fortunate fact that they were mutually regulated. Numbers of immature double or single positive thymocytes were not affected. On the other hand, further analysis of lymphocyte composition of peripheral lymphoid tissues, i.e. spleen and PBMCs (blood) indicate a mild T cell lymphopenia in combination with increased numbers of double negative ($CD3^{low}/B220^{low}$) cells whereas numbers of B cells were unaffected. These findings point into the direction, that CerS2H/A mice have an impaired thymic egress of mature T cells. Although we have not measured S1P level in blood (serum) and thymic parenchyma, we assume a similar distortion of the S1P gradient as it was described for $CerS2^{gt/gt}$ deficient mice due to lack of catalytic activity and loss of CerS2-specific ceramides and sphingolipids (Imgrund et al., 2009; Rieck et al., 2017).

Moreover, publications from recent years clearly demonstrate that even minor alterations of the S1P gradient formed between thymus and blood or lymph nodes and blood has major effects regarding the emigration and migration of T cells. Vogel (2009) demonstrated by the application of a S1PL null mice, which lack in S1P lyase activity, that those mice had higher proportions of mature CD4+ and CD8+ cells which were additionally depicted by a complete loss of CD69 surface expression. Furthermore, the S1PL-/- mice show a complete loss of peripheral T cells. Additionally, mice lacking the sphingosine kinases (SPHK 1, 2) maintain normal plasma S1P level, but show a strong reduction of S1P in lymph nodes which results in the block of lymphocyte egress from LNs and Peyer's patches (Pham et al.,2010). Moreover, not only the precise expression of synthesizing and degrading enzymes, but also the proper function of S1P specific receptors has a major influence on the T cell distribution. Resop (2016) could show for example that S1PR1 is the main S1P receptor expressed in the human thymus and that it plays a major role in thymocyte egress. Additionally, Matloubian (2004) demonstrated with the application of mice which lack S1PR1 in hematopoietic stem cells, that

they show strong ablation of naïve T cells in circulation and on the other hand an accumulation of mature CD4 and CD8 single positive cells within the thymus, whereas numbers of immature double positive (CD4+/CD8+) cells were not affected. Furthermore, they pointed out that these results are comparable to that found in mice treated with FTY720. FTY720 is a derivative of myriocin, which inhibits sphingolipid metabolism and acts as an immunosuppressive drug that negatively affects T cell egress (Matloubian et al., 2004; Braumrunker et al., 2007).

Based on our results and findings performed by others it might be most likely, that loss of CerS2's catalytic activity has a major influence on the maintenance/impairment of the S1P gradient. Moreover, the occurrence of weaker accumulation and milder T cell lymphopenia in peripheral tissues could have one reason in the low, i.e. mixed C57BL-6/SV129 background of the mice. The latter experiments performed with the CerS2$^{gt/gt}$ mice showed at least 93.75 % of C57BL/6N or J, with some animals having the NNT mutation in the genome (Ronchi et al., 2013). Mice used in our experiments were only of at least 75 % C57BL/6N, but tested-free of NNT mutation. For further analysis, or cell-type specific CerS2 mutation it should be considered to backcross several times in an appropriate genetic background. Additionally, it needs to be verified if the S1P-gradient is distorted in the newly generated CerS2H/A mice, by quantitative analysis of S1P levels in plasma, thymus and other lymphoid tissues. Furthermore, it should be also recapitulated and further investigated in which cell types and to which amount CerS2 is expressed to ascertain the precise microenvironment that contributes to the phenotype. Additionally, it should be considered to directly measure the surface expression of S1PR1, by application of new protocols.

Nevertheless, the newly generated conditional CerS2H/A mice recapitulated recent findings performed with CerS2$^{gt/gt}$ mice (Rieck et al., 2017). Thereby reflecting that ceramide synthase 2 is a further factor which somehow is involved in the maintenance of the S1P homeostasis and an additional modulator in facilitating thymic egress of mature T cell.

These recent findings also emphasise CerS2 as a potent regulator, in terms of pharmacological treatment, to prevent the development of immune-diseases based on reduced numbers of naïve T cells.

# 7 Summary

Ceramide species are the precursor of sphingolipids, which serve as structural components of biological membranes or are bioactive molecules. In mammals, ceramides are synthesised by a family of ceramide synthases (CerS) 1 to 6. They catalyse the N-acylation of a sphingoid long chain base and a fatty acyl-CoA of varying chain length. All ceramide synthases harbour a lag1p motif essentially necessary for catalytic activity and all CerS, except CerS1, contain a homeodomain of unknown function.

During this PhD thesis, different CerS2-overexpression constructs were generated and investigated to identify mutations suitable to analyse the catalytic function independent from homeodomain function of the mCerS2 protein. Consequently, two different CerS2 conditional mouse lines were generated, CerS2$^{H212A/H213A}$ (H/A) and CerS2$^{Del79-120}$ (Del). Both mouse lines show a high mortality rate and develop severe phenotypic alterations.

In H/A mice, the coding region of *cers2* was exchanged by a CerS2H212A/H213A-eGFP fragment, resulting in the expression of a CerS2 point-mutated protein. Additional IRES-driven GPF-expression was used to monitor *cers2H/A* expression and to verify the presence of the CerS2H/A protein. *In vitro* assays confirmed that catalytic activity of CerS2 is lost in H/A mice. Additional qRT-PCR and immunoblot analyses confirmed expression of the CerS2H/A protein in all analysed tissues. Expression levels (mRNA or protein) however do not always correlate with that of WT control. Furthermore, the H/A replacement-mutation results in alterations of lipid and energy metabolism. First, Mass spectrometric analysis showed strong reduction in C22/ C24/ C24:1 ceramide species and an increase in long-chain ceramides (C16/C18), which does not restore the total sphingolipid content. Analysis regarding the storage lipid content of liver highlight significant reduction in TAG, DAG and FFA levels in mutated mice, which is accompanied by reduction in white adipose tissue (WAT) mass. Morphological and histological investigations of H/A mice revealed reduced body weight as well as size, while adipocyte size is even more disproportionately reduced. On standard diet, H/A mice ingest more food, but show less weight gain, which is not based on altered intestinal lipid absorption. Liver sections showed loss of lipid droplet formation and an unexpected loss of glycogen-content. Moreover, catalytic ablation also leads to the development of hepatocellular carcinoma. Transcriptome analyses performed in combination with detailed qRT-PCR analyses show down regulation of genes involved in lipid metabolism. Immunological analyses of H/A mice showed that depletion of catalytic activity and loss of corresponding ceramide species negatively affects egress of mature single positive T cells from the thymus into the periphery. Accumulation of naïve T cells within the thymus results in a mild T cell lymphopenia.

The CerS2$^{Del79-120}$ mutation was verified in cell culture experiments first. After transient transfection of the CerS2Del79-120 plasmid, the mutated CerS2 protein was expressed and further investigations indicate, that the deletion within the homeodomain had no effect on the catalytic activity. Yet, the Del mice show complete loss of the CerS2Del protein, leading to a loss of catalytic activity and a lack of C22-24 ceramide species. Del mice show the same phenotype as the CerS2$^{gt/gt}$ and H/A mice.

All findings indicate that the catalytic domain of CerS2 is important for the synthesis of C22/C24 ceramide species. It is also necessary to maintain CerS2s regulatory functions in lipid and energy metabolism and to facilitate those functions, which allow the thymic egress of mature T cells.

# 8 References


Akiko Iwasaki and Ruslan Medzhitov. Control of adaptive immunity by the innate immune system. Nat Immunol. 2015 April ; 16(4): 343–353.

Alberts, B. (2008): Molecular biology of the cell. 5th Edt. New York: Garland Science.

Alfatah M1, Wong JH1, Nge CE1, Kong KW2, Low KN1, Leong CY1, Crasta S1, Munusamy M1, Chang AML1, Hoon S2, Ng SB3, Kanagasundaram Y4, Arumugam P5. Hypoculoside, a sphingoid base-like compound from Acremonium disrupts the membrane integrity of yeast cells. Sci Rep. 2019 Jan 24;9(1):710.

Arana L, Gangoiti P, Ouro A, Trueba M, Gómez-Muñoz A. Ceramide and ceramide 1-phosphate in health and disease. Lipids Health Dis. 2010 Feb 5;9:15.

Bandet CL, Tan-Chen S, Bourron O, Le Stunff H, Hajduch E. Sphingolipid Metabolism: New Insight into Ceramide-Induced Lipotoxicity in Muscle Cells. Int J Mol Sci. 2019;20(3):479.

Bartke N, Hannun YA. Bioactive sphingolipids: metabolism and function. J Lipid Res. 2009;50 Suppl(Suppl):S91–S96.

Barz WP, Walter P. Two endoplasmic reticulum (ER) membrane proteins that facilitate ER-to-Golgi transport of glycosylphosphatidylinositol-anchored proteins. Mol Biol Cell. 1999;10(4):1043-59.

Bauer, R, Voelzmann, A, Breiden, B, Schepers, U, Farwanah, H, Hahn, I, Eckardt, F, Sandhoff, K and Hoch, M ( 2009) Schlank, a member of the ceramide synthase family controls growth and body fat in Drosophila. EMBO J 28, 3706– 3716.

Baumruker T1, Billich A, Brinkmann V. (2007) FTY720, an immunomodulatory sphingolipid mimetic: translation of a novel mechanism into clinical benefit in multiple sclerosis, Expert Opinion on Investigational Drugs, 16:3, 283-289.

Becker I., Wang-Eckhardt L., Yaghootfam A., Gieselmann V., Eckhardt M. (2008). Differential expression of (dihydro)ceramide synthases in mouse brain: oligodendrocyte- specific expression of CerS2/Lass2. Histochem Cell Biol. 129 (2): 233-241.

Bellini L, Campana M, Mahfouz R, Carlier A, Véret J, Magnan C, Hajduch E, Le Stunff H. Targeting sphingolipid metabolism in the treatment of obesity/type 2 diabetes. Expert Opin Ther Targets. 2015;19(8):1037-50.

Bibby AC, Litchfield DW. The multiple personalities of the regulatory subunit of protein kinase CK2: CK2 dependent and CK2 independent roles reveal a secret identity for CK2beta. Int J Biol Sci. ;1(2):67–79.

Bickert A, Kern P, van Uelft M, Herresthal S, Ulas T, Gutbrod K, Breiden B, Degen J, Sandhoff K, Schultze JL, Dörmann P, Hartmann D, Bauer R, Willecke K. Inactivation of ceramide synthase 2 catalytic activity in mice affects transcription of genes involved in lipid metabolism and cell division. Biochim Biophys Acta Mol Cell Biol Lipids. 2018 Jul;1863(7):734-749.

Bickert A. (2016). Biological functions of Sphingomyelin synthase related protein and Ceramide synthase 4 investigated with transgenic mouse mutants. PhD thesis, Mathematisch-Naturwissenschaftlichen Fakultaet der Rheinischen Friedrich-Wilhelms-Universitaet Bonn.

Bikman B.T., Summers S.A. (2011). Ceramides as modulators of cellular and whole body metabolism. J Clin Invest. 121(11):4222-30.

Bishop KA, Harrington A, Kouranova E, et al. CRISPR/Cas9-Mediated Insertion of loxP Sites in the Mouse Dock7 Gene Provides an Effective Alternative to Use of Targeted Embryonic Stem Cells. G3 (Bethesda). 2016;6(7):2051-61.

Bligh, E.G. & Dyer, W.J. (1959) A RAPID METHOD OF TOTAL LIPID EXTRACTION AND PURIFICATION. Can. J. Biochem. Physiol., 37, 911–917.

Bouabe H, Okkenhaug K. Gene targeting in mice: a review. Methods Mol Biol. 2013;1064:315-36.

Breslow DK, Collins SR, Bodenmiller B, et al. Orm family proteins mediate sphingolipid homeostasis. Nature. 2010;463(7284):1048–1053.

Bullock, W. O., J. M. Fernandez, and J. M. Short (1987). "XL1-Blue: a high efficiency plasmid transforming recA Escherichia coli strain with beta-galactosidase selection. ." Biotechniques 5: 376-378.

Cano and. Lopera. Chapter 5, Introduction to T and B lymphocytes from Anaya JM, Shoenfeld Y, Rojas-Villarraga A, et al., editors. Autoimmunity: From Bench to Bedside. Bogota (Colombia): El Rosario University Press; 2013.

Carbo A, Hontecillas R, Andrew T, Eden K, Mei Y, Hoops S, Bassaganya-Riera J. Computational modeling of heterogeneity and function of CD4+ T cells. Front Cell Dev Biol. 2014 Jul 29;2:31.

Carlson, C.M., Endrizzi, B.T., Wu, J., Ding, X., Weinreich, M.A., Walsh, E.R. et al, Kruppel-like factor 2 regulates thymocyte and T-cell migration. Nature. 2006;442:299–302.

Cazzolli R, Carpenter L, Biden TJ, Schmitz-Peiffer C. A role for protein phosphatase 2A-like activity, but not atypical protein kinase Czeta, in the inhibition of protein kinase B/Akt and glycogen synthesis by palmitate. Diabetes 2001;50(10):2210-18.

Ceredig, R. & Rolink, T. A positive look at double-negative thymocytes. Nature Rev. Immunol. 2, 888–897 (2002).

Chavez, J. & Summers, S. (2012) A ceramide-centric view of insulin resistance. Cell Metab., 15, 585–594.

Chu VT, Weber T, Wefers B, Wurst W, Sander S, Rajewsky K, Kühn R. Increasing the efficiency of homology-directed repair for CRISPR-Cas9-induced precise gene editing in mammalian cells. Nat Biotechnol. 2015 May;33(5):543-8.

Cong, L. et al. Multiplex genome engineering using CRISPR/Cas systems. Science 339, 819–823, (2013).

Cox MA, Kahan SM, Zajac AJ. Anti-viral CD8 T cells and the cytokines that they love. Virology. 2013 Jan 5;435(1):157-69.

D'Mello N.P., Childress A.M., Franklin D.S., Kale S.P., Pinswasdi C., and Jazwinski S. M. (1994). Cloning and characterization of lag1, a longevity-assurancegene in yeast. J Biol Chem, 269(22):15451–15459.

Degen, J. (2003). Erzeugung und Charakterisierung von konditionalen Knock-in-Reportergen-Mäusen des Connexin36 Ph.D thesis, Mathematisch-Naturwissenschaftlichen Fakultaet der Rheinischen Friedrich-Wilhelms-Universitaet Bonn.

Dupuy, A. D.; Engelman, D. M. (2008): Protein area occupancy at the center of the red blood cell membrane. Proc. Natl. Acad. Sci. U.S.A 105 (8), S. 2848–2852.

Ebel, P., Imgrund, S., Vom Dorp, K., Hofmann, K., Maier, H., Drake, H., Degen, J., Dörmann, P., Eckhardt, M., Franz, T., & Willecke, K. (2014 i) Ceramide synthase 4 deficiency in mice causes lipid alterations in sebum and results in alopecia. Biochem. J., 461, 147–158.

Ebel, P. (2014 ii) Characterization of two transgenic mouse lines deficient in Ceramide Synthase 6 and Ceramide Synthase 4. PhD thesis, Mathematisch-Naturwissenschaftlichen Fakultaet der Rheinischen Friedrich-Wilhelms-Universitaet Bonn.

Eberle M, Ebel P, Wegner MS, Männich J, Tafferner N, Ferreiros N, Birod K, Schreiber Y, Krishnamoorthy G, Willecke K, Geisslinger G, Grösch S, Schiffmann S. (2014). Regulation of ceramide synthase 6 in a spontaneous experimental autoimmune encephalomyelitis model is sex dependent. Biochem Pharmacol. 2014 Nov 15;92(2):326-35.

Eckl KM, Tidhar R, Thiele H, Oji V, Hausser I, Brodesser S, Preil ML, Onal-Akan A, Stock F, Müller D, Becker K, Casper R, Nürnberg G, Altmüller J, Nürnberg P, Traupe H, Futerman AH, Hennies HC. Impaired epidermal ceramide synthesis causes autosomal recessive congenital ichthyosis and reveals the importance of ceramide acyl chain length. J Invest Dermatol. 2013 Sep;133(9):2202-11.

Fabrias, G., Muñoz-Olaya, J., Cingolani, F., Signorelli, P., Casas, J., Gagliostro, V., & Ghidoni, R. (2012) Dihydroceramide desaturase and dihydrosphingolipids: debutant players in the sphingolipid arena. Prog. Lipid Res., 51, 82–94.

Fahy, E., Subramaniam, S., Brown, H.A., Glass, C.K., Merrill, A.H., Murphy, R.C., Raetz, C.R.H., Russell, D.W., Seyama, Y., Shaw, W., Shimizu, T., Spener, F., van Meer, G., VanNieuwenhze, M.S., White, S.H., Witztum, J.L., & Dennis, E.A. (2005) A comprehensive classification system for lipids. J. Lipid.

Fahy, E., Subramaniam, S., Murphy, R.C., Nishijima, M., Raetz, C.R.H., Shimizu, T., Spener, F., van Meer, G., Wakelam, M.J.O., & Dennis, E.A. (2009) Update of the LIPID MAPS comprehensive classification system for lipids. J. Lipid Res., 50 Suppl, S9–S14.

Feil R, Brocard J, Mascrez B, LeMeur M, Metzger D and Chambon P. (1996). Ligand-activated site-specific recombination in mice. Proc Natl Acad Sci U S A. 93:10887-10890.

Feil, S., Valtcheva, N., & Feil, R. (2009) Inducible Cre mice. Methods Mol. Biol., 530, 343–363.

Feng C, Woodside KJ, Vance BA, El-Khoury D, Canelles M, et al. (2002) A potential role for CD69 in thymocyte emigration. Int Immunol 14: 535–544.

Fernandis, A. Z.; Wenk, M. R. (2007): Membrane lipids as signaling molecules. Current Opinion in Lipidology 18 (2), S. 121–128.

Filhol O, Nueda A, Martel V, et al. Live-cell fluorescence imaging reveals the dynamics of protein kinase CK2 individual subunits. Mol Cell Biol. 2003;23(3):975–987.

Fukushima R, Kasamatsu A, Nakashima D, et al. Overexpression of Translocation Associated Membrane Protein 2 Leading to Cancer-Associated Matrix Metalloproteinase Activation as a Putative Metastatic Factor for Human Oral Cancer. J Cancer. 2018;9(18):3326-3333.

Galgani J, Ravussin E. Energy metabolism, fuel selection and body weight regulation. Int J Obes (Lond). 2008 Dec;32 Suppl 7(Suppl 7):S109-19.

Garth L. Nicolson. Cell Membrane Fluid–Mosaic Structure and Cancer Metastasis. Cancer Res. 2015 Apr 1;75(7):1169-76. doi: 10.1158/0008-5472.CAN-14-3216.

Gault CR, Obeid LM, Hannun YA. An overview of sphingolipid metabolism: from synthesis to breakdown. Adv Exp Med Biol. 2010;688:1–23.

Gazit SL, Mariko B, Thérond P, et al. Platelet and Erythrocyte Sources of S1P Are Redundant for Vascular Development and Homeostasis, but Both Rendered Essential After Plasma S1P Depletion in Anaphylactic Shock. Circ Res. 2016;119(8):e110–e126.

Gehring W.J., Qian Y.Q., Billeter M., Furukubo-Tokunaga K., Schier A.F., Resendez-Perez D., Affolter M., Otting G., Wüthrich K. (1994). Homeodomain-DNA recognition. Cell. 29;78(2):211-23.

Getty AL, Pearce DA. Interactions of the proteins of neuronal ceroid lipofuscinosis: clues to function. Cell Mol Life Sci. 2010;68(3):453-74.

Ginkel, C. (2013) Herstellung und Charakterisierung von zwei Mauslinien mit Mutationen im Ceramidsynthase1 Protein und Sphingomyelin Synthase related Protein. PhD Thesis, Mathematisch-Naturwissenschaftlichen Fakultaet der Rheinischen Friedrich-Wilhelms-Universitaet Bonn.

Glenn Dranoff Cytokines in cancer pathogenesis and cancer therapy Nature Reviews Cancer volume 4, pages 11–22 (2004).

Godfrey, D. I., Kennedy, J., Suda, T. & Zlotnik, A. A developmental pathway involving four phenotypically and functionally distinct subsets of CD3−CD4−CD8− triple negative adult mouse thymocytes defined by CD44 and CD25 expression. J. Immunol. 150, 4244–4252 (1993).

Gosejacob D, Jäger PS, Vom Dorp K, Frejno M, Carstensen AC, Köhnke M, Degen J, Dörmann P, Hoch M. Ceramide Synthase 5 Is Essential to Maintain C16:0-Ceramide Pools and Contributes to the Development of Diet-induced Obesity. J Biol Chem. 2016 Mar 25;291(13):6989-7003.

Grösch, S., Schiffmann, S., & Geisslinger, G. (2012) Chain length-specific properties of ceramides. Prog. Lipid Res., 51, 50–62.

Grossi C.E and Lydyard P.M. Spleen. Encyclopedia of Immunology (Second Edition) 1998, Pages 2205-2208.

Guillas, I., P. A. Kirchman, R. Chuard, M. Pfefferli, J. C. Jiang, S. M. Jazwinski and A. Conzelmann (2001). "C26-CoA-dependent ceramide synthesis of Saccharomyces cerevisiae is operated by Lag1p and Lac1p." Embo J 20(11): 2655-2665.

Gulbins E. and Li P.L. (2006). Physiological and pathophysiological aspects of ceramide. Am j Physiol Regul Integr Comp Physiol 290: R11-R26.

Hage H. R, Bourron O, Hajduch E. Defect of insulin signal in peripheral tissues: important role of ceramide. World J Diabetes 2014;5(3):244-57.

Hager-Theodorides AL, Rowbotham NJ, Outram SV, Dessens JT, Crompton T. Beta-selection: abundance of TCRbeta-/gammadelta- CD44- CD25- (DN4) cells in the foetal thymus. Eur J Immunol. 2007;37(2):487–500.

Hait NC, Allegood J, Maceyka M, et al. Regulation of histone acetylation in the nucleus by sphingosine-1-phosphate [published correction appears in Science. 2009 Oct 16;326(5951):366]. Science. 2009;325(5945):1254–1257.

Hajer GR, Haeften TWv, Visseren FL. Adipose tissue dysfunction in obesity, diabetes, and vascular disease. European Heart Journal. 2008;29:2959–2971.

Hanada, K. (1) (2003) Serine palmitoyltransferase, a key enzyme of sphingolipid metabolism. Biochim. Biophys. Acta, 1632, 16–30.

Hanada ,K. (2), Kumagai, K., Yasuda, S., Miura, Y., Kawano, M., Fukasawa, M., & Nishijima, M. (2003) Molecular machinery for non-vesicular trafficking of ceramide. Nature, 426, 803–809.

Hannun Y.A , Obeid L.M. (2002). The ceramide-centric universe of lipid-mediated cell reglation.stress encounters of the lipid kind. . (2002) J. Biol. Chem. 277, 25847–25850.

Hannun, Y. a & Obeid, L.M. (2008) Principles of bioactive lipid signalling: lessons from sphingolipids. Nat. Rev. Mol. Cell Biol., 9, 139–150.

Harvey Lodish, Arnold Berk, and Chris A. Kaiser. Molecular cell biology. 8th revised edition edition, 2016.

Hatoum D, Haddadi N, Lin Y, Nassif NT, McGowan EM. Mammalian sphingosine kinase (SphK) isoenzymes and isoform expression: challenges for SphK as an oncotarget. Oncotarget. 2017;8(22):36898-36929.

Helke K, Angel P, Lu P, Garrett-Mayer E, Ogretmen B, Drake R, Voelkel-Johnson C. Ceramide Synthase 6 Deficiency Enhances Inflammation in the DSS model of Colitis. Sci Rep. 2018 Jan 26;8(1):1627.

Hirschberg, K., J. Rodger and A. H. Futerman (1993). "The long-chain sphingoid base of sphingolipids is acylated at the cytosolic surface of the endoplasmic reticulum in rat liver." Biochem J 290 ( Pt 3): 751-757.

Hoess, R.H., M. Ziese, and N. Sternberg. 1982. P1 site-specific recombination: nucleotide sequence of the recombining sites. Proc. Natl. Acad. Sci. USA. 79:3398–3402.

Holland WL, Summers SA. Sphingolipids, insulin resistance, and metabolic disease: new insights from in vivo manipulation of sphingolipid metabolism. Endocr Rev. 2008;29(4):381–402.

Holthuis, J.C., Pomorski, T., Raggers, R.J., Sprong, H., & Van Meer, G. (2001) The organizing potential of sphingolipids in intracellular membrane transport. Physiol. Rev., 81, 1689–1723.

Holthuis J.C.M. and Levine T.P. (2005). Lipid traffic: floppy drives and a superhighway. Nat Rev Mol Cell Biol, 6(3):209–220.

Imgrund, S., Hartmann, D., Farwanah, H., Eckhardt, M., Sandhoff, R., Degen, J., Gieselmann, V., Sandhoff, K., & Willecke, K. (2009) Adult ceramide synthase 2 (CERS2)-deficient mice exhibit myelin sheath defects, cerebellar degeneration, and hepatocarcinomas. J. Biol. Chem., 284, 33549–33560.

Imgrund, S. (2011) Erzeugung und erste Charakterisierungen zweier Mausmutanten mit Defekten in der Ceramidsynthase 2 und 4. PhD thesis, Mathematisch-Naturwissenschaftlichen Fakultaet der Rheinischen Friedrich-Wilhelms-Universitaet Bonn.

Janeway CA Jr, Travers P, Walport M, et al. Immunobiology: The Immune System in Health and Disease. 5th edition. New York: Garland Science; 2001.

Jennemann, R., Rabionet, M., Gorgas, K., Epstein, S., Dalpke, A., Rothermel, U., Bayerle, A., van der Hoeven, F., Imgrund, S., Kirsch, J., Nickel, W., Willecke, K., Riezman, H., Gröne, H.-J., & Sandhoff, R. (2012) Loss of ceramide synthase 3 causes lethal skin barrier disruption. Hum. Mol. Genet., 21, 586–608.

Jiang, J. C., P. A. Kirchman, M. Zagulski, J. Hunt and S. M. Jazwinski (1998). "Homologs of the yeast longevity gene LAG1 in Caenorhabditis elegans and human." Genome Res 8(12): 1259-1272.

Jinek, M. et al. A programmable dual-RNA-guided DNA endonuclease in adaptive bacterial immunity. Science 337, 816–821 (2012).

Kano, M., Igarashi, H., Saito, I., Masuda, M. (1998) Cre-loxP-mediated DNA flipflop in mammalian cells leading to alternate expression of retrovirally transduced genes. Biochem. Biophys. Res. Commun. 248, 806-811.

Kenneth P. Murphy, Charles A. Janeway, Paul Travers, Mark Walport, Allan Mowat, and Casey T. Weaver. Janeway's immunobiology. Garland Science, London, 8.edition, 2012.

Kihara A. Synthesis and degradation pathways, functions, and pathology of ceramides and epidermal acylceramides. Prog Lipid Res. 2016 Jul;63:50-69.

Kitatani K., Idkowiak-Baldys J., and Hannun Y. A. (2008). The sphingolipid salvage pathway in ceramide metabolism and signaling. Cell Signal, 20(6):1010–1018.

Klein L, Kyewski B, Allen PM, Hogquist KA. Positive and negative selection of the T cell repertoire: what thymocytes see (and don't see). Nat Rev Immunol. 2014 Jun;14(6):377-91.

Kolter T, Proia RL, Sandhoff K. (2002). Combinatorial ganglioside biosynthesis. J Biol Chem. 277(29):25859-62.

Kolter T. (2011). A view on sphingolipids and disease. Chem Phys Lipids. 164(6):590-606. Epub.

Kremser, C., Klemm, A.-L., van Uelft, M., Imgrund, S., Ginkel, C., Hartmann, D., & Willecke, K. (2013) Cell-type-specific expression pattern of ceramide synthase 2 protein in mouse tissues. Histochem Cell Biol (2013) 140: 533.

Kremser, C. (2018) Charakterisierung transgener Mäuse mit Defekten in den Ceramidsynthasen 1, 2, 4 und 6. PhD Thesis, Mathematisch-Naturwissenschaftlichen Fakultaet der Rheinischen Friedrich-Wilhelms-Universitaet Bonn.

Kuhn R, Schwenk F, Aguet M and Rajewsky K. (1995). Inducible gene targeting in mice. Science. 269:1427-1429

Lahiri, S., Lee, H., Mesicek, J., Fuks, Z., Haimovitz-Friedman, A., Kolesnick, R.N., & Futerman, A.H. (2007) Kinetic characterization of mammalian ceramide synthases: determination of K(m) values towards sphinganine. FEBS Lett., 581, 5289–5294.

Lallemand, Y., Luria, V., Haffner-Krausz, R., & Lonai, P. (1998) Maternally expressed PGK-Cre transgene as a tool for early and uniform activation of the Cre site-specific recombinase. Transgenic Res., 7, 105–112.

Lam K.P., Rajewsky K. (1998) Rapid elimination of mature autoreactive B cells demonstrated by Cre-induced change in B cell antigen receptor specificity in vivo. Proc. Natl. Acad. Sci. 95, 13171-13175.

Lamour N. F., Stahelin R. V., Wijesinghe D. S.. (2007). Ceramide kinase uses ceramide provided by ceramide transport protein: localization to organelles of eicosanoid synthesis. Journal of Lipid Research. 2007;48:1293–1301.

Laviad E. L., Albee L., Pankova-Kholmyansky I., Epstein S., Park H., Merrill A. H., and Futerman A. H. (2008). Characterization of ceramide synthase 2: tissue distribution, substrate specificity, and inhibition by sphingosine 1-phosphate. J BiolChem, 283(9):5677–5684.

Levy, M. & Futerman, A.H. (2010) Mammalian ceramide synthases. IUBMB Life, 62, 347–356.

Lewandoski M. (2001). Conditional control of gene expression in the mouse. Nat Rev Genet. 2:743-755.

Linke, T., G. Wilkening, F. Sadeghlar, H. Mozcall, K. Bernardo, E. Schuchman and K. Sandhoff (2001). "Interfacial regulation of acid ceramidase activity. Stimulation of ceramide degradation by lysosomal lipids and sphingolipid activator proteins." J Biol Chem 276(8): 5760-5768.

Liu, P., Jenkins, N. A., und Copeland, N. G. (2003) A highly efficient recombineering-based method for generating conditional knockout mutations. Genome Res, 13(3):476–484.

Magin, T.M., McWhir, J., & Melton, D.W. (1992) A new mouse embryonic stem cell line with good germ line contribution and gene targeting frequency. Nucleic Acids Res., 20, 3795–3796.

Mali P, Yang L, Esvelt KM, Aach J, Guell M, et al.RNA-guided human genome engineering via Cas9.Science 2013; 339: 823–6.

Mandon, E. C., I. Ehses, J. Rother, G. van Echten and K. Sandhoff (1992). "Subcellular localization and membrane topology of serine palmitoyltransferase, 3-dehydrosphinganine reductase, and sphinganine N-acyltransferase in mouse liver." J Biol Chem 267(16): 11144-11148.

Mao, C. and L. M. Obeid (2008). "Ceramidases: regulators of cellular responses mediated by ceramide, sphingosine, and sphingosine-1-phosphate." Biochim Biophys Acta 1781(9): 424-434.

Marchesini N., Osta W., Bielawski J., Luberto C., Obeid L.M., Hannun Y.A. (2004). Role for mammalian neutral sphingomyelinase 2 in confluence-induced growth arrest of MCF7 cells. J Biol Chem. 279 (24): 25101-25111.

Mashiko D, Young SA, Muto M, Kato H, Nozawa K, Ogawa M, Noda T, Kim YJ, Satouh Y, Fujihara Y, Ikawa M. Feasibility for a large scale mouse mutagenesis by injecting CRISPR/Cas plasmid into zygotes. Dev Growth Differ. 2014 Jan;56(1):122-9.

Matloubian M1, Lo CG, Cinamon G, Lesneski MJ, Xu Y, Brinkmann V, Allende ML, Proia RL, Cyster JG. Lymphocyte egress from thymus and peripheral lymphoid organs is dependent on S1P receptor 1. Nature. 2004 Jan 22;427(6972):355-60.

McGinnis W., Levine M.S., Hafen E., Kuroiwa A., Gehring W.J. (1984). A conserved DNA sequence in homoeotic genes of the Drosophila Antennapedia and bithorax complexes. Nature. 308: 428-433.

McLeod M, Craft S and Broach JR. (1986). Identification of the crossover site during FLP-mediated recombination in the Saccharomyces cerevisiae plasmid 2 microns circle. Mol Cell Biol. 6:3357-3367.

Mencarelli, C. und Martinez-Martinez, P. (2012) Ceramide function in the brain: when a slight tilt is enough. Cellular and molecular life sciences : CMLS.

Merrill A. H, Jr. (2011). Sphingolipid and Glycosphingolipid Metabolic Pathways in the Era of Sphingolipidomics Chem. Rev. 111, 6387–6422.

Mesika, A., Ben-Dor, S., Laviad, E.L., & Futerman, A.H. (2007) A new functional motif in Hox domain-containing ceramide synthases: identification of a novel region flanking the Hox and TLC domains essential for activity. J. Biol. Chem., 282, 27366–27373.

Mizutani, Y., Kihara, A., & Igarashi, Y. (2005) Mammalian Lass6 and its related family members regulate synthesis of specific ceramides. Biochem. J., 390, 263–271.

Morell P, Radin NS. Specificity in ceramide biosynthesis from long chain bases and various fatty acyl coenzyme A's by brain microsomes. J Biol Chem. 1970 Jan 25;245(2):342-50.

Morell, P., E. Costantino-Ceccarini and N. S. Radin (1970). "The biosynthesis by brain microsomes of cerebrosides containing nonhydroxy fatty acids." Arch Biochem Biophys 141(2): 738-748.

Mosbech, M.-B., A. S. B. Olsen, D. Neess, O. Ben-David, L. L. Klitten, J. Larsen, A.Sabers, J. Vissing, J. E. Nielsen, L. Hasholt, A. D. Klein, M. M. Tsoory, H. Hjalgrim, N. Tommerup, A. H. Futerman, R. S. Møller and N. J. Færgeman (2014). "Reduced ceramide synthase 2 activity causes progressive myoclonic epilepsy." Annals of Clinical and Translational Neurology 1(2): 88-98.

Mullen TD, Hannun YA, Obeid LM. Ceramide synthases at the centre of sphingolipid metabolism and biology. Biochem J. 2012;441(3):789-802.

Nagy, A., Gertsenstein, M., Vintersten, K., Behringer R., 2003. Manipulating the Mouse Embryo, Cold Spring Harbor Laboratory Press, New York.

NetNGlyc1.0; R. Gupta, E. Jung and S. Brunak. Prediction of N-glycosylation sites in human proteins. In preparation, 2004.

NetOGlyc3.1; Karin Julenius, Anne Mølgaard, Ramneek Gupta, Søren Brunak, Prediction, conservation analysis, and structural characterization of mammalian mucin-type O-glycosylation sites, *Glycobiology*, Volume 15, Issue 2, February 2005, Pages 153–164.

NetPhos3.1; Blom N1, Gammeltoft S, Brunak S. Sequence and structure-based prediction of eukaryotic protein phosphorylation sites. J Mol Biol. 1999 Dec 17;294(5):1351-62.

Newton J, Lima S, Maceyka M, Spiegel S. Revisiting the sphingolipid rheostat: Evolving concepts in cancer therapy. Exp Cell Res. 2015;333(2):195–200.

Ng CL, Oresic K, Tortorella D. TRAM1 is involved in disposal of ER membrane degradation substrates. Exp Cell Res. 2010;316(13):2113-22.

Ng ML, Wadham C, Sukocheva OA. The role of sphingolipid signalling in diabetes-associated pathologies (Review). Int J Mol Med. 2017;39(2):243–252. doi:10.3892/ijmm.2017.2855

NLStradamus-Server: Nguyen Ba AN, Pogoutse A, Provart N, Moses AM. NLStradamus: a simple Hidden Markov Model for nuclear localization signal prediction. BMC Bioinformatics. 2009 Jun 29;10(1):202.

Nitta T, Suzuki H. Thymic stromal cell subsets for T cell development. Cell Mol Life Sci. 2016 Mar;73(5):1021-37.

NucPred - Predicting Nuclear Localization of Proteins. Brameier M, Krings A, Maccallum RM. Bioinformatics, 2007. PubMed id: 17332022

Nutt, Hodgkin, Tarlinton, and Corcoran. The generation of antibody-secreting plasma cells. Nature reviews. Immunology, 15(3):160_171, 2015.

Ogretmen B., Hannun Y.A. (2004). Biologically active sphingolipids in cancer pathogenesis and treatment. Nat Rev Cancer. 4 (8): 604-616.

Ordoñez M, Presa N, Dominguez-Herrera A, Trueba M, Gomez-Muñoz A. Regulation of adipogenesis by ceramide 1-phosphate. Exp Cell Res. 2018 Nov 15;372(2):150-157.

Park, W.-J., Park, J.-W., Erez-Roman, R., Kogot-Levin, A., Bame, J.R., Tirosh, B., Saada, A., Merrill, A.H., Pewzner-Jung, Y., & Futerman, A.H. (2013) Protection of a ceramide synthase 2 null mouse from drug-induced liver injury: role of gap junction dysfunction and connexin 32 mislocalization. J. Biol. Chem., 288, 30904–30916.

Park WJ, Park JW, Merrill AH, Storch J, Pewzner-Jung Y, Futerman AH. Hepatic fatty acid uptake is regulated by the sphingolipid acyl chain length Biochim Biophys Acta. 2014; 1841(12):1754–1766.

Peters, F., Vorhagen, S., Brodesser, S., Jakobshagen, K., Brüning, J.C., Niessen, C.M., & Krönke, M. (2015) Ceramide synthase 4 regulates stem cell homeostasis and hair follicle cycling. J. Invest. Dermatol., 135, 1501–1509.

Pettus B. J., Bielawska A., Subramanian P., et al. Ceramide 1-phosphate is a direct activator of cytosolic phospholipase A2. Journal of Biological Chemistry. 2004; 279:11320–11326.

Pewzner-Jung, Y., S. Ben-Dor and A. H. Futerman (2006). "When do Lasses (longevity assurance genes) become CerS (ceramide synthases)?: Insights into the regulation of ceramide synthesis." J Biol Chem 281(35): 25001-25005.

Pewzner-Jung Y., Park, H., Laviad E. L., Silva L. C., Lahiri S., Stiban J., Erez-Roman R., Brügger B., Sachsenheimer T., Wieland F., Prieto M., Merrill A. H.,and Futerman A. H. (2010 I). A critical role for ceramide synthase 2 in liver homeostasis: I. alterations in lipid metabolic pathways. J Biol Chem, 285(14):10902–10910.

Pewzner-Jung Y., Brenner O., Braun S., Laviad ,E. L., Ben-Dor S., Feldmesser E., Horn-Saban S., Amann-Zalcenstein D., Raanan C., Berkutzki T., Erez-Roman R., Ben-David O., Levy M., Holzman D., Park H., Nyska A., Merrill A. H., and Futerman A. H. (2010 II). A critical role for ceramide synthase 2 in liver homeostasis: II. insights into molecular changes leading to hepatopathy. J Biol Chem, 285(14):10911–10923.

Pham TH, Baluk P, Xu Y, Grigorova I, Bankovich AJ, Pappu R, Coughlin SR, McDonald DM, Schwab SR, Cyster JG. Lymphatic endothelial cell sphingosine kinase activity is required for lymphocyte egress and lymphatic patterning. J Exp Med. 2010 Jan 18;207(1):17-27.

Phillips, R.; Ursell, T.; Wiggins, P.; Sens, P. (2009): Emerging roles for lipids in shaping membrane-protein function. Nature 459 (7245), S. 379–385.

Phyre2 Server: Kelley LA1, Mezulis S1, Yates CM1, Wass MN1, Sternberg MJ1. The Phyre2 web portal for protein modeling, prediction and analysis. Nat Protoc. 2015 Jun;10(6):845-58. doi: 10.1038/nprot.2015.053.

Pietzsch, J. (2004). Mind the membrane. Horizon Symposia: Living Frontier, 1-4.

Poitout V., Robertson R.P. Glucolipotoxicity: Fuel Excess and Beta-cell Dysfunction. Endocr. Rev. 2008;29:351–366.

Powell DJ, Hajduch E, Kular G, Hundal HS. Ceramide disables 3-phosphoinositide binding to the pleckstrin homology domain of protein kinase B (PKB)/Akt by a PKCzeta-dependent mechanism. Mol Cell Biol. 2003 Nov;23(21):7794-808. doi: 10.1128/mcb.23.21.7794-7808.2003.

Proia RL, Hla T. Emerging biology of sphingosine-1-phosphate: its role in pathogenesis and therapy. J Clin Invest. 2015;125(4):1379–1387. doi:10.1172/JCI76369

Pruett ST1, Bushnev A, Hagedorn K, Adiga M, Haynes CA, Sullards MC, Liotta DC, Merrill AH Jr. Biodiversity of sphingoid bases ("sphingosines") and related amino alcohols. J Lipid Res. 2008 Aug;49(8):1621-39.

Raichur S, Brunner B, Bielohuby M, et al. The role of C16:0 ceramide in the development of obesity and type 2 diabetes: CerS6 inhibition as a novel therapeutic approach. Mol Metab. 2019;21:36–50.

Raichur, S., Wang, S.T., Chan, P.W., Li, Y., Ching, J., Chaurasia, B., Chaurasia, B., Dogra, S., Öhman, M.K., Takeda, K., Sugii, S., Pewzner-Jung, Y., Futerman, A.H., & Summers, S.A. (2014) CerS2 haploinsufficiency inhibits β-oxidation and confers susceptibility to diet-induced steatohepatitis and insulin resistance. Cell Metab., 20, 687–695.

Rajewsky K, Gu H, Kühn R, et al. Conditional gene targeting. J Clin Invest. 1996;98(3):600-3.

Regard JB, Sato IT, Coughlin SR. Anatomical profiling of G protein-coupled receptor expression. Cell. 2008;135(3):561–571.

Resop RS, Douaisi M, Craft J, Jachimowski LC, Blom B, Uittenbogaart CH. Sphingosine-1-phosphate/sphingosine-1-phosphate receptor 1 signaling is required for migration of naive human T cells from the thymus to the periphery. J Allergy Clin Immunol. 2016 Aug;138(2):551-557.e8.

Rickert, R., K. Rajewsky, and J. Roes. 1995. Impairment of T-cell dependent B-cell responses and B1 cell development in CD19-deficient mice. Nature (Lond.). 376:352–355.

Rieck M, Kremser C, Jobin K, Mettke E, Kurts C, Gräler M, Willecke K, Kolanus W. Ceramide synthase 2 facilitates S1P-dependent egress of thymocytes into the circulation in mice. Eur J Immunol. 2017 Apr;47(4):677-684. doi: 10.1002/eji.201646623.

Rodriguez, C. I., Buchholz, F., Galloway, J., Sequerra, R., Kasper, J., Ayala, R., Stewart, A. F., Dymecki, S. M., und Rodríguez, C. I. (2000) High-efficiency deleter mice show that FLPe is an alternative to Cre-loxP. Nature genetics, 25(2):139–140.

Rother J., van Echten G., Schwarzmann G., Sandhoff K. (1992). Biosynthesis of sphingolipids: dihydroceramide and not sphinganine is desaturated by cultured cells. Biochem Biophys Res Commun.189(1):14-20.

Saba JD. The low down on sphingosine-1-phosphate lyase as a regulator of thymic egress. J Immunol Sci. 2017;1(1):1–8.

Sandhoff, K. and T. Kolter (2003). "Biosynthesis and degradation of mammalian glycosphingolipids." Philos Trans R Soc Lond B Biol Sci 358(1433): 847-861.

Sandhoff, R. (2010) Very long chain sphingolipids: tissue expression, function and synthesis. FEBS letters, 584(9):1907–1913.

Sassa T, Kihara A. Metabolism of very long-chain Fatty acids: genes and pathophysiology. Biomol Ther (Seoul). 2014;22(2):83–92.

Sassa T, Hirayama T, Kihara A. Enzyme Activities of the Ceramide Synthases CERS2-6 Are Regulated by Phosphorylation in the C-terminal Region. J Biol Chem. 2016 Apr 1;291(14):7477-87.

Schiffmann, S., K. Birod, J. Mannich, M. Eberle, M. S. Wegner, R. Wanger, D. Hartmann, N. Ferreiros, G. Geisslinger and S. Grosch (2013). "Ceramide metabolism in mouse tissue." Int J Biochem Cell Biol 45(8): 1886-1894.

Schultze, N., Y. Burki, Y. Lang, U. Certa, and H. Bluethmann. 1996. Efficient control of gene expression by single step integration of the tetracycline system in transgenic mice. Nat. Biotechnol. 14:499–503.

Schulze, H. & Sandhoff, K. (2014) Sphingolipids and lysosomal pathologies. Biochim. Biophys. Acta, 1841, 799–810.

Schwab SR, Pereira JP, Matloubian M, Xu Y, Huang Y, Cyster JG. Lymphocyte sequestration through S1P lyase inhibition and disruption of S1P gradients. Science. 2005;309(5741):1735–1739.

Seoane-Collazo P, Fernø J, Gonzalez F, Diéguez C, Leis R, Nogueiras R, López M. Hypothalamic-autonomic control of energy homeostasis. Endocrine. 2015 Nov;50(2):276-91.

Shiow LR, Rosen DB, Brdickova N, Xu Y, An J, Lanier LL, Cyster JG, Matloubian M. CD69 acts downstream of interferon-alpha/beta to inhibit S1P1 and lymphocyte egress from lymphoid organs. Nature. 2006;440:540–544.

Simanshu DK, Kamlekar RK, Wijesinghe DS, Zou X, Zhai X, Mishra SK, Molotkovsky JG, Malinina L, Hinchcliffe EH, Chalfant CE, Brown RE, Patel DJ. (2013). Non-vesicular trafficking by a ceramide-1-phosphate transfer protein regulates eicosanoids. Nature. 2013 Aug 22;500 (7463):463-7.

Singer, A., Bosselut, R.. , T Cell Subsets: Cellular Selection, Commitment and Identity in Advances in Immunology, 2004

Singer, S.J. & Nicolson, G.L. (1972) The fluid mosaic model of the structure of cell membranes. Science, 175, 720–731.

Sociale M, Wulf AL, Breiden B, Klee K, Thielisch M, Eckardt F, Sellin J, Bülow MH, Löbbert S, Weinstock N, Voelzmann A, Schultze J, Sandhoff K, Bauer R. Ceramide Synthase Schlank Is a Transcriptional Regulator Adapting Gene Expression to Energy Requirements. Cell Rep. 2018 Jan 23;22(4):967-978.

Spassieva, S., Seo, J.-G., Jiang, J.C., Bielawski, J., Alvarez-Vasquez, F., Jazwinski, S.M., Hannun, Y. a, & Obeid, L.M. (2006) Necessary role for the Lag1p motif in (dihydro)ceramide synthase activity. J. Biol. Chem., 281, 33931–33938.

Speakman JR. Measuring energy metabolism in the mouse - theoretical, practical, and analytical considerations. Front Physiol. 2013;4:34.

Spiegel S, Milstien S. The outs and the ins of sphingosine-1-phosphate in immunity. Nat Rev Immunol. 2011;11(6):403–415.

Spiegel, S. and S. Milstien (2003). "Sphingosine-1-phosphate: an enigmatic signalling lipid." Nat Rev Mol Cell Biol 4(5): 397-407.

Stanley P, Taniguchi N, Aebi M. N-Glycans. 2017. In: Varki A, Cummings RD, Esko JD, et al., editors. Essentials of Glycobiology [Internet]. 3rd edition. Cold Spring Harbor (NY): Cold Spring Harbor Laboratory Press; 2015-2017. Chapter 9.

Sternberg, N., and D. Hamilton. 1981. Bacteriophage P1 site-specific recombination. I. Recombination between loxP sites. J. Mol. Biol. 150:467–486.

Stoffel, W., D. LeKim and G. Sticht (1968). "Biosynthesis of dihydrosphingosine in vitro." Hoppe Seylers Z Physiol Chem 349(5): 664-670.

Swiss-Model Server:

Waterhouse, A., Bertoni, M., Bienert, S., Studer, G., Tauriello, G., Gumienny, R., Heer, F.T., de Beer, T.A.P., Rempfer, C., Bordoli, L., Lepore, R., Schwede, T. SWISS-MODEL: homology modelling of protein structures and complexes. Nucleic Acids Res. 46(W1), W296-W303 (2018).

Bienert, S., Waterhouse, A., de Beer, T.A.P., Tauriello, G., Studer, G., Bordoli, L., Schwede, T. The SWISS-MODEL Repository - new features and functionality. Nucleic Acids Res. 45, D313-D319 (2017).

Guex, N., Peitsch, M.C., Schwede, T. Automated comparative protein structure modeling with SWISS-MODEL and Swiss-PdbViewer: A historical perspective. Electrophoresis 30, S162-S173 (2009).

Benkert, P., Biasini, M., Schwede, T. Toward the estimation of the absolute quality of individual protein structure models. Bioinformatics 27, 343-350 (2011).

Bertoni, M., Kiefer, F., Biasini, M., Bordoli, L., Schwede, T. Modeling protein quaternary structure of homo- and hetero-oligomers beyond binary interactions by homology. Scientific Reports 7 (2017).

Takaba H, Takayanagi H. The Mechanisms of T Cell Selection in the Thymus. Trends Immunol. 2017 Nov;38(11):805-816.

Takahama Y1. Journey through the thymus: stromal guides for T-cell development and selection. Nat Rev Immunol. 2006 Feb;6(2):127-35.

Tayama, M., S. Soeda, Y. Kishimoto, B. M. Martin, J. W. Callahan, M. Hiraiwa and J. S. O'Brien (1993). "Effect of saposins on acid sphingomyelinase." Biochem J 290 ( Pt 2): 401-404.

Teufel, A., Maass, T., Galle, P.R., & Malik, N. (2009). The longevity assurance homologue of yeast lag1 (Lass) gene family (Review). International Journal of Molecular Medicine, 23, 135-140.

Tidhar, R., Ben-Dor, S., Wang, E., Kelly, S., Merrill, A.H., & Futerman, A.H. (2012) Acyl chain specificity of ceramide synthases is determined within a region of 150 residues in the Tram-Lag-CLN8 (TLC) domain. J. Biol. Chem., 287, 3197–3206.

Tidhar, R. & Futerman, A.H. (2013) The complexity of sphingolipid biosynthesis in the endoplasmic reticulum. Biochim. Biophys. Acta, 1833, 2511–2518.

Tidhar R, Zelnik ID, Volpert G, Ben-Dor S, Kelly S, Merrill AH Jr, Futerman AH. Eleven residues determine the acyl chain specificity of ceramide synthases. J Biol Chem. 2018 Jun 22;293(25):9912-9921.

Tippetts TS1, Holland WL1, Summers SA2. The ceramide ratio: a predictor of cardiometabolic risk. J Lipid Res. 2018 Sep;59(9):1549-1550.

Tress, O. (2006) Vorarbeiten zur Einführung einer Mutation in das Mausgenom, die im Menschen die Pelizaeus-Merzbacher ähnliche Krankheit verursacht. Diplomarbeit, Mathematisch-

Naturwissenschaftlichen Fakultaet der Rheinischen Friedrich-Wilhelms-Universitaet Bonn.

Turban S, Hajduch E. Protein kinase C isoforms: mediators of reactive lipid metabolites in the development of insulin resistance. FEBS Lett. 2011;585(2):269-74.

Turpin, S.M., Nicholls, H.T., Willmes, D.M., Mourier, A., Brodesser, S., Wunderlich, C.M., Mauer, J., Xu, E., Hammerschmidt, P., Brönneke, H.S., Trifunovic, A., LoSasso, G., Wunderlich, F.T., Kornfeld, J.-W., Blüher, M., Krönke, M., & Brüning, J.C. (2014) Obesity-induced CerS6-dependent C16:0 ceramide production promotes weight gain and glucose intolerance. Cell Metab., 20, 678–686.

UniprotKB: UniProt Consortium. UniProt: a worldwide hub of protein knowledge. Nucleic Acids Res. 2019 Jan 8;47(D1):D506-D515.

van Meer, G. & Holthuis, J.C. (2000) Sphingolipid transport in eukaryotic cells. Biochim. Biophys. Acta, 1486, 145–170.

van Uelft, M. (2012) The effect of the Hox- domain on the activity of mouse ceramide synthase 2 in transfected cells. M. thesis, Mathematisch-Naturwissenschaftlichen Fakultaet der Rheinischen Friedrich-Wilhelms-Universitaet Bonn.

Véret J, Bellini L, Giussani P, Ng C, Magnan C, Le Stunff H. Roles of Sphingolipid Metabolism in Pancreatic Cell Dysfunction Induced by Lipotoxicity. J Clin Med. 2014;3(2):646–662. Published 2014 Jun 20.

Véret, J., Coant, N., Berdyshev, E., Skobeleva, A., Therville, N., Bailbé, D., Gorshkova, I.A., Natarajan, V., Portha, B., & Stunff, H.L. (2011). Ceramide synthase 4 and de novo production of ceramides with specific N-acyl chain lengths are involved in glucolipotoxicity-induced apoptosis of INS-1 β-cells. The Biochemical journal, 438 1, 177-89 .

Vincent Poitout, R. Paul Robertson, Glucolipotoxicity: Fuel Excess and β-Cell Dysfunction, Endocrine Reviews, Volume 29, Issue 3, 1 May 2008, Pages 351–366.

Voelzmann, A. and Bauer, R. (2010). Ceramide synthases in mammalians, worms, and insects: emerging schemes. BioMolecular Concepts, 1(5-6):411–422.

Voelzmann A. (2013). The homeodomain of the Drosophila Ceramide Synthase Schlank confers nuclear import information and DNA binding capabilities. PhD thesis, Mathematisch-Naturwissenschaftlichen Fakultaet der Rheinischen Friedrich-Wilhelms-Universitaet Bonn.

Voelzmann, A., Wulf, A.-L., Eckardt, F., Thielisch, M., Brondolin, M., Pesch, Y.,Bauer, R., and Hoch, M. Nuclear drosophila ceramide synthase schlank regulates lipid homeostasis. FEBS Lett. 2016 Apr;590(7):971-81.

Vogel P, Donoviel MS, Read R, Hansen GM, Hazlewood J, Anderson SJ, Sun W, Swaffield J, Oravecz T. Incomplete inhibition of sphingosine 1-phosphate lyase modulates immune system function yet prevents early lethality and non-lymphoid lesions. PLoS One. 2009;4(1):e4112. doi: 10.1371/journal.pone.0004112. Epub 2009 Jan 1. PubMed PMID: 19119317; PubMed Central PMCID: PMC2606024.

Wang H, Yang H, Shivalila CS, Dawlaty MM,Cheng AW, et al. One-step generation of mice carrying mutations in multiple genes by CRISPR/Cas-mediated genome engineering. Cell 2013; 153: 910–8.

Wattenberg, B.W. (2010) Role of sphingosine kinase localization in sphingolipid signaling. World J. Biol. Chem., 1, 362–368.

Winter, E. & Ponting, C.P. (2002) TRAM, LAG1 and CLN8: members of a novel family of lipid-sensing domains? Trends Biochem. Sci., 27, 381–383.

Woo-Jae Park/ Joo-Won Park. The effect of altered sphingolipid acyl chain length on various disease models. Biol Chem. 2015 Jun;396(6-7):693-705. doi: 10.1515/hsz-2014-0310. Review.

Wulf, A. (2015). Analysis of Domain Specific Functions of the Ceramide Synthase Schlank in Drosophila melanogaster. PhD Thesis, Mathematisch-Naturwissenschaftlichen Fakultaet der Rheinischen Friedrich-Wilhelms-Universitaet Bonn.

Yamashita, T. (2011). "Glycosphingolipid modification: structural diversity, functional and mechanistic integration of diabetes." Diabetes Metab J 35(4): 309-316.

Yanagida K, Hla T. Vascular and Immunobiology of the Circulatory Sphingosine 1-Phosphate Gradient. Annu Rev Physiol. 2017 Feb 10;79:67-91.

Yao, J.K. & Rastetter, G.M. (1985) Microanalysis of complex tissue lipids by high-performance thin-layer chromatography. Anal. Biochem., 150, 111–116.

Yeo G. S. and Heisler L. K. (2012). Unraveling the brain regulation of appetite: lessons from genetics. Nat. Neurosci. 15, 1343-1349.

Young SA, Aitken RJ, Ikawa M. Advantages of using the CRISPR/Cas9 system of genome editing to investigate male reproductive mechanisms using mouse models. Asian J Androl. 2015;17(4):623-7.

Zamora-Pineda J, Kumar A, Suh JH, Zhang M, Saba JD. (2016). Dendritic cell sphingosine-1-phosphate lyase regulates thymic egress. J Exp Med. 2016 Nov 14;213(12):2773-2791.

Zhao, L., Spassieva, S.D., Jucius, T.J., Shultz, L.D., Shick, H.E., Macklin, W.B., Hannun, Y. a, Obeid, L.M., & Ackerman, S.L. (2011) A deficiency of ceramide biosynthesis causes cerebellar purkinje cell neurodegeneration and lipofuscin accumulation. PLoS Genet., 7, e1002063.

Zhou J, Saba JD. Identification of the first mammalian sphingosine phosphate lyase gene and its functional expression in yeast. Biochem Biophys Res Commun. 1998;242(3):502–507.

Zúñiga-Pflücker JC. T-cell development made simple. Nat Rev Immunol. 2004 Jan;4(1):67-72. Review.

# 9 List of abbreviations

| | |
|---|---|
| A | Alanine |
| Akt/PKB | protein kinase B |
| APC | antigen-presenting cell |
| ASO | antisense oligonucleotides |
| BAC | bacterial artificial chromosome |
| BAT | brown adipose tissue |
| BCA | Bicinchoninic acid |
| BMD | Bone marrow derived |
| bp | base pairs |
| BSA | Bovine serum albumin |
| C (terminus) | Carboxyl terminus |
| C1P | ceramide-1-phosphate |
| CD | cluster of differentiation |
| cDNA | complementary DANN |
| cEC | cortical epithelial cells |
| CERK | ceramide kinase |
| CerS | ceramide synthases |
| CERT | ceramide transport protein |
| CNS | central nervous system |
| CoA | Coenzyme A |
| CPE | ceramide phosphoethanolamine |
| CPE | ceramide phosphoethanolamine |
| $cPLA_2$ | cytosolic phospholipases A2 |
| Cre | causes recombination |
| DAG | diacylglycerol |
| DCs | dendritic cells |
| Del | $CerS2^{Del79-120}$ mice |
| DES | dihydroceramide desaturase |
| DMEM | Dulbecco's modified Eagle medium |
| DMSO | Dimethyl sulfonide |
| DN | double-negative |
| DNA | Deoxyribonucleic acid |
| DNA | Deoxyribonucleic acid |
| dNTPs | Deoxynucleotide triphosphate |
| DP | double positive |
| e.g. | exempli gratia |
| ECL | enhanced chemiluminescence |
| ECM | extracellular matrix |
| ECM | extracellular matrix |
| EDTA | Ethylenediaminetetraacetic acid |
| ER | endoplasmic reticulum |
| ERT | estrogen-receptor |
| ESCs | embryonic stem cells |
| FFA | free fatty acids |
| Flp | Flippase |
| frt-sites | Flp-recognition target |
| GSL | glycosphingolipid |
| GSL | Glycosphingolipids |
| gt | gene trap |
| H | Histidine |
| H&E | Hematoxylin and eosin staining |
| H/A | $CerS2^{H212A/H213A}$ mice |
| HEK | human embryonic kidney cells |
| HFD | high-fat-diet |
| HOX | Homeobox |
| HRP | horse radish peroxidase |
| i.e. | id est |
| IR | Insulin receptor |
| IRES | internal ribosomal entry site |
| kb | kilo base pairs |
| kbp | kilo base pairs |
| kDa | kilo Dalton |
| KLF-2 | kruppel-like factor 2 |
| Lag | Longevity assurance gene |
| Lass | longevity assurance gene |
| LCB | long chain base |
| Lip3 | lipase3 |

| | |
|---|---|
| loxP-site | locus of X over P1 |
| MAG | myelin-associated glycoprotein |
| mEC | medullary epithelial cells |
| MEF | Mouse embryonic fibroblasts |
| min | minute |
| min | Minute |
| mRNA | messenger RNA |
| N (terminus) | Amino terminus |
| NBD | Nitrobent-2-Oxa.1,3-Diazol-4-yl |
| NLS | nuclear localization signals |
| NMR | nuclear magnetic resonance, |
| Ob | obese |
| ON | overnight |
| ORMDL | Orm like |
| P/S | Penicillin/Streptomycin |
| PBS | Phosphate buffered saline |
| PC | phosphocholine |
| PCR | Polymerase chain reaction |
| PE | phosphoethanolamine |
| PI3K | phosphatidylinositol 3-kinase (PI3K), |
| PKCz | (Protein kinase C). |
| PMSF | Phenylmethanesulfonylfluoride |
| PP2A | protein phosphatase - PP2A |
| rpm | rounds per minute |
| RT | Room temperature |
| RT-PCR | real time-PCR |
| S1P | sphingosine-1-phosphate |
| S1PR1-5 | S1P receptor 1-5 |
| SAPs | sphingolipid activator proteins |
| SCZ | subcapsular zone |
| SDS | Sodium dodecyl sulphate |
| SEM | standard error of the mean |
| SEM | Standard error of the mean |
| SL | Sphingolipids |
| SL | sphingolipid |
| SM | sphingomyelin |
| SP | single positive |
| SPHK1 or 2 | sphingosine kinase 1 and 2 |
| SPT | serine palmitoyl transferase |
| T2D | type 2 diabetes |
| TAG | triacylglycerol |
| Tfh | follicular helper T cell |
| Th | T helper cell |
| TLC | thin layer chromatography |
| TLC | TRAM-Lag-CLN8 |
| TLC domain | TRAM-Lag-CLN8 domain |
| Treg | regulatory T cell |
| WAT | white adipose tissue |
| WT | wilyd type |

# 10 Appendix – supplemental Figures

## 10.1 Supplemental figures of the Introduction

**Figure A1: Main subtypes of long chain bases (LCBs).**

Sphingosine can be distinguished from sphinganine (dihydrosphingosine) by the presence of a double bond at position 4. Additionally, sphinganine is exclusively generated in the *de novo* synthesis pathway of ceramides. Phytosphingosine is the main SL in plants and funghi (Adopted and modified from Hanada et al., 2003; Alfatah et al., 2019)

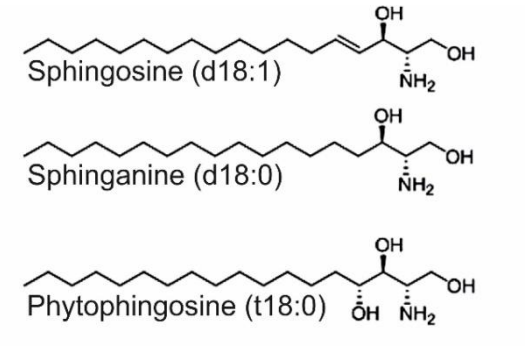


## 10.2 Supplemental figures of the Methods part

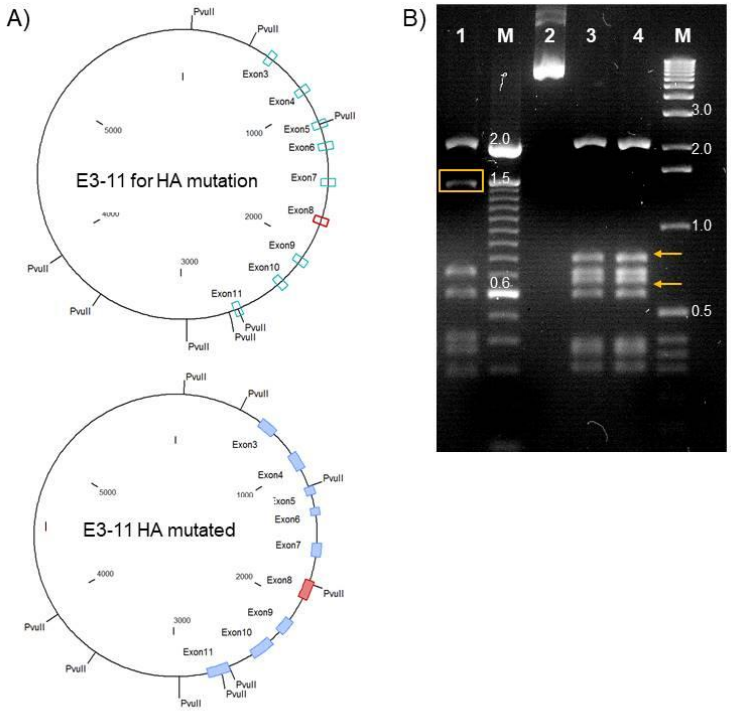


**Figure A2: Validation of H213/213A mutation after PvuII digestion.**

**(A)** Schematic representation of plasmids, before (E3-11 for HA mutation) and after mutagenesis PCR (E3-11 HA mutated). PvuII restriction sites of the plasmids were illustrated. **(B)** PvuII restriction digestion analyses performed with un-modified and mutated E3-11 HA plasmids. The DNA fragment at approximately 1.5 kb (yellow box) decomposed after PvuII digestion into two smaller fragments (0.7/ 0.66 kb) indicated by yellow arrows. Arrows indicate decomposition. Lanes, 1: WT (E3-11 for H mutation), 2: non-digested E3-11 HA mutated vector, 3 and 4: two different bacterial clones digested with PvuII.

## 10.3 Supplemental figures of the Results

```
MLQTLYDYFWWERLWLPVNLTWADLEDKDGRVYAKASDLYITLPLALLFLVIRYFFELYVATPLAALLNVKEKTRLRAPP   80
NATLEHFYQTSGKQPKQVEVDLLSRQSGLSGRQVERWFRRRRNQDRPSLLKKFREASWRFTYYLIAFVAGMAVTVDKPWF  160
YDLRKVWEGYPIQSIIPSQYWYYMIELSFYWSLLFSIASDVKRKDFKEQIIHHVATIILLCFSWFANYVRAGTLIMALHD  240
ASDYLLESAKMFNYAGWKNTCNNLFIVFAIVFIITRLVIMPFWILHCTMIYPLELYPAFFGYYFFNFMMAVLQMLHIFWA  320
YFILRMAHKFITGKLIEDERSDREETESSEGEETAAGAGAKSRLLANGHPILNNNHPKND
```

```
(Threshold=0.5)
---------------------------------------------------------------------
SeqName      Position  Potential    Jury    N-Glyc
                                agreement result
---------------------------------------------------------------------
Sequence       19 NLTW   0.7776      (9/9)   +++
Sequence       81 NATL   0.6829      (9/9)   ++
---------------------------------------------------------------------
```

**Figure A3: Glycosylation studies of ceramide synthase 2**.

**(A)** Depicted is the peptide sequence of CerS2 with possible glycosylation sites highlighted in red. Below; N-glycosylation prediction analysis results performed with the NetNGlyc1.0 server. Possible glycosylation sites were predicted upon the presence of Asn-Pro-Ser/Thr-motif. +++; The 'potential' score is shown as an averaged output of nine neural networks, threshold >0.75. ++; the potential score was given in 9/9 neural networks, threshold >0.5.

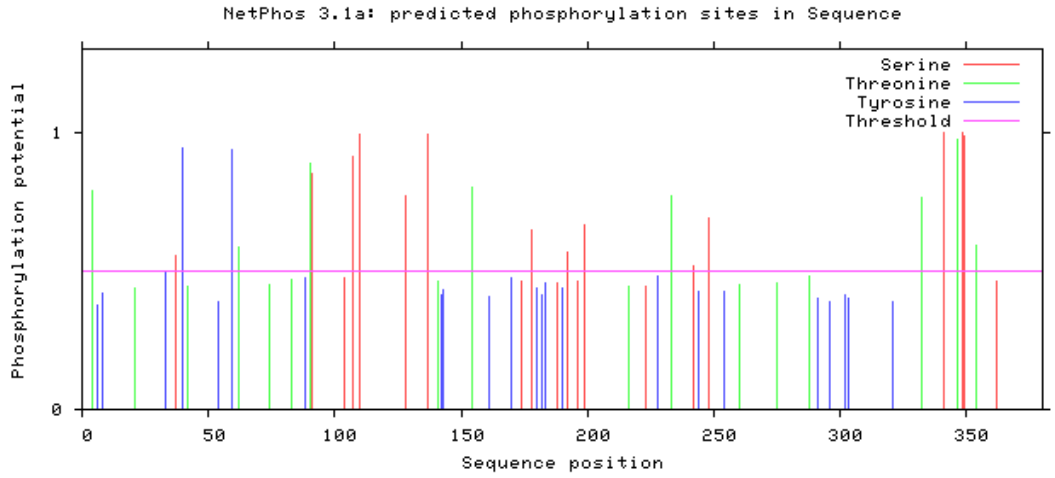


**Figure A4: NetPhos 3.1a Phosphorylation prediction results.**

Shown is the graphical overview resulting from the NetPhos 3.1a prediction tool. Possible phosphorylation sites predicted for the CerS2 protein sequence are indicated. Color- code represents different amino acid residues, which could be used for phosphorylation.

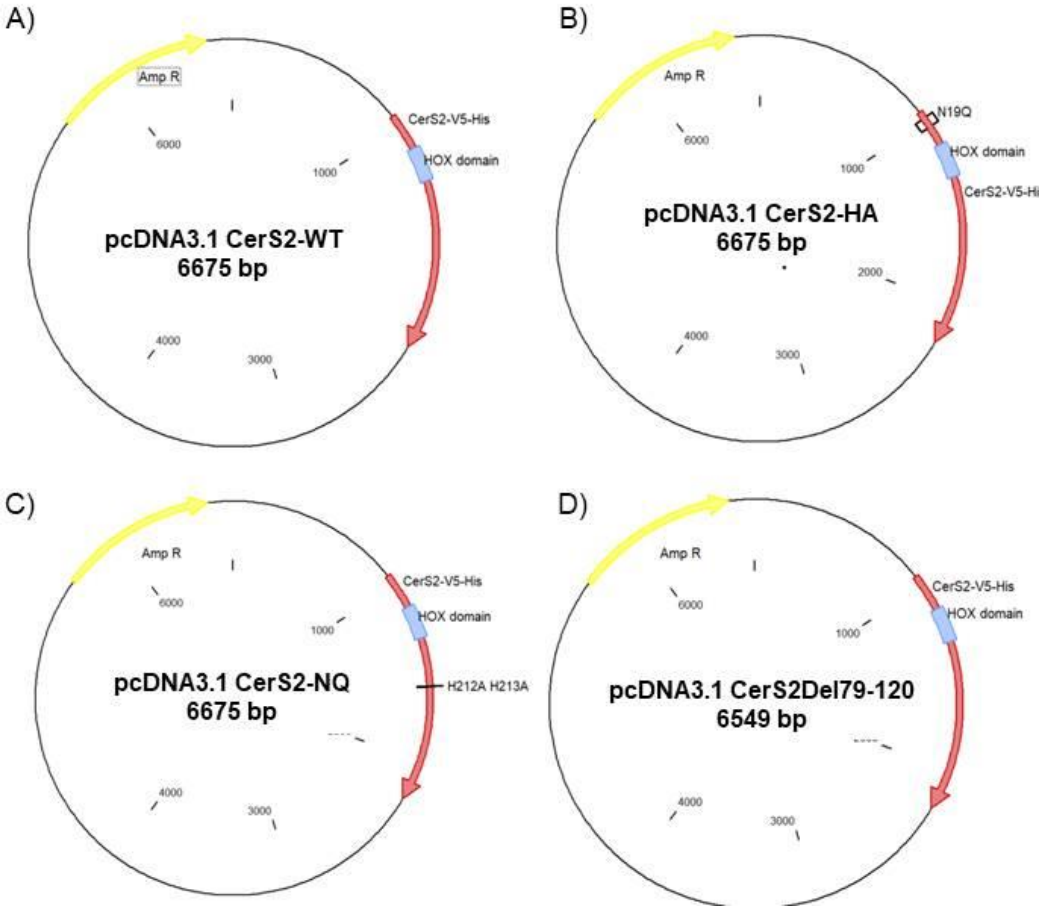


**Figure A5: Generated pcDNA3.1 CerS2 plasmids containing different forms of WT or modified cDNA of *cers2*. (A)** Vector card of the pcDNA3.1 containing the WT sequence of *cers2*. **(B)** pcDNA3.1 CerS2 vector containing the H212A/H213A mutation. **(C)** pcDNA3.1 CerS2 vector containing the cers2, which carries a mutation at the glycosylation site (N19Q) **(D)** Shown is the pcDNA3.1 vector containing the cers2 cDNA coding for the CerS2Del79-120 protein.

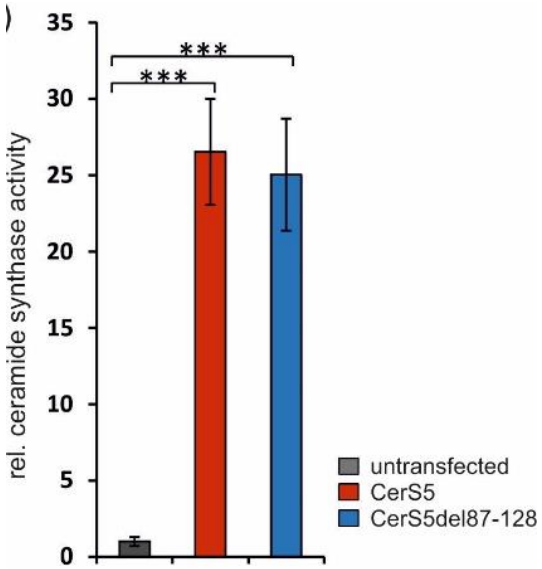


**Figure A6: Analysis of CerS5 activity *in vitro*.** Protein lysates of transiently transfected (cerS5-WT, CerS5del87-128) HEK cells were generated and incubated with NBD-sphinganine and C16-acyl-CoA as substrates. The activity assay was performed as described. Desitometric analysis was performed after lipid extraction and separation by HPTLC. Data are means ±SEM; Quantification was based on three individual experiments. Unpaired t-test, ***P<.001.

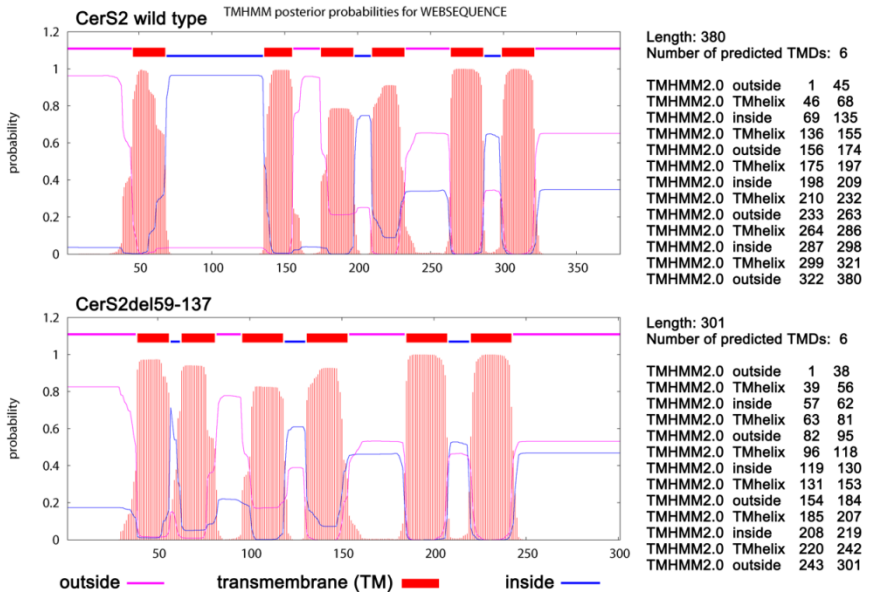


**Figure A7: TMHMM (transmembrane) topology- prediction results.** Shown is the graphical overview of the transmembrane topology-predictions of the CerS2 WT and CerS2Del59-137 protein obtained by the TMHMM 2.0 prediction (http://www.cbs.dtu.dk/services/TMHMM-2.0/). The X axis indicates the position of amino acid residues. The Y axis indicates the probability to which extent the amino acid residues are part of a transmembrane domain (TMD). Blue (inside): cytoplasm facing sequences, purple (outside): sequences facing the ER lumen (Adopted and modified according to Bickert et al., 2018).

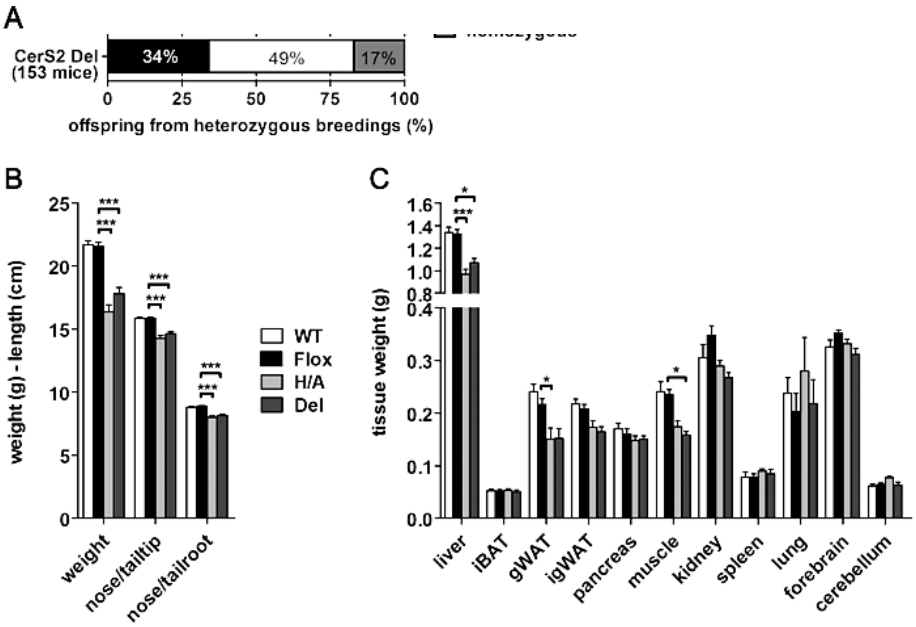


**Figure A8: physiological properties (Mendelian ratio, body weight & organ size): (A) Mendelian ratio CerS2 Del mice.** Shown are the percentages of WT (black), heterozygous (white) and homozygous (grey) mice obtained from heterozygous breedings of +/CerS2Del mice. The total number of analysed mice is shown in brackets (adopted and modified from Bickert et al., 2018). **(B)** Ratio of body weight/ body length determined for CerS2 WT, Flox, H/A and Del mice.(n≥11). (C) Overview of different tissue weights of CerS2 WT, Flox, H/A and Del mice. Data are means ±SEM; unpaired t-test, *P<.05; ***P<.001 (liver: n≥10; other tissues: n≥5) (Adopted and modified according to Bickert et al., 2018).

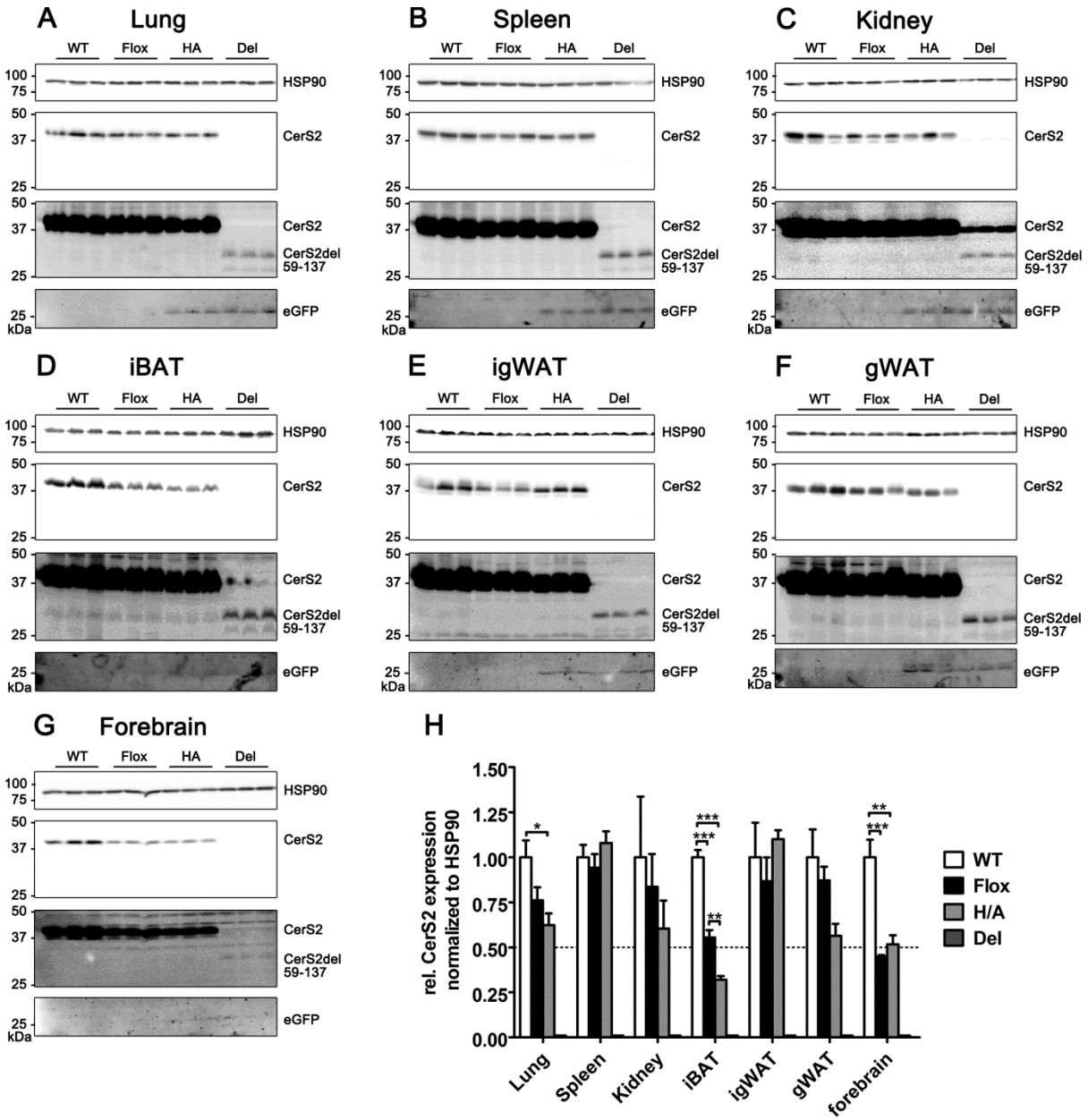


**Figure A9: Protein expression of endogenous and modified CerS2 protein in different tissues of CerS2 WT, Flox, H/A and Del mice. (A-G)** Immunoblot results showing CerS2 (and eGFP) expression under normal exposure (upper blot). The expression levels of the endogenous CerS2 (45 kDa) in CerS2 WT (and also in Flox) mice served as controls. Point mutated CerS2 (44.9 kDa) protein was detectable in CerS2 H/A mice, no signal was detectable for CerS2 Del mice in any of the analysed tissues. Over-exposure of all investigated blots (lower blot) showed a band corresponding to the truncated CerS2 (CerS2del59-137; 35.8 kDa) present in CerS2 Del mice. Expression level of Del protein is under 1% in comparison to the expression of the CerS2 WT protein found in the Flox control mice (CerS2Del79-120 protein appearing at approximately 37 **(H)** Densitometric analysis and quantification of CerS2 expression normalized to HSP90 (after normal-exposure). Data are means ± SEM, (n=3); Unpaired t-test, *P<.05; **P<.01; ***P<.001. gWAT – gonadal white adipose tissue; iBat – interscapular brown adipose tissue; igWAT – inguinal white adipose tissue (Adopted and modified according to Bickert et al., 2018).

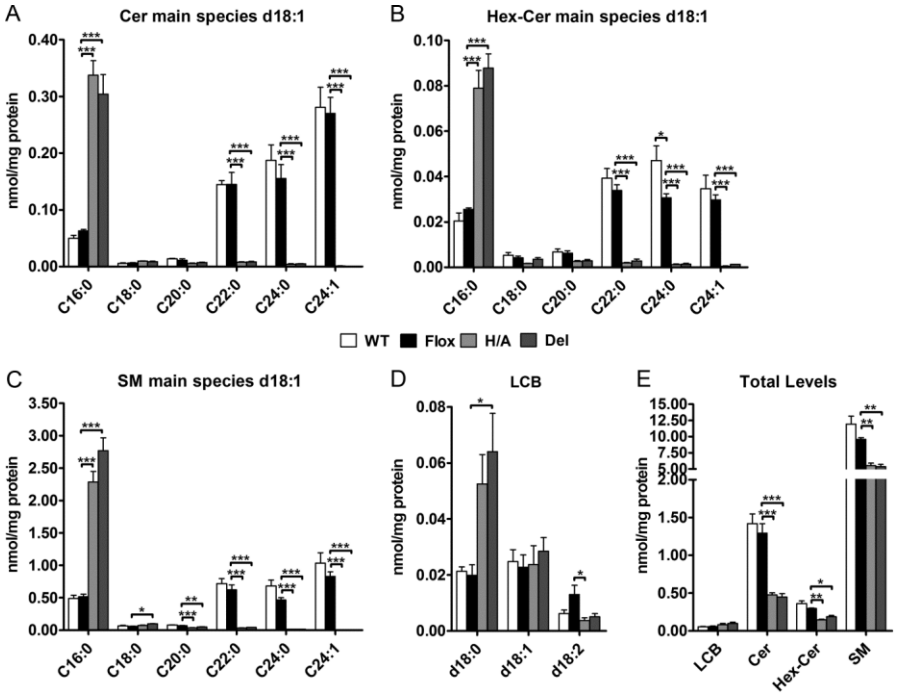


**Figure A 10: Mass spectrometric analyses of liver sphingolipid content in CerS2 WT, Flox, H/A and Del mice. (A)** Quantification of ceramide (Cer), **(B)** hexosylceramide (Hex-Cer) and **(C)** sphingomyelin (SM) species with incorporated sphingosine (d18:1). **(D)** Analysis of less abundant Long chain base species with incorporated sphinganine (d18:0) and sphingadiene (d18:2). **(E)** Quantification of total levels of LCBs, ceramides, hexosylceramides and sphingomyelins. Data are means ± SEM, (n=4); Unpaired t-test, *P<.05; **P<.01; ***P<.001 (Adopted and modified according to Bickert et al., 2018).

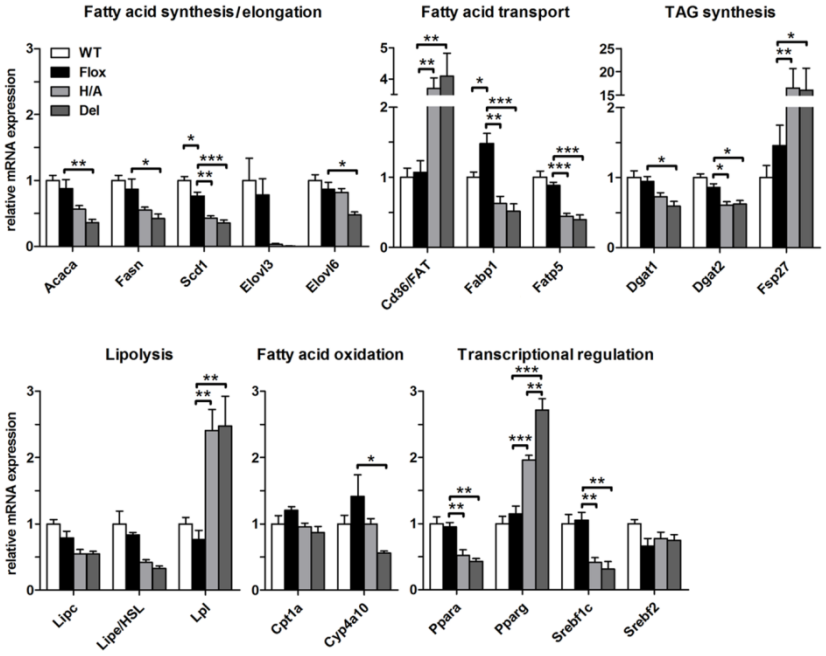


**Figure A 11: Quantitative Real-Time (qRT)-PCR analyses of genes involved in hepatic lipid homeostasis.** Transcript levels of several genes involved in lipid anabolic-, catabolic- and regulatory processes were determined in CerS2 WT, Flox, H/A and Del mice normalized to PPIA (Peptidylprolyl isomerase A) and HPRT (Hypoxanthine-guanine phosphoribosyltransferase) expression (n=5-7). Data are means ± SEM; *, p<0.05; **, p<0.01; ***, p<0.001. (Adopted and modified according to Bickert et al., 2018).

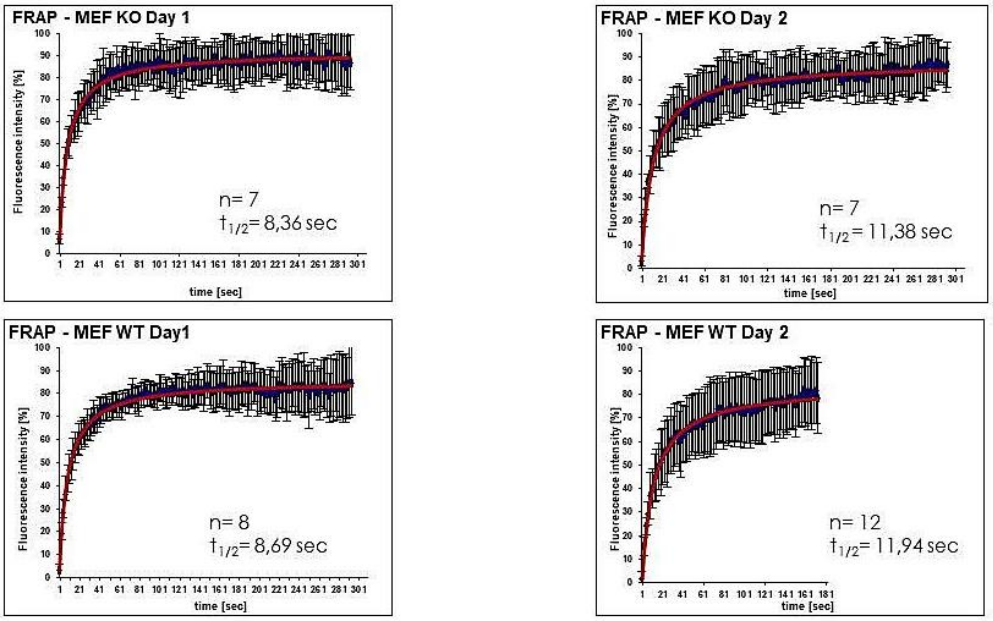


**Figure A 12: Lateral diffusion of the Insulin receptor in membrane sheets of primary MEFs derived from CerS2H/A mice.** Fluorescence recovery (FRAP) experiment was performed in collaboration with Elisa Merklinger, Prof. Lang. No obvious differences were obtained in the capability of the transfected IR-GFP to diffuse within the plasma membrane.

```
schlank      -----MDILNEFSNVFWSTHIWLPPNTTWADIAPGSRPDVVHANYKDLIWPIPFAAVVML 55
CerS2m       -------MLQTLYDYFWWERLWLPVNLTWADLEDK-D-GRVYAKASDLYITLPLALLFLV 51
CerS5m       MATAAAETLGLLWGWLWSESFWLPQNVSWADLEGPGD-GYGYPRAQHVLSVFPLAVCIFS 59
CerS6m       --------MAGILAWFWNERFWLPHNVTWADLKNTEE--ATFPQAEDLYLAFPLAFCIFM 50
                     :  :   :*   :*** * :***:         . . ..:   :*:*  .:

schlank      VRYTLERFWISPVGKSLGIRSSRPKKAANVPILEKTYAKSTRL-DKKKLVPLSKQTDMSE 114
CerS2m       IRYFFELYVATPLAALLNVKEKTRLRAPPNATLEHFYQTSGKQPKQVEVDLLSRQSGLSG 111
CerS5m       VRMLFERFIAKPCALRVGIKDSPVNKVEPNDTLEKVFVSVTKYPDEKRLKGLSKQLDWSV 119
CerS6m       VRLIFERFIAKPCAIALNIQANGPQTAQPNAILEKVFTAITKHPDEKRLEGLSKQLDWDV 110
             :*  :* :  .* .  :.:: .    .     **: :    :  .: .:  **:* . .

schlank      REIERWWRLRRAQDKPSTLVKFCENTWRCIYYLYSFIFGVIVLWDKPWFWDVKSCWYGYP 174
CerS2m       RQVERWFRRRRNQDRPSLLKKFREASWRFTYYLIAFVAGMAVTVDKPWFYDLRKVWEGYP 171
CerS5m       RKIQCWFRHRRNQDKPPTLTKFCESMWRFTYYLCIFCYGIRFLWSMPWFWDTRQCWYNYP 179
CerS6m       RSIQRWFRQRRNQEKPSTLTRFCESMWRFSFYLYVFSYGVRFLKQTPWLWNTRHCWYNYP 170
             *.:: *:* ** *::*  * :* *  **  :**  *  *: .  . **::: :  * .**

schlank      HQSISNDIWWYYMISMSFYWSLTGTQFFDVKRKDFWQMFIHHMVTLLLMSLSWVCNLHRV 234
CerS2m       IQSIIPSQYWYYMIELSFYWSLLFSIASDVKRKDFKEQIIHHVATIILLCFSWFANYVRA 231
CerS5m       YQPLSRELYYYYITQLAFYWSLMFSQFIDVKRKDFLMMFIHHMIGIMLTTFSYVNNMVRV 239
CerS6m       YQPLTADLHYYYILELSFYWSLMVSQFTDIKRKDFGIMFLHHLATIFLITFSYVNNMARV 230
              * :  .  :**: .::*****  :   *:*****   ::**:  ::*  :*:. *  *.

schlank      GSLVLVVHDCADIFLEAAKLTKYAKYQKLCDAIFAIFTVVWIVTRLGFYPRIIYSSS-VE 293
CerS2m       GTLIMALHDASDYLLESAKMFNYAGWKNTCNNLFIVFAIVFIITRLVIMPFWILHCTMIY 291
CerS5m       GALIFCLHDFADPLLEAAKMANYARRERLCTTLFVIFGAAFIVSRLAIFPLWILNTTLFE 299
CerS6m       GTLVLCLHDSADALLEAAKMANYAKFQKMCDLLFVMFAVVFITTRLGIFPLWVLNTTLFE 290
             *:*:: :** :* :**:**: :**  :. *  :* :*  .:* :** : *  :   : .

schlank      APRILPMFPAYYIFNSLLLMLLVLHVIWTYMILKIVVDSLQKGLMSGDIRSSDSEDLTDS 353
CerS2m       PLELYPAFFGYYFFNFMMAVLQMLHIFWAYFILRMAHKFI-TGKLIEDERSDREETESS- 349
CerS5m       SWEIIGPYPSWWLFNALLLILQVLHAIWSYLIVQTASKALSRGKVSKDDRSDVESSSEE- 358
CerS6m       SWEIVGPYPSWWVFNLLLLLLLQGLNCFWSYLIVKIACKTVSKGKVSKDDRSDIESSSDD- 349
               .:   : .::.** :: :*  *: :*:*:*:: . . :  * :  * **. ..   .

schlank      SGNARLTNGSARSKNKSISSAPSDKGSAGGAGSRAGARVATTERREE------------ 400
CerS2m       EGEETA-AG------AGAKSRLLANGHPILNNNH-----------PKND----------- 380
CerS5m       EDETT--HK------NNLSGSSSSNGANCMNGYMGGSHLAEEQGTCKATGNLHFRASPHL 410
CerS6m       EDSEP--PG------KKPHSSTTTNGTSGTNGYLLTGP-------CSVDD---------- 384
             ...               .    :*     .             .

schlank      ----   400
CerS2m       ----   380
CerS5m       HSCD   414
CerS6m       ----   384
```

**Figure A 13: Protein sequence alignment performed with schlank, CerS2/5 and 6:** Identical residues are indicated with asterisks (*) and similar residues with a '**:**' or a '**.**'. The colon depicts amino acids with more similarity to each other than those labeled with a dot. ( Alignments were performed with the CLUSTALW multiple alignment program (ExPASy).